POLYMERIC MICELLE-MEDIATED CURCUMIN DELIVERY FOR SAFE AND EFFICIENT CANCER THERAPY

A THESIS PRESENTED BY

RADHIKA RAVEENDRAN

TO

SREE CHITRA TIRUNAL INSTITUTE FOR MEDICAL SCIENCES AND TECHNOLOGY
THIRUVANANTHAPURAM
INDIA

IN PARTIAL FULFILMENT OF THE REQUIREMENTS
FOR THE AWARD OF
DOCTOR OF PHILOSOPHY

2016

CERTIFICATE

I, ***Radhika Raveendran***, hereby certify that I had personally carried out the work depicted in the thesis entitled, ***"Polymeric micelle - mediated curcumin delivery for safe and efficient cancer therapy"***.

No part of the thesis has been submitted for the award of any other degree or diploma prior to this date.

Date: 24-02-2016
Thiruvananthapuram

Radhika Raveendran
Reg No: PhD/2010/10

Dr. G.S. Bhuvaneshwar Former Head BMT wing, SCTIMST Thiruvananthapuram	Dr. Chandra P Sharma Former Head, Bio-surface Technology BMT Wing, SCTIMST Thiruvananthapuram

This is to certify that **Ms. Radhika Raveendran** in the department of Bio-surface Technology/FADDS of this Institute has fulfilled the requirements prescribed for the Ph.D degree of the Sree Chitra Tirunal Institute for Medical Sciences and Technology, Trivandrum.

The thesis entitled, **"Polymeric micelle-mediated curcumin delivery for safe and efficient cancer therapy"** was carried out under our joint supervision. No part of the thesis was submitted for the award of any degree or diploma prior to this date.

* Clearance was obtained from the Institutional Ethics Committee for carrying out the study.

Date: 24-02-2016

Thiruvananthapuram

Dr. G.S. Bhuvaneshwar
(Guide)

Dr. Chandra P.Sharma
(Co-Guide)

SREE CHITRA TIRUNAL INSTITUTE FOR MEDICAL SCIENCES & TECHNOLOGY, TRIVANDRUM

Thiruvananthapuram – 695011, INDIA
(An Institute of National Importance under Govt. of India)
Phone-(91)0471-2520248 Fax-(91)0471-2341814
Web site – www.sctimst.ac.in

Dr. Chandra P Sharma

Former Scientist G (SG), Head

Bio Surface Technology BMT wing,

SCTIMST, Thiruvananthapuram

This is to certify that **Ms. Radhika Raveendran**, in the Biosurface Technology Division and FADDS, of this Institute has fulfilled the requirements prescribed for the Ph.D degree of the Sree Chitra Tirunal Institute for Medical Sciences and Technology, Trivandrum. The thesis entitled, ***"Polymeric micelle - mediated curcumin delivery for safe and efficient cancer therapy"*** was carried out under my direct supervision. No part of the thesis was submitted for the award of any degree or diploma prior to this date.

*Clearance was obtained from the Institutional Ethics Committee/ Institutional Animal Ethics Committee for carrying out the study

Date: 24-02-2016
Thiruvananthapuram

Dr. Chandra P Sharma
(Co- guide)

The thesis entitled

Polymeric micelle - mediated curcumin delivery for safe and efficient cancer therapy

Submitted by

RADHIKA RAVEENDRAN

for the degree of

Doctor of Philosophy

Of

SREE CHITRA TIRUNAL INSTITUTE FOR MEDICAL SCIENCES AND TECHNOLOGY, THIRUVANANTHAPURAM

is evaluated and approved by

.....	..... 24/2/2016 Dr. J.D. Sudha
Guide	Examiner

Declaration of part of the study done at QUT

The study related to poly (2-oxazoline) polymers, depicted in this thesis, was performed at Queensland University of Technology (QUT), Brisbane, Australia under the supervision of Dr. Tim R Dargaville and co-supervision of Dr. Kathleen Mullen during the period 2013-2014.

Acknowledgments

This thesis would not have seen the light of the day without the support of several individuals and I take this opportunity to thank them. Firstly, I would like to thank my supervisor, Dr. G.S. Bhuvaneshwar for his support and encouragement throughout my PhD tenure. I am indebted to my co-supervisor Dr. Chandra P. Sharma for his assiduous guidance and scientific discussions during the course of this work. I am extremely grateful to Dr. K. Sreenivasan, one of my doctoral advisory committee members, who stepped up to be my guide-in charge after the retirement of my supervisors to facilitate the Institute's official formalities related to my PhD, I also thank him for his critical comments to improvise my thesis. I thank Dr. T.V Kumary, my doctoral advisory committee member, for her input and suggestions to better my work. I owe my gratitude to Dr. C.K.S. Pillai, Former Emeritus Scientist at SCTIMST. His role is crucial in designing this project and if it were not for him, I would not have contemplated this road of PhD journey. I was fortunate enough to get the opportunity to pursue a part of my PhD study at Queensland University of Technology (QUT), Brisbane, Australia for a period of one year. I thank Dr. Sheel Nuna for helping with all the formalities related to this program. I am indebted to Dr. Tim R. Dargaville, my research supervisor at QUT for initiating me to the lab environment at QUT. His conversations have enlightened my way of scientific thinking and I appreciate his constructive criticism to improve the thesis. I also thank Dr. Kathleen Mullen, my associate supervisor at QUT for her assistance.

I wish to express my gratitude and respect to the former and present Director of SCTIMST, BMT Wing for providing me the opportunity and the facilities during the course of my work. I am thankful to the Deputy Registrar (Dr Sundar Jaysingh), Associate Dean for PhD affairs, Dean and all members of the academic division and Director's office for their assistance. I am extremely grateful to Dr. Rekha M.R for her help with all the biological studies projected in my thesis. I truly believe that hands-on training on scientific instruments goes a long way in moulding a PhD scholar. And in this regard, I owe my gratitude to the staff at QUT, especially to Dr. Mark Wellard , Ms. Rachel Hancock , Dr. Jamie Riches for training on

^{1}H NMR spectrometer and transmission electron microscope. I am grateful to Dr. Kaladhar Kamalasanan for his feedback regarding my PhD work and his constant inspiration to think "out of the box". I thank Dr.Jayalekshmi A.C and Dr. Sunita prem Victor for their support. I acknowledge Mr. P.R. Hari for GPC analysis. I thank Dr.H.K Varma and, Dr. Suresh for FTIR facility. Also I wish to acknowledge Dr.Annie John and her staff for TEM analysis. I thank Dr. P.Ramesh and my good friends of POP lab, Dr. Roy Joseph and his lab members, Dr.Kalliyanakrishnan and his lab members, Dr. Lissy Kalliyanakrishna and her lab members, Dr.Maya Nandakumar and her lab members for providing me access to use their laboratory facilities. Also I am really thankful for the support that I received from the past and present lab mates of BST. And I am deeply indebted to my past and present friends in FADDS for the camaraderie and rapport built over the years and most importantly their support during the vicissitudes of my PhD life. My appreciation also extends to all my SCTIMST friends for their friendship throughtout my study period. I also acknowledge the congenial lab atmosphere offered by the Free Radical Chemistry and Biotechnology Group and CRC Polymers Research lab, QUT.

I acknowledge the financial assistance from the project Facility for nano/microparticles based biomaterials- advanced drug deliverysystems #8013, under the Drugs &Pharmaceuticals Research Programme and QUT Post Graduate Research Scholarship Award .

Most importantly, my deepest appreciation and gratitude goes to my family who stood by me and encouraged me to accomplish this task especially my brother Ragesh. I am thankful to Midhun V.S, my husband, for his constant support, motivation and for bearing the brunt of my PhD tantrums. I value the patience and support bestowed by my in-laws to complete the work at my own pace. I am thankful to all my friends; schoolmates, college mates, hostel mates (especially housemates in Brisbane) who always were my constant well-wishers.

And finally, I believe that this day would not have been a reality without the presence of the Supreme Power by whose grace I endured my PhD years with faith, patience, and perseverance. Thank you!

Table of Contents

List of Figures

List of Tables

Abbreviations

CMC	Critical micelle concentration
DCC	Differential scanning calorimetry
DLS	Dynamic light scattering
DMAP	N,N-dimethyl-4-aminopyridine
DMEM	Modified Eagles Medium
DMSO	Dimethyl sulphoxide
DPH	1, 6 Diphenyl-1,3,5 hexatriene
FBS	Fetal bovine serum
FTIR	Fourier transform infrared spectroscopy
GPC	Gel permeation chromatography
MTT	3-(4,5-dimethylthiazol-2-yl)-2,5-diphenyltetrazolium bromide
NMR	Nuclear magnetic resonance spectroscopy
PAGE	Polyacrylamide gel electrophoresis
PBS	Phosphate buffered saline
PCL	Polycaprolactone
PF127	Pluronic 127
POx	Poly (2-oxazolines)
RBC	Red blood cells
WBC	White blood cells
TEA	Triethylamine
TEM	Transmission electron microscope
THF	Tetrahydrofuran

SYNOPSIS

Cancer is a life threatening disease and has been identified to be a global killer. The International Agency for Research on Cancer (IARC) estimated approximately 12.7 million cancer cases worldwide in 2008 and current projections show that this number is expected to double by 2030. While the higher rate of cancer is attributed to demographic changes, it is compounded by various other factors like poor diet, sedentary lifestyle, occupational hazards and genetic propensities. Cancer, if not culminated to a terminal stage, has a possibility to be treated and cured. Various treatment options exist depending on the type and location of the cancer. Chemotherapy is a frequently employed treatment method which involves the systemic approach of using drugs to kill cancer cells. However, most of the traditional chemotherapeutic drugs have deleterious effects on healthy cells as they are incapable in differentiating between a normal and a cancerous cell. Thus, in their course of exerting cytotoxicity, these drugs end up being detrimental to normal cells. Furthermore, the side effects related to these drugs are another cause of major concern. Hence, there is currently a significant unmet medical need for alternatives to these synthetic chemotherapeutic drugs. An effective and ideal alternative is to resort to drugs derived from natural sources. Nature is rightfully termed as the “master chemist” as it is a reservoir of various therapeutic compounds. The toxicity of currently used chemotherapeutic drugs and the safety profile of natural therapeutics have fueled the quest for natural anti-cancer compounds. Scientists are encouraged to delve into

Nature's medicine cabinet to discover compounds that possess chemotherapeutic properties. One such Nature's therapeutic panacea is curcumin, a polyphenolic compound extracted from the well renowned spice turmeric. Extensive research over the last few decades has established the anti-cancer potential of curcumin to induce selective apoptosis on cancer cells. Despite, having considerable promise as a safe and effective anti-cancer drug, curcumin faces obstacles when it comes to clinical administration mainly due its low aqueous solubility and instability at physiological pH. Implementing polymeric micelles for curcumin delivery is an effective strategy to surpass these setbacks. Polymeric micelles are self- assembling nano-constructs based on amphiphilic macromolecules that have distinct hydrophobic and hydrophilic block domains. They are endowed with a host of favourable properties which offer great prospects in the realm of drug delivery and these include solubilization of poorly soluble drugs, stealth property leading to longer systemic circulation, high stability and the ability to be targeted to cancer cells.

This PhD study focuses on the synthesis and investigation of polymeric micelles, based on amphiphilic copolymers / conjugates of water soluble polymers, which are explored for their feasibility in encapsulating curcumin for anti-cancer applications. The thesis is presented as six chapters. The first chapter of the thesis portrays an introduction providing an overview on cancer, its current statistics as a global burden and currently employed treatments in cancer therapy. The drawbacks of chemotherapy and the need for natural alternatives like curcumin are highlighted. Further, adoption of polymeric micelles as a strategy to resolve the clinical administration issues faced by curcumin is also discussed. The second chapter

describes the literature review related to the area of research. A comprehensive survey of literature is presented on various hydrophilic and hydrophobic components based on polymers, fatty acids and macro cyclic compounds which have been incorporated for the preparation of polymeric micelles related to the study. Discussion of the aims of the study and the hypothesis are also projected in this chapter. The following objectives are considered for the study:

- Synthesis of amphiphilic matrices based on biocompatible materials which can self-assemble to form micelles.
- Preparation of curcumin loaded polymeric micelles based on these amphiphilic matrices.
- Attempt to explore these different amphiphilic matrices to attain favourable amount of curcumin loading and release profile at physiological/ acidic pH.
- To gain insight on the solubility parameter of curcumin with the hydrophobic micellar core of synthesized amphiphilic polymers.
- Evaluation of the anti-cancer activity of synthesized curcumin loaded micelles compared to free curcumin.

The third chapter describes the materials and methods section. This chapter is divided into four sections. The first section details the preparation of curcumin loaded micelles based on mPEG laurate, mPEG linolenate and Pluronic linolenate which were synthesized by Steglich esterification. In the second section, synthesis and characterization of curcumin loaded PCL/Pluronic micelles are projected. PCL/Pluronic block copolymer were synthesized by stannous octoate mediated ROP (ring opening polymerization) of ε-caprolactone with Pluronic. This chapter also

sketches an attempt on synthesis and characterization of curcumin loaded calix arene conjugated PCL/Pluronic micelles. The third section focuses on the preparation of curcumin dextran conjugates capable of self assembling in aqueous media. The fourth section elaborates on the preparation of curcumin loaded micelles based on poly-2-oxazoline (POxs) polymers. Cationic ring opening polymerization (CROP) of 2-ethyl-2-oxazoline (EtOx) and 2-(but-3-enyl)-2-oxazoline (ButenOx) afforded P(EtOx-b-ButenOx) block copolymers. Similarly, CROP of 2-methyl-2-oxazoline (MeOx) and 2 isopropyl-2-oxazoline (isoPropOx) produced block and gradient copolymers of P(MeOx-isoPropOx). These polyoxazoline copolymers were investigated for their suitability for curcumin delivery. The curcumin loaded micelles based on different amphiphilic matrices were subjected to physico-chemical characterizations and *in vitro* biological evaluations to establish the feasibility of polymeric micelle mediated curcumin delivery. The general structural characterization of the synthesized amphiphilic matrices was performed by FTIR and ^{1}H NMR spectroscopy. The critical micelle concentration of the micelles was determined by fluorescence spectroscopy using fluorescence probes. The size and zeta potential of the curcumin loaded micelles were determined by dynamic light scattering (DLS) method using Zetasizer Nano ZS. The morphology and size of the micelles were also analysed by transmission electron microscopy (TEM). Curcumin-polymer interactions were validated by differential scanning calorimetric (DSC) studies. Spectral properties of curcumin loaded micelles were studied by UV-visible and fluorescence spectroscopy. Loading and encapsulation efficiencies of the micelles

were determined and quantified spectrophotometrically. Hemolytic studies and blood aggregation studies were carried out to study the compatibility of the micelles with the blood components. *In vitro* cell culture studies were performed in cancer cell lines to assess the effect of the curcumin loaded polymeric micelles compared to the native curcumin. Cytotoxicity of the curcumin loaded micelles was evaluated by MTT assay and was further corroborated by Live Dead assay. Cellular internalization of curcumin loaded micelles in cancer cells was detected by fluorescence microscopy.

The fourth chapter and the fifth chapter of the thesis concentrate on the results and discussions, respectively, pertaining to the study. These chapters are also discussed section wise based on the four amphiphilic matrices. Conjugation of fatty acids to hydrophilic polymers is a facile method to design self-assembling micelles. The impetus to incorporate fatty acids was due to their cell penetrating properties in addition to their ability in solubilizing hydrophobic molecules. PEG conjugation endows stealth properties to the micelles by preventing opsonization. Curcumin loaded mPEG laurate and linolenate micelles exhibited size less than 100 nm and zeta potential in the range of -15 to -24 mV. Curcumin loaded mPEG linolenate exhibited slightly better loading of about 3% (w/w) with an encapsulation efficiency of about 90% than its laurate counterpart and this was substantiated by the comparatively lower value of Flory-Huggins interaction parameter for the linolenate core with respect to curcumin. In order to further enhance curcumin loading, Pluronic was conjugated to linolenic acid. It was observed that the hydrophobic PPO chains in Pluronic had an increment effect on curcumin loading. Curcumin

loading of 7.9 % (w/w) was afforded with the Pluronic linolenate micelles having a hydrodynamic size around 167 nm. Retention of curcumin properties in the loaded micelles was also validated by spectroscopic characterization techniques. It was also confirmed from the study that micellar encapsulation prevented the rapid degradation of curcumin. MTT assay results revealed that curcumin loaded micelles demonstrated negligible toxicity on the normal cells and enhanced cytotoxic activity on human colon adenocarcinoma (Caco2) cells compared to free curcumin. The curcumin loaded Pluronic linolenate micelles rendered the dual benefits of linolenic acid and curcumin which were evident from the enhanced apoptotic effects of curcumin and linolenic acid on Caco2 cells. Cellular uptake images of curcumin loaded micelles showed intracellular green fluorescence proving that the Caco2 cells efficiently took up the curcumin loaded micelles compared to the free curcumin. However, despite having higher release at pH 4.5, around 73% release of curcumin in 72 hours was observed from the Pluronic linolenate micelles at pH 7.4. This is considered to be a drawback while intending to design drug delivery systems for cancer therapy. Since the tumour microenvironment is acidic, negligible release at pH 7.4 and rapid release at acidic pH are desired for anti-cancer applications. In the second section, with a view to further increase the hydrophobicity to enhance curcumin loading and to modulate the release at pH 7.4, PCL was introduced to synthesize PCL/Pluronic block copolymer. Curcumin loaded PCL/Pluronic micelles exhibited size less than 200 nm with curcumin loading of 10 %. It was observed that about 56% of curcumin was released at pH 7.4 in 72 hours which could be explained by incorporating the hydrophobic PCL. Micellar encapsulation endowed

similar properties as in the previous section which includes enhanced curcumin stability, enhanced cytotoxicity and cellular internalization in cancer cells compared to native curcumin. An attempt was carried out to conjugate calix arene to the PCL/ Pluronic copolymer as calix arenes possess hydrophobic cavities which are capable of encapsulating hydrophobic molecules. Curcumin loaded calix[4]arene conjugated PCL/Pluronic micelles exhibited a loading of 17.6 % (w/w). Incorporation of calix[4]arene led to a decreased curcumin release of 35 % at pH 7.4 in 72 hours and an enhanced release of 92 % at acidic pH. However, low reaction yield and use of dioxane during preparation of micelles posed as a problem to work with these matrices on a larger scale. The third section explored the possibility of conjugating curcumin to hydrophilic dextran so as to form a self-assembling micelle. Hemocompatible dextran curcumin conjugates prevented curcumin degradation at physiological pH. In addition, it was observed that conjugation of curcumin did not compromise its therapeutic property and induced cytotoxicity on C6 glioma cells at 50 μM curcumin concentration. Despite having enticing features, a low curcumin loading of 3 % (w/w) posed as a drawback for the dextran curcumin conjugates. The fourth section details the major findings of curcumin loaded micelles prepared from polyoxazoline (POx) polymers, an emerging class of polymers considered to be an alternative to PEG as they confer similar biocompatibility and stealth properties. P($EtOx_{33}$-b-$ButenOx_{26}$) and P ($EtOx_{17}$-b-$ButenOx_{44}$) could form curcumin loaded micelles of size less than 110 nm and loading of 7.5 and 11.6 % (w/w), respectively. The micelles also exhibited pH sensitive release due to micellar deformation at acidic pH. Further, upon investigating the block and gradient copolymers of

P(MeOx-isoPropOx), it was noted that curcumin loaded P($MeOx_{30}$-b-isoPropOx_{30}) showed favourable results among them.

The last chapter of the thesis concludes by summarizing the characteristics of curcumin loaded micelles prepared from the different amphiphilic matrices based on size, loading and release profile. Fortifying the hydrophobic domains of amphiphilic matrices is shown to influence curcumin loading and tune its release profile. It is understood that polymer architecture plays a significant role in influencing the loading and release characteristics of curcumin. Among the investigated matrices, P($EtOx_{17}$-b-ButenOx_{44}), the polyoxazoline based amphiphilic matrix exhibited better loading on a par with pH sensitive release of curcumin and enhanced cytotoxicity and cellular internalization. These attributes project P ($EtOx_{17}$-b-ButenOx_{44}) as a promising candidate among the investigated matrices and is believed to have a potential scope to be extrapolated for safe and efficient anti-cancer drug delivery applications.

CHAPTER 1 - INTRODUCTION

1.1 Cancer –An Overview

Cancer is a complex disease triggered by a set of acquired or heritable changes altering the expression of cell division or cell survival monitoring genes. The aetiology of cancer is defined by the disruption of cellular control mechanisms to cause abnormal multiplication of genetically altered cells. Normal cells display an inherent regime of growth, division and programmed cell death known as apoptosis. Unlike normal cells, cancer cells do not experience apoptosis therefore leading to an uncoordinated or deregulated cellular proliferation of abnormal mass of cells. Medically, cancer is termed as neoplasm which can be malignant or benign. Malignant neoplasm is characterized by uncontrolled cell growth comprising of invasion, destruction of adjacent tissues and metastasis to distant anatomic sites via lymph or blood. Most commonly, cancer mortality owes to these metastatic conditions. Benign neoplasm (tumour), however, does not invade other tissues or form metastasis. The molecular and cellular infrastructure of cancer is constituted by various biological processes that have been identified as "hallmarks of cancer" which include sustaining cell proliferation, dodging growth suppressors, resisting cell death, inducing angiogenesis , acquiring replicative immortality , activating invasion and metastasis processes , genome instability, tumour-promoting inflammation, reprogramming of cell bioenergetics and evading immune surveillance (Hanahan and Weinberg, 2011). Various risk factors contribute to cancers which include genetic

factors, lifestyle factors such as diet, tobacco use, certain types of infection, occupational hazards and environmental exposures to different types of chemicals and radiation.

1.2 Cancer Burden- Global Scenario

The global population is expected to reach 8.3 billion by 2030 and it is regarded that continuing growth and ageing of the world's population would lead to an expected global burden of 20.3 million new cancer cases by 2030 and 13.2 million cancer-related deaths worldwide (Ferlay et al., 2010). Estimates in 2008 indicated that about 12.7 million people were diagnosed with cancer and 7.6 million succumbed to it (Bray et al., 2013; Jemal et al., 2011). In the coming years, changes in lifestyle combined with pre-existing factors are likely to produce dramatic increase in the rate of occurrence of cancer. The most commonly diagnosed cancers are that of lung, breast, colorectum, stomach prostrate, liver and cervix and these cancers together constitute more than 58% of the predicted global cancer burden. A nationwide survey in India confirmed that more than 70% of fatal cancers occur in the age group of 30-69 year indicating that cancer is an important cause of adult deaths (Dikshit et al., 2012). Population growth and increasing life expectancy is bound to enhance the absolute number of cancer deaths in India. Regional and individual differences in cancer trends complicate the termination of the disease, despite enormous funding and research. Further progress in eradicating cancer can be accelerated by applying existing knowledge on cancer control across all segments of the population and by supporting modalities in cancer prevention, early detection and treatment.

1.3 Existing modes in cancer therapy

Despite being dreaded as a fatal disease, early diagnosis of cancer increases the chances of treating and curing it. Location of the cancer, stage of the disease, health status, age and other individual characteristics dictate the therapeutic choice of treatment.

1.3.1 Surgery

Surgery, the oldest known treatment for cancer, involves surgical removing of tumour from a localized part of the body. Prior to 1950s, cancer therapy was largely confined to the province of a surgeon (Chabner and Roberts, 2005). As surgery is more focused in extirpating the localized tumour cells, it proves a limitation when there is a widespread dissemination of the disease.

1.3.2 Chemotherapy

Chemotherapy employs chemicals that interfere with the cell division process by damaging proteins or DNA. Cancer chemotherapeutics are identified by screening compounds that are capable of killing the rapidly dividing cells. The era of chemotherapy was marked with discovery of nitrogen mustards and anti-folate drugs in 1940s. The timeline of chemotherapy witnessed the discovery of many chemotherapeutic drugs with Taxol being the first “blockbuster oncology drug” approved by FDA in 1992 (Chabner and Roberts, 2005). Understanding the molecular profile of human tumours is critical to the effective use of chemotherapeutic drugs. Chemotherapy remains the backbone of cancer treatment as

it is also used in conjunction with other modes of treatments like surgery and radiation therapy. Combination therapies often include multiple types of chemotherapy or chemotherapy combined with other treatment options.

1.3.3 Radiation therapy

Radiation therapy emerged as a valuable tool for control of local disease post 1960s with the invention of the linear accelerator (Chabner and Roberts, 2005). Radiation treatment is performed by focusing high-energy gamma-rays on the cancer cells. Severe side effects are associated with radiation therapy as the energy beams are capable of damaging normal healthy tissue. However, in recent years , improvement in technologies have witnessed accurate targeting of these beams on tumour cells (Gunjur et al., 2014).

1.3.4 Immunotherapy

The landscape of cancer treatment over the last four decades has dramatically changed. The age when surgery and radiotherapy were the only effective ways to combat tumour has ended. Immunotherapy aims to get the innate and adaptive immune systems of the body to fight cancer (Zitvogel et al., 2008) . Recognition of various tumour expressed proteins by the immune system is exploited in this therapy which augments protective antitumor immunity (Dougan and Dranoff, 2001). Immune therapy is also used to treat hematologic malignancies. Investigational immune therapies are focused on building upon established treatments to generate more efficacious and less toxic cancer therapy.

1.3.5 Hormone Therapy

Hormone therapy involves exogenous administration of steroid hormones or hormone antagonist drugs which manipulates the endocrine system. It is designed to alter hormone production in the body to curb the proliferation of cancer cells or to eliminate it completely. Hormonal therapy is effective for cancers affecting the breast, prostate, adrenal cortex and endometrium which are derived from hormonally responsive tissues . Breast and prostate cancers are treated through this mode of therapy by focusing on reducing the estrogen or testosterone levels, respectively.

1.3.6 Gene Therapy

The paradigm of gene therapy is to replace the damaged genes that are prone to cause cancer or to induce apoptosis in a defective cell. Burgeoning number of gene transfer methods and gene cloning techniques have contributed to the advancement of clinical trials of cancer gene therapy (Culver and Michael Blaese, 1994). Various viral and non-viral vectors have been developed and different strategies have been employed to treat the malignant disease. Vector development aims at using retroviral or DNA-virus platforms to increase transfer efficiencies, targeting, transgene expression complemented with expressional targeting or conditional gene expression. Non-viral systems based on synthetic molecules are a recent development in gene therapy to overcome the toxicity and immunogenicity problems encountered by the use of viral vectors (Niidome and Huang, 2002) .

1.4 Drawbacks of chemotherapy

Chemotherapy is indispensable in cancer treatment regimen with its use in conjunction with other treatments like surgery and radiotherapy to ensure the non-recurrence of tumour. But, nowadays use of chemotherapeutics is a double edged sword. Synthetic chemotherapeutic drugs are effective in destroying the proliferating mass of cancer cells. However, these cytotoxic drugs are unable to differentiate between the uncontrolled proliferation of cancer cells and the normal, healthy dividing cells, thereby creating undesirable cytotoxicity. Toxicity of these anticancer chemotherapeutic agents is not always attributed to excessive dose but can also occur within the therapeutic dose range. Bone marrow toxicity is prevalent due to the effect of the drugs on proliferating cell populations. Administration of anthracycline group of agents like doxorubicin and daunorubicin are known to cause cardiomyopathy. Renal failures are associated with the use of cis-platinum drugs, nitrosoureas and high dose methotrexate (Plenderleith, 1990). Peripheral neurotoxicity and central neurotoxicity which include minor cognitive deficits, encephalopathy with dementia or even coma are also common side effects of chemotherapy Methotrexate, cytarabine and ifosfamide are primarily known to induce central neurotoxicity (Verstappen et al., 2003). The chemotherapeutic drugs have adverse effect on the rapidly proliferating cells associated with spermatogenesis or oogenesis leading to sterility. In addition, various other side effects spurning from the continuous administration of the chemotherapeutic drugs adversely affect the quality of life of the patients. Many chemotherapeutic drugs cause alopecia (hair

loss) as they terminate the normal dividing cells of the hair follicles. Nausea, fatigue, vomiting, diarrhoea, mucositis, pain, rashes and infections are few other common problems arising from acute drug toxicity (Johnstone et al., 2002; Loprinzi et al., 2007).

1.5 Natural alternatives to alleviate conventional chemotherapy side- effects

Side effects of chemotherapy are a major impediment in cancer treatment. The deleterious effects on the normal cells have become the impetus for the quest for anti-cancer drugs with safer profile. Recognizing the need for safer approaches to cancer chemotherapy, scientists are delving into the herbal medicine cabinet of Nature. The interest of using natural products for therapeutic applications has gained momentum in the past few decades. Despite revolutionizing modern medicine over the last century, synthetic pharmaceuticals are tagged with undesirable properties and side effects which have inspired a search for natural alternatives as these hold promise of better tolerance than their synthetic counterparts. Although this seems a recent venture, resorting to natural compounds to cure maladies is dated well back to the ancient times. Plants have commonly been the source of phytochemicals which are known to possess anticarcinogenic properties. The NCI (National Cancer Institute) has documented about 35 plant-based foods that possess cancer-preventive properties and exciting findings have been achieved with anti-oxidant vitamins and their precursors derived from fruits and vegetables (Surh, 2003). Prevention of tumour development by chemo-preventive phytochemicals is considered to be the

outcome of the combination of several distinct sets of intracellular effects which include; cell-cycle progression; cell proliferation, differentiation and apoptosis; DNA repair; angiogenesis and metastasis; activation of tumour-suppressor genes and hormonal and growth-factor activity. Chemo-preventive phytochemicals can block or suppress the progression of precancerous cells into malignancy by acting upon various molecular targets implicated in cancer (Gescher et al., 1998; Milner et al., 2001). A new dimension to the standard cancer therapy could be attained by using phytochemical compounds which can eliminate the usual toxicity issues associated with synthetic chemotherapeutic drugs.

1.6 Curcumin - Combating Cancer the Natural Way

Curcumin, a polyphenol, is an active component of the perennial herb *Curcuma longa* (commonly known as turmeric) prevalent in tropical and sub-tropical regions mainly India, China and South East Asia. Turmeric is extensively used as dietary spice in the Asian countries. However, turmeric is not only confined to culinary purposes but also has medicinal properties. This is evident as it is widely used in Indian traditional holistic medicine known as Ayurveda and Chinese medicine (Salem et al., 2014). Turmeric paste is a common home remedy for the treatment of cough, wounds and inflammations. (Chattopadhyay et al., 2004). Turmeric is constituted by curcumin and other curcuminoids and these pigments are obtained through solvent extraction and subsequent crystallization from the rhizomes of *Curcuma longa* [Figure 1] (Goel et al., 2008).

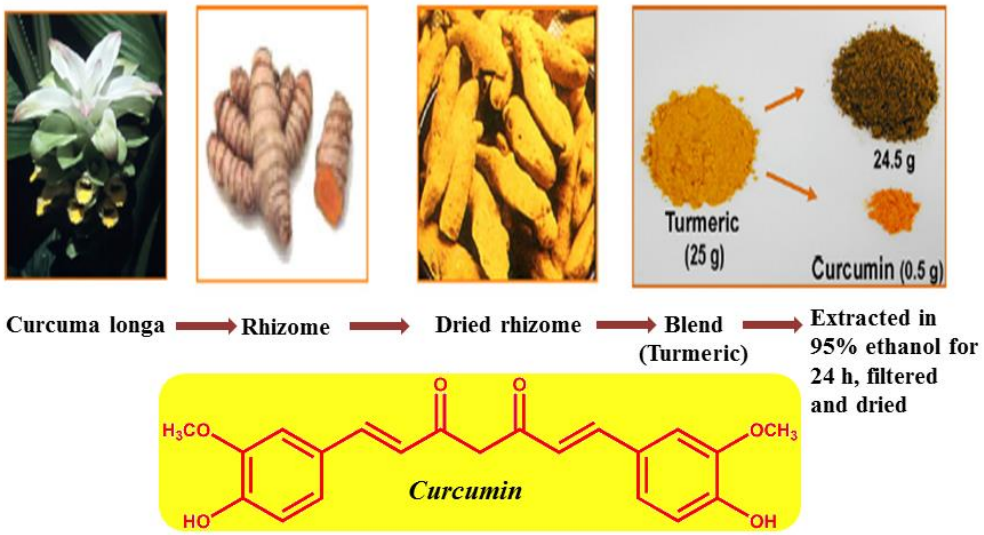

Figure 1. Curcumin is extracted from the dried rhizomes of turmeric (Curcumin longa). Adapted from (Goel et al., 2008)

Research has now established that curcumin is the active agent in turmeric which imparts, not only the yellow hue, but also the multiple therapeutic properties (Esatbeyoglu et al., 2012). Curcumin is one of the most extensively investigated phytochemicals due to its wide spectrum of biological actions which include anti-inflammatory, anti-oxidant, anti-carcinogenic, anti-bacterial, anti-fungal and anti-ulcer activities (Aggarwal et al., 2007). More importantly, it is the anti-cancer potential of curcumin which has brought this molecule into the limelight. This has stemmed from the fact that India revealed lower risk of cancer when compared to the West which was attributed to the regular intake of turmeric (Salem et al., 2014). Onset and progression of cancer involve several molecular markers. Curcumin is known to interfere with several biochemical pathways through its interaction with

molecular targets which include transcription factors, growth factors, RNA, DNA and many proteins (Gupta et al., 2013; Shehzad et al., 2013). Potential therapeutic effects and better tolerance define the motivation for the use of curcumin in comparison to most chemotherapeutic drugs associated with harmful side effects. The safety profile of curcumin has been well assessed and is observed to be tolerated at high doses with negligible toxic effects. As indicated by numerous Phase I studies, no adverse effects were observed with an oral intake of 12 grams of curcumin per day (Hsu and Cheng, 2007; Lao et al., 2006; Shoba et al., 1998).

1.7 Drawbacks in curcumin administration

The chemo-preventive potential of curcumin has been demonstrated by the anti-carcinogenic effects in cell culture and animal models. Despite having considerable promise to be exalted to a status of a safe anticancer drug, curcumin experiences obstacles in clinical administration due to its low aqueous solubility which subsequently leads to low bioavailability. Relatively low intestinal absorption, rapid metabolism in the liver and elimination by gall bladder contribute to the low oral bioavailability of curcumin (Shoba et al., 1998; Wahlström and Blennow, 1978; Yang et al., 2007). Moreover, the plasma concentration of curcumin is found to be negligible following intravenous administration (Ireson et al., 2001). Another setback faced by curcumin is its rapid degradation at physiological pH (Wang et al., 1997).

1.8 Polymeric Micelles to spice up curcumin delivery

Amphiphilic polymers, consisting of hydrophilic and hydrophobic domains, spontaneously self- assemble in aqueous media to form polymeric micelles having a

distinct hydrophobic core surrounded by hydrophilic corona (Miyata et al., 2011). Ringsdorf et al , almost 30 years ago, introduced the concept of utilizing polymeric micelles for the encapsulation of therapeutic agents (Pratten et al., 1985; Winnik et al., 1991). However, during that time, majority of micelles were synthesized from bio-incompatible materials. Recent years have witnessed the introduction of biocompatible materials for polymer micelle syntheses which have revolutionized the realm of drug delivery. It is understood that almost one-third of the discovered drug compounds are shelved from reaching clinical administration due to poor solubility and inherent systemic toxicity which have led to the restriction of the productive application of these potent therapeutic agents (Lipinski, 2000). Advent of polymeric micelles has circumvented these limitations. Moreover, polymeric micelles exhibit better safety profile as alternatives for the administration of hydrophobic drugs compared to the conventional solubilising agents like Cremophor®EL (polyethoxylated castor oil), and Tween 80 that are faced with toxicity issues (Aliabadi and Lavasanifar, 2006). Polymer micelles are endowed with the following advantages that define their stringent success in drug delivery:

1.8.1 Size

The size of polymeric micelles confine to the nanoscale range of 10-200 nm in diameter (Aliabadi and Lavasanifar, 2006). The significance of their small size is crucial in retarding the rate of body clearance by recticuloendothelial system (RES) and renal filtration. Further, the blood residence time of micelles is prolonged which allows them to permeate through leaky inflamed blood vessels, a phenomenon which is observed in the tumour micro-environment (McDonald and Baluk, 2002).

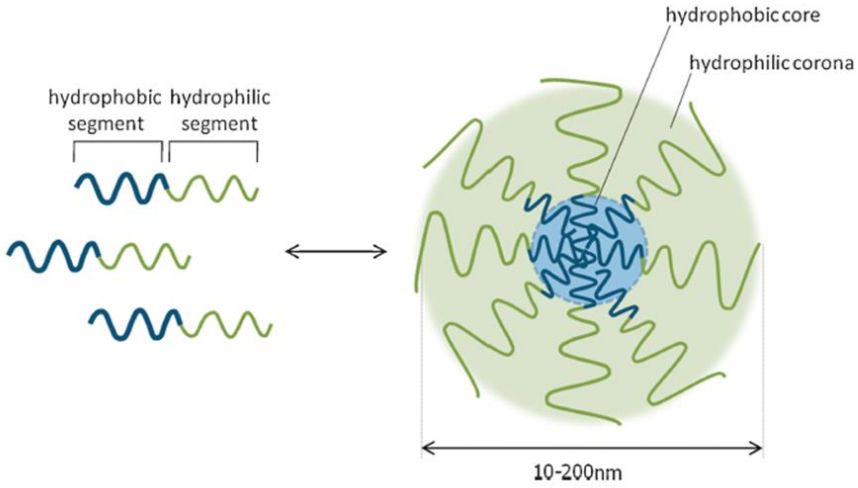

Figure 2. Schematic representation of polymeric micelle formation. Adapted from (Owen et al., 2012).

1.8.2 Stealth properties

A foreign organism or particle upon entering the systemic circulation is swarmed by opsonin proteins which cover it and hence make it visible to phagocytic cells leading to engulfing and eventual destruction or removal of the foreign material from the bloodstream (Owens III and Peppas, 2006). Enhanced adsorbability of blood serum proteins occurs on hydrophobic particles relative to hydrophilic particles (Carrstensen et al., 1992). The hydrophobic core of polymeric micelles, however, can evade phagocytosis. The hydrophilic corona of the polymeric micelle forms a highly water-bound barrier which aids in preventing opsonization (Aliabadi and Lavasanifar, 2006) . This poses as an advantage in longer circulation of drug loaded micelles to attain maximum therapeutic efficacy.

1.8.3 Critical micelle concentration (CMC)

Amphiphilic polymers self-assemble by aggregation of chains constituted by the hydrophobic and hydrophilic segments. A minimum polymer concentration known

as the critical micelle concentration (CMC) is required for the individual chains or unimers to self-assemble in an aqueous milieu. The higher CMC value in conventional low molecular weight surfactants results in rapid precipitation of solubilized drug upon dilution. Polymeric micelles generally have a low CMC value compared to the micelles formed from the small surfactant molecules which ensure their stability and retention of the encapsulated drug for a prolonged duration even upon dilution by biological fluids (Lukyanov and Torchilin, 2004).

1.8.4 Drug loading capacity

Polymeric micelles can carry large payloads of drug entity and also protect it from degradation. Drug loading can be tuned by tailoring the structural design of the core-forming block of the polymer. The drug loading capacity is depended on the compatibility of the hydrophobic core of the micelle and the incorporated drug. The compatibility between the drug and the polymer is dictated by Flory–Huggins interaction parameter [χ_{sp}] (Letchford et al., 2008). This calculated parameter provides information about the compatibility between the drug and micellar core and has been used to qualitatively explain the different extents of solubilization of hydrophobic drugs by micellar drug delivery systems formed from amphiphilic polymers. The lower the χ_{sp} value , the more compatible the drug is with the micellar core which indicates a high predicted amount of solubilization (Lim Soo et al., 2002; Liu et al., 2004).

1.8.5 Tumour targeting

Tumour selective drug delivery is highly desired to avoid the undesirable side-effects on normal cells and to derive maximum therapeutic efficacy. Tumour site can be

zeroed in by exploiting the physiological abnormalities of tumour cells and their cellular targets. Polymeric micelles are efficient in targeting the tumour cells by two mechanisms - passive and active targeting.

1.8.5.1 Passive targeting (EPR effect)

There is a vast difference between the anatomical architecture of normal cells and tumour cells. The blood vessels in the tumour micro-environment are leaky with large fenestrations and in addition, the tumour tissues have poor lymphatic drainage (Matsumura and Maeda, 1986). Polymer micelles, due to their small size, can extravasate into the tumour interstitium via these dilated fenestrations and are further retained in the tumour cells due to the poor lymphatic clearance. This phenomenon, which is the basis of selective targeting of macromolecular drugs, is termed as enhanced permeation and retention (EPR effect) or passive targeting. Through EPR effect, high concentration of polymeric drugs can be achieved locally at the tumour site than in normal tissue (Iyer et al., 2006).

1.8.5.2 Active targeting

Tumour cells are known to overexpress certain surface markers (receptors or antigens) relative to normal cells. Active targeting aims at conjugating ligands, which have affinity to appropriate receptors on the tumour cells, onto the surface of polymer micelles. The ligands home the drug loaded micelles to the tumour site and bind onto their specific receptors on the cell membrane which pave the endocytic internalization of the micelles, thereby achieving higher intracellular drug concentrations (Torchilin, 2008). Specific ligands like proteins, antibodies,

oligosaccharides or aptamers are attached to the shell-forming block of the polymeric micelles. (Mahmud et al., 2007).

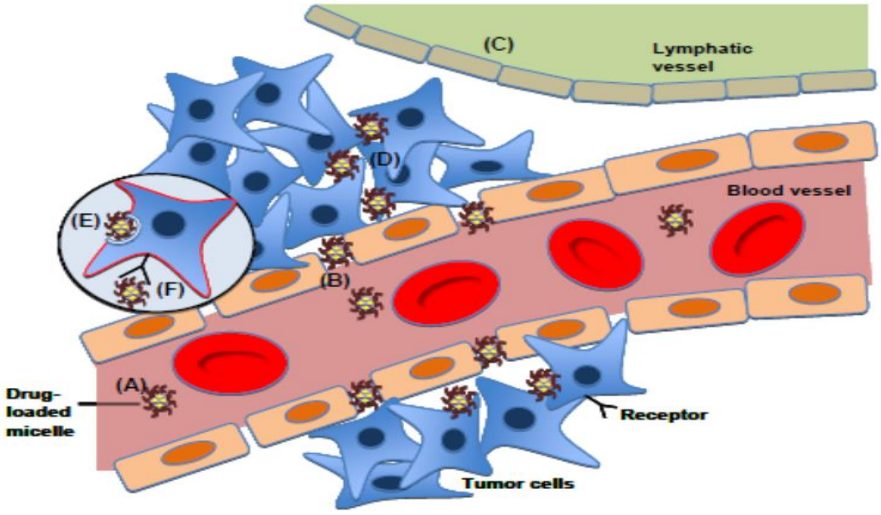

Figure 3. (a) Evasion of innate clearance mechanisms by polymeric micelles resulting in prolonged blood circulation time; (b) extravasation of micelles through the leaky tumor vasculature, where the endothelial gap junctions vary between 400–600 nm (passive targeting); (c) retention of micelles in tumour tissues due to impaired lymphatic drainage; (d) a high interstitial concentration of drug loaded micelles in the tumor; (e) non-specific or (f) specific receptor-mediated internalization of drug-loaded micelles (active targeting). Adapted from (Ebrahim Attia et al., 2011).

1.9 Aim of the study

The efficacy of curcumin is hampered by the obstacles it faces during clinical administration. Encapsulating curcumin in polymer micelles is a pragmatic strategy to overcome the drawbacks. The aim of this study is to fine-tune the properties of polymeric micelles synthesized from various amphiphilic polymers to meet the optimum curcumin delivery profile to cancer cells.

1.10 Objective of the study

The study focuses on the following objectives:

- Synthesis of amphiphilic matrices, based on biocompatible components, that are capable of self assembling into micelles. These micelles are further explored in their utility to encapsulate and solubilize curcumin.
- There is a dearth of amphiphilic polymers that can exhibit better curcumin loading capacity for achieving favourable results *in vivo*. Therefore, an attempt has been carried out in the study to investigate amphiphilic polymers that can enhance the loading of curcumin.
- To identify favourable curcumin loaded micelle carriers that are capable of exhibiting rapid release at acidic pH while maintaining low release at physiological pH.
- To determine the Flory–Huggins interaction parameter [χ_{sp}], which defines the compatibility between curcumin and the micelle core , and to analyse the trend of loading of curcumin with respect to $\chi_{sp.}$
- Evaluation of the anticancer effect of synthesized curcumin loaded micelles compared to free curcumin.

The further chapters in the thesis contribute to fulfilling the objectives of the study. Chapter 2 details the literature review related to the area of research and highlighting the rationale for the study. Chapter 3 describes the materials and methods used for the study. Chapter 4 focuses on the results of the experimental observations and the data generated. Chapter 5 involves the discussion and interpretation of the results

mentioned in the previous chapter. Finally, chapter 6 depicts the major conclusions highlighting the salient findings and projecting favorable matrices for designing future projects.

CHAPTER 2 - LITERATURE REVIEW

2.1 Curcumin

2.1.1 Physico-chemical properties

Curcumin [chemical name: (*E*,*E*)-1,7-bis(4-hydroxy-3-methoxyphenyl)-1,6-heptadiene-3,5 dione) or diferuloylmethane] is a bis-α,β-unsaturated β-diketone with a melting point around 180^{o}C and a molecular weight of 368.37 g/mol (Aggarwal et al., 2007). Curcumin was first isolated in crude form by Vogel in 1815 (Vogel and Pelletier, 1815) and later in 1870, the crystalline form of orange-yellow powder was obtained. The structure of curcumin ($C_{21}H_{20}O_6$) was elucidated by Lampe and Milobedeska in 1910 (Lampe et al., 1910). Curcumin possesses two aromatic rings , functionalized with methoxy and hydroxy groups in ortho positions with respect to each other, linked by a seven carbon spacer that has two α,β unsaturated carbonyl groups. The conjugated double bond along with the two symmetrically placed chromophores of the structural motif C=O–C=C renders the yellow colour. The structural arrangement enables curcumin to exhibit tautomerism where a keto-enol and equilibrating beta-diketone tautomeric forms of curcumin are possible, as shown in Figure 4. Jovanovic et al proposed that curcumin predominately exists in the beta diketone form in mildly acidic and neutral solutions and also suggested that, in this form , the central methylene group acted as a potent hydrogen donor in radical reactions which attributed to the potential biological activity exerted by curcumin (Jovanovic et al., 1999). However, NMR studies performed by Payton et al debated the above proposition as it was observed that curcumin existed in keto-enol form in

solvents over a pH 3-9 range (Payton et al., 2007). This was further corroborated by Shen and Li through density functional theory calculations which supported the pre-dominance of keto-enol tautomers (Shen and Ji, 2007).

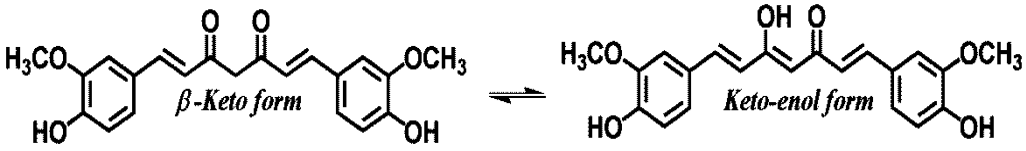

Figure 4. Tautomerism exhibited by curcumin

2.1.2 Curcumin and cancer

Curcumin is endowed with a multitude of therapeutic properties but it is the discovery of anti-cancer activity of curcumin that has, in fact, brought the 'herbal wonder drug' to limelight. The anticancer activity of curcumin is traced back to reports which indicate lower incidence of colon cancers in India, where turmeric consumption is more prominent, compared to the West (Sinha et al., 2003).

2.1.2.1 Molecular targets of curcumin in cancer

Curcumin has the potential to interact with numerous molecular targets involved in inflammation. Inflammation has been linked to cancer and the functional relationship was established by Virchow as early as 1863 (Balkwill and Mantovani, 2001). Neoplastic risk gets potentiated by sustained cell proliferation in an environment rich in inflammatory cells, growth factors and DNA-damage-promoting agents (Coussens and Werb, 2002). Curcumin is known to interfere with several biochemical pathways involved in the proliferation and survival of cancer cells by binding to various molecular targets like , growth factors, transcription factors and several proteins,

which play crucial roles in the onset and progression of cancer (Gupta et al., 2013; Shehzad et al., 2013).

The chemical structure of curcumin offers it versatility and favourability in binding to a variety of molecular markers (Figure 5). The two hydrophobic phenyl groups connected by a flexible linker allows the molecule to attain different conformations that can maximize Van der Waals and π–π interactions with aromatic and other hydrophobic amino acid residues. The phenolic hydroxyl, methoxy groups, as well as the ketone and enol groups are loci for hydrogen bonding interactions. Keto-enol tautomerism allows curcumin to arrange acceptor and donor groups to faciliatate hydrogen bonding in multiple ways. In addition, α,β- unsaturated ketone moiety serves as a Michael acceptor which enables nucleophilic attack by functional groups of amino acids.

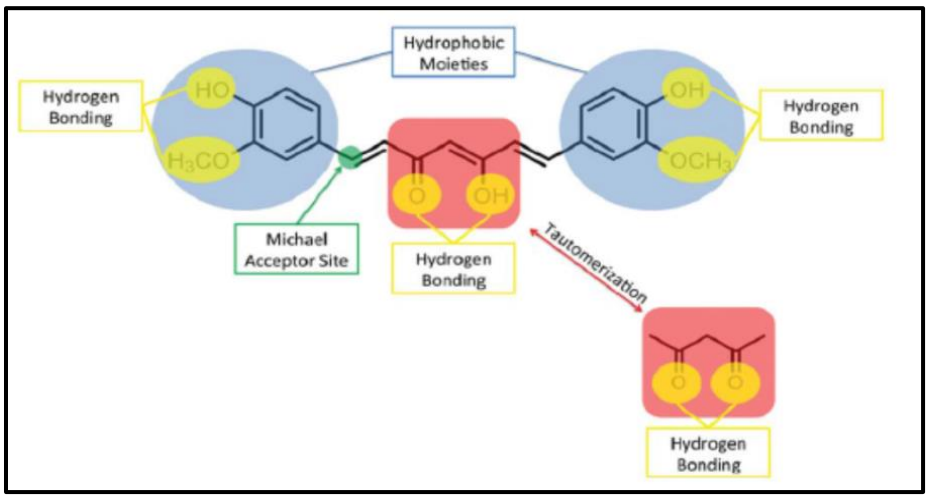

Figure 5. Structural features of curcumin involved in binding to molecular targets (Salem et al., 2014)

Several pathways have been proposed for curcumin to exhibit anti-cancer effect and presence of multiple mechanisms puts curcumin at an advantage while dealing with multi-drug resistant cancers (Salem et al., 2014). The mode of action can occur both via intrinsic (mitochondrial) and extrinsic (mediated by cell surface trans-membrane death receptors) mechanisms (Shehzad et al., 2013). Activation of tumour suppressor p53 and pro-apoptotic members of the B-cell lymphoma 2 (Bcl-2) family initiates the intrinsic pathway. Curcumin up-regulates p53 activity which in turn activates the Bcl-2 homologous antagonist killer (Bak) and Bcl-2 associated x protein (Bax). Apoptosis is promoted by pore formation in the mitochondrial membrane releases cytochrome c into the cytoplasm, thereby triggering the caspase cascade (Shehzad et al., 2013). Molecular docking studies by Luthra et al confirmed the binding of curcumin to the cavity 2 of the protein Bcl-2 through multiple amino acid interactions (Luthra et al., 2009). Curcumin at concentrations less than 30 μM were noticed to cause reduction in the mitochondrial membrane potential to activate caspase cascade in human colorectal cancer cells (Guo et al., 2013). Curcumin is known to suppress nuclear factor kappa-light-chain enhancer of activated B cells (NF-κB), a transcription factor which is extensively studied as a target for treatment of cancer. Under normal circumstances, NF-κB exists in an inactive form in the cytoplasm. Upon stimulation by free radicals, radiations, viral or bacterial antigens, NF-κB gets trans-located to the nucleus activates the expression of genes that are involved in the suppression of apoptosis and promote proliferation (Salem et al., 2014). Induction of apoptosis and inhibition of proliferation are also achieved through tumour necrosis factor (TNF) receptor activation which defines the extrinsic

pathway of curcumin. The TNF pathway leads to pro-apoptotic caspase-8 and caspase-3 activation, resulting in NF-κB activation which regulates the expression of cyclooxygenase-2 (COX-2) enzyme. COX-2 enzyme play critical role in response to inflammation. Van der Waals and hydrogen bonding interactions which arise from the structural features of curcumin enable curcumin to bind to TNF-α. This further inhibits TNF-α to bind to its receptor thereby preventing the activation of NF-κB (Salem et al., 2014). Another transcription factor commonly investigated as a target for cancer therapy is activated protein-1 (AP-1) which accounts for proliferation and oncogenic transformations (Eferl and Wagner, 2003). Curcumin is reported to inhibit the activation pathway of AP-1 by directly interacting with the AP-1 DNA-binding site (Dorai and Aggarwal, 2004). The ability of single molecule like curcumin to exhibit all these effects is still an enigma under scrutiny. However, there is no denying the fact that curcumin is the age old solution for an age old disease like cancer (Anand et al., 2008).

2.2 Polymer micelles

Despite multifarious therapeutic properties, curcumin is not heralded in clinical use and the reticence is attributed to its low aqueous solubility and instability at physiological pH. The low aqueous solubility of curcumin results in suboptimal blood concentrations affecting the bioavailability which makes it difficult to derive the therapeutic efficacy. The challenges faced by curcumin in translating its therapeutic efficacy to clinical forefront can be circumvented by employing delivery systems which can solubilize curcumin, prevent degradation and release it at desired

physiological destinations. Nanoparticle-based drug delivery systems have offered considerable hope in this regard. Enhancement of aqueous solubility of curcumin has been demonstrated in a variety of nano-carriers based on liposomes, polymer nanoparticles, micelles, conjugates, dendrimers, etc (Naksuriya et al., 2014; Salem et al., 2014). However, liposomes are associated with membrane de-stabilization effects which limit their drug loading capacity (Liu et al., 2006). The generality of the approaches to employ dendrimers and conjugates for drug delivery is highly restrained as it is dictated by the covalent conjugation of drug molecules to the carrier which require the availability of functionalizable chemical groups (Blanco et al., 2009). Polymeric micelles confer unique nano platform to the above nano systems for drug delivery applications by permitting facile encapsulation of poorly soluble drugs in the hydrophobic cores of micelles. Smaller size, higher drug loading and timely release of the drugs from micelles can be fine-tuned by varying the hydrophobic blocks. They are efficient in avoiding renal filtration and uptake by reticulo-endothelia system and can circulate in the blood for extended period of time, eventually passing through disrupted capillaries in the tumour micro-environment.

2.2.1 Micelle structure

The common amphiphilic architectures used to build polymeric micelles are di-block (hydrophilic-hydrophobic) or tri-block (hydrophilic-hydrophobic-hydrophilic) polymers. Graft (hydrophilic-g-hydrophobic) or ionic (hydrophilic-ionic) copolymers are also used to form micelles for drug delivery applications (Owen et al., 2012). The hydrophobic part of the block copolymer self-associates into a semi-solid core surrounded by the coronal layer formed from the hydrophilic segment of the

copolymer. The ability of polymer units to self-assemble into nano-scale aggregates defines the characteristic of micelle systems which depends on factors like composition and mass of polymer backbone, concentration of polymer chains and properties of encapsulated drugs (Blanco et al., 2009).

2.2.2 Micellization - thermodynamic and kinetic stability

The impetus for micellization is given by the minimization of the free energy of an amphiphilic polymer by forming selectively ordered structures. The hydrophobic core is shielded by the hydrophilic chains from interaction with the aqueous environment, thus reducing the interfacial free energy of the polymer-solvent system (Owen et al., 2012). Micelles are subjected to lot of environmental changes which include significant dilution in blood, changes in pH and proximity with numerous cells and proteins, upon intravenous administration. In these circumstances, drug loaded micelles must remain intact to retain their drug cargo from untimely release. The tendency of micelles to dissociate is depended on the cohesion and composition of the hydrophobic core (Gaucher et al., 2005). Micelle stability is a function of both thermodynamic and kinetic parameters. Thermodynamic stability defines the state of a system during micelle formation and its way to equilibrium whereas kinetic stability focuses on the behavior of the system over time and describes the rate of polymer exchange and micelle disassembly. The critical micelle concentration (CMC), which is the minimum concentration of polymer required for micelle formation, is the prime factor which characterizes the thermodynamic stability of the micelles. Below the CMC, there exists insufficient number of polymer chains that adsorb at the air-water or aqueous-organic solvent interface. More number of chains

are adsorbed as the concentration of the polymer is increased and eventually at a particular concentration termed as CMC, saturation of polymer chains are attained both at the interface and in the bulk solution. Addition of more polymer chains beyond this point will lead to micelle formation in the bulk solution so as to reduce the free energy of the system (Owen et al., 2012).

2.2.3 Preparation techniques of drug loaded polymeric micelles

Physical encapsulation of drugs in the polymeric micelles is performed by various procedures. Dialysis and oil/ water (o/w) emulsion methods are the common techniques for preparation of polymeric micelles. In the dialysis method, organic solvent containing the polymer and the drug are dialyzed against distilled water to afford the drug loaded polymer micelles. Free drug and the organic solvent are also eliminated via this process (Gaucher et al., 2005). (O/W) emulsion technique induces the formation of an emulsion of small organic solvent droplets by mixing of water-immiscible organic solvent and water that serves as a template for micelle self-assembly. Here, water is added quickly into the water-immiscible organic solvent which contains the polymer and the drug. The mixture upon sonication or stirring triggers emulsification which produces nano-sized droplets dispersed throughout the aqueous phase. The polymer assembles at the organic-water interface with hydrophilic blocks protruding into the aqueous phase which stabilizes the emulsion with the hydrophobic blocks while the hydrophobic blocks clusters along with the drug forming the micellar core. The organic solvent is further removed by evaporation, leaving behind the drug-loaded micelles (Tyrrell et al., 2010).

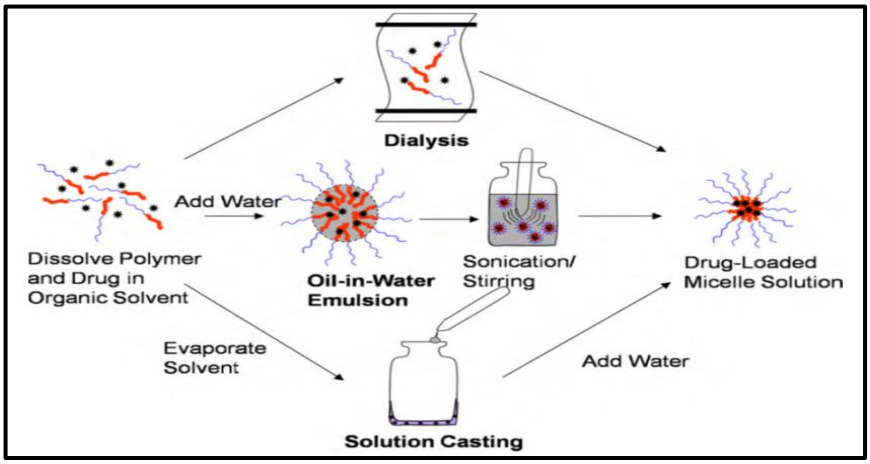

Figure 6. Illustration of different methods of preparation of drug loaded polymeric micelles. Adapted from (Tyrrell et al., 2010)

Moderately hydrophobic polymers can adopt direct dissolution method where the polymer and drug are dissolved in an aqueous solvent which leads to micellization. However, this method cannot be adopted for highly hydrophobic drugs as enough drug would not be available in solution to saturate the micelle core owing to the extremely low drug solubility (Tyrrell et al., 2010). Another method known as solution casting method is employed for micelle preparation. The polymer and drug are dissolved in an organic solvent and upon removal of the solvent, typically under nitrogen, a thin film is created which enhances the interaction of the drug with the hydrophobic polymer block. Subsequently, water is added which triggers micellization. Flash nano-precipitation is a micelle preparation technique based on the rapid mixing of organic and aqueous solvents. The polymer and drug, dissolved in an organic solvent, are pumped into a jet where simultaneously another stream of water is pumped in. Rapid mixing occurs as the fluid streams meet in the confined

space which induces precipitation of drug and polymer with the polymer assembling around the drug (Johnson and Prud'homme, 2003).

2.3 Curcumin loaded polymeric micelles - Rationale for the study

Among the existing strategies to obviate the drawbacks faced by curcumin, implementing polymeric micelles is one of the most attractive alternatives as they are endowed with many advantages like small size, provides enhanced stability and extended systemic circulation of the encapsulated drugs. Polymeric micelles are much sought after, given the fact that most of low water-soluble drugs are shelved away from the threshold of clinical entry despite their proven *in vitro* efficacy (Owen et al., 2012). Curcumin, being lipophilic, can be accommodated in the hydrophobic core of polymeric micelles. Molecular dynamics study of curcumin with Pluronic block copolymers have revealed that the micellar structure helped in the solvation of curcumin in water (Samanta and Roccatano, 2013). The efficacy of micelle encapsulated curcumin is notably enhanced compared to the free form. Bisht et al demonstrated the profound cytotoxicity of curcumin loaded micelles , based on cross-linked random copolymers of N-isopropylacrylamide with N-vinyl-2-pyrrolidone and poly(ethylene glycol) monoacrylate , against pancreatic XPA-1 cells compared to curcumin in its free form (Bisht et al., 2007). This is probably one of the initial investigations on “nano-curcumin” utilizing micellar aggregates. Recent studies have tested the co-delivery of curcumin with platinum drugs within one carrier system to produce enhanced synergistic effects on multi-drug resistant cancers (Scarano et al., 2015). Here, triblock copolymer constituting of PCL, a PEG

based shell and an amine bearing polymer self-assembled into onion-type micelles which could incorporate curcumin in the micellar core with an entrapment capacity of 6%. Polymeric micellar co-delivery of curcumin and resveratrol have been found to mitigate *in vitro* doxorubicin-induced cardio-toxicity (Carlson et al., 2014). However, most of the investigated polymeric micelles for curcumin delivery have low loading capacity accompanied by release of considerable amount of curcumin at physiological pH which exacerbate the overall *in vivo* therapeutic efficacy. A very low loading capacity of 1% w/w has been reported in curcumin loaded mPEG palmitate micelles with 80% release at pH 7.4 in 24 hours. (Sahu et al., 2008). Podaralla et al investigated curcumin loading in mPEG-zein micelles of size 124 nm which afforded a loading of 2 %. High release of about 80% was observed at the physiological pH in 24 hours from these micelles (Podaralla et al., 2012). Micelles based on PLGA (poly lactic glycolic acid) exhibited curcumin loading around 6%, however, release studies at pH 7.4 were not reported (Song et al., 2011). Although it is found that low concentration of curcumin is sufficient in inducing *in vitro* cytotoxicity on cancer cells, these results do not necessarily correlate to the concentrations achieved *in vivo* (Naksuriya et al., 2014). *In vitro* conditions involve prolonged exposure of cells to high static concentrations of curcumin which is responsible for the enhanced cell death. *In vivo* tumour reduction studies by Yallapu et al. investigated the effect of curcumin loaded PLGA nanoparticles in prostate tumour xenografts and demonstrated that 9% w/w curcumin loading led to only 50% tumour regression (Yallapu et al., 2014). Therefore, there is a need for matrices which can exhibit high loading capacity for curcumin so as to achieve better *in vivo*

therapeutic efficacy. Currently, there is a dearth of amphiphilic polymers that can exhibit better curcumin loading capacity for deriving favourable *in vivo* results. Furthermore, there is paucity of information on studying the compatibility factor of curcumin with the micellar core of polymeric micelles. The body of work showcased in this study attempts to focus on these lacunae.

2.4 Building blocks of amphiphilic matrices investigated in the study

To realize the potential of polymeric micelles we embarked on developing amphiphilic matrices to improve the outcomes of curcumin delivery. The following hydrophilic and hydrophobic components were incorporated in our study for designing the amphiphilic carrier.

2.4.1 Fatty acids

Fatty acid based drug delivery systems are frequently used to improve the solubility of sparingly water soluble drugs. The carboxylic acid group of a fatty acid molecule could conveniently be linked to an alcohol via an ester linkage and the resultant product has an inherent amphiphilicity to it.

2.4.1.1 Lauric acid

Lauric acid also known as dodecanoic acid is a saturated fatty acid with a 12-carbon atom chain. It comprises about half of the fatty acid content in coconut oil and palm kernel oil. Lauric acid is also known to exhibit bactericidal properties (Nakatsuji et al., 2009; Yang et al., 2009). Drug delivery systems incorporating lauric acid to solubilize hydrophobic drugs have been widely investigated (Desai et al., 2011; Nam

et al., 2013). Lauric acid is also noted for its penetration enhancing properties which aids in transdermal drug delivery (Pathan and Setty, 2009)

2.4.1.2 α-Linolenic acid

α-Linolenic acid (*all-cis*-9,12,15-octadecatrienoic acid is an essential omega-3 fatty acid with an 18-carbon chain and three *cis* double bonds. Alpha linolenic acid is abundant in flaxseed oil, fish oil, soy and walnut oil exhibits enhanced hydrophobicity and membrane penetrative property (Castelli et al., 2003). Linolenic acid also is known to attenuate activities of inflammatory cytokines including TNF thereby reducing chronic inflammation (Yano et al., 2000) .

2.4.2 Poly ethylene glycol (PEG)

PEG is a polyether compound with repeating units of ethylene oxide. It is also known as polyethylene oxide (PEO) or polyoxyethylene (POE). PEG is considered the gold standard for stealth polymers in the burgeoning field of polymer based drug delivery. PEG imparts hydrophilicity to the drug delivery vehicles that allows both enhancement of aqueous solubility and prevention of opsonization (Knop et al., 2010). Furthermore, it reduces the propensity of particles to aggregate by offering steric stabilization. Shielding or bounding by PEG brings about a change in the pharmacokinetics of administered drugs by resulting in prolonged blood circulation time (Owens III and Peppas, 2006). The concept of PEGylation was introduced in the late 1970s; however, PEG was embraced for widespread applications in drug delivery only in the 1990s (Knop et al., 2010). Kabanov et al were the first to propose the advantage of PEG as a hydrophilic part of linear blockcopolymers for micellization (Kabanov et al., 1989). Later extensive investigations were performed

on the development of PEG-containing block copolymer micelles for designing drug-delivery carriers (Kwon and Kataoka, 1995).

2.4.3 Pluronic block copolymers

Pluronics (also known as Poloxamer) are nonionic triblock copolymers constituted by a central hydrophobic chain of poly propylene oxide (PPO) flanked by two hydrophilic chains of poly ethylene oxide (PEO). Among amphiphilic copolymers, Pluronics are widely investigated and FDA (Food and Drug Administration) approved materials for drug delivery (Tyrrell et al., 2010). Owing to their amphiphilic character, these copolymers are able display surfactant properties including ability to interact with biological membranes and hydrophobic surfaces (Batrakova and Kabanov, 2008). Drug pharmacokinetics and bio-distribution can be improved by incorporating drugs into Pluronic micelles which improves drug solubility and stability. Another appealing aspect includes the suppression of opsonization by the PEO units of Pluronic (Jackson et al., 2000). Pluronic block copolymers are also considered to be potent biological response modifiers efficient in sensitizing multi drug resistant (MDR) cancer cells and enhancing drug transport across cellular barriers (Kabanov et al., 2003). Although Pluronic block copolymers are non-biodegradable, individual free chains with a molecular weight in the 10–15 kDa range have been shown to be removed from the bloodstream through filtration by the kidneys (Batrakova et al., 2004).

2.4.4 Polycaprolactone (PCL)

PCL is a hydrophobic, semi-crystalline polymer that has found applications in fabrication of biomedical devices such as stents, implants, sutures and prosthetics, (Tyrrell et al., 2010). It is commonly synthesized by ring-opening polymerization of ε-caprolactone (Carothers, 1929). Its exceptional blend compatibility and low melting point (59–64 ^{o}C) are the factors that define its potential in biomedical applications like drug delivery and tissue engineering. Enhanced permeability to drugs , exceptional biocompatibility and ability to be completely excreted from the body post bioresorption enables PCL to be used for controlled drug delivery (Woodruff and Hutmacher, 2010). PCL can serve as a reservoir for poorly soluble drugs in micelles prepared from PCL co polymers (Letchford et al., 2008; Raveendran et al., 2013). PCL degradation occurs at a slow rate and hence it is beneficial for long term therapeutic agents. However, for many drug delivery applications, the slow degradation rate of PCL could affect the drug release. It has been demonstrated that co-polymerization of ε-caprolactone with hydrophilic polymers can enhance the rate of bio-degradation of PCL (Siepmann et al., 2012).

2.4.5 Calix[n]arenes

Calix arenes belong to a class of cyclo-oligomers produced by the base catalyzed reaction of formaldehyde and *p*-substituted phenol (Gutsche, 1998). Calixarenes are promising materials for nanomedicine applications such as drug and gene delivery systems, scaffolds and diagnostics. Calix arenes have hydrophobic cavities that can hold smaller molecules or ions and with their unique three-dimensional architecture, they can exhibit excellent host-guest chemistry like cyclodextrins, cryptands and

crown ethers (de Fátima et al., 2009). The classic supramolecular host-guest assembly system has been exploited widely for drug delivery (Tu et al., 2011).The ease of functionalization at either the upper and/or lower rim stimulated extensive research of calix arenes as supramolecular platforms for catalysis, sensing, molecular recognition, drug and gene delivery (Nimse and Kim, 2013).

2.4.6 Dextran

Dextran is a polysaccharide synthesized from sucrose by lactic-acid bacteria mainly *Leuconostoc mesenteroides* and *Streptococcus mutans*. The dextran chain consists of α-1,6 glycosidic linkages between glucose molecules and branches initiate from α-1,3 linkages. The lower molecular weights of dextran widely find use as plasma expander. Hydrophilicity, biocompatibility and biodegradability make dextran ideal for bio-medical applications (Won and Chu, 1998). The high density of hydroxyl groups enables dextran to be conjugated to drugs and proteins which improves the solubility, enhances the circulation time and stabilizes the therapeutic agents. Many studies have demonstrated dextran as the hydrophilic unit in the preparation of amphiphilic polymers (Varshosaz, 2012). Investigations prove that dextran is an alternative to PEG for low protein-binding, cell-resistant coatings on biomaterial surfaces (Massia et al., 2000). Though dextran shares similar anti-fouling properties as that of PEG, the multivalent properties of dextran pose as highly advantageous where high-density surface immobilization of biologically active molecules to is desired. Conjugation of hydrophobic drugs to dextran is known to increase their water solubility (Won and Chu, 1998). Dextran pro-drugs are efficient in achieving controlled drug release and drug targeting. Enhanced effectiveness and improvement

in the cytotoxic effects of chemotherapeutic agents have been reported by implementing various dextran-anti-tumour drug conjugates (Varshosaz, 2012).

2.4.7 Poly (2-oxazolines)

Poly (2-oxazoline)s [POxs] are a versatile class of polymers, which were discovered in the 1960s, prepared by cationic ring opening polymerization (CROP) of 2-oxazolines (Kagiya et al., 1966a). Despite their early discovery, their attributes were only identified until years later owing to the long reaction time required for their synthesis which often ranged from several hours to weeks for attaining complete conversion (Seeliger et al., 1966; Tomalia and Sheetz, 1966). The advent of microwave reactors was crucial in benefitting the POxs syntheses as microwave irradiation in closed reaction vials accelerated the polymerization of 2-oxazolines by a tremendous factor compared to the conventional reflux polymerizations. The end group functionality can be controlled during the initiation and termination stages and the side chain variation is possible by incorporating different 2-oxazoline monomers (Hoogenboom, 2009). Therefore, it is possible to achieve tailor made properties by manipulation of the functional groups of poly (2-oxazolines). This versatility has influenced POx to have an upper hand over PEG despite sharing similar stealth behaviour and biocompatibility as the latter (Barz et al., 2011). POx is now touted to be a promising alternative against the gold standard PEG in biomedical applications and has hence garnered significant attention. The recently rejuvenated interest in POx has validated the polymer as a potential candidate for biomedical applications due to the sharing of similar beneficial properties of PEO regarding the biocompatibility, biodistribution and the stealth behavior. Goddard et al

demonstrated the biocompatibility of poly (2-methyl-2-oxazoline) (PMeOx) through intravenous administration in mice in 1989 (Goddard et al., 1989). The first indication of stealth behaviour of POxs stemmed from the studies demonstrating suppressed platelet adhesion and fibrinogen attachment on silica adsorbed with (PMeOx-b-PeO-b-PMeOx) triblock copolymer (Maechling-Strasser et al., 1989). Later, Zalipsky and co-workers were successful in providing the proof of stealth behaviour of POxs decorated liposomes. Furthermore, the accumulation profile of these liposomes were similar to PEO liposomes (Zalipsky et al., 1996). Extraordinary drug loading capacity has been reported in formulations prepared from poly(2-oxazoline) block copolymers (Luxenhofer et al., 2010).

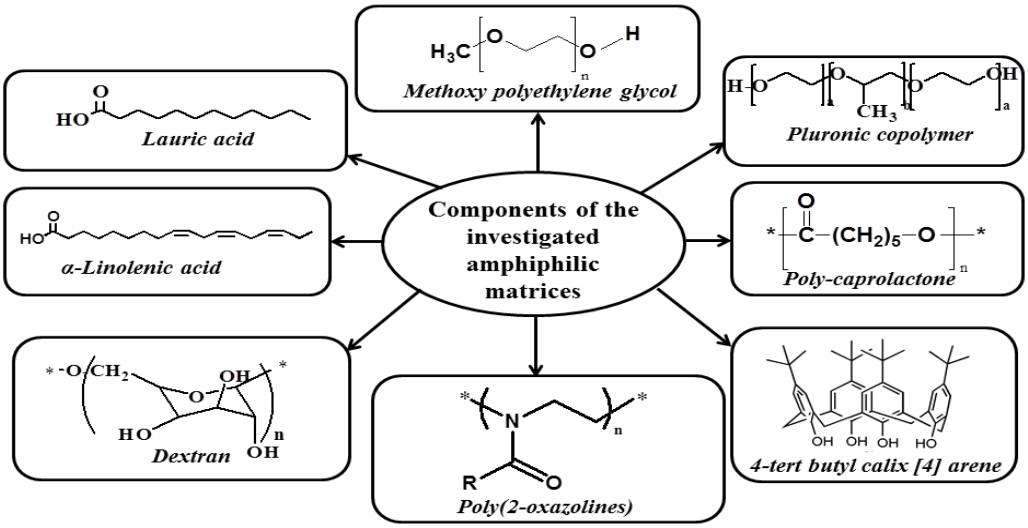

Figure 7. Hydrophilic and hydrophobic components incorporated in our study to prepare the amphiphilic matrices

The quantum of work presented in this thesis focuses on the investigation of amphiphilic matrices synthesized from the above mentioned components (Figure 7) to form polymeric micelles that serve as feasible curcumin carrier systems for anti-cancer applications.

CHAPTER 3 - MATERIALS AND METHODS

3.1 Curcumin loaded micelles based on PEGylated Fatty Esters

3.1.1 Materials

mPEG (M_n =5000 g/mol), Pluronic [PEO-PPO-PEO (polyethylene oxide-poly propylene oxide-polyethylene oxide) triblock copolymer] (M_n = 12,600g/mol) lauric acid, α-linolenic acid, curcumin, N,N'-dicyclohexylcarbodiimide (DCC), 4-dimethylaminopyridine (DMAP), pyrene and 3-(4,5-dimethylthiazol-2-yl)-2,5-diphenyl tetrazolium bromide (MTT), Modified Eagles Medium (DMEM) were purchased from Sigma (Bangalore, India). Fetal bovine serum (FBS) was from GIBCO (USA). HeLa cells, colorectal adenocarcinoma (Caco2) cells and mouse fibroblasts (L929) cells were obtained from National Centre for Cell Science (Pune, India). All the solvents used in the study were of analytical grade and obtained from Merck (India). The blood experiments which involved collection of blood from healthy volunteers were approved by the Institute Ethics Committee.

3.1.2 Synthesis of PEGylated fatty esters

3.1.3 Synthesis of mPEG laurate and linolenate

Steglich esterification was adopted for obtaining mPEG laurate and linolenate (Neises and Steglich, 1978). Lauric acid (0.2003 g, 1mmol) and DMAP (0.122 g, 1mmol) were added into a stirring solution of mPEG (5g, 1mmol) in 50mL of anhydrous dichloromethane. DCC (0.206 g, 1mmol) was added to the mixture at 0^oC

and later stirred at room temperature for 6 hours. Precipitated dicyclohexylurea was filtered off and the solvent of the resulting product was rapidly eliminated using rotary evaporator. The synthesized ester was then dissolved in dichloromethane and upon addition of cold diethyl ether, white precipitate was formed which was filtered and dried to obtain the product in pure form (Yield = 3.8 g, 76%). To obtain the desired linolenate ester, similar reaction methodology was devised where linolenic acid, DMAP and mPEG were added in the molar ratio 2:1:1. Similar work up procedure for the laurate ester was followed (Yield = 3.2 g, 64%).

3.1.4 Synthesis of Pluronic linolenate

Linolenic acid (0.2 g, 0.72 mmol) and DMAP (0.04g, 0.36 mmol) were added into a stirring solution of Pluronic (5 g, 0.36 mmol) in 50 mL of anhydrous methylene chloride. DCC (0.07 g, 0.36 mmol) was added to the mixture at 0^{o}C and later stirred at room temperature for 6 hours. Precipitated dicyclohexylurea was filtered off and the synthesized Pluronic linolenate was precipitated by adding the filtrate to excess cold diethyl ether. The final product was filtered and dried (Yield = 4.1 g, 82%).

3.1.5 Characterization

3.1.5.1 Fourier transform infrared spectroscopy (FTIR)

IR spectra of the synthesized esters were recorded in the range of 4000-400 cm^{-1} on a Fourier transform infrared spectrophotometer (Nicolet 5700) using potassium bromide (KBr) pellet technique.

3.1.5.2 ^{1}H Nuclear magnetic spectroscopy (^{1}H NMR)

The ^{1}H NMR spectrum of the synthesized esters were measured in deuterated chloroform ($CDCl_3$) using a 400 MHz spectrophotometer (Bruker DRX 400) at 25^{o}C.

3.1.5.3 Preparation of curcumin loaded micelles by solvent dialysis method

Loading of curcumin at 3.25, 4.76 and 7.69 and 9.09 % w/w were carried out in 30 mg of synthesized ester. Curcumin and the synthesized ester were dissolved in 10 ml of dimethyl formamide (DMF) solution and were directly dialyzed for 24 hours against 2 litres of ultrapure water (resistivity 18.2 Ωm) using cellulose dialysis membranes (molecular weight cutoff: 3500 Da and 12 kDa, manufacturer, Sigma). The water was changed thrice during the dialysis process. The micellar solution from dialysis bag was collected and centrifuged at 5000 rpm for 15 minutes to settle the unloaded curcumin. The micellar solution obtained, free from the pelleted curcumin, was frozen at -80 °C and then lyophilized using a lyophilizer (Labconco, USA) to obtain a dry powder of curcumin loaded micellar products for further use. To prepare the empty micelles, the above procedure was followed without the presence of curcumin.

3.1.6 Curcumin encapsulation

The percentage of encapsulated curcumin was determined by centrifuging the micellar solution, obtained after dialysis, at 5000 rpm for 15 minutes. The pelleted (un-encapsulated) curcumin was dissolved in methanol and was spectrophotometrically quantified using UV spectrometer (Cary model 100 BioUV-Vis spectrophotometer, Varian Australia) at a wavelength of 430 nm. Standard curcumin solutions in methanol were prepared. Absorbances were recorded and a linear plot for the standards was obtained. The curcumin concentration in the micelles was determined from the standard curve. The encapsulation efficiency and

the drug loading capacity were calculated by the following equation (Sahu et al., 2008):

$$\text{Encapsulation efficiency (\%)} = \frac{(\text{Total amount of curcumin} - \text{Free curcumin})}{\text{Free curcumin}} \times 100$$

$$\text{Drug loading capacity (w/w\%)} = \frac{(\text{Amount of curcumin in micelles})}{\text{Amount of curcumin loaded micelles}} \times 100$$

3.1.7 Curcumin-polymer core compatibility calculations

The compatibility between curcumin and the micelle core forming block was calculated by employing the Hildebrand-Scatchard equation.

$$\chi_{sp} = (\delta_{drug} - \delta_{polymer})\frac{V}{RT} \qquad [1]$$

where χ_{sp} is known as the Flory-Huggins interaction parameter, δ_{drug} is the solubility parameter for the drug (curcumin), $\delta_{polymer}$ is the solubility parameter for the core forming block , R is the gas constant , T is the temperature and V is the molar volume of the drug which is calculated from the group contributions method derived by Fedors (Fedors, 1974). Calculations of δ_{drug} and $\delta_{polymer}$ are obtained by from Van Krevelen's additive group contribution method according to which the solubility parameter is the sum of dispersion(δ_d) , polar (δ_p) and hydrogen bonding components (δ_h) (Van Krevelen, 1997).

$$\delta^2_{drug} = \delta_d^{\,2} + \delta_p^{\,2} + \delta_h^{\,2} \qquad [2]$$

$$\delta^2{}_{polymer} = \delta_d{}^2 + \delta_p{}^2 + \delta_h{}^2 \quad [3]$$

The individual components were calculated by the following equations

$$\delta_{\mathrm{d}} = \frac{\sum F_{di}}{V} \quad [4]$$

$$\delta_{\mathrm{p}} = \frac{\left(\sum F_{pi}^2\right)^{1/2}}{V} \quad [5]$$

$$\delta_h = \left(\sum \frac{E_{hi}}{V}\right)^{1/2} \quad [6]$$

F_{di} , F_{pi} and E_{hi} are the molar dispersion, polar attraction constants and hydrogen bonding energy , respectively for each structural group in the molecules. These values are tabulated by Van Krevelen (Van Krevelen, 1997). The above equations were employed to determine the interaction parameter of curcumin with laurate, linolenate and PPO/linolenate core of mPEG laurate, mPEG linolenate and Pluronic linolenate core, respectively.

3.1.8 Characterization of the micelles

3.1.8.1 Determination of Particle Size and Zeta Potential

The size of the curcumin loaded micelles was assessed by dynamic light scattering (Nano-ZS 90, Malvern Instrument, UK). The temperature was kept at 25 ^{o}C during the measuring process and measurements were recorded as the average of three test runs. For zeta potential determination, the measurement was performed in folded capillary cells using Nanosizer (Malvern Instrument UK). TEM experiments were performed on a Hitachi H-7650 (Tokyo, Japan) at an acceleration voltage of 80 kV. Curcumin loaded micellar suspensions were administered onto a 200 mesh copper grids and air dried prior to imaging.

3.1.8.2 Critical micelle concentration (CMC) study

Critical micelle concentration (CMC) of synthesized esters was determined by fluorescence spectroscopy using pyrene as fluorescence probe. Pyrene stock solution was prepared by dissolving 2.5 mg of pyrene in 5 ml methanol which was further diluted 20 times. 50 µl of diluted pyrene solution was vortexed well with different concentrations of micellar solutions ranging from 3 mg to 0.001 mg. The solutions were vortexed and kept overnight to equilibrate pyrene with the micelles. The fluorescence spectrum was recorded on a fluorescence spectrophotometer (Infinite M200, TECAN) at an emission wavelength of 390 nm (Sahu et al., 2008).

3.1.8.3 Spectral characterization

The spectral properties of the curcumin loaded micelles were analyzed by UV spectrometer (Cary model 100 BioUV-Vis spectrophotometer, Varian Australia Pty Ltd, Victoria, Australia). The absorption intensity of curcumin loaded micelle and free curcumin were studied at 425 nm. The fluorescence emission spectra of free curcumin and curcumin loaded micelle were recorded from 450-700 nm with an excitation wavelength of 425 nm on a fluorescence spectrophotometer (Infinite M200, TECAN).

3.1.8.4 Differential scanning calorimetry (DSC)

DSC was performed on a scanning calorimeter with a thermal analysis data system (DSC Q20). Small amounts of the samples were placed in aluminum pans and heated from 25 ^{o}C to 300 ^{o}C at a heat flow rate of 10 ^{o} C/min under nitrogen flow.

3.1.9 In vitro–release studies

Release studies were performed at physiological (pH 7.4) and acidic (pH 4.5) conditions. Lyophilized curcumin loaded esters were re-dispersed in 33 mL of 0.01 M phosphate-buffered saline solution (pH 7.4) at a formulation concentration of 300 μg/mL. Total volume was divided into 33 Eppendorf tubes giving 11 different sets (each set with 3 Eppendorf tubes for the triplicates) for time-dependent release study at time intervals of 2, 4, 6, 12, 24, 36, 48, 60, 72, 96 and 108 hours. Free curcumin is completely insoluble in PBS; therefore, at predetermined intervals of time, the solution was centrifuged at 1000 rpm for 5 minutes to separate the released (pelleted) curcumin from the micelles. At definite time intervals, released amounts of curcumin loaded in the micelles were first extracted in methanol and quantified at 425 nm using UV visible spectrophotometer. The release was calculated as follows:

$$\text{Release (\%)} = \frac{\text{Released amount of curcumin}}{\text{Total amount of curcumin}} \times 100$$

3.1.10 Stability study

The stability of micellar curcumin and native curcumin in physiological pH were studied using UV-Visible spectrophotometer. Curcumin and micellar curcumin in PBS were incubated in a shaker with 150 rpm rotation for 8 hours. Methanol (1% v/v) was used to dissolve native curcumin. At pre-determined time intervals, the absorbances of the samples were recorded.

3.1.11 Blood compatibility study

For performing the hemolysis and aggregation studies, the human blood sample was collected in a tube containing 3.8 % sodium citrate at ratio 9:1 (blood: anticoagulant). 200 µl of blood was mixed with 800 µl of saline and was centrifuged at 750 rpm for 10 minutes. The erythrocytes obtained after repeated washings (plasma- free) were re-suspended in fresh saline and vortexed. 100 µl of the pellet was added to 5 mg/ml concentration of the empty and curcumin loaded micellar solutions which were kept for incubation at 37^{o}C for 2 hours. The absorbances were measured at 541 nm. Normal saline was used as negative control (0 % lysis) and distilled water as positive control (100 % lysis). Percentage of hemolysis was calculated using the following equation:

$$\text{Percentage of hemolysis} = \frac{\text{OD of test solution} - \text{OD of negative control}}{\text{OD of positive control} - \text{OD of negative control}} \times 100$$

where OD refers to optical density

Red blood cell (RBC) aggregation studies were performed by centrifuging the blood at 700 rpm for 10 minutes to separate the RBC layer. The separated layer was washed twice with saline and diluted with saline in the ratio 1:4 ratio. 2 ml of diluted RBC was incubated for 20 minutes at 37^{o}C with 1 ml each of curcumin loaded micelles (5mg/ml concentration). The diluted RBC was also incubated along with negative and positive control. Normal saline and PEI were used as the negative and positive controls, respectively. The compatibility of white blood cells (WBC) and platelets was demonstrated with anti-coagulated blood (1 ml) overlaid with

histopaque (1 ml) in order to make separated layers and was centrifuged for 15 minutes at 800 rpm at room temperature. The collected WBC and platelets were incubated with the loaded and empty micelles (concentration of 5 mg/ml) for 30 min at 37^{o}C. Similar procedure was carried out for the incubation with the controls. After incubation, the cells were isolated by centrifugation, examined on mounted slides and the images were captured on a phase contrast microscope (Leica DMIRB).

3.1.12 Gel Electrophoresis

Native polyacrylamide gel electrophoresis (PAGE) analysis was performed to detect the interaction of micelles with plasma proteins. The micelles were incubated with human plasma (diluted with saline) for 1 h at 37^{o}C. 20 µL of the supernatant after centrifugation at 10,000 rpm for 10 min was loaded on 7% resolving and 4% stacking gel at 100V for 90 min using Mini-PROTEAN II electrophoresis system (Bio-Rad, CA, United States). The gel after coomassie blue staining was documented using an image analyzer (LAS 4000, Fuji). Plasma incubated with normal saline (0.09% sodium chloride) was used as the control.

3.1.13 *In vitro* Cytotoxicity studies

3.1.13.1 MTT assay

The cytotoxicity of various concentrations of free curcumin and curcumin loaded mPEG-laurate and linolenate micelles were assessed on HeLa cell lines by MTT assay. DMEM medium along with 10% FBS were utilized for seeding the cells prior to their incubation for 24 hours at 37 °C in 5% CO_2 and 95% humidity. The cells were trypsinized and transferred to a 24-well cell culture plate at a density of 1x10^{5}cells/well and were exposed to a series of different concentrations of free and

micellar curcumin in the range of 2.5–20 µM for 24 hours. The cytotoxicity exerted by the empty micelles of mPEG laurate and linolenate ester in the concentration range of 0.5 mg/ml to 6mg/ml was also assessed. MTT assay was performed on curcumin loaded Pluronic linolenate micelles to evaluate their cytotoxicity on Caco2 and L929 cells. The percentage cell viability (CV) was calculated as:

$$CV\ (\%)=\frac{N_t}{N_C}\times 100$$

where N_t is the absorbance of the cells treated with free curcumin or curcumin loaded micelles and N_c was the absorbance of the untreated cells.

3.1.13.2 Live dead assay

The cytotoxicity was further qualitatively assessed using the live/dead viability assay (Molecular Probes, Invitrogen Corp.) as described elsewhere (Takada et al., 2004). Caco2 cells were seeded into 24 well plates at a seeding density of 5×10^4 cells/well and allowed to adhere overnight with 5% CO_2 at 37°C. The cells were then incubated with 100 µl of the samples for 24 hours. An equivalent concentration of 20 µM of curcumin was used in the free and the loaded status. Empty micelles were assessed at a concentration of 5mg/ml. Prior to the assay, cells were washed thrice with phosphate buffered saline, stained with assay reagents containing 2 μM calcein AM (acetomethoxy derivate of calcein) and 4 μM EthD-1 (ethidium homodimer) and incubated for 30 min at 37°C. The cells were then visualized and imaged using fluorescence microscope (Leica DM IRB, Germany).

3.1.14 *In vitro* cellular uptake studies by fluorescene microscopy

To visualize the cellular uptake of curcumin loaded micelles of mPEG laurate and linolenate, HeLa cells were cultured with a seeding density of $2x10^5$cells/well. An equivalent concentration of 10 μM of curcumin as a free and loaded form was used for the uptake study. The samples were dissolved in PBS (0.01 M, pH 7.4) and as free curcumin was insoluble in aqueous solution, it was dissolved with dimethylsulfoxide (DMSO). Cells were treated with free curcumin and curcumin loaded micelles and were incubated at 37^oC for 4 hours. Nucleus staining was done with Hoechst 33342. After 4 h incubation, cells were subjected to PBS wash twice and the cells were fixed using 3.7% paraformaldehyde solution prior to viewing under a fluorescence microscope (Leica DMI3000) for intracellular curcumin fluorescence. Similar procedure was adopted for monitoring the cellular internalization of Pluronic linolenate micelles in Caco2 cells which were grown in 35 mm culture plate up to 80% confluency with a seeding density of $4x10^5$cells/well. Cells were incubated with free curcumin and curcumin loaded micelles at 37^oC for 4 hours. The cells were later washed twice with PBS and the fixed using 3.7% paraformaldehyde solution before viewing under the fluorescence microscope (Leica DMI3000).

3.1.15 Statistical data analysis

Data are represented as mean ± SD (standard deviation) of three independent experiments. Statistical analysis of the MTT assay data was performed by one-way analysis of variance (ANOVA) using SPSS software (SPSS-16, IBM, USA); a value of $p<0.05$ and $p<0.01$was considered significant (n=3).

3.2 Curcumin loaded Pluronic/PCL micelles

3.2.1 Curcumin loaded PCL/Pluronic micelles

3.2.1.1 Materials

ε-caprolactone, Pluronic (molecular weight = 12600 g/mol), stannous octoate, curcumin from *Curcuma longa* (Turmeric) , pyrene, 3-(4, 5-dimethylthiazol-2-yl)-2,5-diphenyl tetrazolium bromide (MTT) and Modified Eagles Medium (DMEM) were purchased from Sigma (Bangalore, India). Fetal bovine serum (FBS) was from GIBCO (USA). Caco2 (colorectal adenocarcinoma) cells were obtained from National Centre for Cell Science (Pune, India).

3.2.1.2 Synthesis of Pluronic/PCL

Pluronic/PCL amphiphilic block copolymers were synthesized by the ring opening polymerization of ε- caprolactone in the presence of Pluronic using stannous octoate as the catalyst (Ha et al., 1999). Calculated amounts of PEO–PPO–PEO triblock copolymer and ε-caprolactone monomer (weight ratio=1:2) were reacted under nitrogen atmosphere. Stannous octoate (0.5% w/w of total feed stock) was added to catalyze the polymerization reaction. The reaction was heated at 140^{o}C for 12 hours. The reaction product was then cooled to room temperature. The obtained viscous material was dissolved in dichloromethane and further precipitated in diethyl ether. The resulting product was filtered and vaccum dried (Yield= 4.7 g, 78%).

3.2.1.3 Polymer characterization

3.2.1.3.1 Fourier transform infrared spectroscopy (FTIR)

The structure of the synthesized block polymer was characterized by Fourier transform infrared spectra and was recorded using a Thermo Nicolet, 5700 (Germany) spectrometer. The FT-IR spectra were obtained in the region 400-4000cm^{-1}.

3.2.1.3.2 ^{1}H nuclear magnetic resonance spectroscopy (^{1}H NMR)

^{1}H NMR spectra of Pluronic/PCL was measured in deuterated chloroform ($CDCl_3$) using a 500MHz spectrometer (Bruker Avance DPX 300). Tetramethylsilane (TMS) was used as the internal standard. The relaxation time of the instrument during measurements was 3.17 s. All other parameters were in the default settings of the instrument as per the specifications of Bruker Avance DPX 300.

3.2.1.3.3 Gel permeation chromatography (GPC)

The molecular weight distribution of the block polymer and weight average molecular weight (Mw) was determined by gel permeation chromatography (GPC, Waters HPLC system 600 Series Pump, Milford, USA). Styragel columns- HR-5E/4E/2/0.5 were used in series. 2414 refractive index detector and Waters 717 plus autosampler were used. Polystyrene standards used for relative calibration was of Mp-100000, 34300, 1470. The mobile phase was THF with a flow-rate of 1 ml /min. The injection volume was usually 100 ml of stock solutions (0.1–0.5 w/v %).

3.2.1.4 Determination of block length of Pluronic/PCL

The block length of the PCL (L_{PCL}) was determined from the NMR spectral analysis according to a previously reported calculation (Ha et al., 1999). The following equation was used for the calculation:

$$L_{PCL} = L_{Pluronic} \times \frac{3\ (\text{Peak intensity of } CH_2 \text{ group of PCL})}{2\ (\text{Peak intensity of } CH_3 \text{ group in PPO of Pluronic})} /2$$

where, $L_{Pluronic}$ is the block length of PPO in Pluronic [7]

A triblock structure was assumed for the Pluronic/PCL copolymer and the number–average molecular weight (M_n) was computed using the equation below

M_n of copolymer = M_n of Pluronic + 2 L_{PCL} x 114 [8]

where 114 is the molecular weight of CL monomer.

3.2.1.5 Preparation of curcumin loaded polymeric micelles by solvent dialysis method

30 mg Pluronic/PCL was dissolved in 10 ml of dimethylformamide (DMF) solution. To this solution varying amounts of 3 mg (9.09% w/w), 4 mg (11.76% w/w), 5 mg (14.28% w/w) and 6 mg (16.66% w/w) of curcumin were added and stirred at room temperature. This DMF solution was directly dialyzed for 24 hours against 3 litres of ultrapure water (resistivity 18.2 Ωm) using cellulose dialysis membranes (molecular weight cutoff: 12 kDa, manufacturer, Sigma). The water was changed three times during the dialysis process. The micellar solution from dialysis bag was collected and centrifuged at 5000 rpm for 15 minutes to settle the unloaded curcumin. The micellar solution obtained, free from the pelleted curcumin, was

frozen at -80 °C and then lyophilized using a lyophilizer (Labconco, USA). The lyophilized product was employed for further experiments.

3.2.1.6 Physico-chemical characterization

3.2.1.6.1 Particle size and zeta potential

The size of the curcumin loaded micelles was assessed by dynamic light scattering (Nano-ZS 90, Malvern Instrument, UK). Lyophilized curcumin loaded Pluronic/PCL was re-dispersed in de-ionized water for DLS measurements. The temperature was kept at 25^{o}C during the measuring process and measurements were recorded as the average of three test runs. The zeta potential of the micellar solutions were measured in folded capillary cells using Nanosizer (Malvern Instrument UK). TEM experiments were performed on a Hitachi H-7650 (Tokyo, Japan) at an acceleration voltage of 80 kV. Curcumin loaded micellar suspensions were administered onto a 200 mesh Formvar-coated copper grids and air dried prior to imaging.

3.2.1.6.2 Differential Scanning Calorimetry (DSC)

DSC curves were recorded on a scanning calorimeter equipped with a thermal analysis data system (DSC Q20). Small amounts of the samples were placed in hermetically sealed aluminum pans and heated from 25˚C to 300˚C at a heat flow rate of 10˚C/min under nitrogen spurge.

3.2.1.7 Spectral characterization

3.2.1.7.1 UV-Visible and fluorescence spectroscopy

The spectral properties of the curcumin loaded polymeric micelles were analyzed by UV spectrometer (Cary model 100 BioUV-Vis spectrophotometer, Varian Australia Pty Ltd, Victoria, Australia). The fluorescence emission spectra of free curcumin and curcumin loaded polymeric micelles were recorded from 450-700 nm with an excitation wavelength of 420 nm on a fluorescence spectrophotometer (Infinite M200, TECAN). The slit widths were set at 5 and 3.5 nm for excitation and emission wavelength, respectively

3.2.1.7.2 Critical micelle concentration (CMC)

Critical micelle concentration (CMC) of the synthesized block polymer was determined by fluorescence spectroscopy using pyrene as fluorescence probe. The fluorescence spectrum was recorded on a fluorescence spectrophotometer (Infinite M200, TECAN). Stock solution of pyrene was prepared by dissolving 2.5 mg of pyrene in 5 ml methanol which was further diluted 20 times. Different concentrations of micellar solutions ranging from 3 mg to 0.001 mg was vortexed with 50 µl of diluted pyrene solution. The solutions were vortexed and kept overnight to equilibrate pyrene with the micelles. The fluorescence spectrum was recorded on a fluorescence spectrophotometer (Infinite M200, TECAN) at an emission wavelength of 390 nm.

3.2.1.8 Curcumin encapsulation

The percentage of encapsulated curcumin was determined by centrifuging the micellar solution, obtained after dialysis, at 5000 rpm for 15 minutes. The pelleted (un-encapsulated) curcumin was dissolved in methanol and was spectrophotometrically quantified using UV spectrometer (Cary model 100 BioUV-Vis spectrophotometer, Varian Australia) at a wavelength of 420 nm. The encapsulation efficiency and loading capacity were calculated by the following equation:

$$\text{Encapsulation efficiency } (\%) = \frac{(\text{Total amount of curcumin} - \text{Free curcumin})}{\text{Free curcumin}} \times 100$$

$$\text{Drug loading capacity } (\text{w/w}\%) = \frac{(\text{Amount of curcumin in micelles})}{\text{Amount of curcumin loaded micelles}} \times 100$$

3.2.1.9 Curcumin- Pluronic/ PCL core compatibility calculations

The compatibility between curcumin and the micelle core forming block was calculated by employing the Hildebrand-Scatchard equation [Equation 1].The group contributions of functional moieties of curcumin and the hydrophobic core of PCL and PPO of Pluronic were calculated by Equations [2]-[6].

3.2.1.10 In vitro release

The release study was performed at acidic as well as physiological pH. Curcumin loaded Pluronic/PCL after lyophilization was re-dispersed in 33 mL of PBS solution (pH 7.4)/acetate buffer solution (pH 4.5) at a formulation concentration of 300μg/mL. Total volume was divided into 33 Eppendorf tubes giving 11 different sets (each set with 3 Eppendorf tubes for the triplicates) for time-dependent release

study at time intervals of 2, 4, 6, 12, 24, 36, 48, 60, 72, 96 and 108 hours. At predetermined intervals of time, the solution was centrifuged at 1000 rpm for 5 minutes to separate the released (pelleted) curcumin from the micelles. At definite time intervals, released amounts of curcumin in loaded micelles were extracted in methanol and quantified at 430 nm using UV visible spectrophotometer. The release was quantified as follows:

$$\text{Release (\%)} = \frac{\text{Released amount of curcumin}}{\text{Total amount of curcumin}} \times 100$$

3.2.1.11 Stability study of curcumin loaded micelles

Free curcumin and curcumin loaded Pluronic/PCL particles were dissolved in PBS to observe the aqueous solubility. To study the stability of curcumin in the micelles, free curcumin and the loaded micelles in PBS (0.01 M, pH 7.4) at a concentration of 40 µg/ml (total of 10ml solution) were incubated in a shaker for 8 hours at 37^{o}C with a rotation speed of 150 rpm. 100 µl of sample solutions were taken and added to 900 µl of methanol and quantified spectrophotometrically at 420 nm.

3.2.1.12 Electrophoresis analysis of polymer –plasma protein interactions

Polyacrylamide gel electrophoresis (native PAGE) analysis was performed to detect the interaction of Pluronic/PCL copolymers with plasma proteins. Pluronic/PCL copolymers were incubated with human plasma (diluted with saline) for one hour at 37^{o}C. The samples were then centrifuged at 10000 rpm for 10 minutes and 20 µl of the supernatant was loaded on 7% resolving and 4% stacking

gel at 100 V for 90 min using Mini-PROTEAN II electrophoresis system (Bio-Rad, CA, USA). The gel was stained with coomassie blue and documented using an image analyzer (LAS 4000, Fuji). Plasma incubated with normal saline (0.09% NaCl) was considered as the control.

3.2.1.13 Blood compatibility study

3.2.1.13.1 Hemolysis

For performing the hemolysis and aggregation studies, the human blood sample was collected in a tube containing 3.8% sodium citrate at ratio 9:1 (blood: anticoagulant). 200µl of blood was mixed with 800µl of saline and was centrifuged at 750 rpm for 10 minutes. The erythrocytes obtained after repeated washings were re-suspended in fresh saline and vortexed. 100µl of the pellet was added to the empty and curcumin loaded micellar solutions which were kept for incubation at 37^{o}C for 2 hours. The absorbances were measured at 541 nm. Normal saline was used as negative control and distilled water as positive control. Percentage of hemolysis was calculated using the following equation:

$$\text{Percentage of hemolysis} = \frac{\text{OD of test solution} - \text{OD of negative control}}{\text{OD of positive control} - \text{OD of negative control}} \times 100$$

3.2.1.13.2 Aggregation study of blood cells

Human erythrocytes were collected by centrifugation of whole blood at 700 rpm for 10 minutes and then diluted with saline at 1:10 ratio. To 100 µl of erythrocytes, 100 µl curcumin loaded and unloaded micelles were added and incubated for 1 h at 37^{o}C. Normal saline (0.09 % NaCl) and PEI (polyethylenimine) were used as the negative and positive controls, respectively. After incubation, the cells were isolated

by centrifugation and the aggregation images were captured on a phase contrast microscope (Leica DM IRB, Germany) .The WBC compatibility study was done with anti-coagulated blood (1 ml) overlaid with histopaque (1 ml) in order to make three separate layers and was centrifuged for 15 minutes at 800 rpm at room temperature. The collected WBC was incubated with the micelles for 1 hour. And the aggregation was monitored through phase contrast microscope. The platetet layer was isolated from the anti-coagulated blood overlaid with histopaque and the platelets were incubated with micelles at 37^{o}C for 1 hour before visualizing through microscope.

3.2.1.14 Cytotoxicity studies – MTT assay

In order to check the cytotoxicities of various concentrations of curcumin loaded polymeric micelles, MTT assay was done on Caco2 cell lines. These cells were seeded in culture flasks with DMEM medium along with 10% FBS and incubated for 24 hours at 37°C in 5% CO_2 and 95% humidity to attain a cell growth of 80 % confluency. Prior to the experiment, the cells were trypsinized and transferred to a 24-well cell culture plate at a density of 1 x10^{5}cells/well. DMSO was added to aid the solubility of curcumin in aqueous media. The final concentration of DMSO in the culture medium was ensured to be less than 0.1%. The cells were exposed to a series of different concentrations of free and encapsulated curcumin (2.5-20 µM) for 24 hours followed by addition of 100µl MTT (3-(4,5-dimethylthiazol-2-yl)-2,5-diphenyltetrazolium bromide solution(0.5mg/ml) and incubated for 3 hours at 37^{o}C. Formazan crystals formed were dissolve with the addition 300 µL of DMSO per well. An incubation period of 15 minutes at 37^{o}C was provided. The absorbance was

measured at 570 nm using a plate reader (Finstruments Micro plate Reader USA). The cells treated with medium were used as negative control. Cytotoxicity of the unloaded micelles was also assessed in similar manner. The percentage viability was calculated as:

$$CV\ (\%)=\frac{N_t}{N_C}\times 100$$

where N_t was the absorbance of the cells treated with free curcumin or curcumin loaded micelles and N_c was the absorbance of the untreated cells.

3.2.1.15 Cellular uptake studies – Fluorescence microscopy

Caco2 cells were grown in culture plate up to 80% confluency to visualize the cellular uptake of curcumin loaded micelles. The molar concentration of curcumin used for the uptake study was 10 μM. All the samples were dissolved in PBS (0.01M , pH 7.4) and as free curcumin was insoluble in aqueous solution, it was dissolved with the aid of dimethylsulfoxide (DMSO) and then diluted with PBS. Cells were treated with free curcumin and curcumin loaded micelles. They were incubated for 4 hours prior to viewing under a fluorescence microscope (Leica DMI3000) for intracellular curcumin fluorescence.

3.2.2 Curcumin loaded calix[4]arene conjugated Pluronic / PCL micelles (CX-Pluronic/PCL)

3.2.2.1 Materials

4-tert butyl calix [4] arene, potassium iodide, 4-toluene sulphonyl chloride, potassium carbonate, Pluronic/PCL co polymer (synthesized in the previous section),

curcumin, pyrene and membrane dialysis bag (molecular weight cutoff 12kDa) were obtained from Sigma-Aldrich.3-(4,5-dimethylthiazol-2-yl)_2,5-diphenyl tetrazolium bromide (MTT), and Dulbecco's modified eagles medium (DMEM) were purchased from Sigma (Bangalore, India). Fetal bovine serum (FBS) was from GIBCO (United States). C6 glioma cells were obtained from National Centre for Cell Science (Pune, India).

3.2.2.2 Synthesis of CX-Pluronic/PCL

3.2.2.2.1 Monotosylation of Pluronic/PCL

Pluronic/PCL was synthesized according to the procedure in our previous section. Pluronic/PCL (1 g, 0.029 mmol) was dissolved in 50ml CH_2Cl_2 and chilled to 0^oC. Under vigorous stirring, Ag_2O (0.01 g, 0.044 mmol) followed by KI (0.034 g, 0.029 mmol) and p-toluenesulfonyl chloride (0.084 g, 0.054 mmol) were added to the chilled Pluronic/PCL. The reaction mixture was stirred further for 2 h at 0^oC and filtered over celite. The obtained white solid, post reduction under vacuum, was then dissolved in 50 mL H_2O Further, it was filtered, extracted with CH_2Cl_2 and precipitated using ice-cold diethyl ether. The residual solvent was removed under vaccum to get a white solid. (Yield= 0.78 g, 78%).

3.2.2.2.2 Removal of tert-butyl groups of 4-tert-butyl calix[4]arene

In order to enlarge the cavity of calix arene so as to accommodate the drug molecules, the tert-butyl groups which created steric hindrance were removed17. A slurry of 4-tert-butyl calix[4]arene (0.5 g,0.77 mmol), phenol(0.35 g, 3.71 mmol) and AlCl3 (0.54 g, 4.1 mmol) were stirred in 10 ml toluene at room temperature for 1 h

in an inert atmosphere. The mixture was then poured into 20 ml of 0.2 N HCl. The organic phase was separated and toluene was evaporated. Upon addition of methanol, a precipitate was formed which was filtered. The filtered solid was recrystallized from 1:1 MeOH/CHCl3 to afford the purified product (Yield= 0.36 g, 72%).

3.2.2.2.3 Reaction of calix arene with mono tosylated PCL/Pluronic (CX- Pluronic/PCL)

A slurry of 4-tert-butyl calix[4]arene (0.24 g, 0.3 mmol), mono tosylated Pluronic/PCL (0.5 g, 0.02 mmol) and K2CO3 (1.28 g, 9.2 mmol) was refluxed in dry acetonitrile (100 ml) for 48 h under a nitrogen atmosphere. After the reaction, the solvent was removed by rotatory evaporator. Then the mixture was dissolved in de-ionized water (30 ml) and extracted with dichloromethane (2 x 100 mL). The combined organic extracts were evaporated under reduced pressure to afford yellowish paste and then further purified using silica column chromatography. A solvent mixture of 9:1 (v/v) CH_2Cl_2/CH_3OH was taken as eluent. The purified fraction was precipitated in ice-cold diethyl ether to obtain white powder. (Yield= 0.12 g, 24%).

3.2.2.3 Characterization by Fourier transform infrared spectroscopy (FTIR)

The structure of the CX-Pluronic/PCL was characterized by Fourier transform infrared spectra and was recorded using a Thermo Nicolet, 5700 (Germany) spectrometer. The FT-IR spectra were obtained in the region 400–4000 cm^{-1}.

3.2.2.4 Preparation of curcumin loaded CX- Pluronic/PCL by solvent dialysis method

Lyophilized Cur-CX-Pluronic/PCL was sonicated in methanol (1mg/ml) and the absorbance of the solution was recorded on a UV–visible spectrophotometer at 425 nm. The amount of curcumin in the micelles was determined from the concentration correlated from a standard linear plot which was obtained by preparing different standard solutions of curcumin in methanol (1-10 µg/ml) and recording their absorption intensities at 425 nm .The drug loading capacity and the encapsulation efficiency was determined the following equations:

$$\text{Drug loading capacity (w/w\%)} = \frac{(\text{Amount of curcumin})}{(\text{Amount of Cur-CX-Pluronic/PCL micelles})} \times 100$$

$$\text{Encapsulation efficiency (\%)} = \frac{(\text{Encapsulated amount of curcumin})}{(\text{Initial amount of curcumin added})} \times 100$$

3.2.2.4.1 Particle size and zeta potential determination

The size of the curcumin loaded CX-Pluronic/PCL micelles was assessed by dynamic light scattering (Nano-ZS 90, Malvern Instrument, UK). The temperature was kept at 25^{o}C during the measuring process and measurements were recorded as the average of three test runs. The zeta potential of the curcumin loaded CX- Pluronic/PCL was measured in folded capillary cells using Nanosizer (Malvern Instrument UK).

3.2.2.4.2 Differential Scanning Calorimetry (DSC)

DSC was performed on curcumin loaded CX- Pluronic/PCL and calix[4]arene. The thermograms were recorded on a scanning calorimeter equipped with a thermal analysis data system (DSC Q20). Samples were placed in hermetically sealed aluminum pans and heated from 25 ˚C to 300 ˚C at a heat flow rate of 10˚C/min under nitrogen purge.

3.2.2.4.3 Critical micelle concentration

Critical micelle concentration (CMC) of CX-Pluronic/PCL was determined by using pyrene as fluorescence probe. Pyrene stock solution was prepared by dissolving 2.5 mg of pyrene in 5 ml methanol which was further diluted 20 times. 50 µl of diluted pyrene solution was vortexed well with different concentrations of micellar solutions ranging from 3 mg to 0.001 mg. The solutions were vortexed and kept overnight to equilibrate pyrene with the micelles. The fluorescence spectrum was recorded on a fluorescence spectrophotometer (Infinite M200, TECAN) at an emission wavelength of 390 nm.

3.2.2.5 Curcumin encapsulation in CX-Pluronic/PCL micelles

The pelleted (unencapsulated) curcumin, obtained after centrifuging the micellar solution at 5000 rpm for 15 minutes, was dissolved in methanol and was spectrophotometrically quantified using UV spectrometer (Cary model 100 BioUV-Vis spectrophotometer, Varian Australia) at a wavelength of 420 nm. The encapsulation efficiency and loading capacity were calculated using the following equation:

$$\text{Encapsulation efficiency } (\%) = \frac{(\text{Total amount of curcumin} - \text{Free curcumin})}{\text{Free curcumin}} \times 100$$

$$\text{Drug loading capacity } (\text{w/w}\%) = \frac{(\text{Amount of curcumin in micelles})}{\text{Amount of curcumin loaded micelles}} \times 100$$

3.2.2.6 Curcumin- CX Pluronic/PCL core compatibility

Using Hildebrand-Scatchard equation [Equation 1], the compatibility between curcumin and the micelle core forming block was calculated. The group contributions of functional moieties of curcumin and the hydrophobic core of PCL and PPO of Pluronic and calix arene were calculated by Equations [2]-[6].

3.2.2.7 Blood compatibility study

3.2.2.7.1 Hemolysis

The human blood sample was collected in a tube containing 3.8 % sodium citrate at ratio 9:1 (blood: anticoagulant). 200µl of blood mixed with 800µl of saline was centrifuged at 750 rpm for 10 minutes. The erythrocytes obtained after repeated washings were re-suspended in fresh saline and vortexed. 100µl of the pellet was added to the empty and curcumin loaded CX- Pluronic/PCL solutions which were kept for incubation at 37 ^{o}C for 2 hours. Normal saline and distilled water was used as negative control and positive control, respectively. The absorbances were measured at 541 nm.Percentage of hemolysis was calculated using the following equation:

$$\text{Percentage of hemolysis} = \frac{\text{OD of test solution} - \text{OD of negative control}}{\text{OD of positive control} - \text{OD of negative control}} \times 100$$

where OD refers to optical density.

3.2.2.7.2 RBC aggregation

Human red blood cells were collected by centrifugation of whole blood at 700 rpm for 10 minutes and then diluted with saline at 1:10 ratio. To 100 µl of red blood cells, 100 µl curcumin loaded and unloaded micelles were added and incubated for one hour at 37^{o}C. Normal saline (0.09 % NaCl) and PEI (polyethylenimine) were used as the negative and positive controls, respectively. After incubation, the cells were isolated by centrifugation and the aggregation images were captured on a phase contrast microscope (Leica DM IRB, Germany)

3.2.2.7.3 WBC aggregation

The WBC compatibility study was performed with anti-coagulated blood (1 ml) overlaid with histopaque (1 ml) in order to make three separate layers and was centrifuged for 15 minutes at 800 rpm at room temperature. The collected WBC was incubated with the micelles for one hour. Aggregation was detected through phase contrast microscope (Leica DM IRB, Germany)

3.2.2.7.4 Platelet aggregation

The platetet layer was isolated from the anti-coagulated blood overlaid with histopaque and the platelets were incubated with curcumin loaded and unloaded micelles at 37 ^{o}C for one hour. The extent of aggregation was observed through phase contrast microscope (Leica DM IRB, Germany).

3.2.2.8 In vitro release study

Release of curcumin from CX-Pluronic/PCL was investigated at acidic and physiological pH. 10 mg of the lyophilized CX-Pluronic /PCL was re dispersed in

10 ml PBS (pH 7.4) /acetate buffer (pH 4.5). The solution was divided equally into ten Eppendorf tubes, one ml each, for time-dependent release study at different time intervals in a shaker maintained at 37^{o}C. At pre-determined intervals of time, the solution was centrifuged to separate the released (pelleted) curcumin from the micelles. The released curcumin was extracted in methanol and quantified at 420 nm using UV visible spectrophotometer. The release was calculated as follows :

$$\text{Release (\%)} = \frac{\text{Released amount of curcumin}}{\text{Total amount of curcumin}} \times 100$$

3.2.2.9 In vitro cytotoxicity study -MTT assay

C6 (glioma) cells were seeded in culture flasks at a density of 2x10^{5}cells/well with DMEM medium along with 10% FBS and incubated for 24 hours at 37°C in 5% CO_2 and 95% humidity to attain a cell growth of 70% confluency. Prior to the experiment, the cells were trypsinized and transferred to a 24-well cell culture plate. The cells were exposed to a series of different concentrations of free and encapsulated curcumin (2.5-20 µM) for 48 hours followed by addition of 100µl MTT [3-(4,5-dimethylthiazol-2-yl)-2,5-diphenyltetrazolium bromide] solution and incubated for 3 hours at 37^{o}C. Formazan crystals formed were dissolve with the addition 300 µL of DMSO per well. The absorbance was measured at 570 nm using a plate reader (Finstruments Micro plate Reader USA). The cells treated with medium were used as negative control. Cytotoxicity of the unloaded micelles was also assessed in the similar manner. The percentage viability was calculated as:

$$CV\ (\%) = \frac{N_t}{N_C} \times 100$$

where N_t was the absorbance of the cells treated with free curcumin or curcumin loaded micelles and N_c was the absorbance of the untreated cells.

3.2.2.10 Cellular internalization of curcumin loaded CX-Pluronic/PCL

C6 glioma cells were seeded in a 4-well plate at a density of $3x10^5$ cells /well and uptake study was performed after 80% confluent growth. The molar concentration of curcumin used for the uptake study was 10 μM. Cells were treated with free curcumin and curcumin loaded CX-PCL/Pluronic prior to incubation for 4 hours after which the cells were washed with PBS and fixed. The intracellular green fluorescence of curcumin was viewed under a fluorescence microscope.

3.2.2.11 Statistical analysis

Data are represented as mean ± SD (standard deviation) of three independent experiments. Statistical analysis of the MTT assay data was performed by one-way analysis of variance (ANOVA) using SPSS software (SPSS-16, IBM, USA); a value of $p<0.05$ and $p<0.01$was considered significant (n=3).

3.3 Curcumin-dextran conjugates

3.3.1 Materials

Dextran (molecular weight=70,000g/mol), curcumin, succinic anhydride, N,N^1 dicyclohexylcarbodiimide (DCC), 4-dimethylaminopyridine (DMAP), pyrene and 3-(4,5-dimethylthiazol-2-yl)-2,5-diphenyl tetrazolium bromide (MTT), Modified

Eagles Medium (DMEM) were purchased from Sigma (Bangalore, India). Fetal bovine serum (FBS) was from GIBCO (USA). C6 glioma cells were obtained from National Centre for Cell Science (Pune, India).

3.3.2 Synthesis

3.3.2.1 Synthesis of curcumin hemi-succinate

Curcumin (0.5 g, 1.4 mmol) was dissolved in 15 ml of THF. Succinic anhydride (0.07 g, 0.7 mmol), TEA (0.07 g, 0.7 mmol), DMAP (0.08 g, 0.7 mmol) were added and the reaction was stirred for 24 h at 60^{o}C. The solvent was removed using a rotary vapour and the resulting residue was dissolved in 1:9 v/v methanol/methylene chloride solution and column chromatography was performed to obtain the pure fraction (10% methanol/methylene chloride was used as eluent) which was concentrated and dried in vaccum (Yield = 0.27 g, 54%).

3.3.2.2 Synthesis of curcumin dextran conjugate

Dextran (2 g, 0.02 mmol) was reacted with curcumin hemi-succinate (0.2 g, 0.4 mmol), DCC (0.09 g, 0.4 mmol), DMAP (0.05g, 0.4 mmol) and TEA (0.04 g, 0.4 mmol) in 20 ml DMSO. The solution was stirred under nitrogen atmosphere for 24 hours. The reaction mixture was filtered and diethyl ether was added to obtain a distinct yellow coloured layer. This layer was separated and dialysed against distilled water (dialysis bag with 10,000 MW cut off) overnight. The solution was lyophilized to obtain curcumin dextran conjugate (Yield= 1.4 g, 68%).

3.3.3 Characterization of curcumin-dextran conjugate

3.3.3.1 FTIR spectroscopy

FTIR spectrum of the curcumin dextran conjugates was recorded in the range of 4000-400 cm^{-1} on a Fourier transform infrared spectrophotometer (Nicolet 5700). IR spectra of dextran and curcumin were also compared for analyzing the successful synthesis of the conjugate.

3.3.3.2 ^{1}H NMR spectroscopy

The ^{1}H NMR spectrum of the curcumin dextran conjugate and dextran were measured in deuterated dimethyl sulfoxide using a 400 MHz spectrophotometer (Bruker DRX 400) at 25^{o}C.

3.3.3.3 Critical micelle concentration

Critical micelle concentration (CMC) of curcumin dextran conjugates were determined by fluorescence spectroscopy using pyrene as fluorescence probe. 2.5 mg of pyrene in 5 ml methanol was diluted 20 times and 50 µl of diluted pyrene solution was vortexed well with different concentrations of solutions of curcumin dextran conjugates. The solutions were vortexed and kept overnight prior to obtaining their fluorescence spectra at an emission wavelength of 390 nm.

3.3.3.4 Determination of particle size

3.3.3.4.1 DLS

The hydrodynamic size of the curcumin dextran conjugates was assessed by dynamic light scattering (Nano-ZS 90, Malvern Instrument, UK). It was ensured that the temperature was maintained at 25 ^{o}C during the measurements.

3.3.3.4.2 TEM

The size of curcumin dextran conjugates was also determined TEM experiments which was done using Hitachi H-7650 (Tokyo, Japan) at an acceleration voltage of 80 kV. Curcumin dextran conjugates were administered onto a 200 mesh copper grids and air dried prior to imaging.

3.3.3.5 Zeta potential

The zeta potential of curcumin dextran conjugates was determined using Nanosizer (Malvern Instrument UK). TEM experiments were performed on a Hitachi H-7650 (Tokyo, Japan) at an acceleration voltage of 80 kV. Curcumin loaded micellar suspensions were administered onto a 200 mesh copper grids and air dried prior to imaging.

3.3.3.6 DSC

Curcumin dextran conjugates were subjected to DSC measurements which were performed on a scanning calorimeter with a thermal analysis data system (DSC Q20). The samples were placed in aluminum pans and heated from 25^{o}C to 300^{o}C at a heat flow rate of 10^{o} C/min under nitrogen flow.

3.3.4 Drug loading capacity

Standard curcumin solutions in DMSO were prepared. Absorbances were recorded at 450 nm and a linear plot for the standards was obtained. Curcumin dextran conjugate was dissolved in DMSO (1mg/ml) and the absorbance was recorded on UV-Vis spectrophotometer at 450 nm. The amount of curcumin in conjugate was determined from the concentration correlated with the standard plot.

$$\text{Drug loading capacity (w/w\%)} = \frac{(\text{Amount of curcumin})}{\text{Amount of curcumin dextran conjugate}} \times 100$$

3.3.5 Spectral characterization

The spectral properties of the curcumin dextran conjugates were analyzed by UV-Visible and fluorescence spectroscopy. The absorption intensity of curcumin dextran conjugate and free curcumin was studied at 420 nm. The fluorescence emission spectra of free curcumin and curcumin dextran conjugates were recorded from 450-700nm with an excitation wavelength of 420 nm.

3.3.6 Stability study

The stability of curcumin conjugated to the dextran backbone was studied in physiological pH using UV-Visible spectroscopy. Free curcumin and conjugated curcumin at equivalent curcumin concentration were prepared in PBS (0.01M, pH 7.4) incubated in a shaker with 150 rpm rotation for 8 hours. Methanol (1% v/v) was used to dissolve native curcumin. At pre-determined time intervals, 100 µl of the solution from the samples were withdrawn and mixed with 900µl of methanol to quantify the stability of curcumin with time.

3.3.7 Blood compatibility

The hemocompatibility of curcumin dextran conjugates were monitored by hemolysis and aggregation studies. Human blood sample was collected in a tube containing 3.8% sodium citrate at ratio 9:1 (blood: anticoagulant). 200 µl of blood was mixed with 800 µl of saline and was centrifuged at 750 rpm for 10 minutes. The erythrocytes were with thrice washed with saline and vortexed after re-suspending in

saline. 100 µl of the erythrocyte pellet was incubated with curcumin dextran conjugates (5mg/ml concentration) at 37^{o}C for 2 hours. The absorbances were measured at 541 nm. Normal saline was used as negative control (0% lysis) and distilled water as positive control (100% lysis). Percentage of hemolysis was calculated using the following equation:

$$\text{Percentage of hemolysis} = \frac{\text{OD of test solution} - \text{OD of negative control}}{\text{OD of positive control} - \text{OD of negative control}} \times 100$$

where OD refers to optical density

Compatibility of curcumin dextran conjugates with blood components were further assessed by aggregation studies. Blood was centrifuged at 700 rpm for 10 minutes to separate the RBC layer which was subjected to saline wash and diluted in the ratio 1:4. 1 ml of curcumin dextran conjugate (5mg/ml) was incubated with 2 ml of diluted RBC for 20 minutes at 37^{o}C. The diluted RBC was also incubated along with negative and positive control. Normal saline and PEI were used as the negative and positive controls, respectively. The compatibility of WBC and platelets was demonstrated with anti-coagulated blood (1 ml) overlaid with histopaque (1 ml) in order to make separated layers and was centrifuged for 15 minutes at 800 rpm at room temperature. The collected WBC and platelets were incubated with the curcumin dextran conjugate solution (concentration of 5mg/ml) for 30 min at 37^{o}C. Similar procedure was carried out for the incubation with the controls. After incubation, the cells were isolated by centrifugation and examined on mounted slides and the images were captured on a phase contrast microscope (Leica DMIRB).

3.3.8 Polyacrylamide gel electrophoresis (PAGE)

The interaction of curcumin dextran conjugates with plasma proteins was assessed by native polyacrylamide gel electrophoresis (PAGE) analysis. Curcumin dextran conjugates were incubated with 100µl of human plasma (diluted with saline) for 1 h at 37^{o}C. The sample was centrifuged 10,000 rpm for 10 min and 20 µL of the supernatant was loaded on 7% resolving and 4% stacking gel at 100V for 90 min using Mini-PROTEAN II electrophoresis system (Bio-Rad, CA, United States). The gel after coomassie blue staining was documented using an image analyzer (LAS 4000, Fuji). Plasma incubated with normal saline (0.09% sodium chloride) was used as the control.

3.3.9 *In vitro* release study

The *in vitro* release study was performed at acidic as well as physiological pH. 10 mg of the lyophilized curcumin dextran conjugate was re-dispersed in 10 ml PBS (pH 7.4) /acetate buffer (pH 4.5). Total volume was divided into ten Eppendorf tubes, one ml each, for time-dependent release study at different time intervals in a shaker maintained at 37^{o}C. At pre-determined intervals of time, the solution was centrifuged for to separate the released (pelleted) curcumin from the conjugate. The released curcumin was extracted in DMSO and quantified at 450 nm using UV visible spectrophotometer. The release was calculated as follows:

$$\text{Release (\%)} = \frac{\text{Released amount of curcumin}}{\text{Total amount of curcumin}} \times 100$$

3.3.10 *In vitro* cytotoxicity studies

3.3.10.1 MTT assay

The cytotoxicity of curcumin dextran conjugates were evaluated by MTT assay on C6 glioma cells. The glioma cells were trypsinized and transferred to a 24-well cell culture plate at a density of $2x10^5$cells/well and were exposed to different concentrations of free and conjugated curcumin in the range of 10–50 µM for 24 hours. The percentage cell viability (CV) was calculated as:

$$CV\ (\%)=\frac{N_t}{N_C}\times 100$$

where, N_t is the absorbance of the cells treated with free curcumin or curcumin loaded micelles and N_c was the absorbance of the untreated cells.

3.3.10.2 Live Dead assay

The cytotoxicity of curcumin dextran conjugate was qualitatively assessed by live/dead viability assay on C6 glioma cells. Glioma cells were seeded into a 4 well plate at a seeding density of 4 x 10^4 cells/well and allowed to adhere overnight with 5% CO2 at 37°C. 100 µl of the samples were incubated with the glioma cells where an equivalent concentration of 20 µM of curcumin was maintained in the free and the conjugated form. After 24 hour incubation period, cells were washed thrice with phosphate buffered saline, stained with assay reagents containing 2 µM calcein AM (acetomethoxy derivate of calcein) and 4 µM EthD-1 (ethidium homodimer) and incubated for 30 min at 37°C. The cells were then visualized and imaged using fluorescence microscope (Leica DM IRB, Germany).

3.3.11 *In vitro* cellular uptake of curcumin dextran conjugate

The cellular internalization of curcumin dextran conjugates was visualized by fluorescence microscope .C6 glioma cells were cultured with a seeding density of

$2x10^5$cells/well. An equivalent concentration of 10 μM of curcumin as a free and conjugated form was used for the uptake study. The samples were dissolved in PBS (0.01 M, pH 7.4) and as free curcumin was insoluble in aqueous solution, it was dissolved with dimethylsulfoxide (DMSO). After PBS wash, the cells were fixed using 3.7 % paraformaldehyde solution prior to viewing under a fluorescence microscope (Leica DMI3000) for intracellular curcumin fluorescence.

3.4 Curcumin loaded POx micelles

3.4.1 Curcumin loaded Poly [2-ethyl-2-oxazoline-b-2-(but-3-enyl)-2-oxazoline] P(EtOx-b-ButenOx) micelles

3.4.1.1 Materials

2-ethyl-2-oxazoline (EtOx), methyl *p*-toluenesulfonate methyl tosylate, 4-pentenoic acid, N-hydroxysuccinimide, 2-chloroethylamine hydrochloride, 1,6 Diphenyl-1,3,5 Hexatriene (DPH) and curcumin , 2,5-diphenyl tetrazolium bromide (MTT) and Modified Eagles Medium (DMEM) were obtained from Sigma Aldrich Fetal bovine serum (FBS) was from GIBCO (USA). C6 glioma cells were obtained from National Centre for Cell Science (Pune, India).

3.4.1.2 Synthesis

3.4.1.2.1 Synthesis of Butenox monomer

2-(but-3-enyl)-2-oxazoline (ButenOx) was synthesized from 4-pentenoic acid by the following three step procedure described by Gress et al (Gress et al., 2007b)

Step 1: Synthesis of N-succinimidyl pentenate

A solution of 4-pentenoic acid (14.72 g, 0.15 mol) in 300 ml dry dichloromethane was stirred in an ice bath with the addition of N-hydroxy succinimide [NHS] (16.91 g, 0.15 mol). DCC (30.33 g, 0.15 mol) was dissolved in 100 ml dry dichloromethane and was added dropwise to the above solution and was stirred vigorously for two hours. White cloudy precipitate was filtered off .The filtrate was evaporated and further dissolved in a mixture of diethyl ether and hexane (2:1 v/v). The solution was filtered and the solvent was evaporated to obtain a white product (Yield =18.5 g, 63%).

Step 2: Synthesis of N-(2- chloro ethyl)-4-pentenamide

To a stirring solution of N-succinimidyl pentenate (18.48 g , 0.092 mol) in 500 ml dry dichloromethane, 2-chloroethyl amine hydrochloride (21.43 g, 0.1848 mol) and sodium hydroxide (7.4 g, 0.1848 mol) dissolved in 200 ml de-ionized water were added drop wise. The solution was allowed to stir vigorously overnight after which the organic layer was separated and washed twice with water and dried over sodium sulphate. The solution was filtered and the solvent was evaporated to yield a yellow oily product. (Yield=11.82 g, 79.2 %).

Step 3: Synthesis of 2-(but-3-enyl)-2-oxazoline

N-(2-chloro ethyl)-4-pentenamide (11.82 g, 0.073 mol) was dissolved in 100 ml dry methanol (methanol dried over molecular sieves). To this solution, potassium hydroxide (4.09 g, 0.073 mol), dissolved in 100 ml dry methanol, was added drop wise. The reaction mixture was stirred for 48 h at 85^{o}C under argon atmosphere. After the reaction, the precipitated salt was filtered off using a filter paper and the

filtrate was evaporated using rotary evaporator to obtain a yellow solution. Additional precipitate was filtered off by passing the solution through a 0.45µm syringe filter. The product was further purified by Kugelrohr distillation (Yield= 4.079 g, 44.7%).

3.4.1.2.2 Synthesis of P(EtOx-b-ButenOx) block co polymers

3.4.1.2.2.1 Synthesis of P($EtOx_{30}$-b-$ButenOx_5$) block co polymer

0.25 ml of EtOx (0.25 g, 2.5 mmol) in 0.6 ml acetonitrile (4 M concentration) was reacted with 0.015 ml methyl tosylate (0.018 g, 0.096 mmol in a microwave vial). The vial was capped and argon was bubbled through the solution for 20 minutes. The reaction solution was heated in the microwave synthesizer (Biotage) for 15 minutes at a temperature of 140^{o}C after which 0.3 ml ButenOx (0.3 g , 2.4 mmol) was added and further heated for 15 minutes. Reaction was quenched by adding 0.02 ml KOH solution. The reaction solution was dissolved in chloroform. It was subjected to sodium bicarbonate wash (twice), water wash (twice) and brine wash (once) and the organic layer was separated and dried over sodium sulphate. It was concentrated and added drop wise to ice cold diethyl ether. Formation of white precipitate occurred. Ether was decanted off and the precipitate was washed twice with ether and dried overnight under vaccum (Yield=0.21g, 38%).

3.4.1.2.2.2 Synthesis of P($EtOx_{33}$-b-$ButenOx_{26}$) block co polymer

Similar stoichiometric amounts of reagents were taken as above and the reaction conditions were same except for the ButenOx polymerization which was heated for 30

minutes before quenching with KOH solution. The work up procedure was similar to the previous synthesis (Yield= 0.34 g, 59%).

3.4.1.2.2.3 Synthesis of P(EtOx$_{17}$-b-ButenOx$_{44}$) block co polymers

0.15 ml of EtOx (0.15 g, 1.5 mmol) in 0.4 ml acetonitrile (4 M concentration) was reacted with 0.009 ml methyl tosylate (0.01 g, 0.06 mmol in a microwave vial). The vial was capped and argon was bubbled through the solution for 20 minutes. The reaction solution was heated in the microwave for 15 minutes at a temperature of 140 ^{0}C. Sample for NMR was taken after 15 minutes to ensure complete EtOx polymerization after which 0.3 ml ButenOx (0.3 g , 2.4 mmol) was added and heated for 30 minutes. The reaction solution was pale yellow in colour and viscous. Complete disappearance of ButenOx monomer peaks was observed by ^{1}H NMR. Reaction was quenched by adding 0.02 ml KOH solution. The reaction solution, dissolved in chloroform, was subjected to sodium bicarbonate wash (twice), water wash (twice) and brine wash (once) and the organic layer was separated and dried over sodium sulphate. Later, it was concentrated and added drop wise to ice cold diethyl ether leading to the formation of white precipitate. Ether was decanted off and the precipitate was washed twice with ether and dried overnight under vaccum (Yield=0.3 g, 67%).

3.4.1.3 Characterization of synthesized polymers

3.4.1.3.1 ^{1}H NMR

^{1}H NMR spectra were obtained using a Varian spectrometer operating at 400 MHz. $CDCl_3$ and DMSO were used as solvents. An acquisition time of 5 seconds and a

relaxation delay of 8 seconds were employed for the collection of ^{1}H NMR spectra of block polymers.

3.4.1.3.2 DSC

The DSC thermograms of the block polymers were recorded using Q10. 5 mg of the samples were placed in aluminum pans and heated from 25^{o}C to 200^{o}C at a heat flow rate of 10^{o} C/min under nitrogen flow.

3.4.1.4 Preparation of micelles

The micelles were prepared by nano-precipitation method with slight modifications. 6 mg polymer and 1 mg curcumin were dissolved in 0.5 ml acetone and added drop wise to 10 ml de-ionized water stirring at 1300 rpm. The solution was further diluted with 10 ml de-ionized water and allowed to stir for 4 hours to remove acetone. Precipitation of curcumin was not observed after acetone removal. Empty micelles of block polymers were prepared by similar method without curcumin addition.

3.4.1.5 Characterization of micelles

3.4.1.5.1 Determination of critical micelle concentration (CMC)

Stock solution of 1, 6 Diphenyl-1,3,5 hexatriene (DPH) was prepared by dissolving 2.5 mg in 5 ml methanol. The solution was diluted 20 times. 50 µl of the diluted DPH solution was added to 11 different concentrations of empty micellar solutions of synthesized block polymers. The solutions were vortexed and kept overnight to equilibrate DPH with the micelles. Fluorescence intensity of the micellar solutions were measured (excitation= 358 nm; emission= 400 nm).

3.4.1.5.2 Particle Size measurement

3.4.1.5.2.1 Dynamic light Scattering

The size of the micelles was assessed by dynamic light scattering (Nano-ZS, Malvern Instrument, UK). The temperature was kept at 25^{o}C during the measuring process and measurements were recorded as the average of three test runs.

3.4.1.5.2.2 Transmission electron microscopy

TEM experiments were performed on a JEOL 1400 at an acceleration voltage of 120 kV. Micelle solutions were administered onto a 200 mesh copper grids, air dried and negatively stained using uranyl acetate prior to imaging.

3.4.1.5.3 Determination of curcumin loading in the micelles

Calculated amounts of lyophilized curcumin loaded micelles were dissolved in methanol and the absorbance was recorded on UV-Vis spectrophotometer at 420 nm. Standard curcumin solutions in methanol were prepared. Absorbances were recorded and a linear plot for the standards was obtained which was used for the calculation of curcumin loading in the micelles. Drug loading capacity of the micelles was calculated:

$$\text{Drug loading capacity (w/w\%)} = \frac{(\text{Amount of curcumin})}{\text{Amount of curcumin loaded}\atop \text{P(EtOx-b-ButenOx)micelles}} \times 100$$

3.4.1.5.4 Drug-polymer compatibility calculations

The compatibility between curcumin and the micelle core forming block (ButenOx) was calculated by employing the Hildebrand-Scatchard equation (equation 1) and equations [2]-[6] based on van Krevelen's additive group contribution method.

3.4.1.5.5 Spectral characterization

The spectral property of the curcumin loaded micelles was analyzed. The fluorescence emission spectra of free curcumin and curcumin loaded micelle were recorded from 450-700nm with an excitation wavelength of 420 nm on a fluorescence spectrophotometer.

3.4.1.5.6 In vitro release study

5 mg of the lyophilized Curcumin loaded polymer was re-dispersed in 10 ml PBS (pH 7.4) /acetate buffer pH 4.5). Total volume was divided into ten Eppendorf tubes, one ml each, for time-dependent release study at different time intervals in a shaker maintained at 37^{o}C. At pre-determined intervals of time, the solution was centrifuged for to separate the released (pelleted) curcumin from the micelles. The released curcumin was extracted in methanol and quantified at 420 nm using UV- visible spectrophotometer. The release was calculated as follows:

$$\text{Release (\%)} = \frac{\text{Released amount of curcumin}}{\text{Total amount of curcumin}} \times 100$$

3.4.1.5.7 In vitro cytotoxicity

3.4.1.5.7.1 MTT Assay

The cytotoxicity of empty and curcumin loaded POX micelles were assessed on C6 glioma cells by MTT assay. DMEM medium along with 10% FBS were utilized for seeding the cells prior to their incubation for 24 hours at 37°C in 5% CO_2 and 95% humidity. The cells were trypsinized and transferred to a 24-well cell culture plate and were exposed to different concentrations of empty and loaded POx micelles ranging from 5-20 µM. Concentration range of 1-5 mg/ml empty POxs micelles were tested for their cytotoxicity.Cytotoxicity of the loaded micelles were assessed where the concentration of curcumin was in the range of 5 µM-20 µM. The percentage cell viability (CV) was calculated as:

$$\text{CV } (\%) = \frac{N_t}{N_C} \times 100$$

where N_t is the absorbance of the cells treated with free curcumin or curcumin loaded micelles and N_c was the absorbance of the untreated cells.

3.4.1.5.7.2 Live Dead Assay

The cytotoxicity was further qualitatively assessed using the live/dead viability assay. C6 glioma cells were seeded into 24 well plates and allowed to adhere overnight with 5% CO_2 at 37°C. The cells were then incubated with 100 µl of the samples for 24 hours. An equivalent concentration of 20 µM of curcumin was used in the free and the loaded form. Prior to the assay, cells were washed thrice with phosphate buffered saline, stained with assay reagents containing 2 μM calcein AM (acetomethoxy derivate of calcein) and 4 μM EthD-1 (ethidium homodimer) and

incubated for 30 min at 37°C. The cells were then visualized and imaged using fluorescence microscope (Leica DM IRB, Germany).

3.4.1.5.8 In vitro cellular uptake studies by fluorescene microscopy

An equivalent concentration of 5 μM of curcumin as a free and loaded form was used for the uptake study. The samples were dissolved in PBS (0.01 M, pH 7.4). Cells treated with free curcumin and curcumin loaded micelles were incubated at 37^{o}C for 4 hours. After PBS wash, the cells were fixed using 3.7% paraformaldehyde solution prior to viewing under a fluorescence microscope (Leica DMI3000).

3.4.2 Curcumin loaded Poly(2-methyl-2 oxazoline -b-2- isopropyl 2-oxazoline) and Poly(2-methyl-2 oxazolin-g-2-isopropyl 2-oxazoline)micelles

Block and gradient copolymers of P(MeOx-isoPropOx) were a gift from Prof. Richard Hoogenboom of Ghent University, Belgium. These block and gradient polymers were synthesized by CROP reaction between the two commercially available monomers, 2-methyl-2 oxazoline and 2-isopropyl 2-oxazoline. Poly(MeOx-isoPropOx) were in 5 different ratios of MeOx: iso PropOx mainly 10:50, 20:40, 30:30, 40:20 and 50:10. In this section, we explored these polymers to elucidate their potential as micelles for curcumin delivery.

3.4.2.1 Preparation of Curcumin loaded micelles using nano precipitation method

10 mg polymer and 1.5 mg curcumin were dissolved in 0.5 ml acetone/ acetonitrile (block polymers $MeOx_{10}$-$IsoPropOx_{50}$ and $MeOx_{20}$-$IsoPropOx_{40}$ were insoluble in acetone and it was solubilized in acetonitrile by warming at 60^{o}C). The solution was

added drop wise to 10 ml de-ionized water stirring at 1300 rpm and was further diluted with 10 ml de-ionized water. It was allowed to stir for couple of hours for acetone/ acetonitrile removal. Empty micelles were prepared in the same procedure without addition of curcumin.

3.4.2.2 Determination of critical micelle concentration

Stock solution of 1, 6 Diphenyl-1,3,5 hexatriene (DPH) was prepared by dissolving 2.5 mg in 5 ml methanol. The solution was diluted 20 times. 50 µl of the diluted DPH solution was added to 11 different concentrations of empty micellar solutions of synthesized block polymers. The solutions were vortexed and kept overnight to equilibrate DPH with the micelles. Fluorescence intensity of the micellar solutions were measured (excitation= 358 nm; emission= 400nm).

3.4.2.3 Characterization of the micelles

3.4.2.4 DLS

The size of the micelles was assessed by dynamic light scattering (Nano-ZS, Malvern Instrument, UK). The temperature was kept at 25^{o}C during the measuring process and measurements were recorded as the average of three test runs.

3.4.2.4.1 TEM

TEM experiments were performed on a JEOL 1400 at an acceleration voltage of 120 kV. Micelle solutions were administered onto a 200 mesh copper grids, air dried and negatively stained using uranyl acetate prior to imaging.

3.4.2.5 Curcumin loading in micelles

Calculated amounts of lyophilized curcumin loaded micelles were dissolved in methanol and the absorbance was recorded on UV-Vis spectrophotometer at 420 nm. Standard curcumin solutions in methanol were prepared. Absorbances were recorded and a linear plot for the standards was obtained. The loading capacity of the micelles was calculated:

$$\text{Drug loading capacity (w/w\%)} = \frac{(\text{Amount of curcumin})}{\underset{\text{P(MeOx-isoPropOx)micelles}}{\text{Amount of curcumin loaded}}} \times 100$$

3.4.2.6 Drug polymer compatibility

The compatibility between curcumin and the micelle core forming block (isoPropOx) was calculated by employing the Hildebrand-Scatchard equation (equation 1) and equations [2]-[6] based on van Krevelen's additive group contribution method.

3.4.2.7 Spectral characterization

The spectral property of the curcumin loaded micelles was analyzed. The UV-visible aborption spectra of free curcumin and curcumin loaded micelles were recorded. The fluorescence emission spectra of free curcumin and curcumin loaded micelles were recorded from 450-700nm with an excitation wavelength of 420 nm on a fluorescence spectrophotometer.

3.4.2.8 In vitro release study

The *in vitro* release was studied at acidic and physiological pH. Similar procedure for the P(EtOx-b-Butenox)s was followed. Curcumin loaded micelles with hydrodynamic size greater than 500 nm which had very low loading were not included for the release study.

3.4.2.9 In vitro cytotoxicity

3.4.2.9.1 MTT Assay

It was observed from the results that curcumin loaded P ($MeOx_{30}$-b-$isoPropOx_{30}$) exhibited better results compared to the other ratios. Hence, the micelles prepared from this polymer ratio were chosen for cell culture experiments. The cytotoxicity of empty and curcumin loaded P ($MeOx_{30}$-b-$isoPropOx_{30}$) POX micelles were assessed on C6 glioma cells by MTT assay. DMEM medium along with 10% FBS were utilized for seeding the cells prior to their incubation for 24 hours at 37 °C in 5% CO_2 and 95% humidity. The cells were trypsinized and transferred to a 24-well cell culture plate and were exposed to different concentrations of empty and loaded Pox micelles. Concentration ranges of 1-5 mg/ml empty P($MeOx_{30}$-b-$isoPropOx_{30}$) micelles were tested for their cytotoxicity. Cytotoxicity of the loaded micelles was assessed where the concentration of curcumin was in the range of 5 µM-20 µM. The percentage cell viability (CV) was calculated as:

$$CV\ (\%) = \frac{N_t}{N_C} \times 100$$

where N_t is the absorbance of the cells treated with free curcumin or curcumin loaded micelles and N_c was the absorbance of the untreated cells.

3.4.2.9.2 Live dead assay

The cytotoxicity of P ($MeOx_{30}$-b-$isoPropOx_{30}$) was further qualitatively assessed using the live/dead viability assay. C6 glioma cells were seeded into 24 well plates and allowed to adhere overnight with 5% CO_2 at 37°C. The cells were then incubated with 100 µl of the samples for 24 hours. An equivalent concentration of

20 µM of curcumin was used in the free and the loaded form. Prior to the assay, cells were washed thrice with phosphate buffered saline, stained with assay reagents containing 2 μM calcein AM (acetomethoxy derivate of calcein) and 4 μM EthD-1 (ethidium homodimer) and incubated for 30 min at 37°C. The cells were then visualized and imaged using fluorescence microscope (Leica DM IRB, Germany).

3.4.2.10 Cellular uptake

An equivalent concentration of 5 µM of curcumin as a free and loaded form was used for the uptake study. The samples were dissolved in PBS (0.01 M, pH 7.4). Cells treated with free curcumin and curcumin loaded micelles were incubated at 37^{o}C for 4 hours. After PBS wash, the cells were fixed using 3.7% paraformaldehyde solution prior to viewing under a fluorescence microscope (Leica DMI3000).

Statistical data analysis

Data are represented as mean ± SD (standard deviation) of three independent experiments.

CHAPTER 4 - RESULTS

4.1 Curcumin loaded micelles based on PEGylated Fatty Esters

4.1.1 Curcumin loaded mPEG-laurate and mPEG-linolenate micelles

4.1.1.1 Synthesis of mPEG laurate and linolenate

The mPEG-fatty esters were synthesized by Steglich esterification using DCC and DMAP (Figure 8 and Figure 9). The characteristic bands of synthesized fatty esters were confirmed by FTIR spectroscopy (Figure 10). Both mPEG-laurate and mPEG-linolenate showed a peak in the region 1720-1730 cm^{-1} due to the stretching vibration of carbonyl group. The peak around 2858 cm^{-1} denoted the C-H stretching vibration. At 2973 cm^{-1}, the olefinic C-H stretching in linolenic acid was observed.

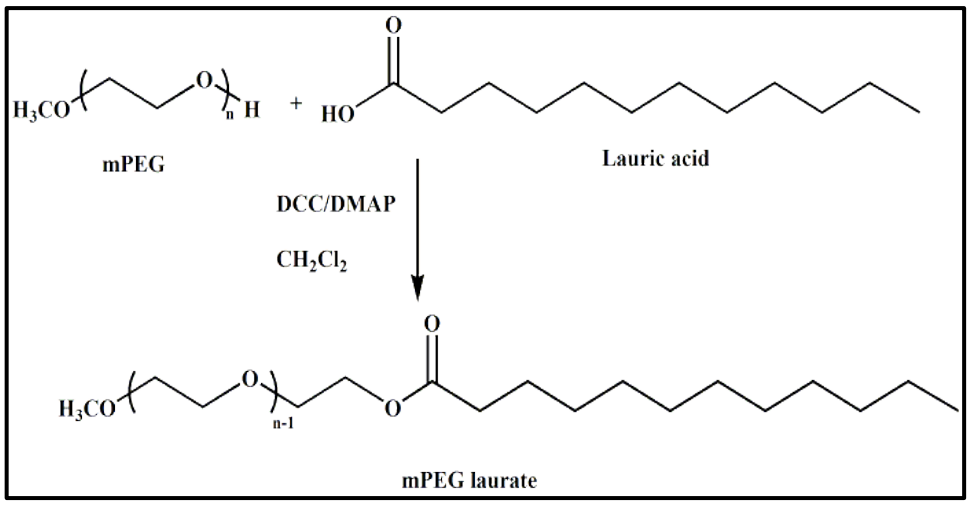

Figure 8. Schematic representation of synthesis of mPEG laurate

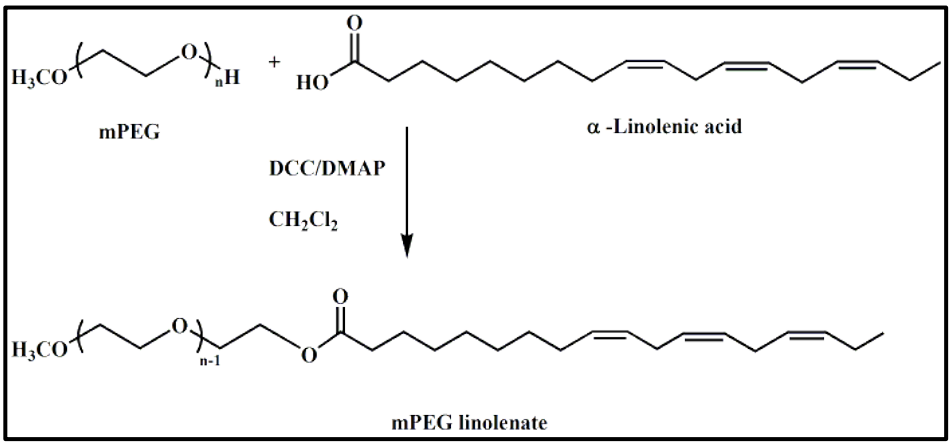

Figure 9. Schematic representation of synthesis of mPEG linolenate

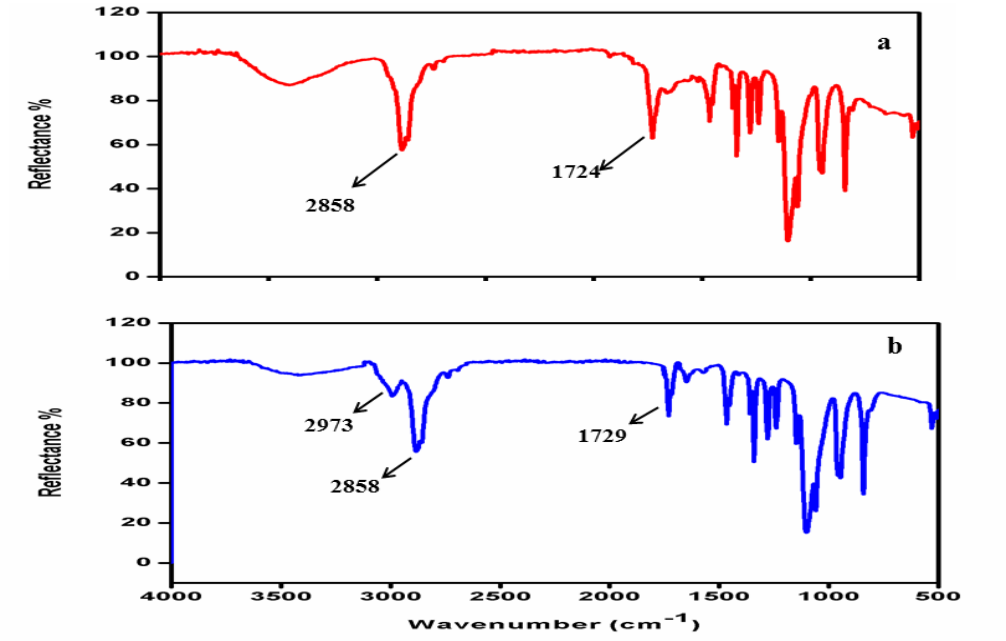

Figure 10. FTIR spectrum of (a) mPEG laurate (b) mPEG linolenate

The chemical structures of polymeric fatty esters were further fortified with ^{1}H NMR spectra. The characteristic peaks of laurate ester were observed at 3.3 ppm [$–(CH_2)_n–$] and 0.88 ppm ($–CH_3$). In addition, the methylene protons in the mPEG

chain were present at 3.46 ppm and the protons of methoxy group were seen at 1.25 ppm (Figure 11). The corresponding linolenate ester exhibited the protons of the conjugated double bonds 6.48 and 8.18 ppm (Figure 12). The peaks at 1.25 and 3.46 ppm corresponded to the protons of the methylene repeat units of mPEG.

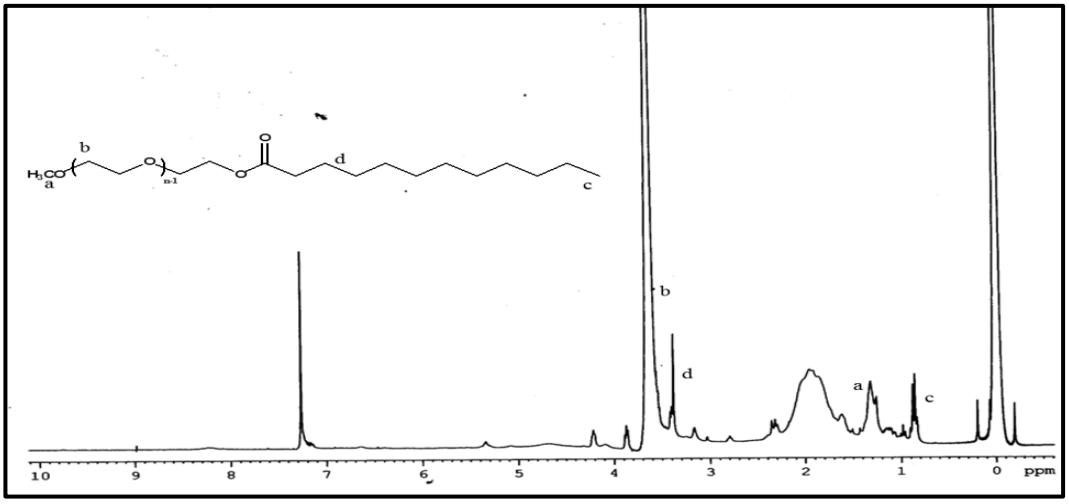

Figure 11. ^{1}H NMR of mPEG -laurate

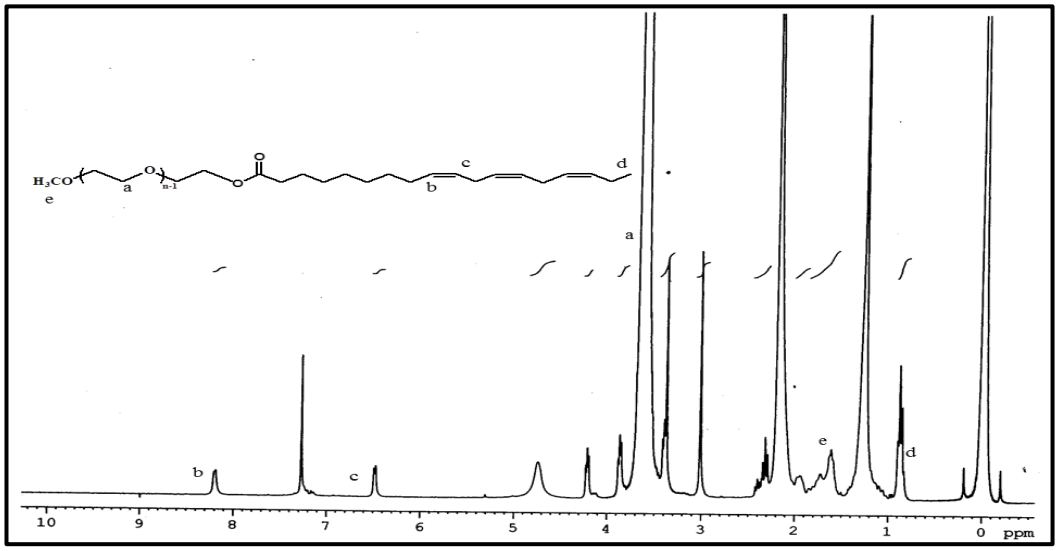

Figure 12. ^{1}H NMR of mPEG –linolenate

4.1.1.2 Curcumin loaded micelles

4.1.1.2.1 Loading characteristics and determination of size and zeta potential

Curcumin loaded micelles were prepared by dialysis method and it was observed that encapsulation in micelles rendered curcumin soluble in aqueous medium while compared to free curcumin (Figure 13). Curcumin loading was performed at 3.23% w/w, 4.76% w/w and 7.69% w/w. The loading capacities and the encapsulation efficiencies are tabulated in Table1.

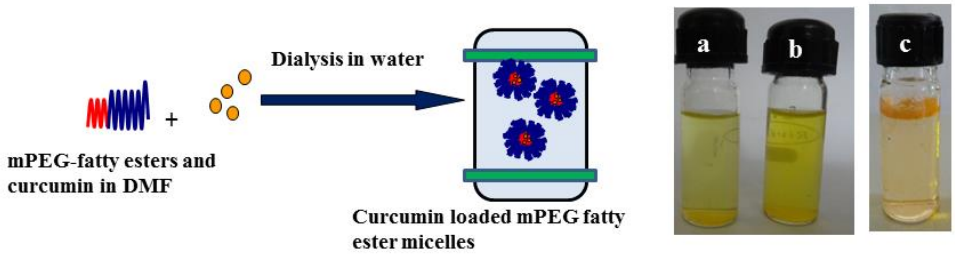

Figure 13. Schematic illustration of preparation of curcumin loaded micelles by dialysis method. (a) Curcumin loaded mPEG laurate micelles (b) Curcumin loaded mPEG linolenate micelles (c) Free curcumin in aqueous media.

Theoretical loading (% w/w)	**mPEG laurate**		**mPEG linolenate**	
	Loading capacity (% w/w)	Encapsulation efficiency (%)	Loading capacity (% w/w)	Encapsulation efficiency (%)
3.23	2.4 ± 0.2	74.2 ±6.3	2.91 ± 0.06	92.7 ± 3.8
4.76	2.3 ±0.2	50.2 ± 4.1	2.8 ± 0.4	59.1 ± 7.5
7.69	2.7 ± 0.4	35.5 ±5.6	3.4 ± 0.4	45.5 ± 4.4

Table 1. Curcumin loading characteristics in mPEG fatty ester micelles

The particle sizes of the unloaded and curcumin loaded micelles (3.23% w/w) of mPEG laurate were determined as 41.3 ± 4.2 nm and 59.5 ± 4.3 nm , respectively.

For the linolenate micelles, the unloaded and loaded size was 52.5 ± 5.2 nm and 77.5 ± 3.2 nm, respectively. The zeta potential of unloaded and curcumin loaded mPEG-laurate were –13.2 ± 2.6 mV and –15.5 ± 1.5 mV, respectively. The zeta potential of unloaded and loaded linolenate counterpart was –25.3 ± 5.3 mV and –23.7 ± 3.2 mV, respectively. The TEM image of the curcumin loaded micelles (Figure 14) showed that micelles were spherical in shape and the size was found to be in the range of 30-50 nm.

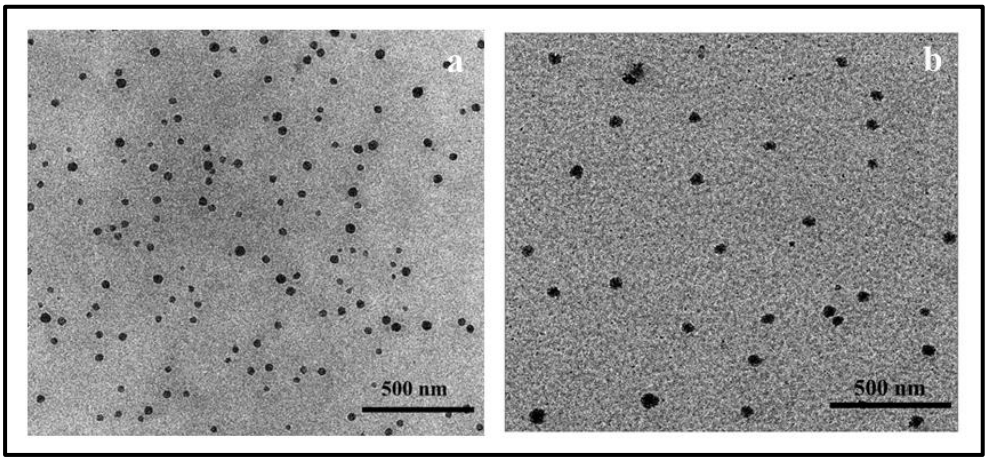

Figure 14. TEM image of curcumin loaded (a) mPEG laurate (b)mPEG linolenate micelles

4.1.1.2.2 Curcumin and fatty ester core compatibility

The compatibility of curcumin with the micellar core was evaluated by determining χ_{sp} , the Flory-Huggins interaction parameter. The contributions of functional groups of curcumin mainly the $–CH_3$, –OH, –CO–, $–C_6H_6–$, =CH– and $–CH_2–$ was employed for calculating the dispersion (δ_d) , polar (δ_p) and hydrogen bonding components (δ_h). Similarly, for the laurate and linolenate moiety the group contributions corresponding to the functional groups were used in the calculations. The molar

volume of the curcumin was obtained as 253.1 cm^3/mol based on the group contributions tabulated by Fedors (Fedors, 1974). The calculated values of solubility parameters $\delta_{curcumin}$, $\delta_{laurate}$, $\delta_{linolenate}$ were 24.84, 17.63 and 17.9, respectively. The interaction parameter ($\chi_{sp)}$, which defines the solubility capacity, of curcumin with the fatty ester core was evaluated to be 0.736 and 0.708 for the laurate and linolenate core , respectively.

4.1.1.2.3 Critical micelle concentration

Critical micelle concentration was evaluated using pyrene as the fluorescence probe. The critical micelle concentration of mPEG laurate and mPEG linolenate micelles was obtained from the point of inflection as 0.901and 0.665 mg/ml, respectively (Figure 15).

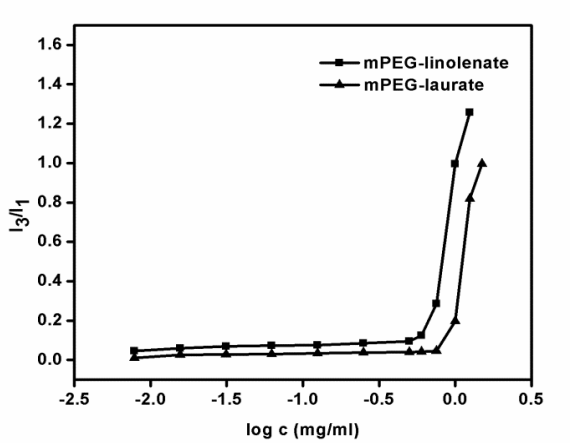

Figure 15. CMC plot of mPEG fatty ester micelles

4.1.1.2.4 Spectral characterization

Distinct spectral properties were exhibited by the curcumin loaded micelles. Free curcumin exhibited an absorption peak at 425 nm. The absorption peak of curcumin

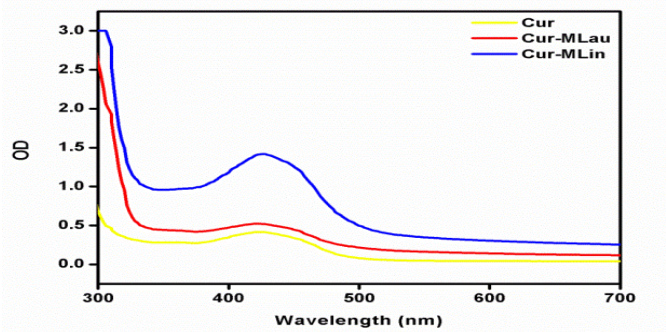

Figure 16. UV-visible spectrum of free curcumin (Cur), curcumin loaded mPEG laurate (Cur-MLau) and curcumin loaded mPEG linolenate (Cur-MLin).

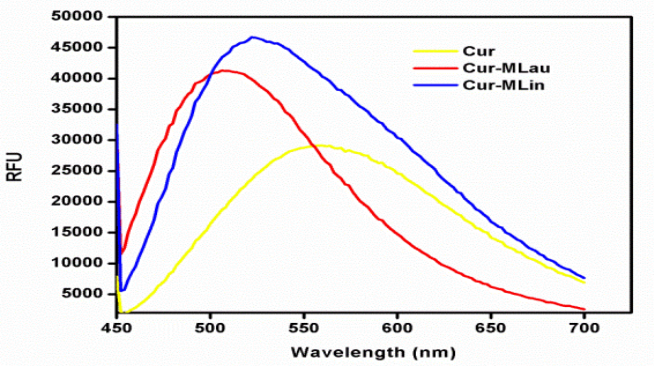

Figure 17. Fluorescence spectrum of free curcumin (Cur), curcumin loaded mPEG laurate (Cur-MLau) and curcumin loaded mPEG linolenate (Cur-MLin).

loaded mPEG fatty ester micelles was seen to be more enhanced compared to that of free curcumin (Figure 16). Curcumin showed a weak broad peak at 560 nm and the curcumin loaded mPEG fatty esters showed a well-defined high intensity blue-shifted fluorescent peak in the range of 500-525 nm (Figure 17).

4.1.1.2.5 Differential scanning calorimetry

In the DSC thermogram, curcumin exhibited an endothermic melting peak at 181.3^{o}C. The characteristic melting peaks of curcumin loaded mPEG linolenate and mPEG laurate were observed at 50.8^{o}C and 57.7^{o}C, respectively. The endothermic peak of curcumin was not visible in the thermograms of curcumin loaded polymers (Figure 18).

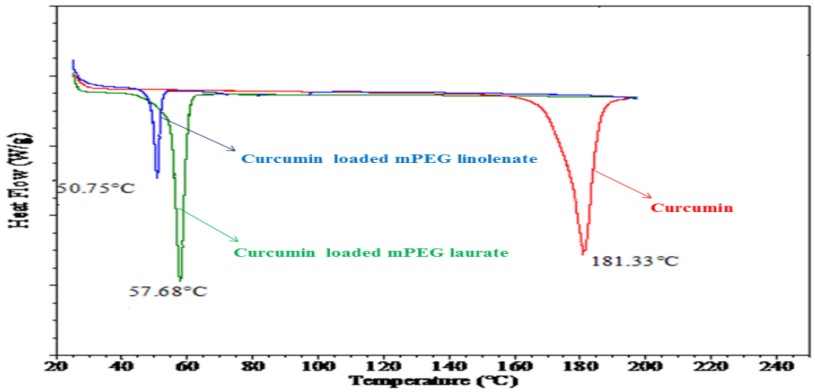

Figure 18. DSC thermograms of curcumin loaded micelles and free curcumin

4.1.1.2.6 Curcumin release study

The release of curcumin from the micelles were studied at pH 7.4 and 4.5 (Figure 19). Slightly higher release was observed at acidic pH compared to pH 7.4. Also higher release was seen from mPEG-laurate micelles compared to mPEG-linolenate. Sustained release was observed after 40 hours in both the micelles. After 108 hours, at both pH, above 90% curcumin was released from the micelles.

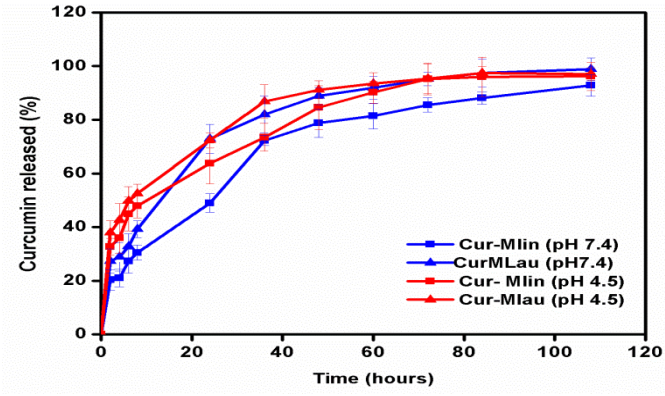

Figure 19. Release study of curcumin from mPEG fatty ester micelles

4.1.1.3 In vitro studies

4.1.1.3.1 Cytotoxicity study – MTT assay

MTT assay was performed on empty and curcumin loaded mPEG fatty ester micelles (Figure 20). Above 80% cells were viable upon treatment with the empty micelles indicating their biocompatibility. However, curcumin loaded micelles produced cytotoxic effects on cancer cells. Dose dependent cytotoxicity was exhibited. About 30% cells were viable with the effect of curcumin loaded micelles having 20 µM curcumin concentration. Similar concentration of free curcumin had 65% of cell viability.

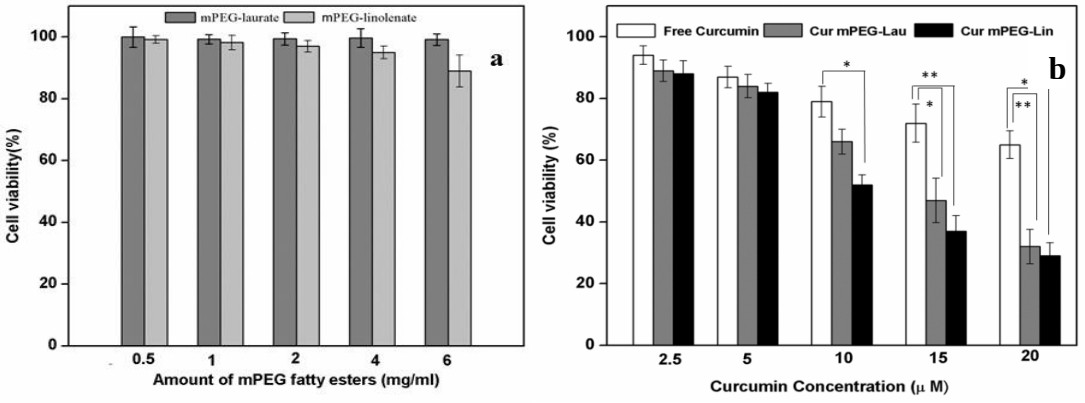

Figure 20. MTT assay on HeLa cells (a) Effect of empty micelles of mPEG laurate and linolenate (b) Effect of curcumin loaded micelles of mPEG laurate and linolenate

4.1.1.3.2 Cellular uptake

The cellular internalization of curcumin loaded mPEG fatty ester micelles in HeLa cells was investigated. The intrinsic green fluorescence of curcumin enables it to be traced inside cells. It was noted that curcumin encapsulated in the micelles were better internalized in the cells compared to free curcumin (Figure 21).

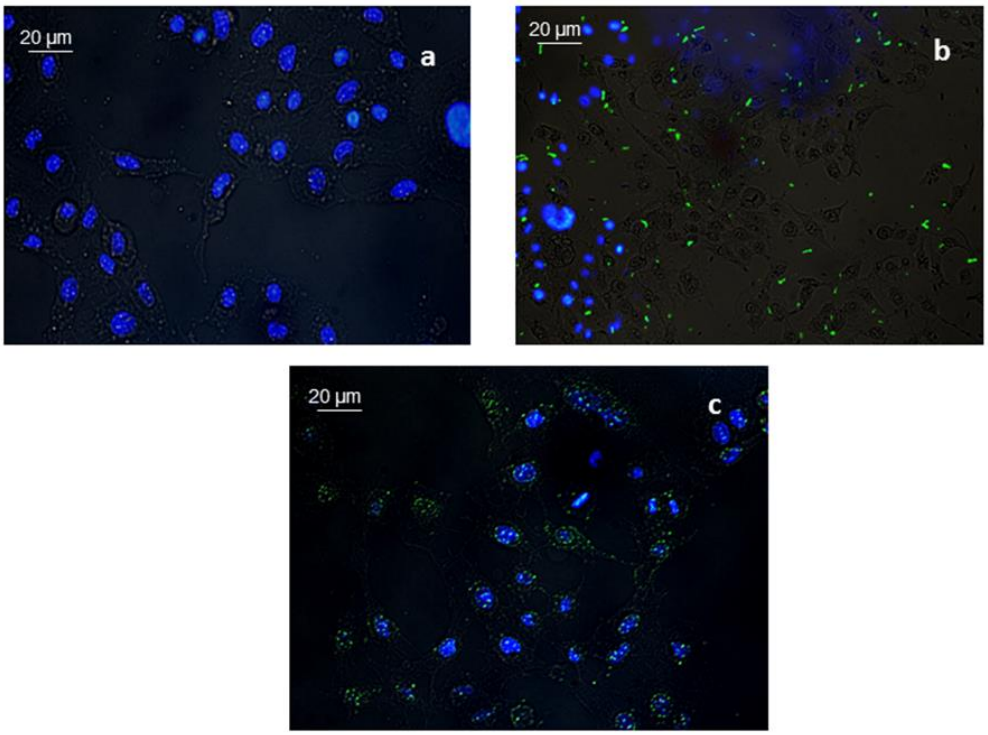

Figure 21. Cell uptake in HeLa cells (a) curcumin (b) curcumin loaded mPEG laurate (c) curcumin loaded mPEG linolenate

4.1.2 Curcumin loaded Pluronic linolenate micelles

4.1.2.1 Synthesis of Pluronic linolenate

Pluronic linolenate was synthesized by Steglich esterification using DCC and DMAP. The reaction scheme is depicted in Figure 22. The IR spectrum of Pluronic linolenate was characterized by principle absorption peaks at 2882 cm^{-1} (C-H aliphatic stretch) and at 1737 cm^{-1} (C=O stretching) [Figure 23]. In the ^{1}H NMR spectra, Pluronic linolenate exhibited the protons of the conjugated double bonds at 6.64, 7.26 and 8.19 ppm. Protons of the methyl group of propylene oxide units were present at 1.13 ppm and protons of the methylene units occurred at 3.6 ppm (Figure 24).

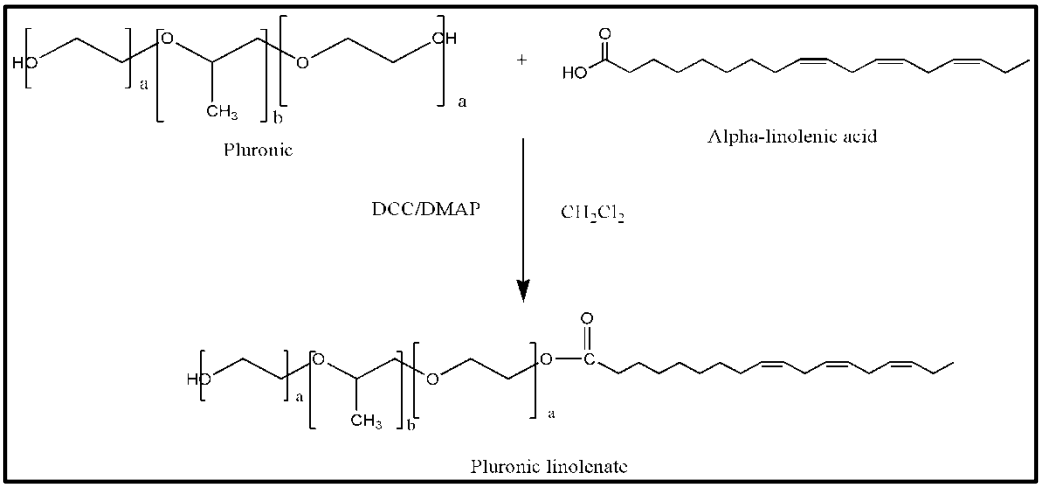

Figure 22. Reaction scheme for the synthesis of Pluronic linolenate

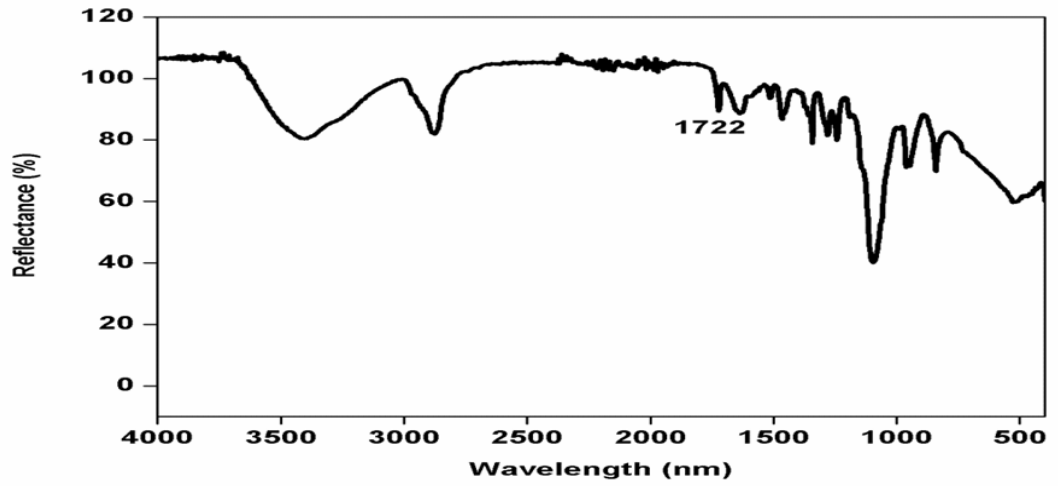

Figure 23. IR spectrum of Pluronic linolenate

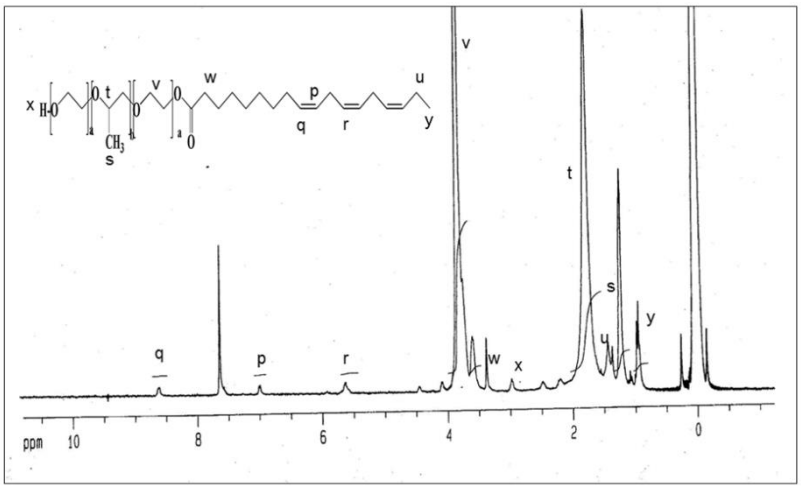

Figure 24. ^{1}H NMR spectrum of Pluronic linolenate

4.1.2.2 Curcumin loaded Pluronic linolenate micelles

4.1.2.2.1 Loading, size and zeta potential determination

Physical incorporation of curcumin into Pluronic linolenate micelles was accomplished through dialysis method. Self-association of the micelles was triggered by the gradual replacement of the organic solvent with water. Hydrophobic curcumin was encapsulated in the hydrophobic core of the micelles. From the DLS experiment, curcumin loaded Pluronic linolenate micelles exhibited a particle size of 167 ± 5 nm compared to the unloaded micelles which had a size of 139 ± 4 nm. However, the actual size of curcumin loaded micelles obtained from TEM analysis was about 60 nm with a range from 60-80 nm (Figure 25). The curcumin loaded and unloaded Pluronic linolenate micelles exhibited negative charge of –17.2 ± 0.4 mV and –14.4 ± 1.5 mV, respectively. Pluronic linolenate micelles exhibited negative charge of –17.2 ± 0.4 mV and –14.4 ± 1.5 mV, respectively. For theoretical loading of 9.09% w/w, an encapsulation efficiency of 89.3 ± 3.2% was obtained in the Pluronic linolenate micelles rendering a loading capacity of 7.9 ± 0.3 % w/w.

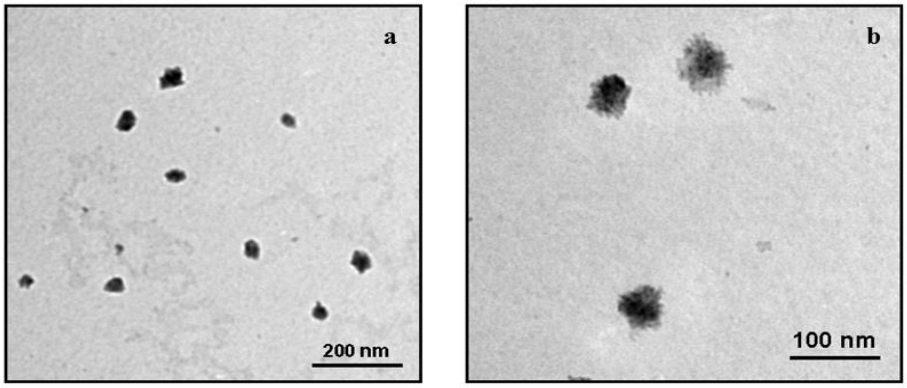

Figure 25. (a) TEM image of curcumin loaded Pluronic linolenate micelles (b) TEM image of the same taken at higher magnification.

4.1.2.2.2 Calculation of Flory-Huggins interaction parameter between curcumin and Pluronic linolenate

Flory-Huggins interaction parameter ($\chi_{sp)}$ determined to assess the compatibility of curcumin with the Pluronic linolenate micellar core. The calculated values of solubility parameters $\delta_{curcumin}$ and $\delta_{Pluronic\ linolenate}$ were calculated as 24.84 and 19.45, respectively. A value of 0.55 was obtained as the interaction parameter ($\chi_{sp)}$ between curcumin and Pluronic linolenate.

4.1.2.2.3 Critical micelle concentration

CMC value was calculated from the point of inflection from the plot showing the relationship between changes in intensity (I_3/I_1) of pyrene with the log [concentration] of micelles and was found to be 0.41mg/ml (Figure 26).

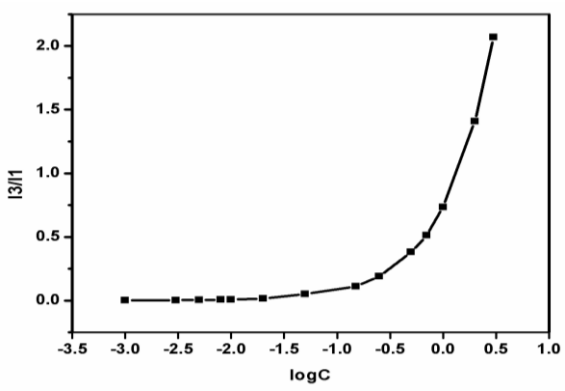

Figure 26. CMC of Pluronic linolenate

4.1.2.2.4 Spectral properties

An enhanced absorption peak of curcumin loaded Pluronic linolenate was obtained at 425 nm (Figure 27). Similar behaviour was also encountered in fluorescence spectra. In addition, curcumin loaded Pluronic linolenate showed a well- defined high intensity blue-shifted fluorescent peak at 540 nm while curcumin showed a broad peak at 570 nm.

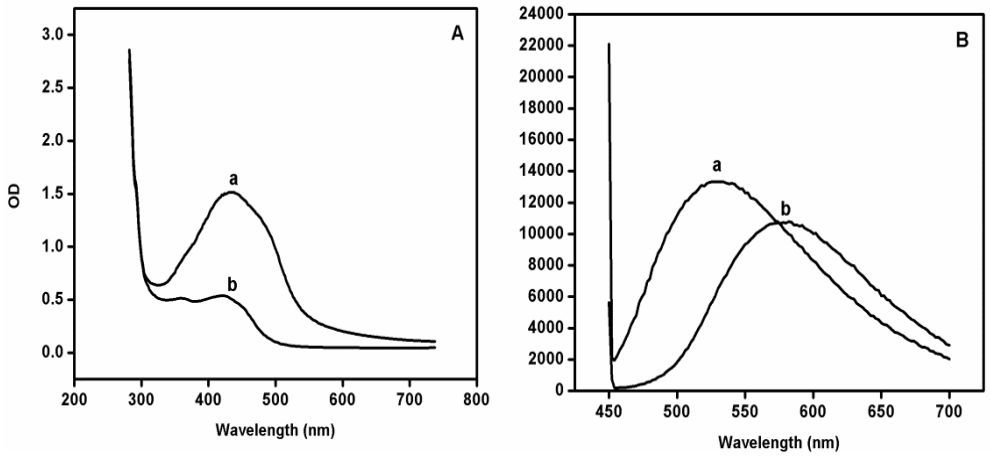

Figure 27. (A) UV-visible spectrum (B) Fluorescence spectrum of curcumin loaded Pluronic linolenate micelles depicted as (a) and free curcumin depicted as (b).

4.1.2.2.5 DSC

The endothermic melting peak of curcumin was observed at 177.2^{o}C. This characteristic peak was not seen in the DSC thermogram of curcumin loaded Pluronic linolenate and only the melting peak of Pluronic linolenate was observed at 51.5^{o}C (Figure 28).

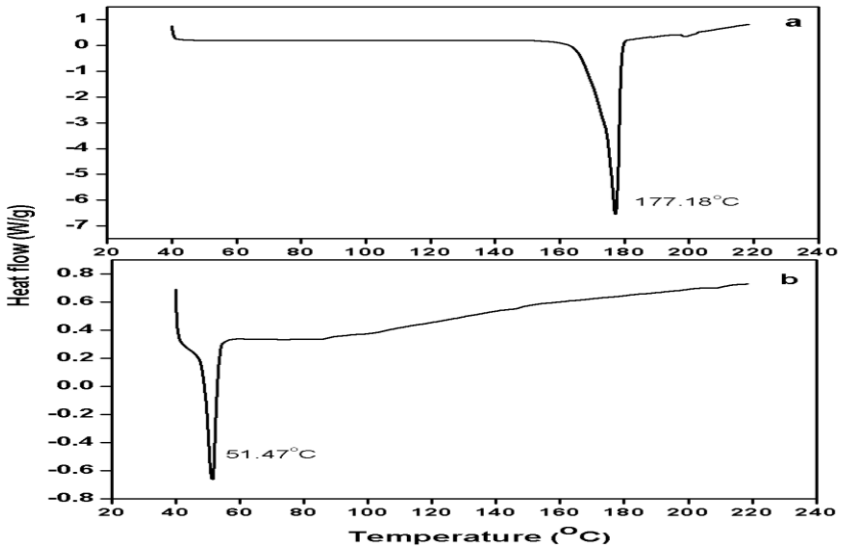

Figure 28. DSC thermogram of (a) free curcumin (b) curcumin loaded Pluronic linolenate

4.1.2.2.6 Stability study

It was observed that the micellar curcumin was completely water soluble compared to native curcumin (Figure 29). We attempted to study the instability and biodegradation of curcumin and micellar curcumin in PBS. Rapid degradation was exhibited by native curcumin. It was noted that only 8% of curcumin remained intact after 8 hours. However, micellar curcumin showed 90% stability under similar conditions.

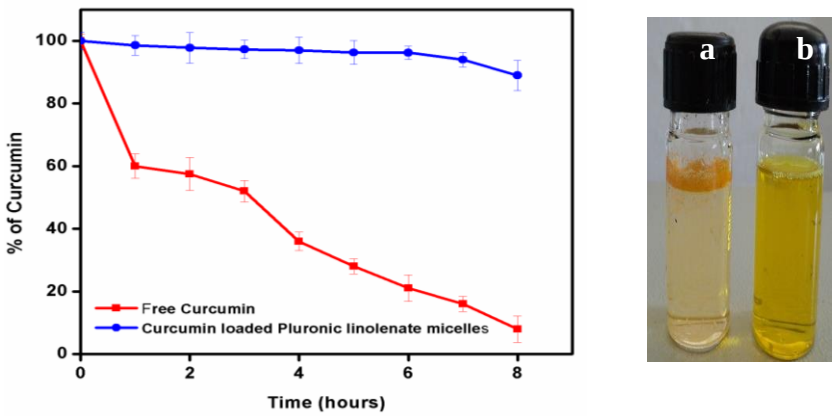

Figure 29. The graph depicts the stability of curcumin in the loaded and free form at pH7.4. The picture on the right shows the solubility of curcumin in aqueous media (a) curcumin (b) curcumin loaded Pluronic linolenate micelles

4.1.2.3 Curcumin release study

The release of curcumin from the core of the Pluronic linolenate micelles was studied in acidic as well as physiological pH (Figure 30). Sustained release of curcumin was observed after 20 hours at both pH. After 72 h, there was about 88% and 73% release at pH 7.4 and pH 4.5, respectively.

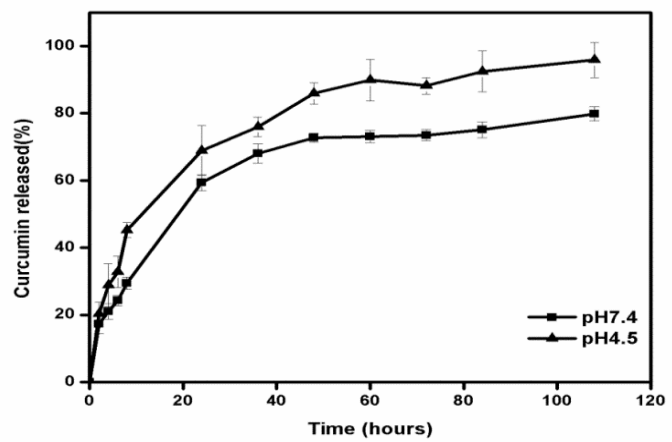

Figure 30. Release of curcumin from Pluronic linolenate micelles at pH 7.4 and pH 4.5

4.1.2.4 Hemocompatibility

The percentage hemolysis of the blank and curcumin loaded micelles was found to be negligible (less than 1 %) which indicated that the synthesized nanoparticles were RBC compatible. Blood compatibility of the loaded micelles was further evaluated from aggregation study. The micrographs of human blood cells and platelets along with normal saline and PEI as controls are shown in Figure 31, Figure 32, Figure 33. No aggregation was detected in RBC, WBC and platelets incubated with the micelles indicating the non-toxic effect of the micelles on normal cells.

4.1.2.4.1 Gel Electrophoresis

The binding extent of plasma proteins on to the Pluronic micelles was examined by performing PAGE (Figure 34). Lanes 2 and 3 corresponded to unloaded and curcumin loaded Pluronic linolenate micelles. There was no inhibition of protein bands and the obtained bands were similar to those of the control placed in lane 1.

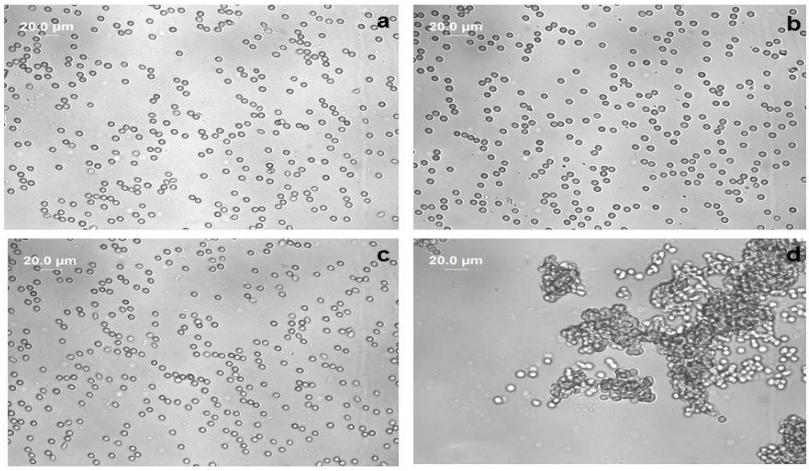

Figure 31. RBC aggregation in (a) saline (b) Pluronic linolenate micelles (c) curcumin loaded Pluronic linolenate micelles (d) PEI

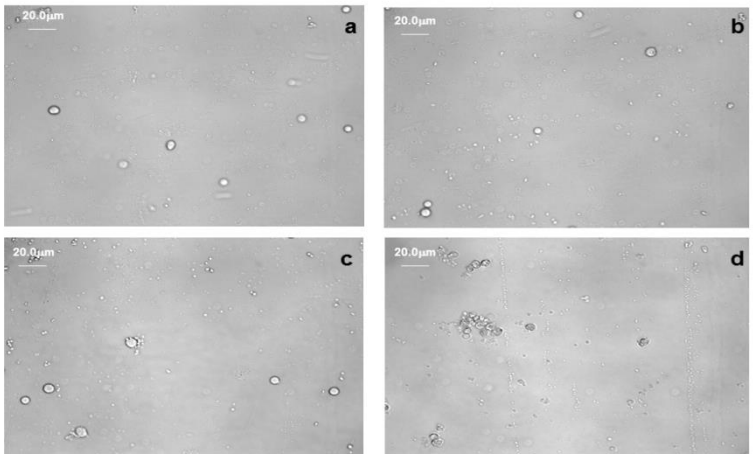

Figure 32. WBC aggregation in (a) saline (b) Pluronic linolenate micelles (c) curcumin loaded Pluronic linolenate micelles (d) PEI

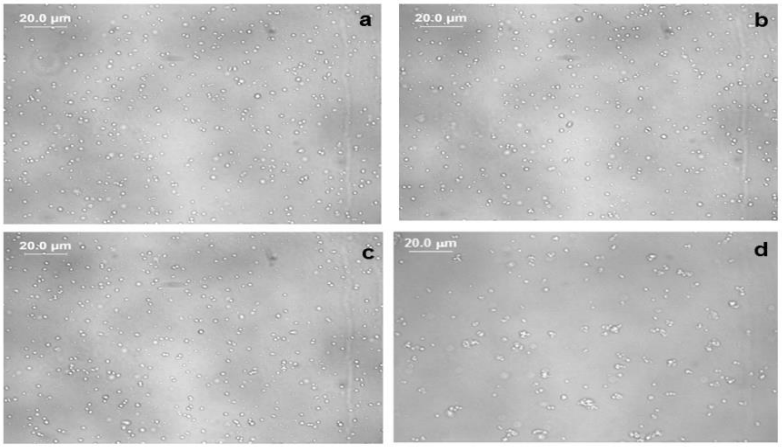

Figure 33. Platelet aggregation in (a) saline (b) Pluronic linolenate micelles (c) curcumin loaded Pluronic linolenate micelles (d) PEI

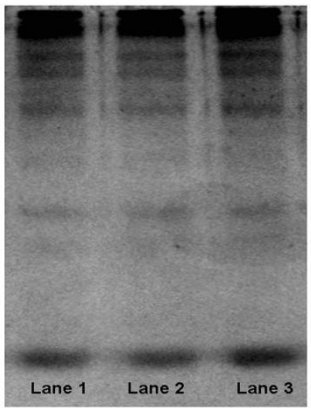

Figure 34. PAGE showing the interactions of micelles with the plasma proteins. Lane 2 and 3 corresponds to empty and curcumin loaded Pluronic linolenate micelles , respectively. Lane 1 is the control performed with saline.

4.1.2.5 In vitro cytotoxicity study

4.1.2.5.1 MTT assay

MTT assay was performed on the micelles to evaluate its cytotoxicity on Caco2 and L929 cells. Reduction of cell viability of Caco2 cells was observed with empty Pluronic linolenate micelles (Figure 35a). However, it was seen that modified Pluronic did not induce any reduction in cell viability of Caco2 cells. Dose dependent toxicity was observed with curcumin and curcumin loaded micelles (Figure 35 b).

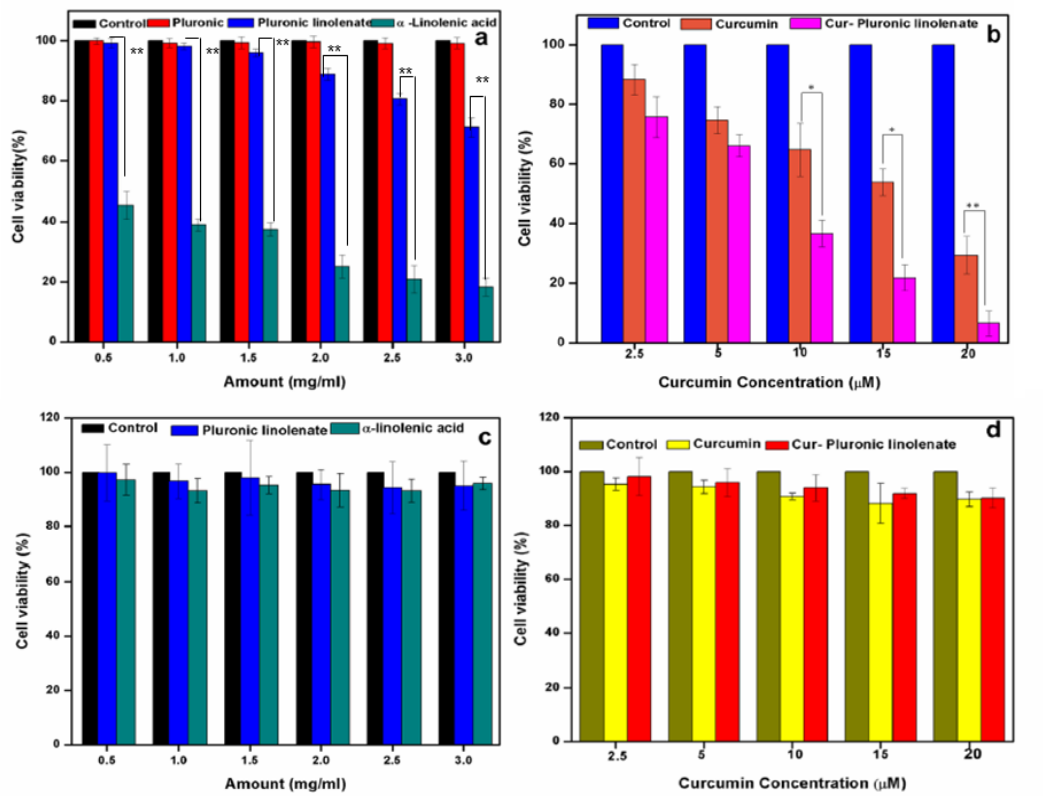

Figure 35. Cytotoxicity study of empty Pluronic linolenate micelles on Caco2 cells. Values reported are mean ± SD, n=3 (b) Cytotoxicity study of curcumin loaded Pluronic linolenate micelles in Caco2 cells. Significant difference was observed between curcumin and curcumin-loaded micelles for all concentrations. Statistically significant difference ($p<0.05$) is denoted by* and ($p< 0.01$) is denoted by **.Values exhibited are mean±SD, n=3.

Curcumin loaded micelles and empty micelles did not create any cytotoxicity on L929 cells (Figure 35 c and d). In addition, we observed that linolenic acid induced dose depend cytotoxicity on Caco2 cells and did not have any cytotoxic effect on L929 cells. It was observed in our MTT assay that almost 90% L929 cells were viable upon treatment with the loaded and unloaded micelles and this non-toxicity was in alignment with the hemolysis and aggregation studies.

4.1.2.5.2 Live dead assay

This assay employs mainly two dyes to infer intracellular esterase activity and plasma membrane integrity. While calcein, a polyanionic dye, is retained within live cells, ethidium bromide homodimer dye enters cells through damaged membranes and bind to nucleic acids. Calcein AM produces green fluorescence (excitation, 488 nm; emission, 507 nm) in live cells and ethidium homodimer produces a red fluorescence in dead cells (excitation, 530 nm; emission, 595 nm).

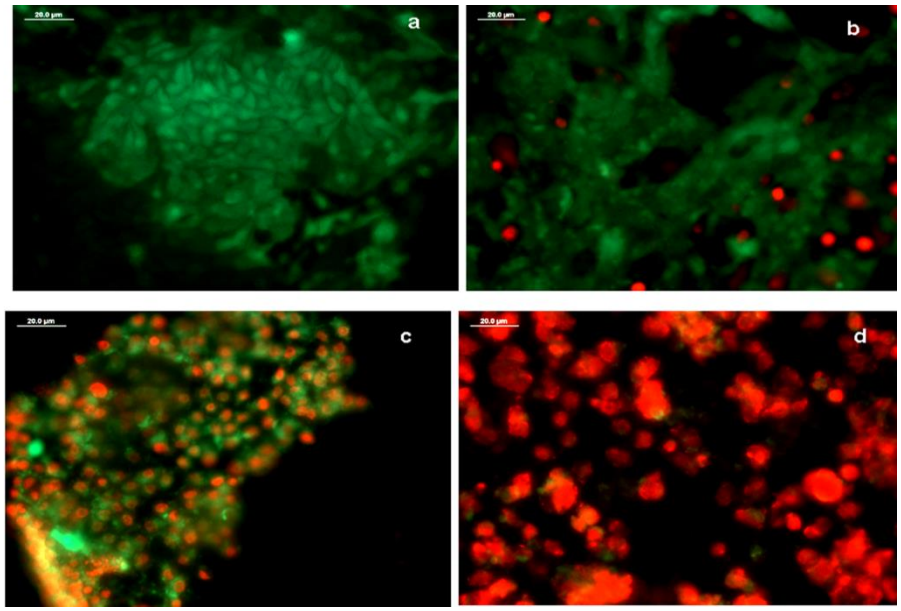

Figure 36. Live dead assay performed on Caco2 cells (a)) control (b) native curcumin (c) Pluronic linolenate micelles (d) curcumin loaded Pluronic linolenate micelles.

The assay performed was a qualitative study to visualize the cytotoxic effect of the curcumin loaded micelles compared to the free curcumin (Figure 36).The red fluorescence was observed in cells incubated with both Pluronic linolenate micelles and curcumin loaded micelles and the cell death more prominent with the loaded micelles.

4.1.2.5.3 Cellular uptake of Pluronic linolenate micelles

Curcumin, being fluorescent, has the advantage to be traced inside cells. Fluorescence microscope images confirmed cellular internalization of the curcumin loaded Pluronic linolenate micelles. Curcumin loaded micelles showed enhanced intracellular green fluorescence compared to the free curcumin (indicated by white arrows in Figure 37). Entry of free curcumin was not prominent in the cells.

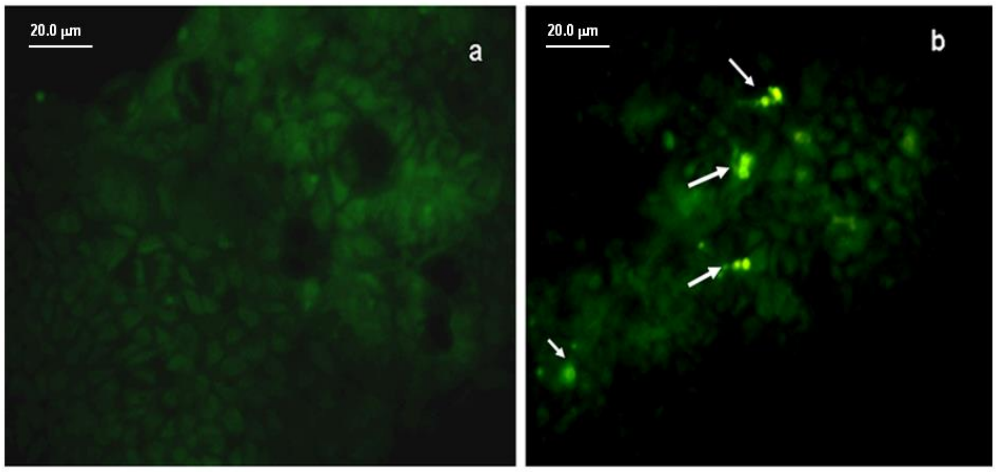

Figure 37. Cellular internalization in Caco2 cells (a) free curcumin (b) curcumin loaded Pluronic linolenate micelles.

4.2 Curcumin loaded micelles based on Pluronic/PCL co polymer

4.2.1 Curcumin loaded Pluronic /PCL micelles

4.2.1.1 Synthesis and characterization of Pluronic/PCL co polymer

Stannous octoate mediated ring- opening polymerization of ε-caprolactone and Pluronic afforded the formation of Pluronic/PCL block copolymer. Figure 38 represents the reaction scheme for the synthesis. In the IR spectrum, apart from bands at 2943 and 2865 cm^{-1}, a strong carbonyl band at 1736 cm^{-1} indicated the formation of Pluronic/PCL block copolymer (Figure 39).

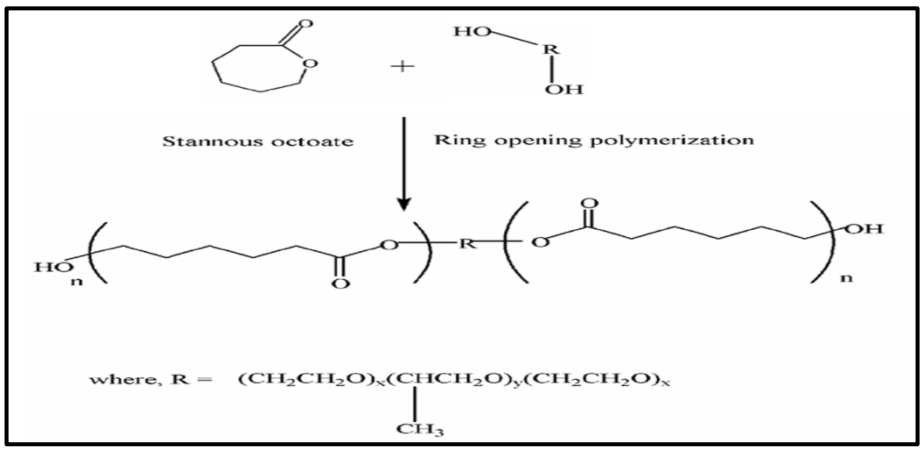

Figure 38. Reaction scheme for the ring opening polymerization of ε−caprolactone and Pluronic using stannous octoate as catalyst.

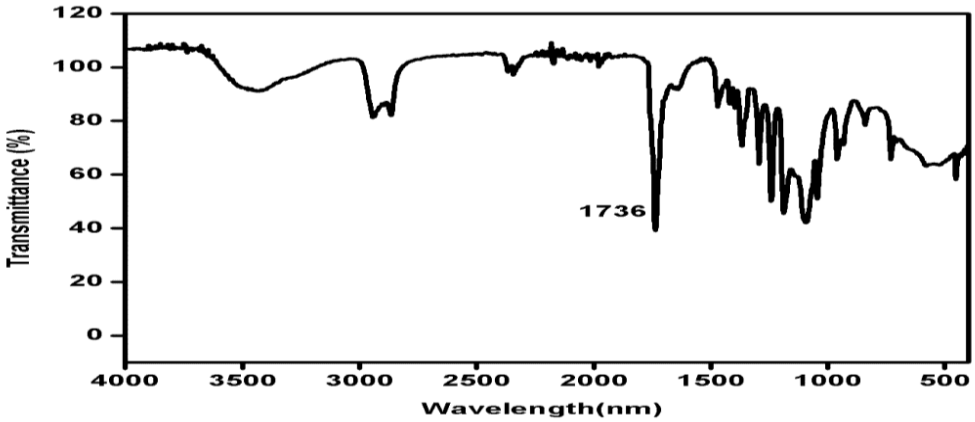

Figure 39. IR spectrum of Pluronic/PCL copolymer

^{1}H NMR spectra showed a sharp singlet at ~3.63 ppm due to the protons of CH_2CH_2 units of PEO. The doublet at 1.13 ppm corresponded to CH_3 protons in PPO. CH and CH_2 units of PPO were depicted by the peaks at ~3.39 and 3.5 ppm. Two intense triplets at 4.05 and 2.30 ppm were observed in addition to the multiplets at ~ 1.4 and 1. 6 ppm which were attributed to the PCL block (Figure 40). The average molecular weight (Mn) of the co-polymer , calculated using the ^{1}H NMR data and applying the Equations 7 and 8, was 28201 g/mol. L_{PCL} in Pluronic/PCL was calculated as 68.34. The molecular weight obtained from GPC was 26663 g/mol with a polydispersity index of 1.66.

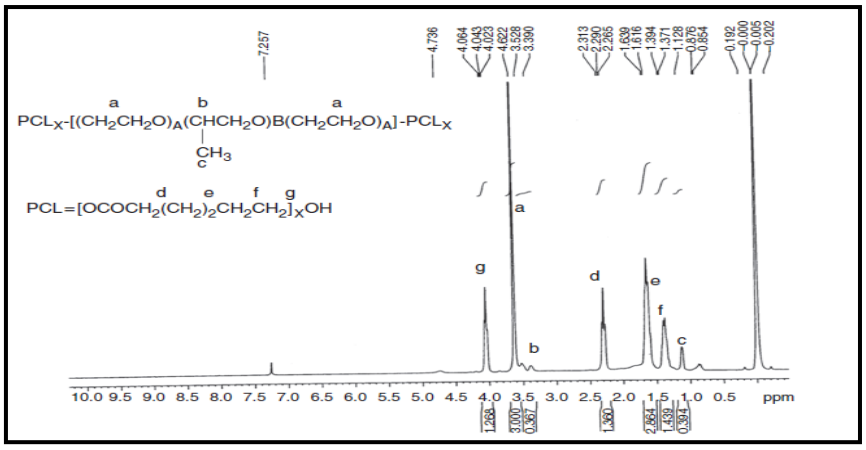

Figure 40. ^{1}H NMR spectrum of Pluronic/PCL copolymer

4.2.1.2 Critical micelle concentration

CMC value was determined from the point of inflection from the plot between the ratio of intensity (I_3/I_1) of pyrene with the log [concentration] of micelles. The CMC of Pluronic/PCL was calculated as 0.195 mg/ml.

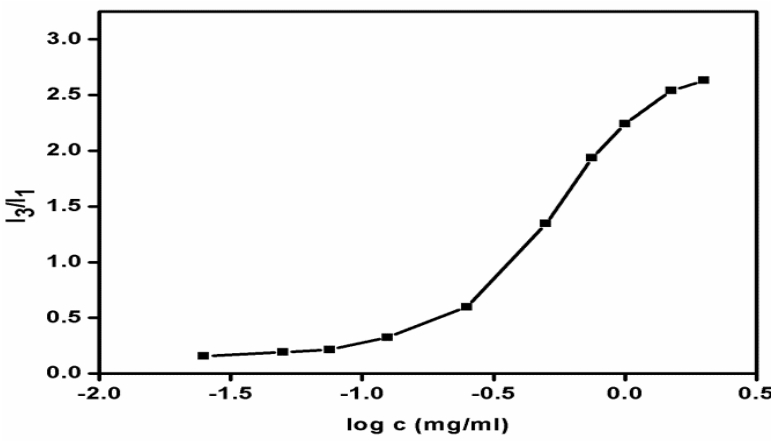

Figure 41. CMC of Pluronic/PCL

4.2.1.3 Preparation of curcumin loaded Pluronic /PCL micelles

4.2.1.3.1 Loading and encapsulation

Curcumin loading in Pluronic/PCL micelles was carried out at 9.09%, 11.76% and 14.28% w/w which afforded an encapsulation efficiency of 96 ± 1, 87 ± 2 and 72 ± 4 % respectively. This corresponded to an actual loading of 8.78 ± 0.09, 10.2 ± 0.3 and 10.3 ± 0.6 % w/w, respectively. Precipitation of curcumin was observed when 16.66% w/w loading was performed and hence loading of 10.2 ± 0.3 % w/w was chosen as the optimized loading efficiency for further *in vitro* studies.

4.2.1.3.2 Curcumin compatibility with Pluronic/PCL core

The compatibility of curcumin with the Pluronic/PCL core was evaluated by determining χ_{sp}, the Flory-Huggins interaction parameter. In addition to the group contributions of the functional moieties of curcumin, atoms and groups of Pluronic and PCL were employed in the calculations. The calculated values of solubility

parameters $\delta_{curcumin}$, $\delta_{Pluronic/PCL}$ were 24.8 and 23.15, respectively. The interaction parameter (χ_{sp}), was calculated as 0.172 for Pluronic/PCL core .

4.2.1.3.3 Determination of particle size and zeta potential of the micelles

The particle size and zeta potential of curcumin loaded Pluronic/PCL micelles were determined by DLS and are tabulated in Table 2. Figure 42 depicts the TEM image of curcumin loaded Pluronic/PCL (10.2% w/w).

Theoretical loading (% w/w)	Actual loading (% w/w)	Particle size (nm)	Zeta potential (mV)
0	–	59.2 ± 0.6	–14.6 ± 1.2
9.09	8.78 ± 0.09	88.4 ± 0.9	–16.5 ± 0.2
11.75	10.2 ± 0.3	159 ± 3	–15.4 ± 0.5
14.21	10.3 ± 0.6	195 ± 7	–17.6 ± 0.4

Table 2. Characteristics of curcumin loaded Pluronic/PCL micelles

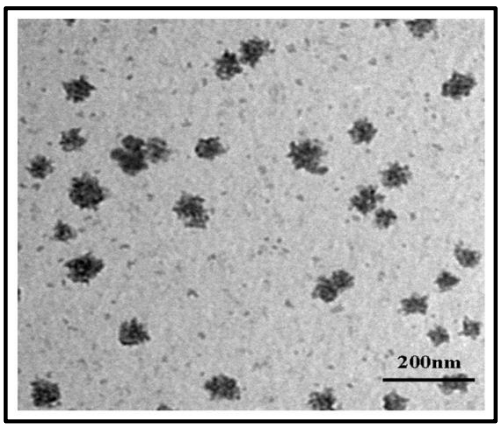

Figure 42. TEM image of curcumin loaded Pluronic/PCL micelles.

4.2.1.4 Differential scanning calorimetry

The physical status of curcumin encapsulated in the polymeric micelles was investigated by DSC. Free curcumin exhibited an endothermic melting peak at 177.2^{o}C implying its crystalline state .This peak was absent in the thermogram of curcumin loaded Pluronic/PCL copolymers which only exhibited the characteristic melting peaks of Pluronic/PCL around 58^{o}C (Figure 43).

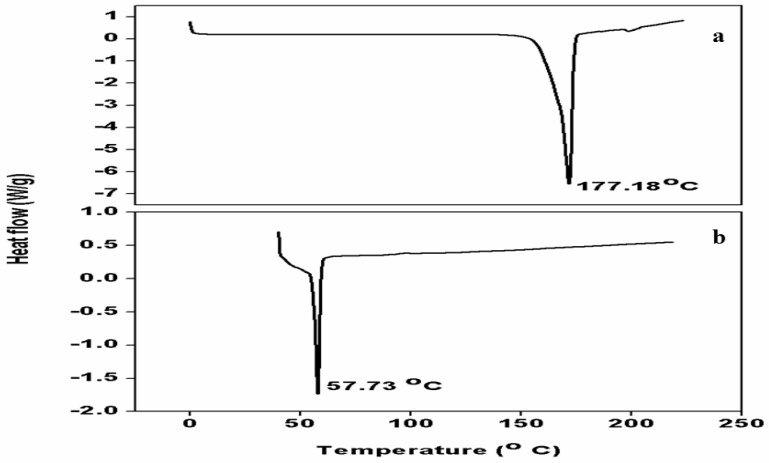

Figure 43. DSC thermogram of (a) curcumin (b) curcumin loaded Pluronic/PCL

4.2.1.5 Spectral characterization

Absorbance spectra of free curcumin were observed at 425 nm and curcumin loaded Pluronic/PCL exhibited strong and intense absorption band at the same wavelength. (Figure 44).The fluorescence spectra also exhibited similar behavior of encapsulated curcumin showing higher intensity. The fluorescence peak of curcumin was seen around 550 nm. There was, however, a well-defined blue shift from 550 nm to 525 nm regarding the fluorescence peak of encapsulated curcumin.

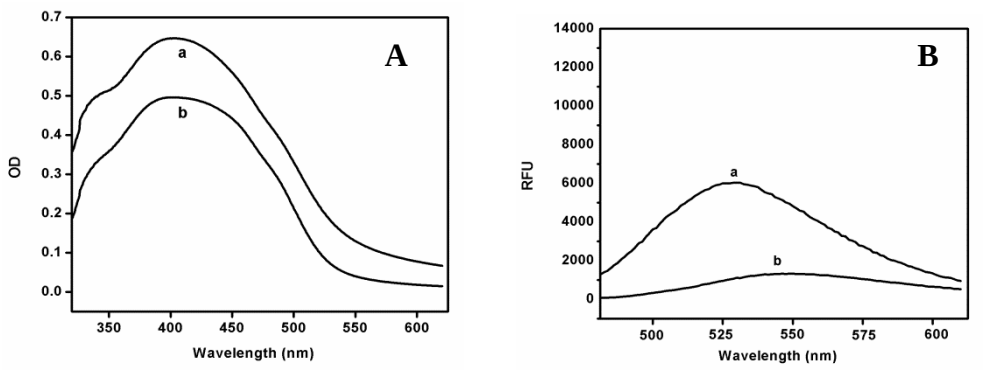

Figure 44. (A) UV-visible spectrum (B) Fluorescence spectrum of (a) curcumin loaded Pluronic/PCL and (b) curcumin

4.2.1.6 Blood compatibility

Negligible percentage (less than 1 %) of hemolysis was observed in the case of empty and curcumin loaded micelles which indicated that the synthesized nanoparticles were compatible with the erythrocytes (Table 3).

Sample	Hemolysis (%)
1. Pluronic/PCL micelles	0.072±0.03
2. Curcumin loaded Pluronic/PCL	0.077±0.023
3. Saline (negative control)	0
4. Distilled water (positive control)	100

Table 3. Hemolysis results

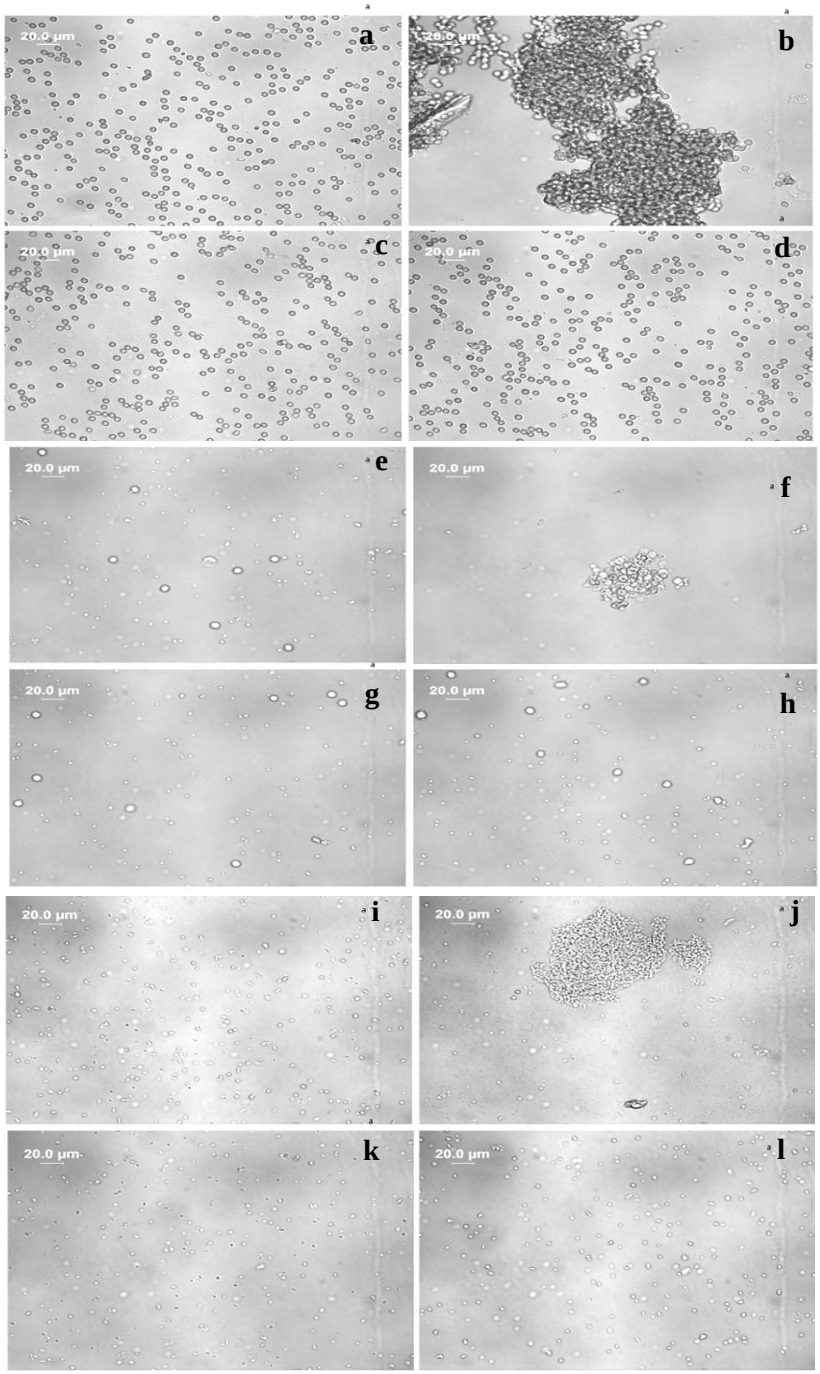

Figure 45. RBC aggregation in (a) saline (b) PEI (c) Pluronic/PCL micelles (d) curcumin loaded Pluronic/PCL micelles. WBC aggregation in (e) saline (f) PEI (g) Pluronic/PCL micelles (h) curcumin loaded Pluronic/PCL micelles. Platelet aggregation in (i) saline (j) PEI (k) Pluronic/PCL micelles (l) curcumin loaded Pluronic/PCL micelles.

Aggregation was not detected in RBC, WBC and platelets incubated with the micelles. The micrographs of human blood cells (RBC, WBC and platelets) upon interaction with the loaded and unloaded micelles along with the controls are shown (Figure 45). It was observed that the micelles did not promote aggregation like the positive control, PEI.

4.2.1.7 Gel Electrophoresis

The binding extent of plasma proteins with Pluronic/PCL micelles was examined by performing native PAGE (Figure 46). Lane 2 and 3 corresponded to Pluronic/PCL and curcumin loaded Pluronic/PCL, respectively. It was observed that the protein bands corresponding to most of the low molecular weight globular proteins were present in all the polymer- plasma samples. The protein bands were similar to the band obtained in lane 1 which corresponded to normal saline indicating that the micelles did not bind with the plasma proteins.

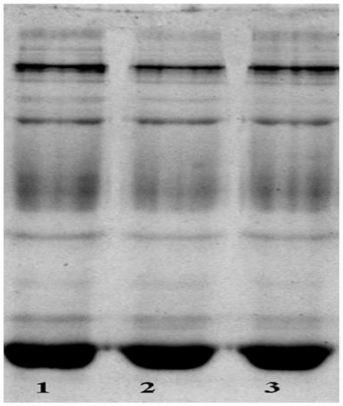

Figure 46. PAGE showing the interactions of curcumin loaded Pluronic/PCL micelles with the plasma proteins.

4.2.1.8 Curcumin release study

The curcumin release profile from the Pluronic/PCL micelles at acidic as well as physiological pH is pictured in Figure 47. After 72 hours, about 56% and 85% of curcumin were released from the micelles at pH 7.4 and pH 4.5, respectively.

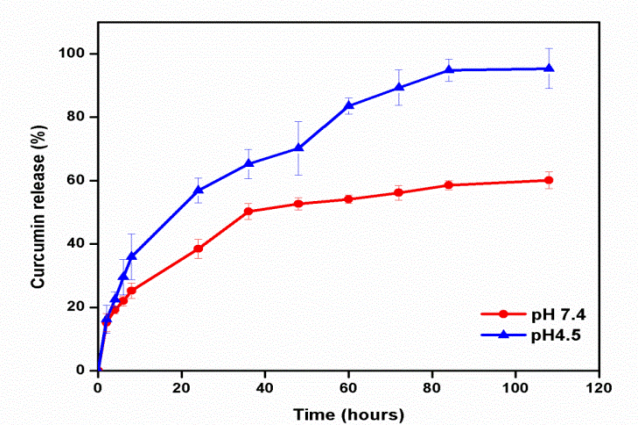

Figure 47. Curcumin release from Pluronic/PCL micelles

4.2.1.9 Stability study

Free curcumin was found to be sparingly soluble in aqueous solution with formation of visible undissolved microscopic flakes compared to the curcumin loaded micellar solution (Figure 48).

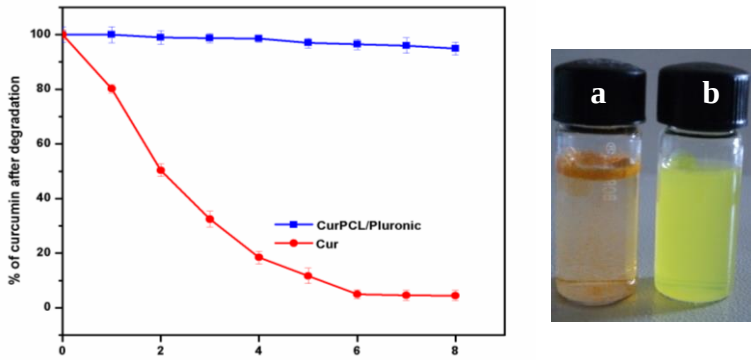

Figure 48. Stability of curcumin in the micelles. The picture on the right shows the solubility of curcumin loaded Pluronic/PCL micelles (b) compared to free curcumin (a).

The biodegradation and stability of curcumin was studied by incubating both free and encapsulated curcumin in PBS and quantifying spectrophotometrically. It was observed that only 5% of free curcumin remained intact after an incubation of 8 hours where as 94% of curcumin encapsulated in the Pluronic/PCL micelles remained intact (Figure 48).

4.2.1.10 In vitro study

4.2.1.10.1 Cytotoxicity study- MTT assay

MTT assay was performed on the empty and curcumin loaded micelles. It was observed that Pluronic/PCL micelles did not exhibit any reduction in cell viability. 100% cell viability was encountered at 3 mg/ml copolymer concentration (Figure 49 a). Less than 60% cells were viable at a curcumin concentration of 10 μM in the curcumin loaded micelles (Figure 49 b).

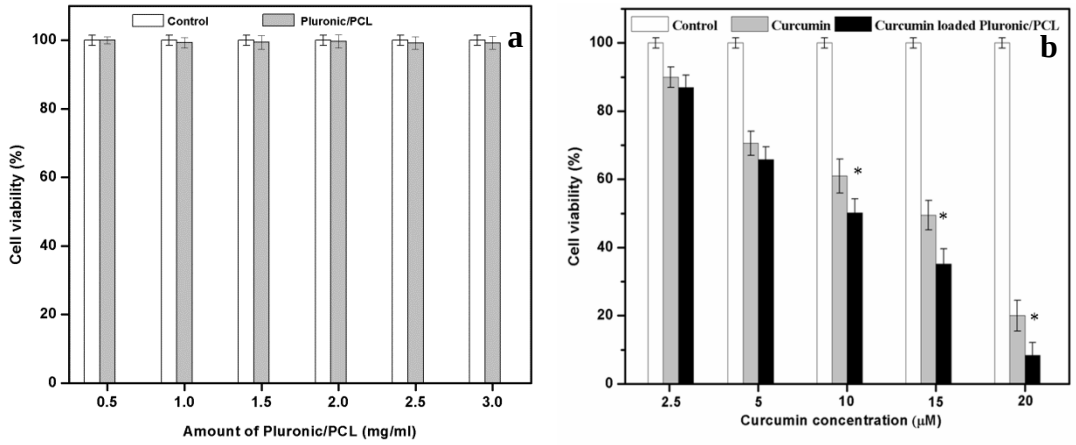

Figure 49. Cytotoxicity study of (a) empty Pluronic/PCL micelles on Caco2 cells (b) curcumin loaded Pluronic/PCL micelles compared to native curcumin.

4.2.1.10.2 Cell uptake

We confirmed the cellular internalization of curcumin loaded Pluronic/PCL micelles by fluorescence microscopy in Caco2 cells. The empty Pluronic/PCL micelles did not exhibit any fluorescence Curcumin loaded micelles showed intracellular green fluorescence proving that the Caco2 cells efficiently took up the micelles compared to the free curcumin (Figure 50). However, entry of free curcumin was not prominent in the cells.

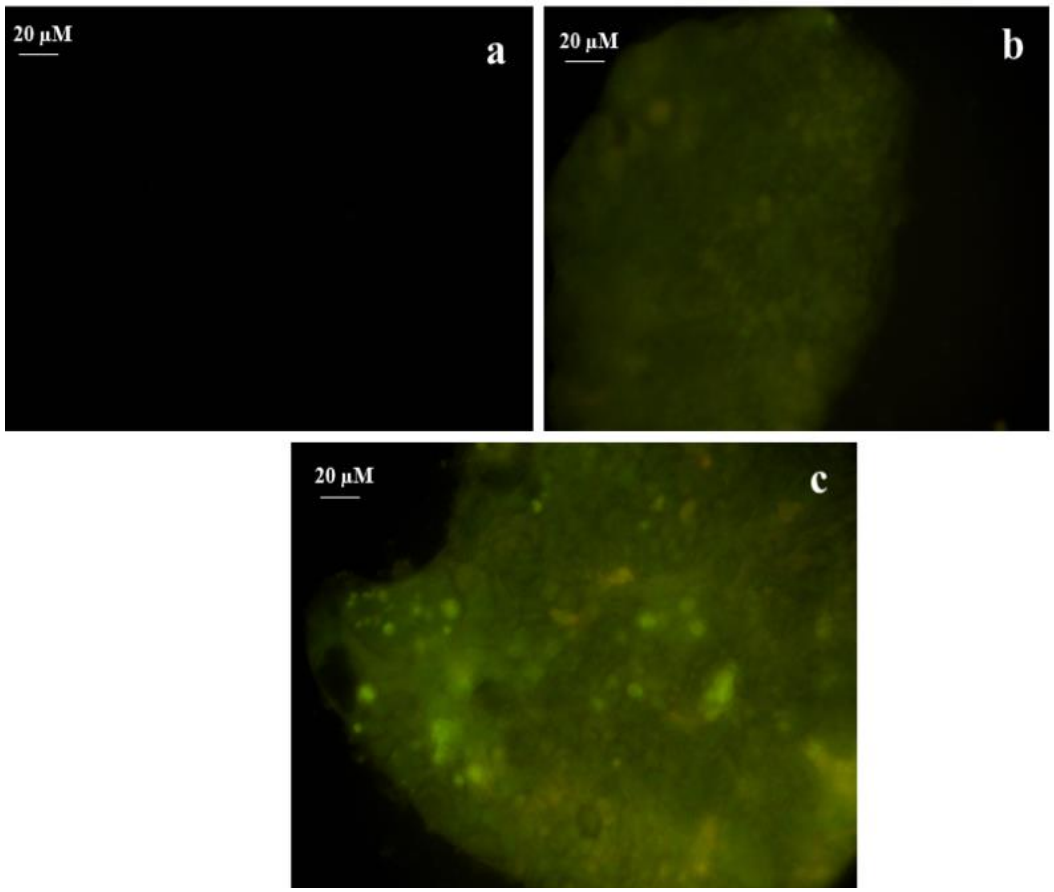

Figure 50. Cellular uptake in Caco 2 cells (a) empty Pluronic/PCL micelles (b) curcumin(c) curcumin loaded Pluronic/PCL micelles

4.2.2 Curcumin loaded calix [4] arene conjugated Pluronic /PCL micelles

4.2.2.1 Synthesis and characterization of calix arene conjugated Pluronic / PCL (CX-Pluronic/PCL)

Under the catalyzing effect of a weak base, Pluronic/PCL-OTs chains were reacted with the hydroxyl groups at contraposition of lower rim of calix [4]arene to afford calix arene conjugated Pluronic/PCL (Figure 51). From the IR spectrum it was observed that the OH peak of CX-Pluronic/PCL at 3122 cm^{-1} disappeared. At 2831 cm^{-1}, the symmetric stretch of CH_2 was encountered. Peaks at 1640, 1466, 1341, 1279, 1241, 1103 cm^{-1} corresponded to the asymmetric stretching of C-O-C. The aromatic peaks of calix arene were observed at 959 and 841 cm^{-1} (Figure 52).

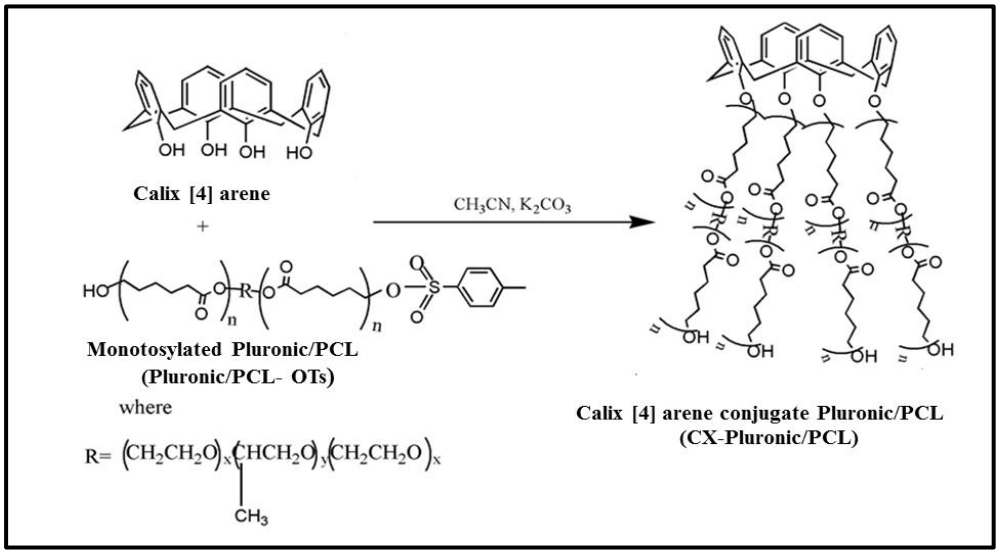

Figure 51. Reaction scheme of synthesis of CX-Pluronic/PCL

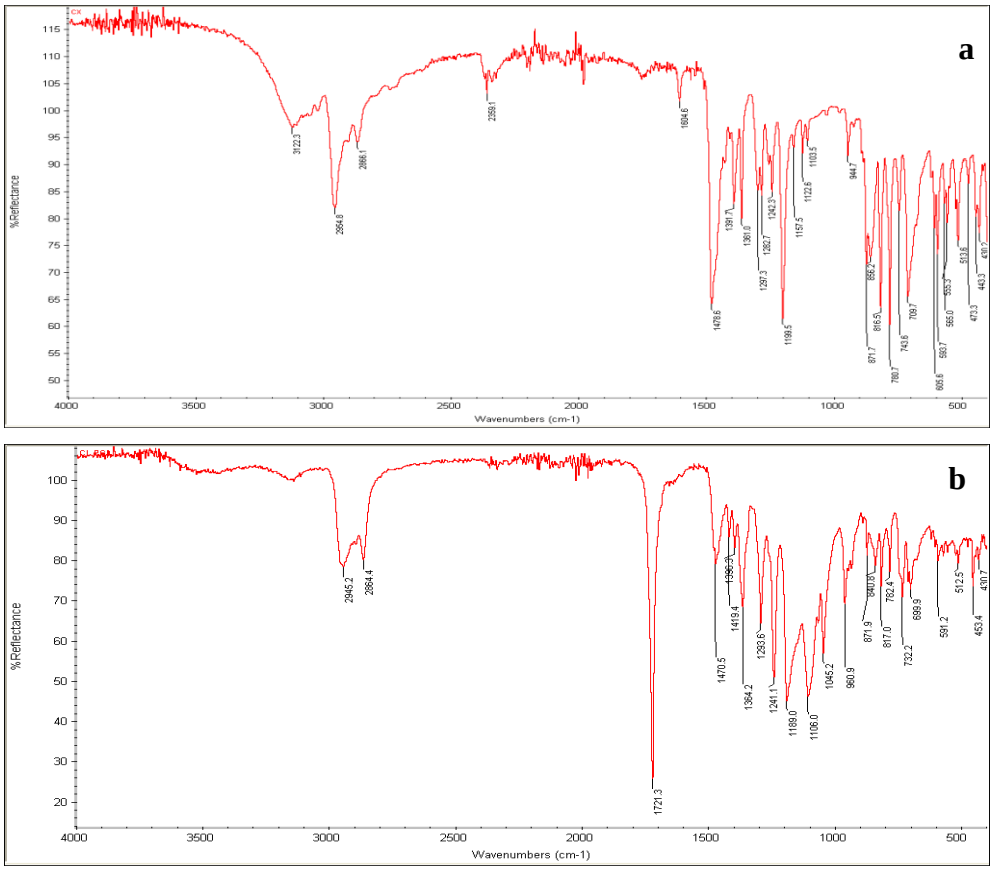

Figure 52. IR spectrum (a) calix[4]arene (b) calix[4]arene conjugated Pluronic/PCL.

4.2.2.2 Preparation of curcumin loaded CX-Pluronic/PCL micelles

4.2.2.2.1 Loading and encapsulation

Curcumin loaded CX-Pluronic/PCL micelles were prepared by dialysis method. CX-Pluronic/PCL was capable of accommodating curcumin in its hydrophobic cavity by host-guest interaction and the self-assembling of these host-guest complex lead to the formation of supra-molecular polymeric micelles (Figure 53). For a theoretical loading of 20% (w/w) actual loading of 17.6 ± 1.2% w/w was obtained which corresponded to an encapsulation efficiency of 78.2 ± 4.4%.

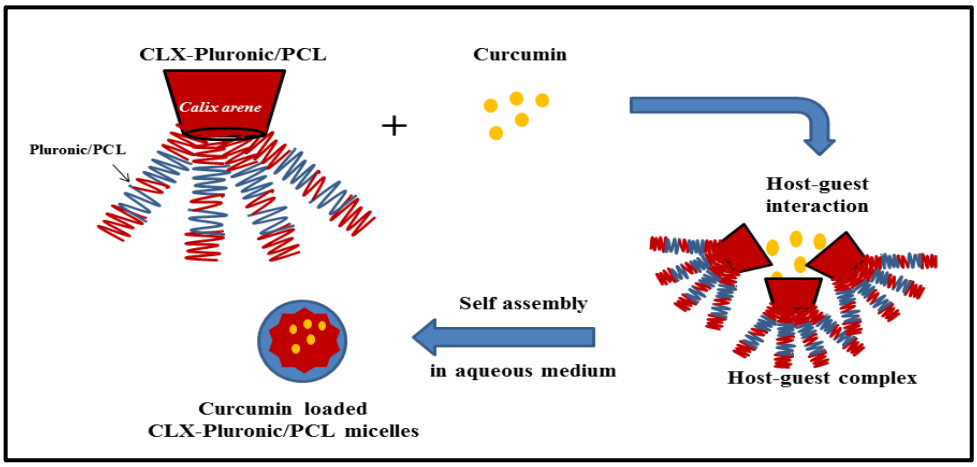

Figure 53. Schematic representation of self-assembly of curcumin loaded CX-Pluronic/PCL in aqueous medium

4.2.2.2.2 Determination of size and zeta potential

Curcumin loaded CX-Pluronic/PCL micelles exhibited a particle size of 230 ± 9 nm and the zeta potential of -26.1 ± 3.2 mV (Figure 54). TEM measurements indicated the size of curcumin loaded CX-Pluronic/PCL micelles to be in the range of 110-130 nm.

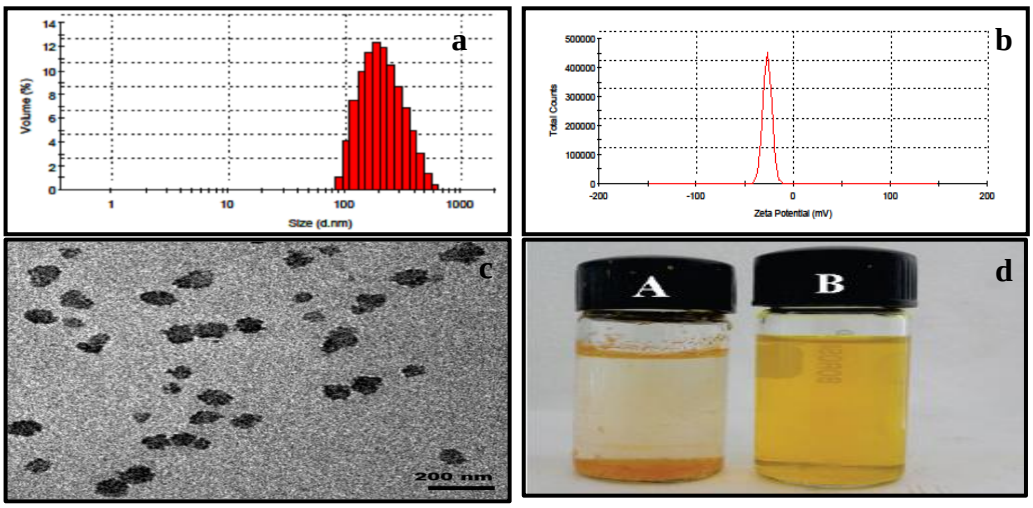

Figure 54 (a) Size of curcumin loaded CX-Pluronic/PCL by DLS (b) Zeta potential of curcumin loaded CX-Pluronic/PCL(c) TEM image of CX-Pluronic/PCL (d) Picture showing the solubility of (A) curcumin (B) curcumin loaded CX-Pluronic/PCL in aqueous medium

4.2.2.2.3 Compatibility of curcumin with CX-Pluronic/PCL core

The compatibility of curcumin with the CX-Pluronic/PCL core was understood from calculating the χ_{sp} , the Flory-Huggins interaction parameter. The calculated values of solubility parameters $\delta_{curcumin}$ and $\delta_{CX\text{-}Pluronic/PCL}$ were 24.8 and 32.67. The value obtained for the interaction parameter (χ_{sp}) was – 0.799 with respect to CX-Pluronic/PCL core.

4.2.2.2.4 Critical micelle concentration

Critical micelle concentration of CX-Pluronic /PCL was determined by plotting the intensity ratio of third and first peak of pyrene as a function of micelle concentration. The CMC calculated for CX-Pluronic/PCL was found to be 0.013 mg/ml (Figure 55).

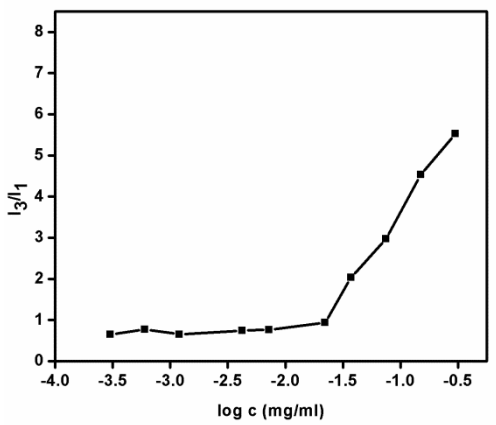

Figure 55. CMC of CX-Pluronic/PCL

4.2.2.3 Spectral Characterization

The CX-Pluronic/PCL micelle-encapsulated curcumin showed distinct spectral properties (Figure 56). Curcumin exhibited absorption with a peak around 425 nm. Absorption intensity of encapsulated curcumin was found to increase sharply. Similar behavior was observed in the fluorescence spectra. Curcumin showed a weak

broad peak at 550 nm, whereas the micelle-loaded curcumin exhibited a well-defined blue-shifted fluorescent peak at 520 nm with high intensity.

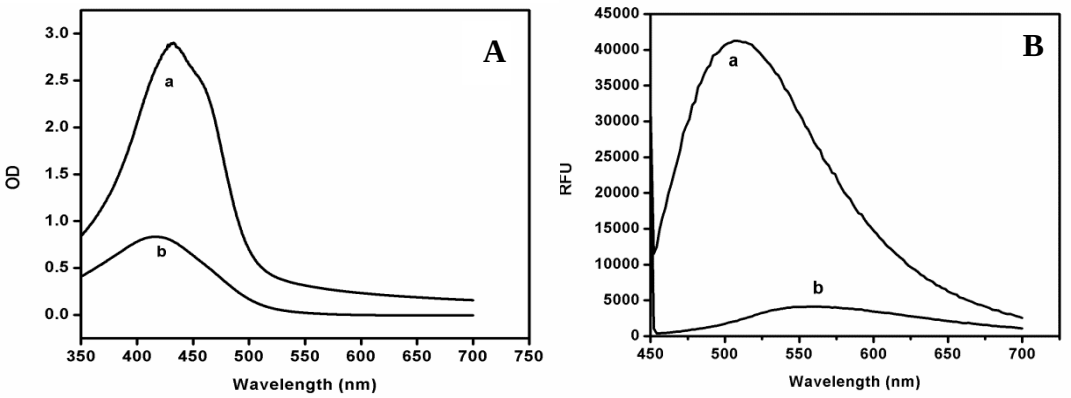

Figure 56. (A) UV-visible spectrum (B) Fluorescence spectrum of (a) curcumin loaded CX-Pluronic/PCL micelles and (b) curcumin

4.2.2.4 Blood compatibility

Less than 1% hemolysis was observed in the case of empty and curcumin loaded micelles which indicated that the synthesized micelles were compatible with the erythrocytes and did not induce lysis as the positive control (Figure 57). The blood compatibility of the micelles was further visually revealed through aggregation studies. It was seen that the micelles did not cause any aggregation of the blood cells.

4.2.2.5 Curcumin release study

At pH 7.4, it was noted that there was decreased release of curcumin. About 35% was released after 72 hours. However, it was observed that there was rapid release of curcumin at acidic pH with about 92% released after a span of 72 hours (Figure 58).

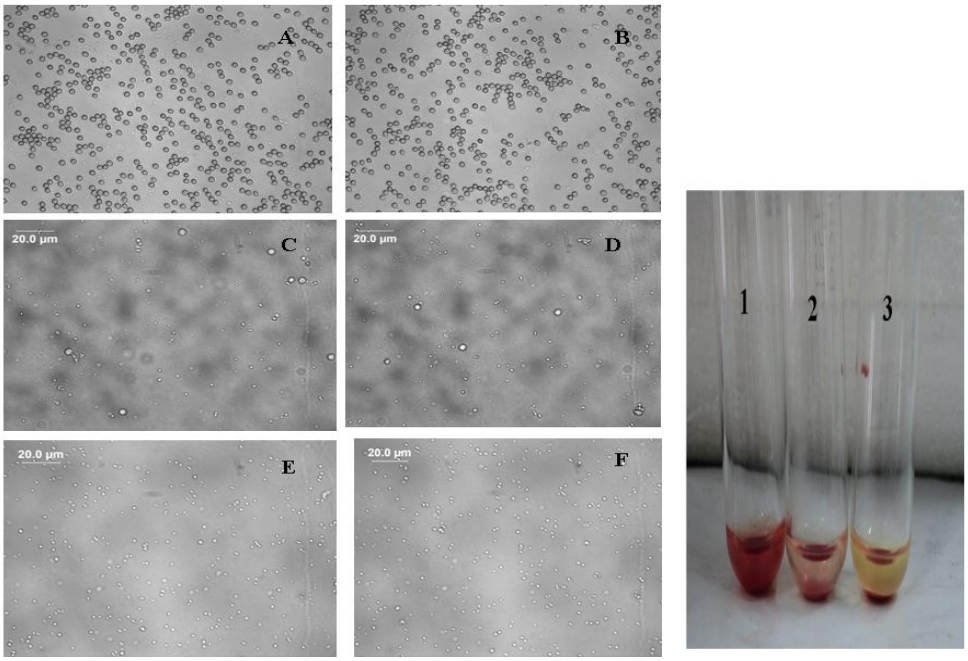

Figure 57. RBC aggregation in (A) saline (B) Cur CX-Pluronic/PCL micelles; WBC aggregation in (C)) saline (D) Cur CX-Pluronic/PCL micelles; Platelet aggregation in (E) saline (F) Cur CX-Pluronic/PCL micelles. Picture on the right shows the hemolysis study (1) positive control (2) negative control (3) Curcumin loaded CX-Pluronic/PCL micelles.

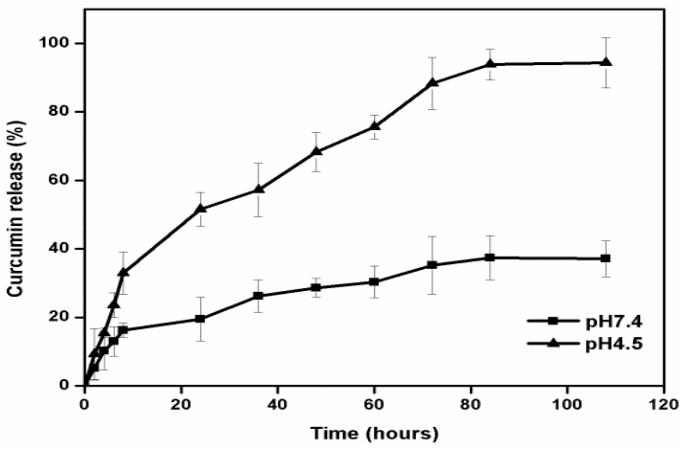

Figure 58. Release of curcumin from CX-Pluronic/PCL micelles.

4.2.2.6 In vitro studies

4.2.2.6.1 Cytotoxicity study- MTT assay

MTT assay was performed on the empty and curcumin loaded CX-Pluronic/PCL micelles. It was observed that CX-Pluronic/PCL micelles did not exhibit any toxicity which was in accordance with the hemolytic study (Figure 59). Curcumin loaded CX-Pluronic/PCL micelles exhibited enhanced cytotoxicity in cancer cells compared to curcumin in free form. At a curcumin concentration of 10 μM in the curcumin loaded micelles, less than 60% cells were viable.

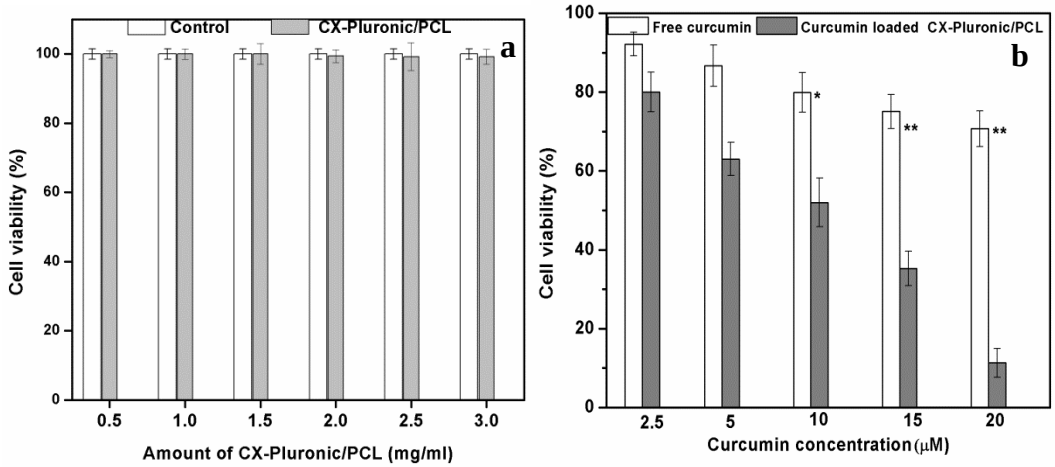

Figure 59. Cytotoxicity on C6 glioma cells (a) empty micelles (b) curcumin loaded CX-Pluronic/PCL micelles

4.2.2.6.2 Cellular internalization in C6 glioma cells

Curcumin loaded CX-Pluronic/PCL showed prominent cellular internalization in C6 glioma cells compared to the free curcumin as evident from the enhanced green fluorescence exhibited by curcumin in the loaded micelles. The reduced entry of free curcumin into the cancer cells was marked by faint green fluorescence (Figure 60).

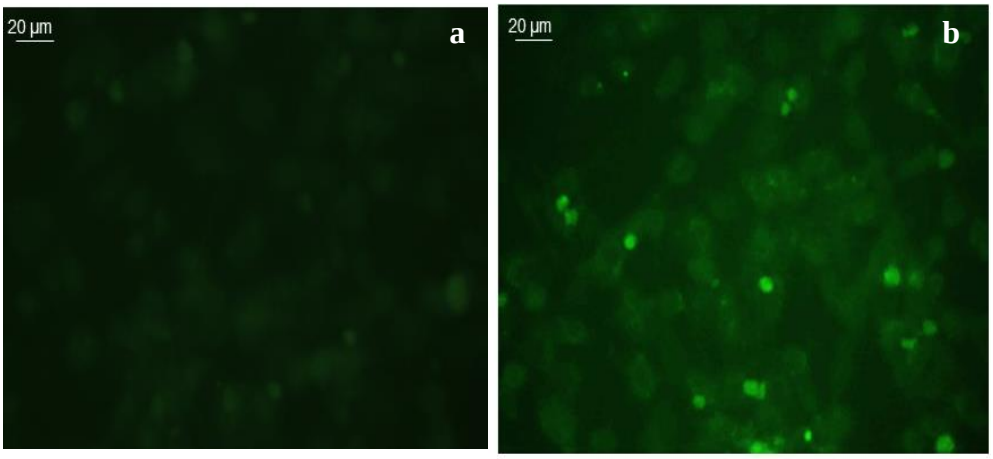

Figure 60. Cellular uptake in C6 glioma cells (a) curcumin (b) curcumin loaded CX-Pluronic/PCL micelles.

4.3 Curcumin-dextran conjugates

4.3.1 Synthesis of curcumin- dextran conjugate

Curcumin-dextran conjugate (Cur-Dex) was prepared by esterification of dextran with curcumin hemi-succinate (Figure 61). Succinic acid acted as the spacer to link the hydrophobic drug with the hydrophilic polymer. The synthesis of the conjugate was confirmed by IR spectra. The conjugation was affirmed by the presence of C-H aliphatic stretch at 2882 cm^{-1}, reduction of – OH stretching peak at 3250 cm^{-1} and presence of prominent curcumin peaks at 3505 cm^{-1} and 1620 cm^{-1} (Figure 62). The synthesis was further confirmed by ^{1}H NMR spectrum (Figure 63). The protons of the dextran backbone were seen between 2-5 ppm and the aromatic protons of curcumin were observed between 6.3 ppm and 6.6 ppm confirming the conjugation.

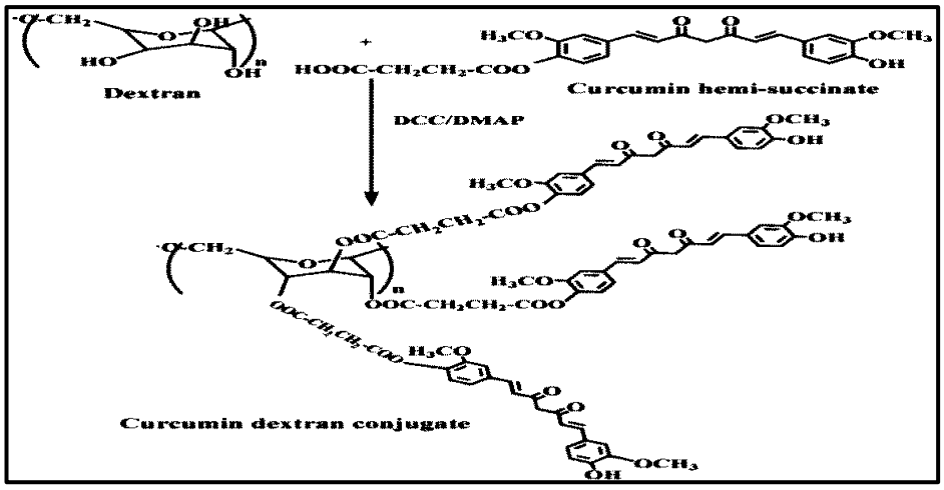

Figure 61. Reaction scheme illustrating the conjugation of curcumin to dextran.

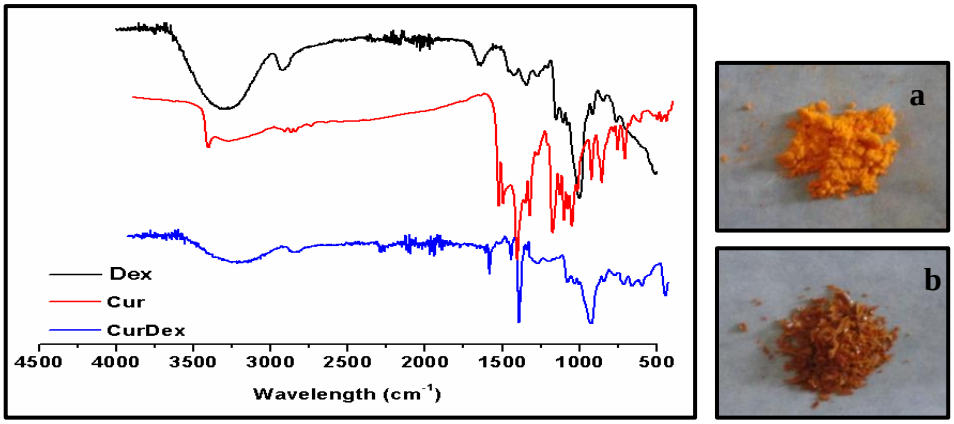

Figure 62. IR spectra confirming the synthesis of curcumin dextran conjugate. Picture on the right shows (a) curcumin (b) curcumin dextran conjugate.

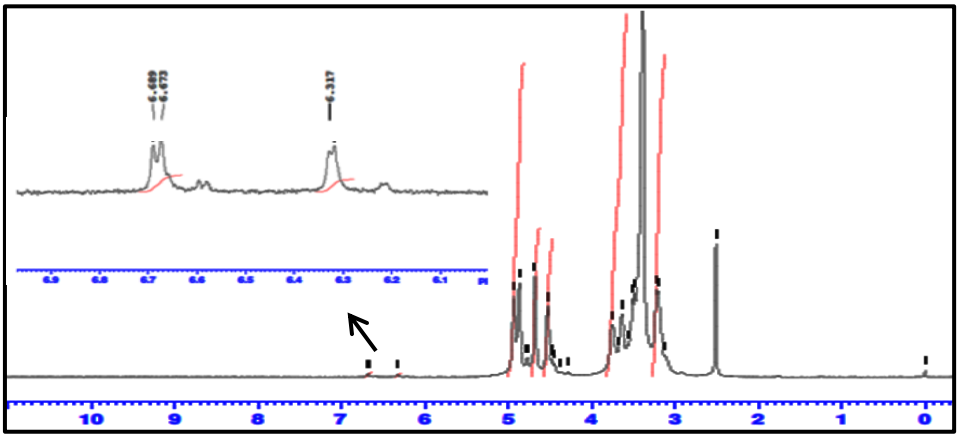

Figure 63. ^{1}H NMR spectrum of curcumin dextran conjugate. Inset picture exhibits the magnified area between 6.3 ppm-6.7 ppm which corresponds to the aromatic protons of curcumin

4.3.2 Critical micelle concentration

It was speculated that Cur-Dex conjugates could self-assemble in aqueous media (Figure 64). In order to determine whether the curcumin dextran conjugates could self-assemble into micelles, CMC was determined (Figure 65). The CMC of Cur –Dex was calculated to be 0.469mg/ml.

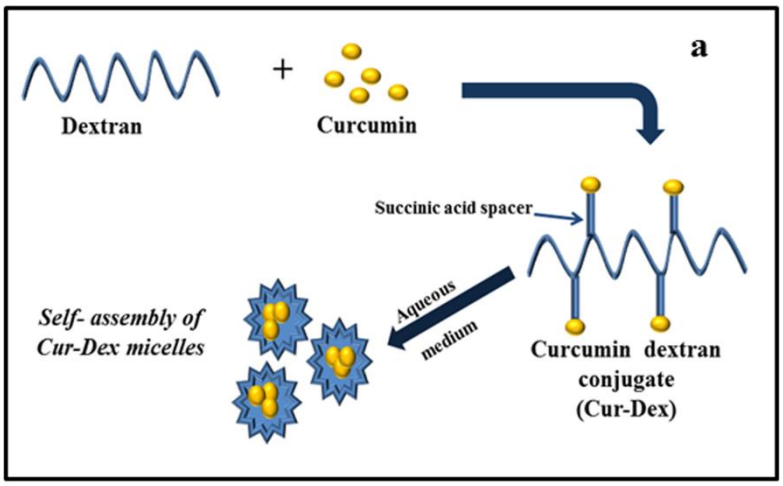

Figure 64. Schematic diagram depicting self-assembly of Cur-Dex

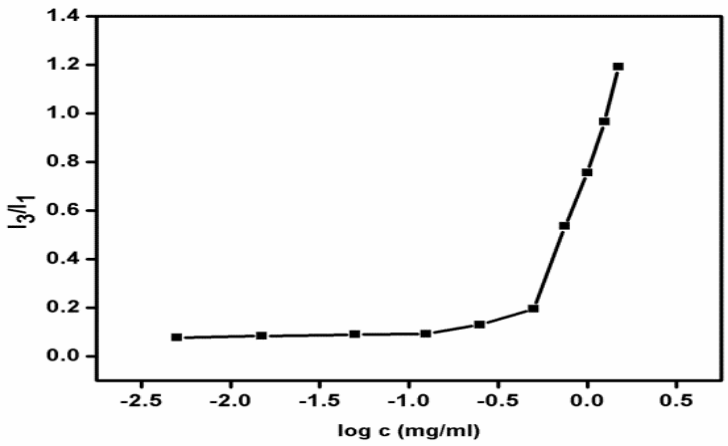

Figure 65. CMC of Cur-Dex

4.3.3 Determination of particle size and zeta potential

The hydrodynamic size of Cur-Dex micelles was 222 ± 33 nm. The size of the micelles from TEM was seen to be less than 50 nm. The zeta potential of Cur-Dex micelles was −15.2 ± 2.2 mV (Figure 66).

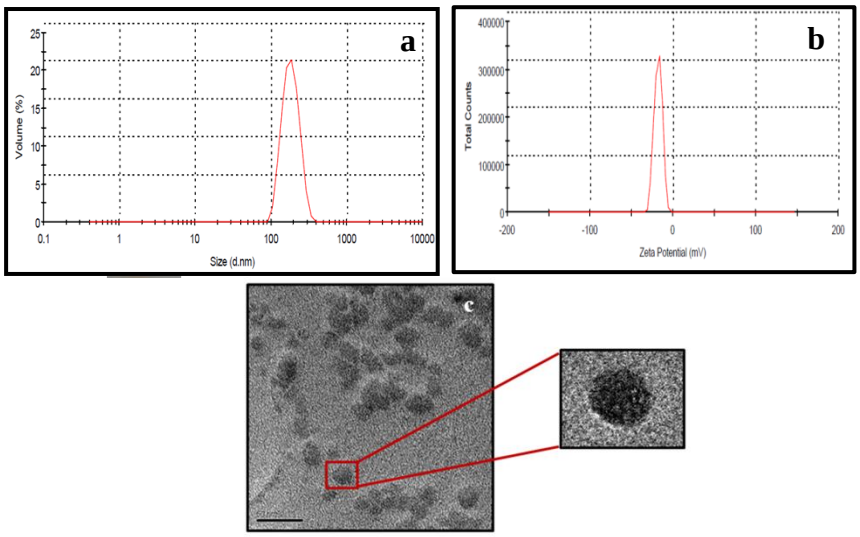

Figure 66. (a) Hydrodynamic size of Cur- Dex micelles.. (b) Zeta potential of Cur-Dex (c) TEM image of Cur-Dex. Inset picture shows the picture of Cur-Dex micelles in aqueous medium (Scale bar =50 nm).

4.3.4 DSC

The DSC thermogram of curcumin-dextran conjugate was recorded and compared with that of dextran. The characteristic curcumin melting point around 180^{o}C as seen in previous thermograms was absent in the conjugated curcumin (Figure 67).

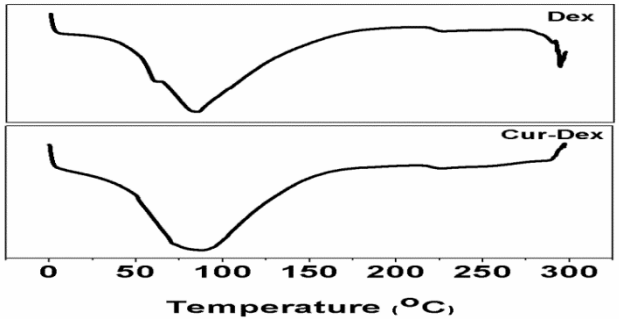

Figure 67. DSC thermograms of dextran and curcumin-dextran conjugate

4.3.5 Drug loading capacity

Amount of curcumin conjugated to dextran was quantified by UV-visible spectroscopy. It was calculated that 1 mg of curcumin conjugated dextran contained 38 µg of curcumin. The loading capacity was obtained as 3.3 ± 1.2 %.

4.3.6 Spectral characterization

The spectral characterization of the conjugates where performed by photo spectroscopy. Cur-Dex exhibited a broad and enhanced absorbance peak at 425 nm which indicated the presence of curcumin. The fluorescence spectrum showed a blue shift in the case of Cur-Dex at 522 nm compared to free curcumin which exhibited a peak at 550 nm (Figure 68).

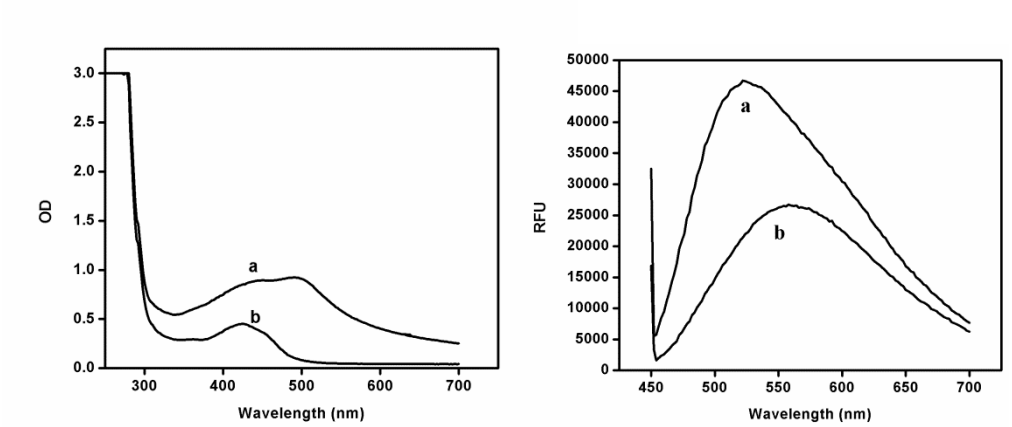

Figure 68. Spectral characterization (A) UV-visible spectrum and (B) Fluoresence spectrum of (a) Cur-Dex and (b) curcumin

4.3.7 Blood compatibility

4.3.7.1 Hemolysis and aggregation study

The curcumin dextran conjugates did not induce any hemolysis of red blood cells and the percentage of hemolysis was 0.06 ± 0.01 %. It was observed from the blood

aggregation study that the conjugates were compatible with the blood components as they did not induce any aggregation (Figure 69).

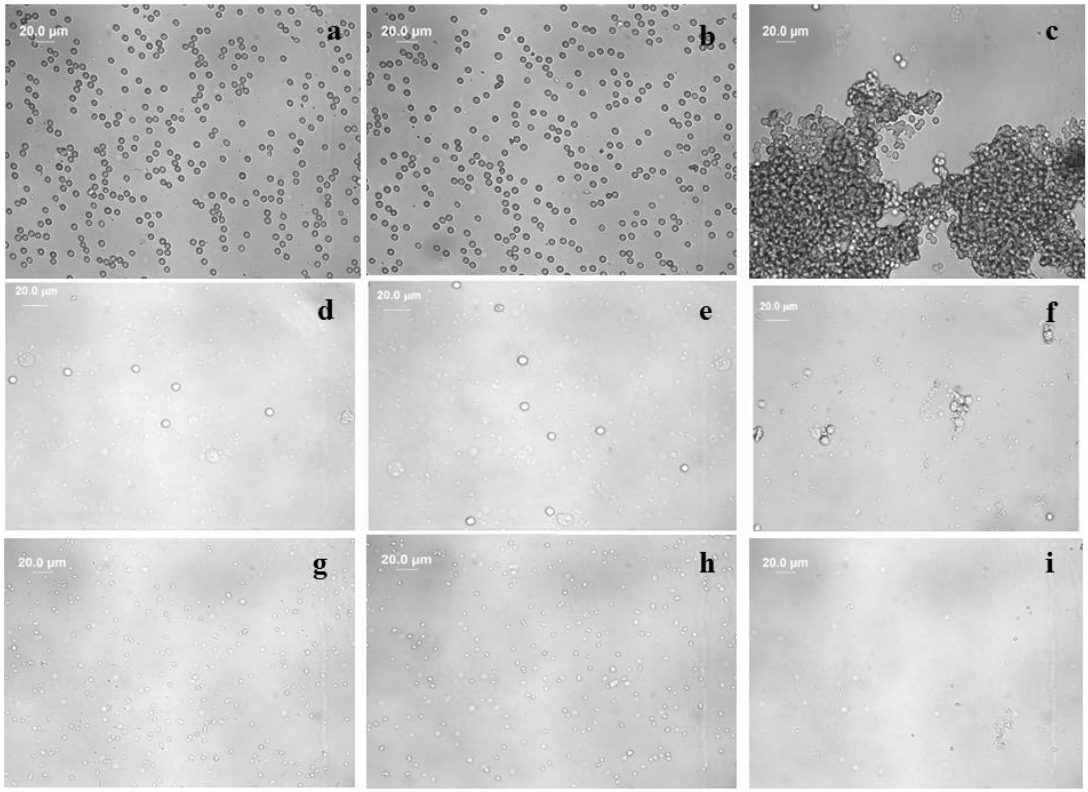

Figure 69. RBC aggregation in (a) saline (b) (c) PEI. WBC aggregation in (e) saline (f) Cur-Dex (g) PEI . Platelet aggregation (h) saline (i) Cur-Dex (j) PEI.

4.3.8 Gel Electrophoresis

Native PAGE was performed on plasma samples incubated with curcumin dextran conjugates. These were compared with saline and dextran. It was evident from the presence of protein bands that the conjugates did not induce adsorption of plasma proteins as there was no inhibition of protein bands and the obtained bands were similar to those of the control (Figure 70).

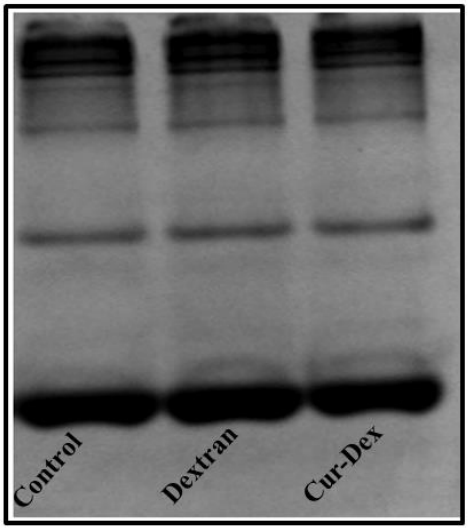

Figure 70. Native PAGE showing the interaction of Cur-Dex on plasma proteins (compared with saline as control and dextran.

4.3.9 Stability study

The stability of curcumin in the conjugated system was monitored relative to the free curcumin. Rapid degradation was exhibited by free curcumin within a span of 8 hours (Figure 71 a). Conjugation of curcumin to dextran was efficient in retaining the stability of curcumin by 80% in PBS.

4.3.10 Curcumin release study

The release of curcumin from Cur-Dex conjugates was assessed at acidic and physiological pH. A reduced and sustained release of curcumin was encountered at pH 7.4. About 30% of the curcumin was released in 72 hours. However, a higher release of curcumin from the conjugate was observed at pH 4.5. About 97% of curcumin was released in 60 hours (Figure 71 b).

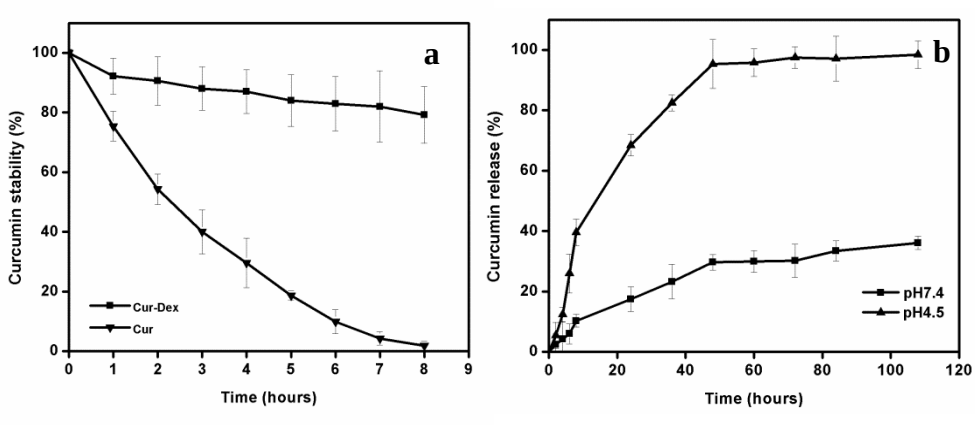

Figure 71. (a) Stability of curcumin in Cur-Dex (b) Curcumin released from Cur-Dex at pH 7.4 and pH 4.5

4.3.11 In vitro studies

4.3.11.1 In vitro cytotoxicity

4.3.11.1.1 MTT Assay

Cytotoxicity of Cur-Dex and free curcumin were assessed on C6 glioma cell with equivalent curcumin concentration maintained in the conjugated as well as free form. It was evident from the MTT results that above 30 µM curcumin concentration in the conjugate form exerted cytotoxic activity in the glioma cells. 60% of cell viability occurred with the conjugated curcumin at 30µM. In case of free curcumin, about 60% of glioma cells were viable at 50 µM whereas for similiar curcumin concentration in the conjugated system less than 20 % cells were viable (Figure 72).

4.3.11.1.2 Live Dead assay

The glioma cells were incubated with curcumin concentration of 50 µM in free and conjugated form. Enhanced red fluorescence was observed with Cur-Dex relative to free curcumin indicating increased death in cancer cells (Figure 73).

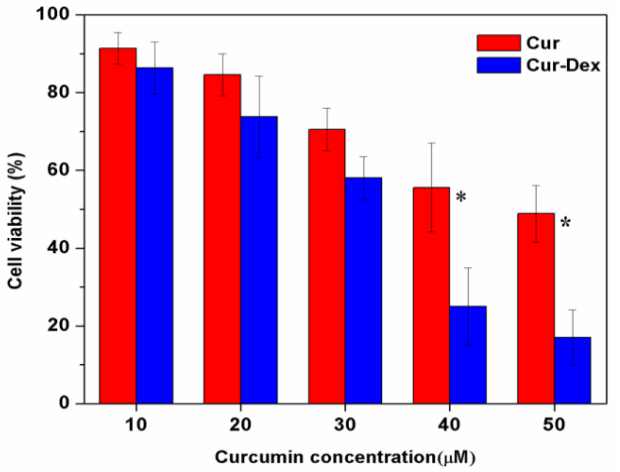

Figure 72. MTT assay on C6 glioma cells to compare the effects of free curcumin and Cur-Dex

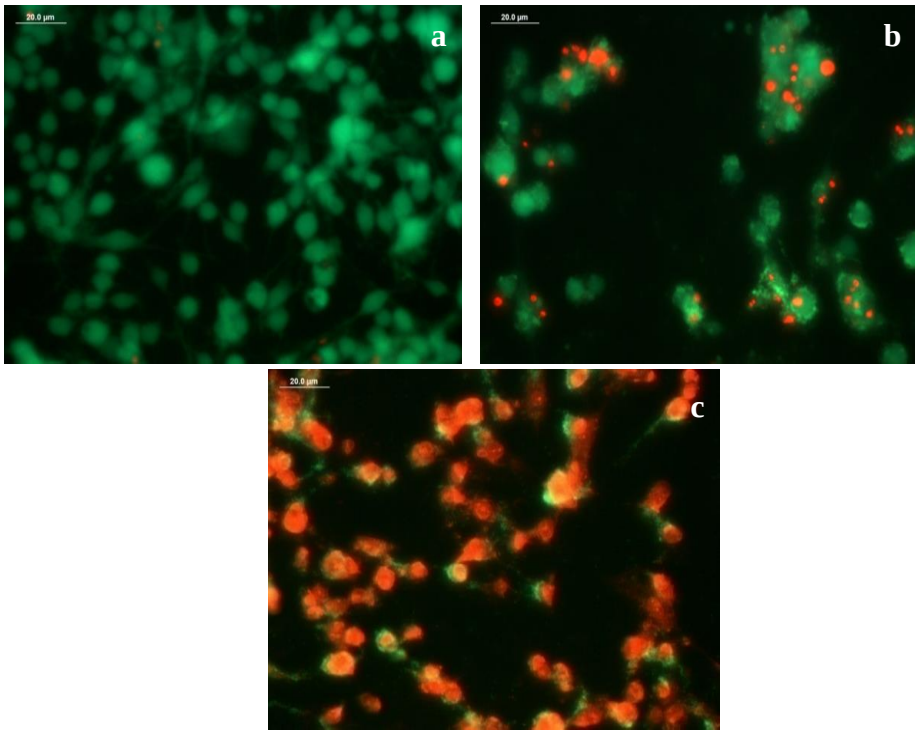

Figure 73. Live dead assay on C6 glioma cells (a) control (b) curcumin (c) Cur-Dex

4.3.11.2 Cellular uptake

Cellular uptake studies of curcumin dextran conjugates were performed by visualizing the intrinsic fluorescence of curcumin using fluorescence microscopy (Figure 74). Green fluorescence was more enhanced in Cur-Dex compared to free curcumin.

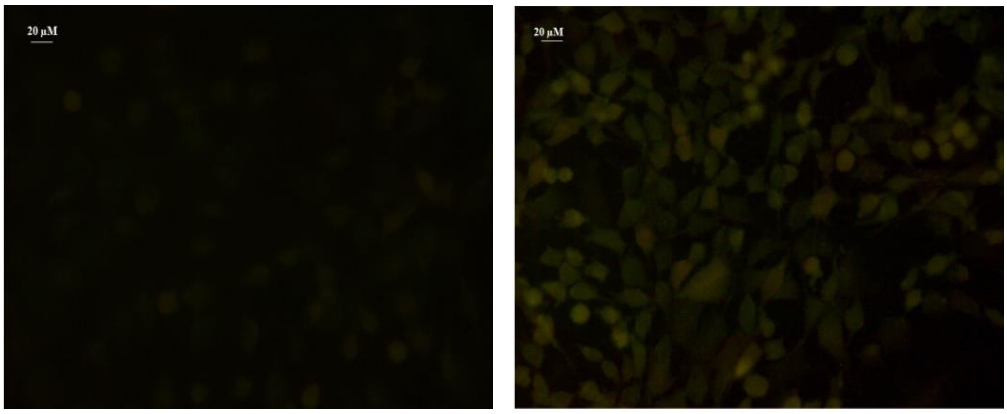

Figure 74. Cell uptake in C6 glioma cells (a) curcumin (b) Cur-Dex

4.4 Curcumin loaded POx micelles

4.4.1 Curcumin loaded Poly [2-ethyl-2-oxazoline-b-2-(but-3-enyl)-2-oxazoline] P(EtOx-b-ButenOx)micelles

4.4.1.1 Synthesis of Poly [2-ethyl-2-oxazoline-b-2-(but-3-enyl)-2-oxazoline] {P(EtOx-b-ButenOx)}

P($EtOx_{30}$-b-$ButenOx_5$), P($EtOx_{33}$-b-$ButenOx_{26}$)and P($EtOx_{17}$-b-$ButenOx_{44}$) di-block polymers were synthesized by the living cationic ring opening polymerization (Figure 75).

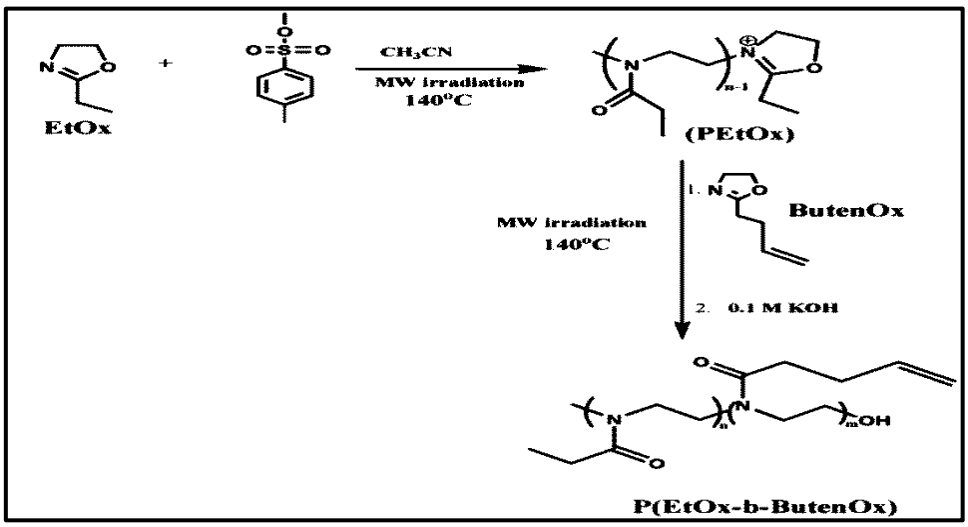

Figure 75. Synthesis of P(EtOx-b-ButenOx)

Formation of di-block polymers was afforded by ensuring complete polymerization of the first monomer i.e. EtOx monomer before reacting the second monomer. This was affirmed by the disappearance of the EtOx monomer peaks at 3.7 and 4.2 ppm and appearance of a broad peak, corresponding to methylene repeat units of EtOx block, at 3.4 ppm. Furthermore, ButenOx polymerization was also confirmed by the disappearance of the monomer peaks and appearance of the peak at 3.4 ppm. However, formation of P($EtOx_{30}$-b-$ButenOx_5$) occurred with incomplete conversion of monomer peaks due to reaction time of 15 minutes (Figure 76). It was noted that complete ButenOx polymerization required 30 minutes reaction time.

^{1}H NMR of P($EtOx_{30}$-b-$ButenOx_5$) ($CDCl_3$, 298K)= 5.75-5.89 (m, 10H, C*H*$_2$=CH-)); 4.96-5.12 (m, 5H, CH_2=C*H*-)); 3.45(br, 140H, (N-C*H*$_2$C*H*$_2$)); 2.5-2.2 (m, 60H, CO-C*H*$_2$-CH_3)); 1.59 (br, 20H (-C*H*$_2$-C*H*$_2$-CH=CH_2)); 1.11 (br, 90H, CO-CH_2-*CH*$_3$).

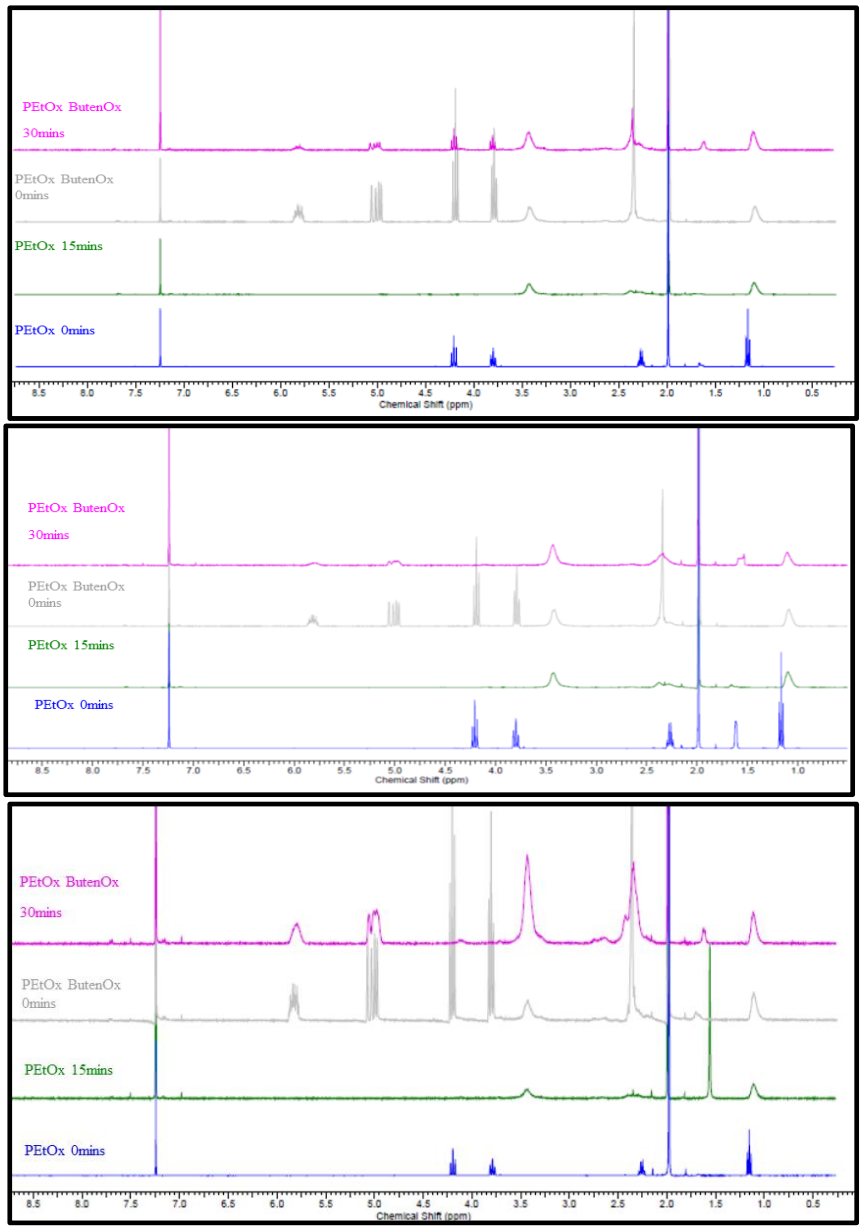

Figure 76. NMR of synthesis of [a] P($EtOx_{30}$-b-$ButenOx_5$) [b] P($EtOx_{33}$-b-$ButenOx_{26}$) [c] P($EtOx_{17}$-b-$ButenOx_{44}$)

^{1}H NMR of P($EtOx_{33}$-b-$ButenOx_{26}$) = 5.75-5.89 (m, 52H, CH_2=CH-)); 4.96-5.12 (m, 26H, CH_2=C*H*-)); 3.45(br, 236H, (N-CH_2CH_2)); 2.5-2.2 (m, 66H, CO-CH_2-CH_3)); 1.59 (br, 104H (-CH_2-CH_2-CH=CH_2)); 1.11 (br, 99H, CO-CH_2-*CH_3*). ^{1}H NMR of P($EtOx_{17}$-b-$ButenOx_{44}$) = 5.75-5.89 (m, 88H, CH_2=CH-)); 4.96-5.12 (m, 44H, CH_2=C*H*-)); 3.45(br, 244H, (N-CH_2CH_2)); 2.5-2.2 (m, 34H, CO-CH_2-CH_3)); 1.59 (br, 176H (-CH_2-CH_2-CH=CH_2)); 1.11 (br, 51H, CO-CH_2-*CH_3*). The number

average molecular weights of the di-block polymers were calculated from ^{1}H NMR by determining the number of EtOx and ButenOx units. Number of EtOx units was calculated from the ratio of integration of signals assigned to the backbone protons of the polymer (δ 3.45 ppm) and the initiator protons (δ 7.1 ppm and 7.7 ppm). The number of ButenOx units were determined from the sum of the proton integrals of the CH_2=CH- side chain (δ 5.75-5.89 ppm and 4.96-5.12 ppm).

4.4.1.2 DSC of synthesized P(EtOx-b-ButenOx)polymers

The DSC measurements were performed on the synthesized P(EtOx-b-ButenOx)} b polymers. The glass transition temperatures of P($EtOx_{30}$-b-$ButenOx_5$), P($EtOx_{33}$-b-$ButenOx_{26}$)and P($EtOx_{17}$-b-$ButenOx_{44}$) were observed at 22.7, 23.2 and 17.8^{o}C, respectively (Figure 77).

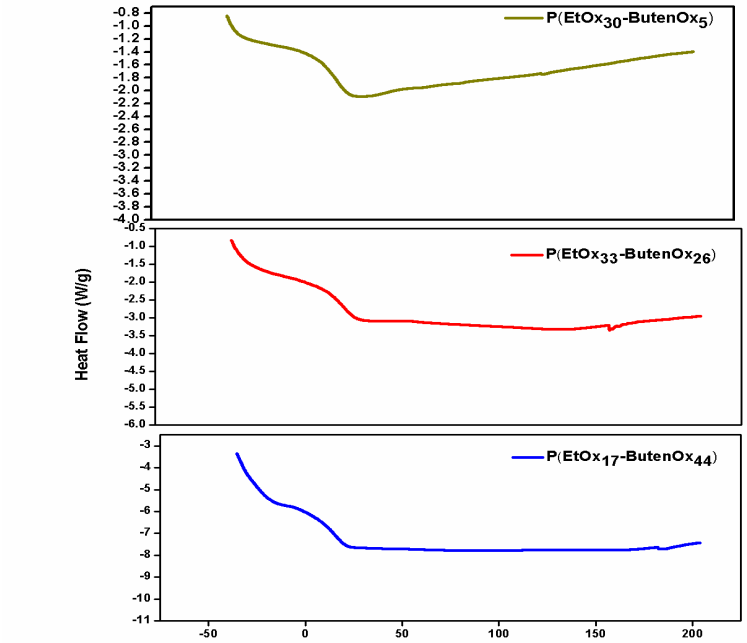

Figure 77. DSC thermogram depicting the glass transition temperatures of P(EtOx-ButenOx)s

4.4.1.3 CMC of the micelles of P(EtOx-b-ButenOx) polymers

Micelles of P(EtOx-b-ButenOx) polymers were prepared by nano-precipiation method. For P($EtOx_{30}$-b-$ButenOx_5$), the CMC value could not be derived as it did not give a definite inflection curve. The CMCs of P($EtOx_{33}$-b-$ButenOx_{26}$)and P($EtOx_{17}$-b-$ButenOx_{44}$) were calculated to be 0.12 mg/ml and 0.07 mg/ml respectively and are tabulated in Table 4.

4.4.1.4 Preparation of Curcumin loaded micelles

Empty and loaded micelles of the block polymers were prepared by nano-precipitation method which is based on the interfacial deposition due to the displacement of a solvent with non-solvent (Figure 78).

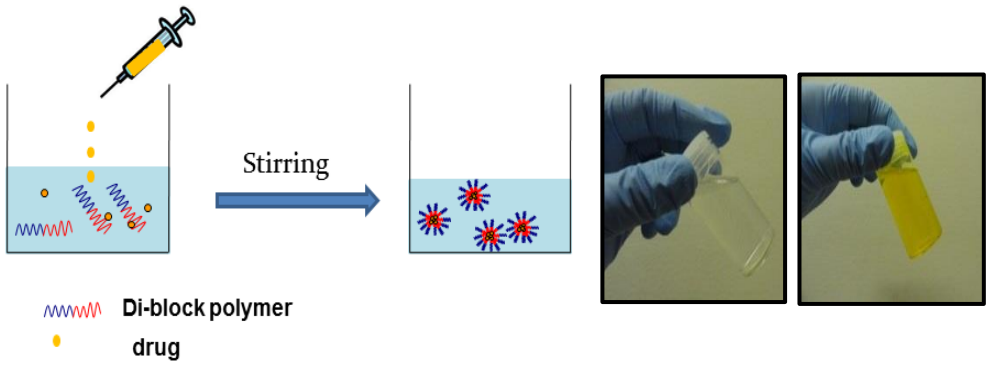

Figure 78. Schematic diagram of micelle formation by nano-precipitation method. Picture on the right shows the empty and curcumin loaded $PE_{17}B_{44}$ micelles.

4.4.1.4.1 Determination of size of micelles

From DLS measurements, it was observed that the micelles were of 70-110 nm exhibiting a monomodal distribution (Table 4). Size of particles obtained by TEM was smaller compared to the DLS measurements (Figure 79).

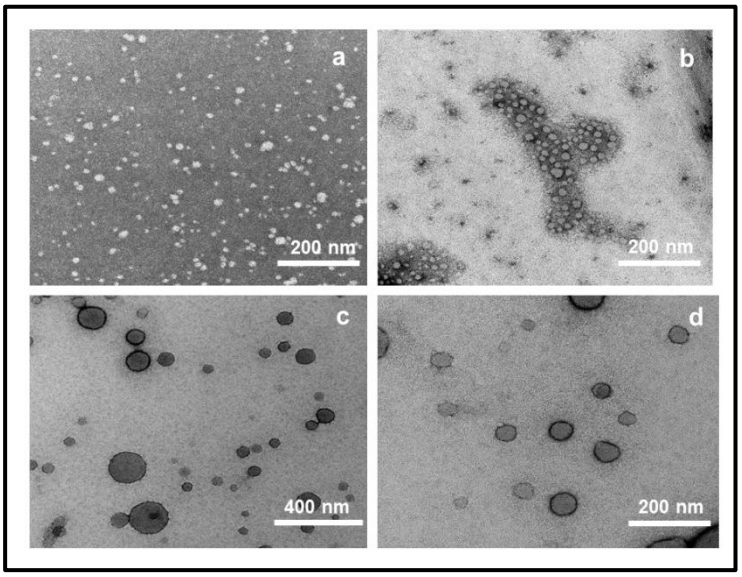

Figure 79. TEM image (a) P($EtOx_{17}$-b-$ButenOx_{44}$) micelles (b) curcumin loaded P($EtOx_{17}$-b-$ButenOx_{44}$) (c) P($EtOx_{33}$-b-$ButenOx_{26}$) and micelles (d) curcumin loaded P($EtOx_{33}$-b-$ButenOx_{26}$) micelles

4.4.1.4.2 Curcumin loading in the micelles

Curcumin loading of 7.5 ±1.7 % and 11.8 ± 2.2 % were obtained from P($EtOx_{33}$-b-$ButenOx_{26}$) and P($EtOx_{17}$-b-$ButenOx_{44}$) micelles, respectively (Table 4).

4.4.1.4.3 Curcumin compatibility with micelle core

The compatibility of curcumin with the micellar core was evaluated by determining χ_{sp} , the Flory-Huggins interaction parameter. The contributions of functional groups of curcumin and ButenOx were employed for calculating the dispersion (δ_d) , polar (δ_p) and hydrogen bonding components (δ_h). The molar volume of the curcumin was obtained as 253.1 cm^3/mol based on the group contributions tabulated by Fedors (Fedors, 1974). The calculated values of solubility parameters $\delta_{curcumin}$ and $\delta_{ButenOx}$ were calculated as 24.84 and 24.16, respectively. The interaction parameter of curcumin with the ButenOx core (χ_{sp}) was calculated as 0.07.

P(EtOx-ButenOx)s	CMC (mg/ml)	Size (nm)		Loading capacity (%)	Encapulation efficiency (%)
		Empty micelles	Loaded micelles		
1. $P(EtOx_{30}ButenOx_5)$	–	–	–	–	–
2. $P(EtOx_{33}ButenOx_{26})$	0.12	97.7 ± 8.5	107.5 ± 2.1	7.4 ± 1.7	51.9 ± 1.9
3. $P(EtOx_{17}ButenOx_{44})$	0.07	69.4 ± 1.1	79.5 ± 1.4	11.8 ± 2.2	82.7 ± 4.7

Table 4. Size, CMC and loading characteristics of synthesized P(EtOx-ButenOx)s

4.4.1.4.4 Spectral characterization

Spectral characterization study further confirmed the encapsulation of curcumin in the micelles. Characteristic absorbance peak of curcumin at 425 nm in the loaded micelles indicated the successful encapsulation. The absorption intensity of curcumin loaded in the $P(EtOx_{17}$-b-$ButenOx_{44})$ micelles was more enhanced compared to that of from $P(EtOx_{33}$-b-$ButenOx_{26})$ micelles and free curcumin. In the fluorescence spectra, curcumin showed a weak broad peak at 560 nm and the curcumin-loaded $P(EtOx_{33}$-b-$ButenOx_{26})$ and $P(EtOx_{17}$-b-$ButenOx_{44})$ micelles showed a well-defined high intensity blue shifted peak at 548 and 538 nm respectively (Figure 80).

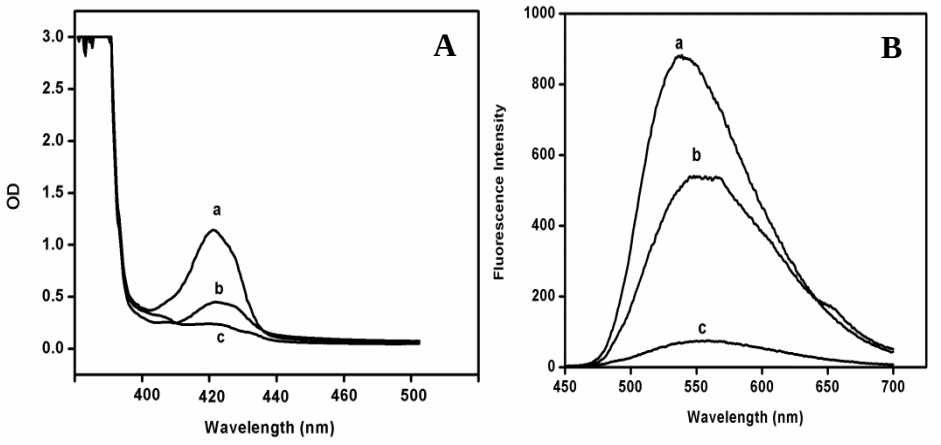

Figure 80. (A) UV-visible spectrum (B) Fluorescence spectrum of (a) curcumin loaded P($EtOx_{17}$-b-$ButenOx_{44}$) micelles (b) curcumin loaded P($EtOx_{33}$-b-$ButenOx_{26}$) micelles (c) curcumin

4.4.1.4.5 Stability of the micelles

The size of the $PE_{17}B_{44}$ micelles was almost constant for over a period of 30 days and was evidently more kinetically stable than $PE_{33}B_{26}$ (Figure 81 a). Empty micelles of $PE_{33}B_{26}$ exhibited increase in size after 8 days, however the curcumin, loaded micelles of the same did not follow similar trend.

4.4.1.4.6 Curcumin release from P(EtOx-ButenOx) micelles

From the release experiments it was noted that P(EtOx-ButenOx) polymers depicted a pH dependent curcumin release. About 12% and 34% of curcumin were released from P($EtOx_{17}$-b-$ButenOx_{44}$) and P($EtOx_{33}$-b-$ButenOx_{26}$) , respectively in 168 hours at pH 7.4 whereas at pH 4.5 , around 87% of curcumin was released (Figure 81 b). Relatively lower release of curcumin was exhibited by P($EtOx_{17}$-b-$ButenOx_{44}$) micelles when compared to P($EtOx_{33}$-b-$ButenOx_{26}$) micelles.

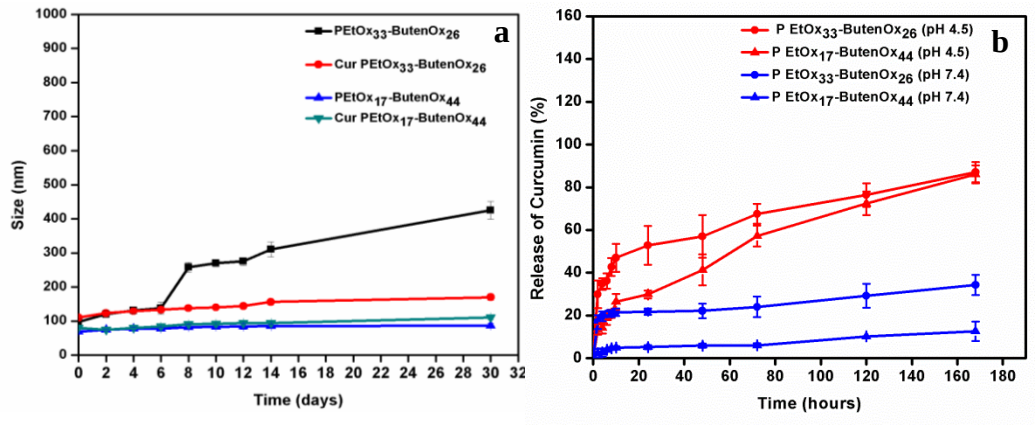

Figure 81. (a) Stability of the P(EtOx-ButenOx) micelles (b) Release study of P(EtOx-ButenOx) micelles

4.4.1.5 In vitro cell studies

4.4.1.5.1 Cytotoxicity study

4.4.1.5.1.1 MTT Assay

It was observed that the empty micelles did not exhibit any toxic effect on the cell lines indicating the biocompatibility of synthesized polyoxazoline micelles (Figure 82 a). Curcumin loaded POx micelles showed enhanced cell death compared to free curcumin (Figure 82 b). Dose dependent cytotoxicty was observed. At 20 µM of equivalent curcumin concentration, 14.04 ± 3.11% , 24.28 ± 4.05%, 71.64 ± 5.73% cell viability were observed with curcumin loaded P($EtOx_{17}$-b-$ButenOx_{44}$), curcumin loaed P($EtOx_{33}$-b-$ButenOx_{26}$) and free curcumin, respectively.

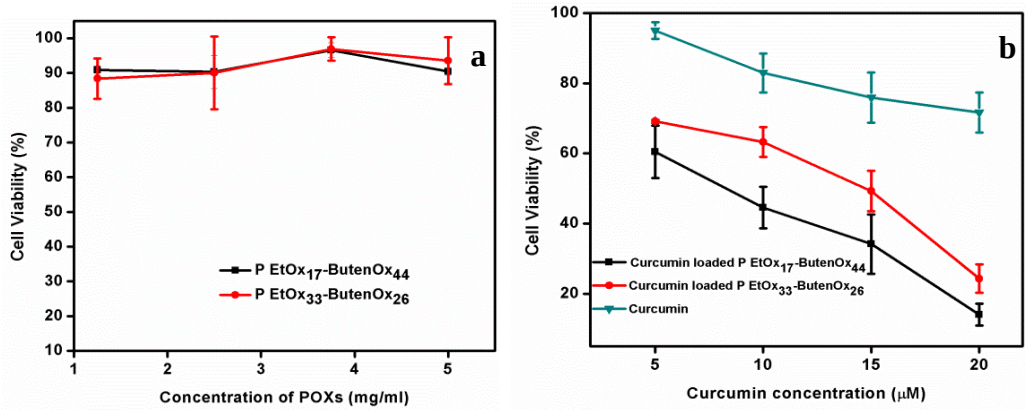

Figure 82. Cytotoxicity study (a) Empty P(EtOx-ButenOx) micelles (b) Curcumin loaded P(EtOx-ButenOx) micelles

4.4.1.5.1.2 Live dead assay

The assay performed was a qualitative study to visualize the cytotoxic effect of the curcumin loaded micelles compared to the free curcumin. Curcumin loaded POx micelles exhibited enhanced cell death compared to free curcumin indicated by the enhanced red fluorescence and negligible green colour (Figure 83).

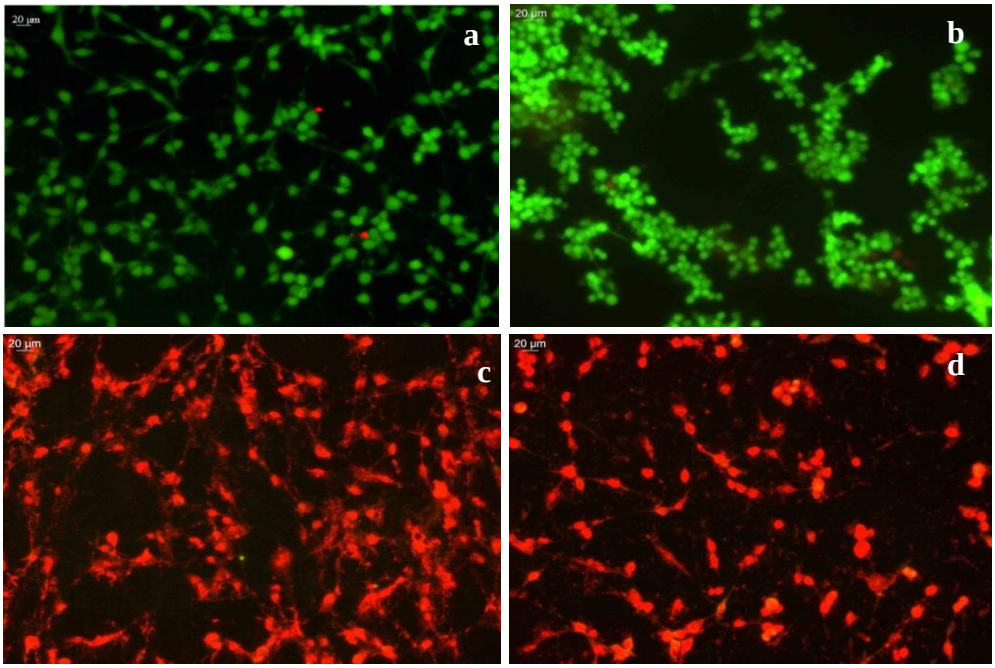

Figure 83. Live dead Assay on C6 glioma cells: (a) Control (b) curcumin (c) curcumin loaded P($EtOx_{17}$-b-$ButenOx_{44}$) micelles (d) curcumin loaded P($EtOx_{33}$-b-$ButenOx_{26}$) micelles

4.4.1.5.2 Cellular internalization

From the fluorescence microscopy images, it was observed that free curcumin was not readily taken up by the cancer cells which was evident from the diminished green fluorescence. Curcumin loaded P(EtOx-b-ButenOx)micelles exhibited prominent green fluorescence indicating relatively better uptake than the free curcumin (Figure 84).

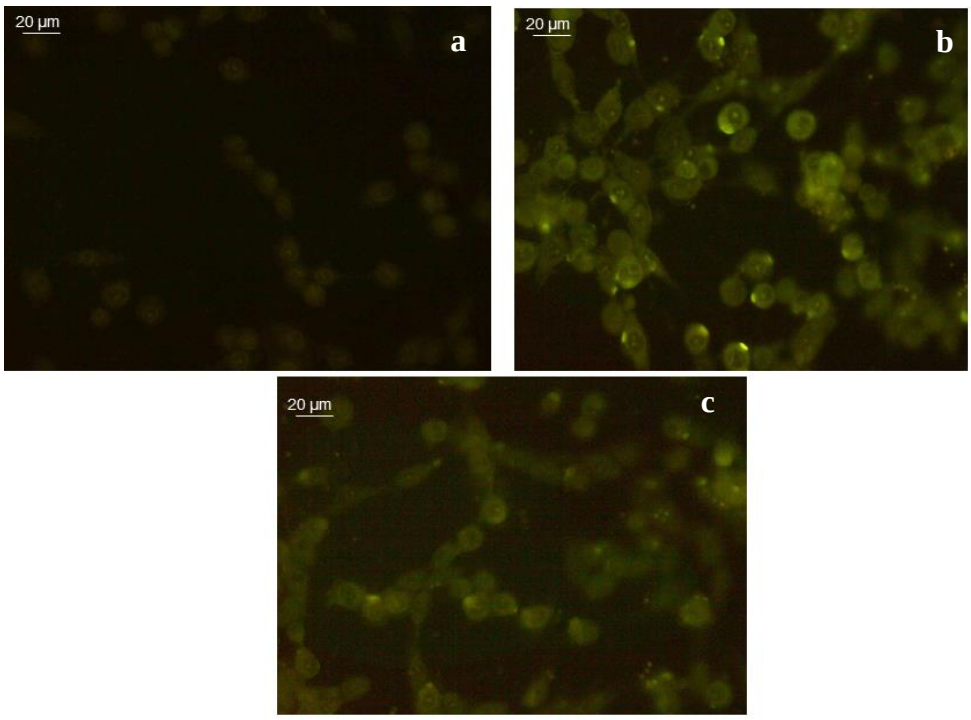

Figure 84. Cellular uptake in C6 glioma cells (a) curcumin(b) curcumin loaded P($EtOx_{17}$-b-$ButenOx_{44}$) micelles (c) curcumin loaded P($EtOx_{33}$-b-$utenOx_{26}$)micelles

4.4.2 Curcumin loaded block and gradient P(MeOx-isoPropOx) micelles

4.4.2.1 CMC of P(MeOx-isoPropOx) micelles

CMCs of the block and gradient polymers were determined using DPH as the fluorescent probe and the results have been tabulated (Table 5 and 6). The polymers

followed the standard trend of decreasing CMCs for increasing number of hydrophobic (isoPropOx) units. Among same ratios, it was observed that the block polymers had comparatively lower CMCs than their gradient counterparts.

4.4.2.2 Preparation of curcumin loaded micelles

The micelles were prepared by nano-precipitation method. The particle sizes of the micelles were evaluated by DLS. Interestingly, the DLS results showed that size of the micelles of few ratios decreased after loading of curcumin which was contradictory to the P(EtOx-b-ButenOx) micelles. The results are tabulated in Table 5 and 6. The gradient polymers also exhibited similar trend in size decrease with curcumin loading except P($MeOx_{40}$-g-isoPropOx_{20}) and P($MeOx_{50}$-g-isoPropOx_{10}) which had lower number of hydrophobic units. The gradient polymers had larger size compared to block ones. The TEM images depicted smaller sizes compared to DLS results due to the drying up of hydrophilic chains during sample preparation. Block polymers with greater number of hydrophobic units retained their spherical structure. It was observed that curcumin loading in P($MeOx_{50}$-b-isoPropOx_{10}) helped in retaining the spherical structure (Figure 85). In case of loading capacity, the gradient polymers showed very low loading compared to the block polymers and this is not unusual.

P(MeOx-isoPropOx) (Block)	Solubility in Acetone	CMC (mg/ml)	Size (nm)		Loading capacity (%)	Encapsulation efficiency (%)
			Empty micelles	Loaded micelles		
10:50	× *	0.09	311.5 ±19.6	279.5 ± 16.2	6.1 ± 0.3	47.3 ± 5.2
20:40	× *	0.14	302.5± 23.2	148.9 ± 65.9	5.7 ± 0.8	44.6 ± 7.2
30:30	✓	0.19	334 ± 25.7	71.6 ± 4.2	5.4 ± 0.9	37.5 ± 3.9
40:20	✓	0.21	254.3 ±29.4	196.5 ± 8.8	1.7 ± 0.2	12.1 ± 1.6
50:10	✓	0.32	227 ± 37	408.5 ± 115.7	0.25 ±0.1	1.74 ± 0.7

Table 5. Physicochemical data for block PMeOx-iso PropOx polymers

(* solubilized in acetonitrile)

P(MeOx-isoPropOx) (Gradient)	Solubility in Acetone	CMC (mg/ml)	Size (nm)		Loading capacity (%)	Encapsulation efficiency (%)
			Empty micelles	Loaded micelles		
10:50	✓	0.15	450.3 ± 55.3	353.8 ± 29.1	1.4 ± 0.2	10.2 ± 1.8
20:40	✓	0.16	518.4 ± 28	253.6 ± 12.9	1.0 ± 1.4	7.4 ± 3.6
30:30	✓	0.21	588.1 ± 45.4	302.5 ± 28.5	0.9 ± 0.4	6.3 ± 2.5
40:20	✓	0.27	644.2 ± 41	717 ± 112.9	0.3 ± 0.04	2.2 ± 0.5
50:10	✓	0.48	775 ± 77.2	>1 µm	0.05± 0.03	0.4 ± 0.1

Table 6. Physicochemical data for gradient PMeOx-iso PropOx polymers

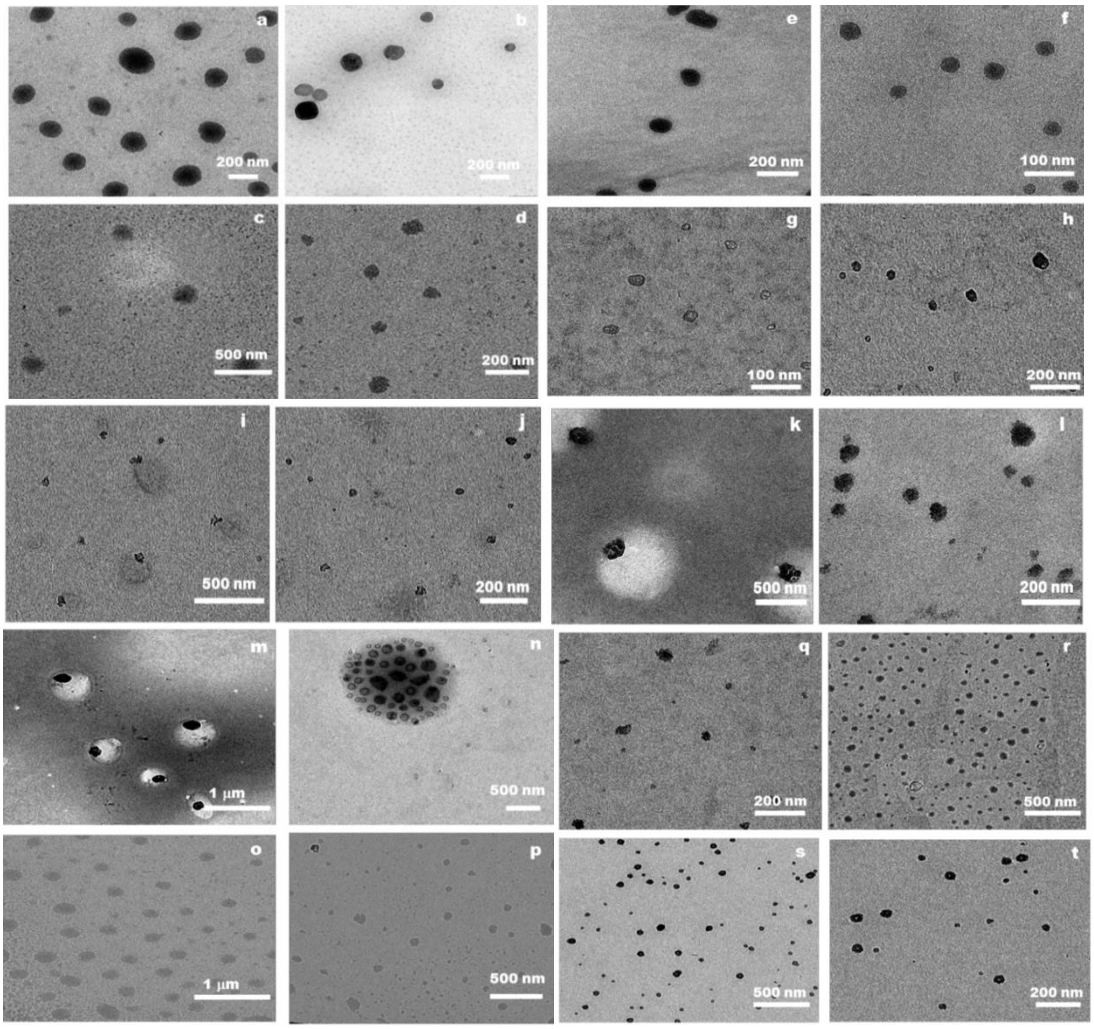

Figure 85. TEM images of (a) $MeOx_{10}$-b-$isoPropOx_{50}$ (b) Curcumin loaded $MeOx_{10}$-b-$isoPropOx_{50}$ (c) $MeOx_{20}$-b-$isoPropOx_{40}$(d) Curcumin loaded $MeOx_{20}$-b-$isoPropOx_{40}$ (e) $MeOx_{30}$-b-$isoPropOx_{30}$ (f) Curcumin loaded $MeOx_{30}$-b-$isoPropOx_{30}$ (g) $MeOx_{40}$-b-$isoPropOx_{20}$ (h) Curcumin loaded $MeOx_{40}$-b-$isoPropOx_{20}$ (i) $MeOx_{50}$-b-$isoPropOx_{10}$ (j) Curcumin loaded $MeOx_{50}$-b-$isoPropOx_{10}$ (k) $MeOx_{10}$-g-$isoPropOx_{50}$ (l) Curcumin loaded $MeOx_{10}$-g-$isoPropOx_{50}$ (m)$MeOx_{20}$-g-$isoPropOx_{40}$ (n)Curcumin loaded $MeOx_{20}$-g-$isoPropOx_{50}$ (o) Curcumin loaded $MeOx_{30}$-g-$isoPropOx_{30}$ (p) $MeOx_{30}$-g-$isoPropOx_{30}$ (q) Curcumin loaded $MeOx_{40}$-g-$isoPropOx_{20}$ (r) $MeOx_{40}$-g-$isoPropOx_{20}$ (s) $MeOx_{50}$-g-$isoPropOx_{10}$ (t)Curcumin loaded $MeOx_{50}$-g-$isoPropOx_{10}$

4.4.2.3 Curcumin compatibility with isoPropOx core

The group contibutions for isoPropOx core were calculated using the equations 6,7 and 8 to determine χ_{sp} . $\delta_{isoPropOx}$ obtained from calculations was 18.72. χ_{sp} between curcumin and isoPropOx was determined to be 0.625.

4.4.2.4 Spectral characterization

The absorbance spectra of curcumin loaded block and gradient polymers were measured (Figure 86 a). Curcumin loaded micelles exhibited the characteristic absorbance peak at 420 nm. The block polymers showed higher intensity peaks compared to gradient ones. Among the block polymers, enhancement of peak intensity was achieved with increasing isoproPOx units. Fluorescence emission spectra of the block and gradient polymers with same concentration of curcumin were recorded (Figure 86 b). The intensity of curcumin emission was higher in the block polymers compared to the gradient polymers. Polymers with low CMC showed enhanced emission intensity of curcumin. However, curcumin loaded P($MeOx_{40}$-b-$isoPropOx_{20}$), P($MeOx_{50}$-b-$isoPropOx_{10}$) and P($MeOx_{10}$-g-$isoPropOx_{50}$) showed slight red shift in the intensity.

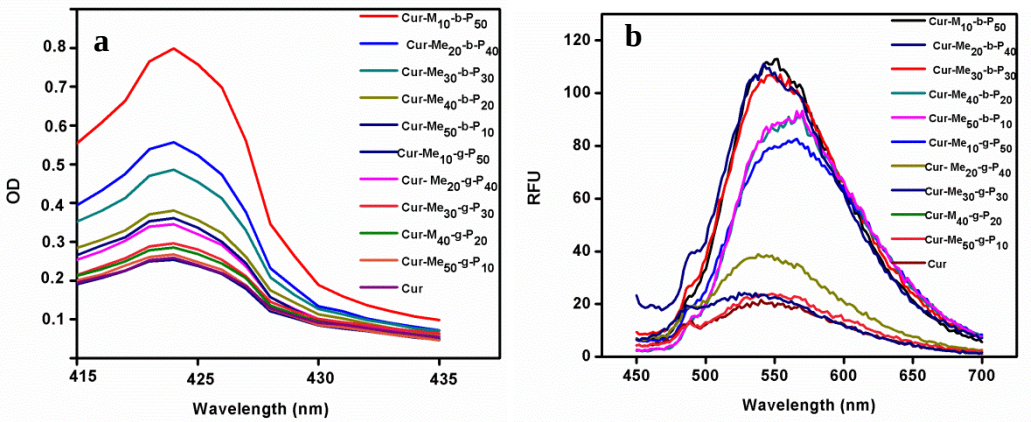

Figure 86. (a) UV-visible spectra and (b) Fluorescence spectrum of curcumin loaded P(MeOx- isoPropOx)s

4.4.2.5 Curcumin release study

The *in vitro* release of curcumin from the block and gradient polymers were performed at two different pH. Gradient polymers of sizes around 300 nm were only

studied. The polymers afforded slow release of curcumin at pH 7.4 and faster release at acidic pH similar to the observations with ButenOx polymers, except P (MeOx $_{50}$-b-EtOx$_{10}$) which exhibited a faster release in PBS (Figure 87).

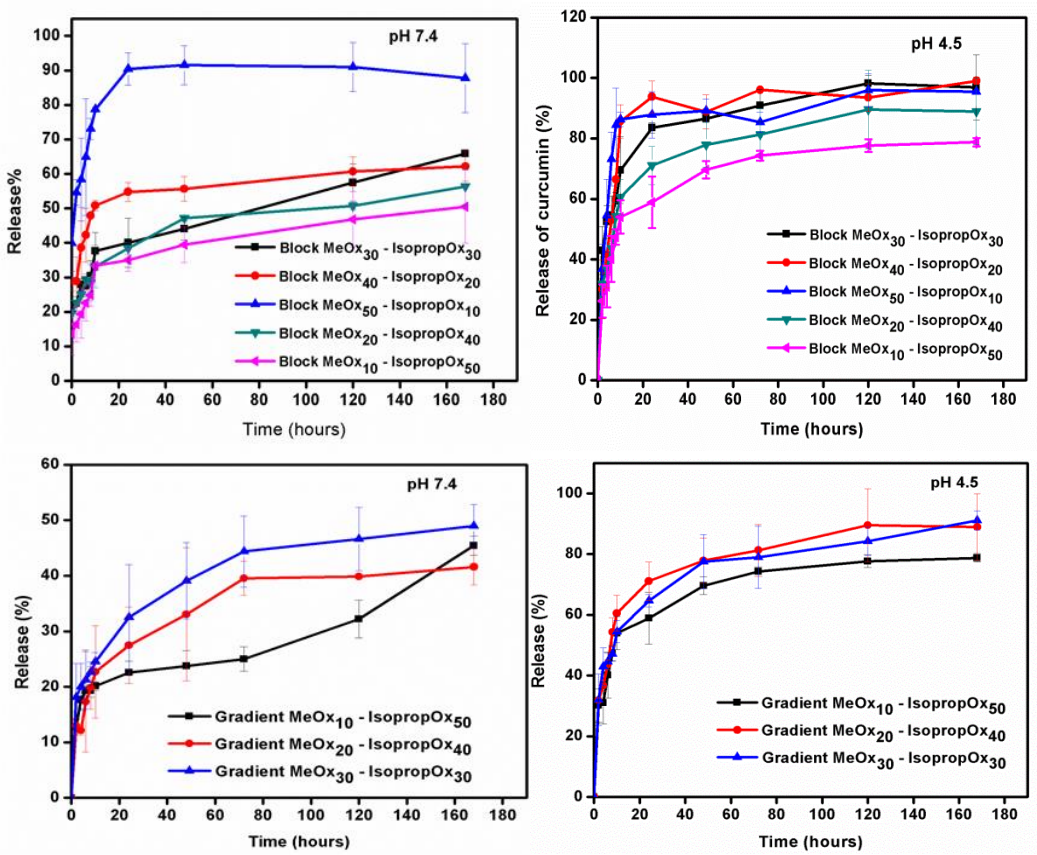

Figure 87. Release study of curcumin from block and gradient co polymers of P(MeOx-isoPropOx) at pH 7.4 and 4.5

4.4.2.6 In vitro studies

Based on loading, size and release studies , P(MeOx $_{30}$-b-EtOx$_{30}$) exhibited favourable results and this ratio was only investigated for futher *in vitro* experiments.

4.4.2.6.1 Cytotoxicity studies

4.4.2.6.1.1 MTT assay

Empty P($MeOx_{30}$-$isoPropOx_{30}$) micelles did not exhibit any toxic effect on the cell lines (Figure 88 a). Enhanced cell death in cancer cells was achieved by curcumin loaded P($MeOx_{30}$-$isoPropOx_{30}$) micelles compared to free curcumin (Figure 88 b). At 20 µM of equivalent curcumin concentration, loaded P($MeOx_{30}$-$isoPropOx_{30}$) exhibited 36.05 ± 4.35% cell viability.

4.4.2.6.1.2 Live dead assay

The assay performed was a qualitative study to visualize the cytotoxic effect of the curcumin loaded P($MeOx_{30}$-$isoPropOx_{30}$) micelles compared to the free curcumin. Live dead assay was consistent with the MTT assay results. Curcumin loaded P($MeOx_{30}$-$isoPropOx_{30}$) micelles exhibited greater cell death compared to free curcumin (Figure 89).

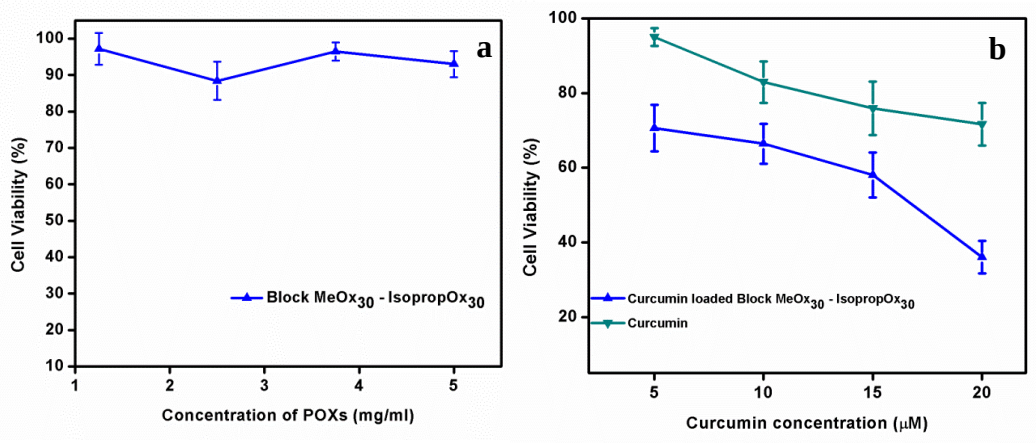

Figure 88. Cytotoxicity study (a) empty P($MeOx_{30}$-$isoPropOx_{30}$) micelles (b) curcumin loaded P($MeOx_{30}$-$isoPropOx_{30}$)micelles

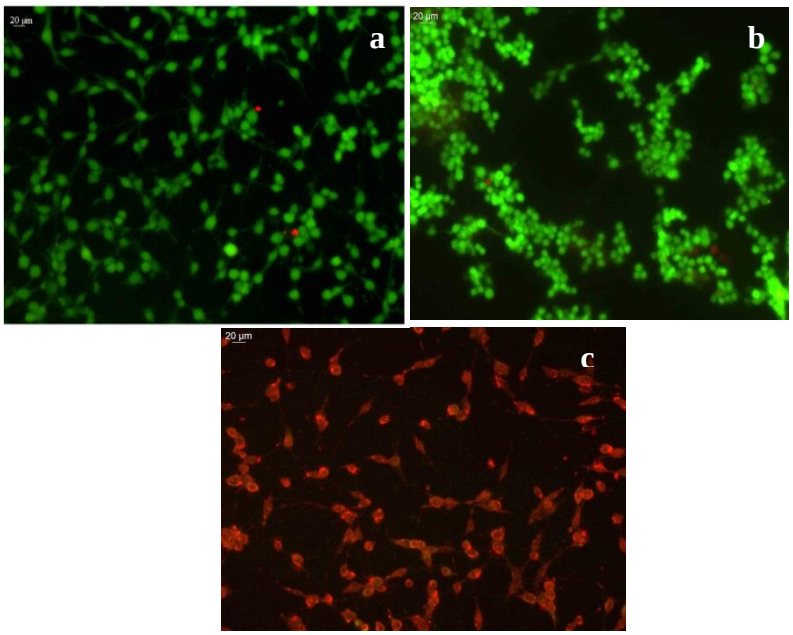

Figure 89. Live dead Assay on C6 glioma cells: (a) Control (b) curcumin (c) curcumin loaded P ($MeOx_{30}$-$isoPropOx_{30}$) micelles

4.4.2.6.2 Cell uptake

Free curcumin exhibited diminished green fluorescence indicatin decreased uptake by the cancer cells. Curcumin loaded P ($MeOx_{30}$-$isoPropOx_{30}$) micelles exhibited prominent green fluorescence indicating relatively better uptake than the free curcumin (Figure 90).

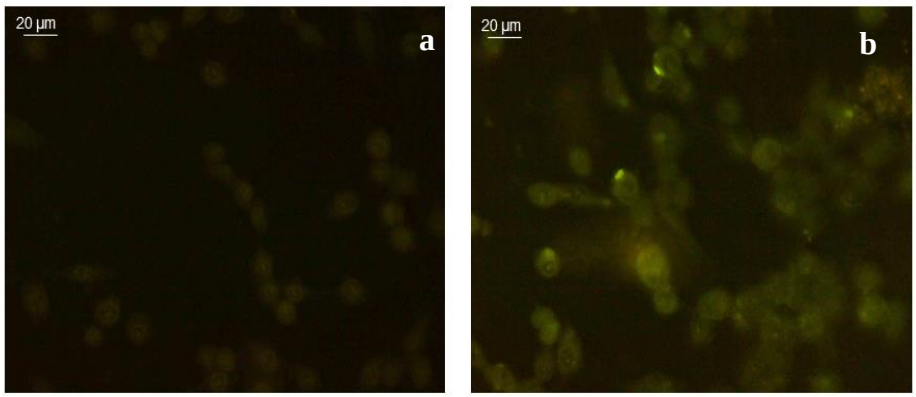

Figure 90. Cellular uptake in C6 glioma cells (a) curcumin(b) curcumin loaded micelles P ($MeOx_{30}$-$isoPropOx_{30}$).

CHAPTER 5 - DISCUSSION

Deleterious effects of synthetic anticancer drugs on healthy cells have fueled the quest for medicines from natural sources. Nowadays, natural biologically active compounds have become much sought after remedy for curing various ailments due to their safe profile and efficacy. In this regard, curcumin which is the active component in turmeric, has garnered wide attention especially due to its ability to exert anti-cancer activity through its pleiotropic effects (Shehzad et al., 2013) . However, low aqueous solubility and susceptibility to degradation pose as setbacks in the clinical administration of curcumin. Encapsulation of curcumin in polymeric micelles can circumvent these limitations. The hydrophobic core of micelles is efficient in accommodating curcumin and the hydrophilic corona is capable of offering stealth properties. Loading of curcumin in polymeric micelles has always been a compromised factor despite the high encapsulation efficiencies reported (Das et al., 2010; Sahu et al., 2008). Drug loaded micelles, after intravenous administration, are subjected to various biological factors that can compel the gradual release of the drug before reaching the physiological destination. Hence, low drug loading can pose as a major disadvantage in attaining the intended effect of the drug at the target site. Release of the drug from these matrices at the physiological pH is a perturbing factor which cannot be completely ignored, thus emphasizing the requirement for enhanced drug loading. It has always been a challenge to achieve

high curcumin loading on par with developing curcumin loaded micelles of size less than 200 nm. Therefore, there has been a growing need for amphiphilic polymers which are capable of forming small sized micelles with enhanced curcumin loading. This study explores the utility of polymeric micelles by incorporating different hydrophobic and hydrophilic components to design amphiphilic matrices that can fine-tune the loading and delivery characteristics of curcumin for optimal clinical administration.

5.1 Curcumin loaded micelles based on PEGylated Fatty Esters

5.1.1 Curcumin loaded mPEG laurate and mPEG linolenate micelles

PEGylated fatty esters were prepared by a facile synthesis of conjugating PEG to fatty acids to produce esters which were capable of self- assembling into micelles in aqueous medium medium. The hydrophobic core contributed by the fatty acids has the potential to encapsulate curcumin. Enhanced hydrophobicity, membrane penetrative property (Castelli et al., 2003) and its potential to induce apoptosis in cancer cells (Deshpande et al., 2013) were the impetus for our selection of linolenic acid. Previously, in the work of Abhishek et al, curcumin loading in palmitate micelles was found to be very low, around 1% w/w, despite high encapsulation efficiency (Sahu et al., 2008). It was comprehended that a better loading capacity could be attained with linolenic acid as the hydrophobic core. Lauric acid, a saturated fatty ester, was incorporated for a comparative study with the unsaturated linolenic acid to evaluate any change in curcumin loading due to structural effects. PEG is often an obvious choice when it comes to imparting hydrophilicity to hydrophobic

surfaces, intended for biomedical applications, as the PEG chains create a layer of barrier prevent opsonization (Owens III and Peppas, 2006).

The mechanism of esterification of mPEG fatty esters, occured with the initial formation of an O-acyl urea formed by the reaction of carboxylic acid and DCC. Nucleophilic attack of the carboxylate formed an anhydride that reacted with the catalyst DMAP to generate an acyl pyridinium carboxylate ion pair which further upon reaction with alcohol gave the ester, liberating the catalyst and carboxylate. The synthesized esters were characterized by FTIR and ^{1}H NMR spectroscopy. From the IR spectra the conjugation was affirmed by stretching vibration of carbonyl group in the region 1720-1730 cm^{-1}. In the NMR spectra, the presence of characteristic peaks corresponding to the protons of the functional groups of fatty acids along with the peaks of protons of mPEG confirmed the syntheses. At 3.3 ppm and 0.88 ppm, the methylene and methyl protons of lauric acid were observed, respectively. The corresponding mPEG linolenate ester exhibited the protons of the conjugated double bonds at 6.48 ppm along with the peaks corresponding to the methylene repeat units of mPEG at 3.46 ppm. Physical incorporation of curcumin into mPEG fatty ester micelles was accomplished through dialysis method. Self- association of the micelles was triggered by the gradual replacement of the organic solvent with water (Aliabadi and Lavasanifar, 2006). Hydrophobic curcumin was encapsulated in the hydrophobic core of the micelles (Figure 13).

From the results of different loading (% w/w) of curcumin in the micelles (Table 1), it was evident that linolenate ester exhibited better loading capacity and better encapsulation efficiency relative to its laurate counterpart. Linolenic acid possesses

conjugated double bonds that can interact with aromatic rings or other conjugated bonds through π-π orbital overlapping (Heard et al., 2005). As curcumin is a polyphenolic compound with a conjugated system, it is believed that linolenic moiety can afford to interact with curcumin via this π-π orbital overlapping and as a result can strengthen the encapsulation of curcumin in the linolenate core. Such interactions were absent in saturated lauric acid. Increasing the theoretical loading led to a decrease in encapsulation efficiency. Higher drug concentration gradient outside the micelles tends to drive out the encapsulated drug leading to a decrease in encapsulation efficiency. Initiation of precipitation, caused by insoluble curcumin, was encountered at 4.76 and 7.69% w/w loading indicating that the amount of curcumin loaded exceeded the solubilization capacity of the micelles. Loading above 7.69 % w/w led to mass precipitation of curcumin. 3.25% w/w loading exhibited better loading capacity on par with better encapsulation efficiency and hence this percentage loading was chosen for further studies.

The *in vivo* fate of polymeric micelles is dictated by their physiochemical properties such as size, zeta potential and shape (Yue et al., 2013). Micellar size also plays a fundamental role in targeting of tumors through EPR effect. Polymeric micelles less than 200 nm is efficient in extravasating into the tumour interstitium and gets retained due to the poor lymphatic drainage system in the tumour vasculature (Maeda et al., 2006). The curcumin loaded micelles of mPEG-laurate ester and linolenate ester exhibited an average hydrodynamic diameter of 59.5 ± 4.3 nm and 77.5 ± 3.2 nm, respectively. It was seen that loading of curcumin in the micelles lead to an increment in their size. Solubilization of a drug in the micellar core leads to the

expansion of the core thereby overall increasing the particle size (Uchegbu and Schatzlein, 2010). The size of the curcumin loaded micelles analyzed by TEM was smaller compared to that measured by DLS. The hydrated state of micelle accounted for the increased size in DLS as compared to the size obtained by TEM (Chen et al., 2007). Surface charge is an important factor for the stability of a nanoparticle suspension and this property is characterized by zeta potential (Couvreur et al., 2002). It reflects the electrical potential of particles and is influenced by the particle composition and the dispersion medium. The curcumin loaded and unloaded mPEG micelles exhibited negative zeta potential in the range of –13 to –25 mV, respectively. The particle zeta potential between +30 mV and –30mV signifies stability in suspension (Clogston and Patri, 2011). The unloaded and loaded micelles showed negligible change in the zeta potential value and it was observed that with increased loading, the particle size increased but the zeta potential remained same. The zeta potential can substantiate the presence of a charged active material encapsulated within the centre of the nanocapsule or adsorbed onto the surface. Negligible change in the zeta potential indicated that curcumin was encapsulated inside the micelles.

The retention of hydrophobic drugs in the core of polymer micelles is significant to the development of efficient delivery vehicles. The compatibility between the drug and the core-forming polymer block is critical in explaining the capacity of a micellar system to solubilize and retain a drug within its core. Most of the performance related characteristics of the delivery systems which include drug loading capacity, encapsulation efficiency and drug release kinetics depend on the

miscibility and the degree of interaction between the polymer and the drug (Mikhail and Allen, 2009). Flory–Huggins interaction parameter (χ_{sp}) was initially implemented to describe the experimental solubilization capacity and unusual selectivity of the various low molecular weight hydrocarbon solutes by block copolymer micelles (Nagarajan et al., 1986). This calculated parameter is useful in evaluating the compatibility between the solute and micellar core and has been used to qualitatively explain the different extents of solubilization of hydrophobic drugs by micellar drug delivery systems formed from amphiphilic polymers (Letchford et al., 2008; Lim Soo et al., 2002; Liu et al., 2004). Determination of the solubility parameter can expedite the selection of highly compatible polymer-drug pairs and could be considered as a promising approach for the rapid screening of polymer systems for a specific drug or, conversely, of various drugs compatible with a specific polymer. The lower the χ_{sp} value, the higher predicted amount of solubilization which indicates enhanced compatibility of the solute with the micellar core. Location of a drug in a micelle has been hypothesized to occur in both core and corona requiring a prediction of overall compatibility (Latere DwanIsa et al., 2007). However, as curcumin is extremely hydrophobic, the possibility of its partitioning into the corona is ruled out and is concentrated only in the core when solubilized.

χ_{sp} value calculated for laurate and linolenate ester was 0.736 and 0.708, respectively. We expected linolenate moiety to have much lower value than the calculated value, owing to the presence of conjugated bonds which could enhance the interaction with curcumin. However, it was seen that the χ_{sp} value for linolenate was only slightly lower than laurate. But this was consistent with the obtained loading capacity of the

micelles as laurate and linolenate micelles exhibited a loading of 2.4 ± 0.2 % and 2.91 ± 0.06 %, respectively.

Critical micelle concentration (CMC) of amphiphilic polymers is crucial for gaining an understanding about their micellar microenvironment in aqueous media. It is the minimum concentration of polymer required for micelles to form and is the key parameter which defines the formation and thermodynamic stability of micelles. The major driving force for the formation of micelles is the hydrophobic effect which minimizes the interfacial energy (Martin et al., 2011; Tadros, 2006). As the polymer chains possess many points of interaction, the polymeric micelles have lower CMC values compared to the low molecular mass surfactants. CMC of mPEG fatty esters were measured using pyrene as the fluorescent probe. This method is based on changes in the vibrational band intensities of pyrene solubilized in water and in micellar solutions. The relative peak intensity of pyrene undergoes significant perturbation upon moving from polar to nonpolar region. The ratio of the fluorescence intensity of the first vibrational band (I_3), the highest energy vibrational band, to that of the third vibrational band (I_1) has been shown to correlate with solvent polarity (Sahu et al., 2008). In polar environment, pyrene behaves as a self-quenching agent but when located in the proximity of hydrophobic domain of a micelle, it exhibits intense fluorescence. The formation of mPEG fatty ester micelles forced pyrene to move into the micelles from the aqueous phase which altered the intensity ratio of I_3/I_1 pyrene fluorescence bands. It was also apparent that with increased micellar concentration, the intensity also increased as pyrene was shifted to the hydrophobic interior. CMC value was calculated from the point of inflection

from the plot showing the relationship between changes in intensity (I_3/I_1) of pyrene with the log (concentration) of micelles and was found to be 0.901and 0.665 mg/ml, respectively (Figure 15). Linolenate core is more hydrophobic than laurate and the CMC trend is in accordance with previous observations that an increase in hydrophobicity leads to lower CMC values (Yang et al., 2010). Lower CMC is attributed to increment in the hydrophobic units which results in enhanced cohesion of the core (Gaucher et al., 2005; Lee et al., 2004; Van Domeselaar et al., 2003). It is imperative for the micelles intended for drug delivery to have a low CMC value as higher CMC would make the micelles face the dire consequences of disassembling into unimers upon dilution after intravenous injection, thereby resulting in the untimely release of the drug.

The encapsulation and binding of curcumin was confirmed by spectral characterization of the curcumin loaded micelles. Curcumin loaded micelles exhibited the characteristic absorption peak of curcumin at 425 nm indicating its encapsulation in the micelles. The intensities of absorption peaks of loaded curcumin were more enhanced compared to free curcumin due to micellar encapsulation. The reason could be attributed to more localized concentration of curcumin in the core of the micelles (Figure 16 a). Similar behaviour was also encountered in fluorescence spectra. A weak broad peak at 560 nm was exhibited by curcuminand the curcumin loaded mPEG fatty ester micelles exhibited well- defined high intensity blue-shifted fluorescent peak in the range of 500-525 nm (Figure 16 b). The shift in fluorescence spectra of curcumin is due to the binding of curcumin in the hydrophobic domain of the micelles. Adikary et al reported the existence of curcumin in the enol form which

is capable of executing excited state intra molecular hydrogen atom transfer (ESIHT) when encapsulated in surfactant micelles and this is attributed to the presence of strong intra-molecular hydrogen bonding between the proton donor and the acceptor atom (Adhikary et al., 2010). We believe that similar interactions occur with curcumin encapsulated in polymeric micelles as is evident from the blue-shift in the emission wavelength of the curcumin loaded micelles. Intensity enhancements and shifts are observed to be a characteristic photo-physical property of curcumin encapsulated in hydrophobic matrices and are in coherence with previously published reports (Sahu et al., 2008)

The physical status of curcumin encapsulated in mPEG-fatty esters was investigated by DSC. Curcumin exhibited an endothermic melting peak around 180^{o}C, which implied that curcumin was in crystalline state (Avgoustakis et al., 2003). In the thermogram of loaded matrices, the endothermic peak of curcumin was not present and only the characteristic melting peaks of mPEG-fatty esters were observed Figure 17). The absence of the melting peak of curcumin suggested that curcumin, encapsulated in the micelles, existed in an amorphous state. Cytotoxic studies on cancer cells in the later part of our study were done to ascertain whether the potential of encapsulated curcumin to induce apoptosis has not been lost due to its transformation into amorphous state.

The release of encapsulated drug from micelles is usually proceeded by diffusion (Aliabadi and Lavasanifar, 2006). The release of curcumin from the core of the mPEG fatty ester micelles was observed (Figure 18). It was observed that the release of curcumin from the micelles was dependent on the hydrophobicity of the micelles.

Relatively lower release of curcumin was exhibited by mPEG-linolenate micelles and this could be explained by the enhanced hydrophobic cohesive interaction between curcumin and the linolenate core. In the initial hours, a pH dependent release was encountered. However, after 108 hours, 90% of curcumin was released at pH 7.4 and 4.5 from both the micelles. Faster release in acidic pH is significant as it relates to the lower pH in the endocytic compartment of tumor cells where the pH is between 4.5-6.5 (Manju and Sreenivasan, 2011). However, mPEG-laurate and linolenate exhibited accelerated release at pH 7.4 and rapid release at physiological pH is not encouraged as this contributes to the loss of drug before reaching the target site.

Curcumin is known to exert cytotoxic effects in multiple cancers by binding to several molecular targets and diminishing undesirable cellular signaling pathway activities (Shehzad et al., 2013). MTT assay was performed to examine the cytotoxic effects of curcumin in the loaded micelles relative to the free curcumin. The empty micelles of mPEG esters did not create any cytotoxicity. The cell viability was well above 85% at 6 mg/ml concentration of mPEG fatty esters (Figure 19 a). However, in the case of curcumin loaded micelles, a dose dependent toxicity was observed. At 20 µM concentration of curcumin, the loaded micelles exhibited less than 30 % cell viability whereas equivalent concentration of free curcumin had around 65% cell viability. Inadequate solubility of curcumin in aqueous medium prevented it to exert its cytotoxic effect on cancer cells. Encapsulation of curcumin in the core of mPEG fatty ester micelles enhanced its aqueous solubility as evident from its reduction in cell viability.

Cellular uptake study is an important parameter that needs to be probed for explaining successful drug delivery of micelles to cancer cells. Curcumin, being fluorescent, has the advantage to be traced inside cells. Fluorescence microscope images confirmed cellular internalization of the curcumin loaded mPEG fatty ester micelles. Non-toxic concentration of curcumin (10 µM) was employed to view the cells in undisrupted morphology. Entry of free curcumin was not prominent in the cells owing to its low aqueous solubility. Curcumin loaded micelles showed intracellular green fluorescence indicating the efficient uptake of encapsulated curcumin owing to the small size of micelles (Figure 20). Curcumin loaded mPEG linolenate micelles afforded more uniform internalization which could be attributed to its membrane penetrative property (Castelli et al., 2003)

5.1.2 Curcumin loaded Pluronic linolenate micelles

Among the mPEG fatty esters synthesized in the previous section, mPEG linolenate exhibited better curcumin loading capacity and encapsulation efficiency along with enhanced cytotoxicity and cellular internalization in cancer cells. However, there was a need to improve the loading capacity of 2.91 ± 0.06 % w/w and modulate the release of curcumin from the micelles at pH 7.4. In order to achieve these objectives, Pluronic was incorporated with linolenic acid so as to enhance the hydrophobicity of the micelles. Increasing the hydrophobic block leads to bigger micellar core which can entrap high amount of the hydrophobic drug (Uchegbu and Schatzlein, 2010). In addition, the release of hydrophobic drug from an enhanced hydrophobic core would be slow due to the strong hydrophobic cohesive interaction between the drug and the micelle core. In this section, we discuss a facile preparation of curcumin loaded

Pluronic linolenate. The hydrophobic environment for solubilizing curcumin was provided by alpha linolenic acid and the poly propylene oxide units of Pluronic. The appealing aspect of Pluronic lies in imparting, to the micelles, the potential to prevent opsonization (Jackson et al., 2000). Studies also have shown that Pluronic is effective in the treatment of multi-drug resistant (MDR) tumors (Kabanov et al., 2003; Wang et al., 2008).

Pluronic linolenate was synthesized by Steglich esterification using DCC and DMAP. The IR spectrum of Pluronic linolenate showed principle absorption peaks corresponding to the C-H aliphatic stretch 2882 cm^{-1} and C=O stretching at 1737 cm^{-1} (Figure 22). The ^{1}H NMR spectrum indicated the protons of the conjugated double bonds at 6.64, 7.26 and 8.19 ppm corresponding to linolenic acid. Protons of the methyl group of propylene oxide units were observed at 1.13 ppm and protons of the methylene units of Pluronic were present at 3.6 ppm (Figure 24). Curcumin loaded Pluronic linolenate micelles were prepared by dialysis method. From the DLS experiment, curcumin loaded Pluronic linolenate micelles exhibited a particle size of 167 ± 5nm compared to the unloaded micelles which had a size of 139 ± 4 nm. Size increase was evident with drug loading. Micelle size is a critical parameter which decides the targeting of tumors through EPR effect. However, the actual size of curcumin loaded micelles obtained from TEM analysis was about 60 nm with a range from 60-80 nm (Figure 24). The size decrease is due to the drying up of micelles during TEM measurements. The morphology of the micelles was also realized from the TEM images. It was observed that TEM image of the micelles depicted a distorted morphology. When Pluronic linolenate is

subjected to aqueous medium, the linolenic group attached to the polymer chain tends to self - assemble to form the hydrophobic core and the hydrophobic PPO on the polymer chain will also be forced to loop itself in to accommodate into the hydrophobic core thereby giving a distorted morphology rather than a spherical shape (Tominaga et al., 2010). The curcumin loaded and unloaded Pluronic linolenate micelles exhibited negative charge of –17.2 ± 0.4mV and –14.4 ± 1.5 mV, respectively. The curcumin loaded micelles with optimum zeta potential explained its stability in aqueous medium.

An encapsulation efficiency of 89.3 ± 3.2 % was obtained in the Pluronic linolenate micelles rendering a loading of 7.9 ± 0.3 %. A loading efficiency of about 4-5% has been reported in unmodified Pluronic (Sahu et al., 2011). Hence, increase in the loading efficiency to 8% was attributed to the conjugation of Pluronic with hydrophobic linolenic acid. Earlier reports on curcumin loading in methoxy polyethylene glycol conjugated palmitic acid micelles showed low percentage of loading (about 1 %) despite better encapsulation efficiency (Sahu et al., 2008). It was deduced from our investigation that enhanced curcumin loading was possible by expansion of the hydrophobic core. In this system, the formation of hydrophobic interactions or hydrogen bonds between the micelle and curcumin provided the basis for the solubilization and stabilization of curcumin in the polymeric micelles. The binding affinity of drugs to polymers depends not only on their hydrophobic compatibility, but also on physical interactions, such as hydrogen bonding, π-π stacking, or hydrophobic interactions (Costache et al., 2009). The role of π-π interactions arising from the double bonds present in linolenic moiety and curcumin

could also be another factor for effective solubilization of curcumin. Curcumin solubilization in the core of Pluronic linolenate micelles was qualitatively assessed by Flory-Huggins interaction parameter ($\chi_{sp)}$. A χ_{sp} value of 0.55 was obtained as the interaction parameter ($\chi_{sp)}$ between curcumin and Pluronic linolenate. Previously, the core of mPEG linolenate had a χ_{sp} value of 0.702. Involvement of the PPO hydrophobic units of Pluronic contributed to the overall reduction in the χ_{sp} value indicating that Pluronic linolenate was more compatible with curcumin. This was further corroborated by the relatively enhanced loading capacity of Pluronic linolenate micelles compared to mPEG linolenate micelles. PPO chains of Pluronic linolenate also were instrumental in reducing the CMC of the micelles to 0.41 mg/ml.

A lower CMC value for Pluronic linolenate micelles accounted for its stability highlighting its enticing property as an effective drug carrier since the micellar structure could be retained even upon dilution with a large volume of blood.

Curcumin encapsulation in Pluronic micelles were affirmed by spectral characterization. The absorption peak of curcumin loaded Pluronic linolenate was observed at 425 nm with enhanced intensity compared to free curcumin (Figure 26 A). In the fluorescence spectra curcumin showed a broad peak at 570 nm and the curcumin loaded Pluronic linolenate showed a well-defined high intensity blue-shifted fluorescent peak at 540 nm (Figure 26 B). These observations suggested that curcumin was bound to the core of the micelles. The physical status of curcumin encapsulation in Pluronic linolenate was analyzed by DSC. The existence of free curcumin in crystalline state was confirmed from the endothermic

melting peak at 177.2^{o}C. The characteristic melting peak of Pluronic linolenate was observed at 51.5^{o}C. The absence of endothermic peak of curcumin in the thermogram of curcumin loaded Pluronic linolenate indicated that encapsulated curcumin existed in an amorphous state (Figure 27). Encapsulation of curcumin in Pluronic linolenate also ensured its stability in aqueous medium. Instability and biodegradation in physiological pH remain one of the major challenges of drug delivery (Das et al., 2009). We attempted to study the instability and biodegradation of curcumin and micellar curcumin in PBS. Rapid degradation was put forth by native curcumin (Figure 28). It was noted that only 8% of curcumin remained intact after 8 hours. Curcumin undergoes rapid hydrolytic degradation into vanillin, feruloyl methane, and ferulic acid above neutral pH and these degraded molecules have negligible spectrophotometric contribution (Leung et al., 2008; Wang et al., 1997). However, micellar curcumin showed 90% stability under similar conditions. Thus, Pluronic linolenate micelles formulation increased the stability of curcumin in PBS by protecting it against hydrolysis and biotransformation. Encapsulation of curcumin in Pluronic linolenate afforded comparatively lower release at pH 7.4 than mPEG linolenate. The release of curcumin from the core of the Pluronic linolenate micelles was observed (Figure 29). Sustained release of curcumin was observed after 20 hours and at pH 7.4, after 72 hours, 73.5 ± 1.7% of curcumin was released whereas 88.2 ± 2.5% was released at pH 4.5. Slightly higher release at acidic pH could be attributed to the acid hydrolysis of the ester bonds of Pluronic linolenate. Hydrolysis of ester bonds should exhibit a rapid release, however, it is understood

that the cohesive force between the hydrophobic moieties of the micelle and curcumin prevents the faster release.

While developing matrices for biomaterial applications it is stringent to have an insight on their interactions with blood components especially for materials that come in contact with blood. Therefore, we assessed the hemolytic property and also conducted aggregation studies with the micelles. Hemocompatibility is a significant parameter to evaluate the responses that arises between drug carrier and blood and it determines the safety parameter of the material in the human body. The percentage hemolysis of the blank and curcumin loaded micelles was found to be negligible (less than 1 %) which indicated that the synthesized nanoparticles were RBC compatible. The ability of curcumin to induce apoptosis in cancer cells without cytotoxic effects on healthy cells is well documented in the literature (Sanoj Rejinold et al., 2011). Blood compatibility of the loaded micelles was further evaluated from aggregation studies. The micrographs of human blood cells and platelets along with normal saline and PEI as controls are shown in Figure 30, 31 and 32. Negligible aggregation was detected in RBC, WBC and platelets incubated with the micelles indicating the non-toxic effect of the micelles on normal cells.

Nanoparticle-protein interaction has to be well comprehended so as to reduce or prevent possible adverse effects to the biological systems caused by nanoparticles (Klein, 2007; Owens III and Peppas, 2006). The binding extent of plasma proteins with nanoparticles has to be evaluated as opsonization can be a major hinderance in the systemic circulation of nanoparticles in the body. Therefore, the binding extent of plasma proteins on to the Pluronic linolenate micelles was examined by

performing PAGE (Figure 33). Lanes 2 and 3 corresponded to unloaded and curcumin loaded Pluronic linolenate micelles. There was no inhibition of protein bands as the obtained bands were similar to those of the control placed in lane 1. The clinical applications of blood-contacting materials face the problem of surface induced thrombosis which is triggered by adsorption of plasma proteins to the surface (Horbett, 1993). Protein adsorption is prominent on hydrophobic surfaces and prevention of adsorption with the micelles could be attributed to the presence of Pluronic. It is established that the PEO chains in the Pluronic have the caliber to prohibit adsorption of proteins and cells (Jeon et al., 1991). The nature of the hydrophilic shell is a deciding factor in micelle stabilization and interactions with plasma proteins and cell membranes.

Over the last few decades extensive research has been carried out to establish the potential of curcumin as an effective anti-inflammatory agent with strong therapeutic potential against various cancers. Curcumin exerts its anti-cancer ability by suppressing transformation, proliferation, and metastasis of tumors. Inhibition of proliferation of cancer human colon cancer cell growth occurs by suppressing the expression of the *EGFR* gene by reducing the trans-activation activity of Egr-1(Chen et al., 2005). MTT assay was performed on the micelles to evaluate its cytotoxicty on Caco2 and L929 cells. Reduction of cell viability of Caco2 cells was observed with empty Pluronic linolenate micelles (Figure 34 a). We did not obtain any reduction in cell viability of Caco2 cells with unmodified Pluronic, therefore it was affirmed that linolenic acid was the apoptosis inducing moiety. Reports support that alpha linolenic acid is capable of inducing apoptosis of cancer cells. Linolenic acid

regulates the growth of cancer cell lines through induction of lipid peroxidation and modulation of nitric oxide release followed by decrease in the mitochondrial membrane potential as well as activation of caspase-3 leading to apoptosis (Deshpande et al., 2013). Dose dependent toxicity was observed with curcumin and curcumin loaded micelles (Figure 34 b). As these micelles did not create cytotoxicity on L929 cells, we ascertained that cytotoxicity was induced only in the cancer cells (Figure 34 c and d). In addition, we observed that linolenic acid induced dose depend cytotoxicity on Caco2 cells and did not have any cytotoxic effect on L929 cells. Similar results were observed by Abd Ghafar et al where linolenic acid component in kenaf seeds had caused cell death in colon cancer (HT29) cells and had negligible toxicity on normal (NIH/3T3) cells (Abd Ghafar et al., 2013). It was observed from our MTT assay results that almost 90% L929 cells were viable upon treatment with the loaded and unloaded micelles and this non-toxicity was in alignment with our hemolysis and aggregation studies. Our MTT results, thus, confirmed that micellar curcumin demonstrated negligible toxicity on the normal cells and enhanced cytotoxic activity on Caco2 cells resulting in its low viability compared to free curcumin. 36.6 ± 4.5% cell viability was afforded with the loaded micelles in comparison to 64.8 ± 8.9% cell viability exhibited by curcumin at an equivalent concentration of 10 µM. This could be attributed to the enhanced apoptotic activity of linolenic acid and curcumin, coupled with enhanced aqueous solubility of the latter. A native drug in solution undergoes internalization by diffusing across the cell membrane. However, its entry is restricted after its saturation in the cytoplasm which leaves a minor fraction of internalized native drug to perform its anti-proliferative

effect till the time of its existence (Ma et al., 2008). Nanocarriers can enter the cells via endocytosis and provide sufficient availability of the drug for a longer period and can thus exert profound cytotoxicity.

Live Dead Assay further corroborated our MTT results regarding the enhanced cytotoxicity of curcumin loaded micelles over free curcumin. This assay employs mainly two dyes to infer intracellular esterase activity and plasma membrane integrity. While calcein, a polyanionic dye, is retained within live cells, ethidium bromide homodimer dye enters cells through damaged membranes and binds to nucleic acids (Takada et al., 2006) . Calcein AM produces green fluorescence (excitation, 488 nm; emission, 507 nm) in live cells and ethidium homodimer produces a red fluorescence in dead cells (excitation, 530 nm; emission, 595 nm) (Boukany et al., 2011). The assay performed was a qualitative study to visualize the cytotoxic effect of the curcumin loaded micelles compared to the free curcumin (Figure 35). The red fluorescence was more prominent in the Caco2 cells incubated with curcumin loaded micelles compared to free curcumin indicating enhanced cell death which was attributed to the combined action of micellar curcumin and the linolenic ester moiety.

Cellular uptake study is an important parameter that needs to be probed for explaining successful drug delivery of micelles to cancer cells. Curcumin, being fluorescent, has the advantage to be traced inside cells. Fluorescence microscope images confirmed cellular internalization of the curcumin loaded Pluronic linolenate micelles. Curcumin loaded micelles showed intracellular green fluorescence proving that the Caco2 cells efficiently took up the micelles compared to the free curcumin

(indicated by white arrows in Figure 36). Entry of free curcumin was not prominent in the cells owing to its low aqueous solubility.

5.2 Curcumin loaded micelles based on Pluronic/PCL

5.2.1 Curcumin loaded Pluronic/PCL micelles

In this section, hydrophobic PCL was incorporated with Pluronic as this was considered to further enhance the loading capacity of curcumin. Fortifying the hydrophobic core can minimize the release of curcrmin at physiological pH. Pluronic/PCL block copolymer was synthesized by stannous octoate mediated ring-opening polymerization of ε-caprolactone and Pluronic The mechanism involved the metal species functioning as a catalyst and the end hydroxyl group of the Pluronic serving as an initiator. The active hydrogen atom at one end of the Pluronic chain acted as an initiator and induced a selective acyl-oxygen cleavage of ε-caprolactone. A strong carbonyl band at 1736 cm^{-1} indicated the formation of Pluronic/PCL block copolymer in the IR spectrum (Figure 38). The ^{1}H NMR spectrum exhibited the peaks corresponding to the methylene protons of PEO chains and methyl protons of PPO chains pertaining to Pluronic in addition to the peaks of the PCL block (Figure 39). Formation of a tri-block structure was confirmed from the similar values in the molecular weights obtained from NMR and GPC analysis (Ha et al., 1999).

The CMC of Pluronic/PCL copolymer was determined by using pyrene as a fluorescence probe. The block polymer arranged into its micellar form in aqueous medium forcing pyrene molecules to move into the micelles from the aqueous phase. This transition altered the intensity ratio of (I_3/I_1) of pyrene fluorescence bands. It was

observed that with increased polymer concentrations, the intensity also increased as pyrene was shifted to the hydrophobic interior. CMC value was measured from the point of inflection of the sigmoid curve (Figure 40). The CMC value calculated for Pluronic/PCL was 0.195 mg/ml. Incorporation of PCL afforded a lower CMC value which signified enhanced hydrophobicity that enabled the easy micelle formation of Pluronic/PCL. This indicated that the micelles may be useful as drug carriers as they could maintain a micelle structure even upon dilution with a large volume of blood.

Curcumin loaded Pluronic/PCL micelles were prepared by dialysis method. The dialysis method consists in bringing the drug and copolymer from organic solvent in which they are both soluble to a solvent that is selective only for the hydrophilic part of the polymer (e.g. water). As the organic solvent is replaced by the selective one, the hydrophobic portion of the polymer associates to form the micellar core incorporating the insoluble drug during the process. Curcumin was loaded into the inner hydrophobic core of the Pluronic/PCL micelles by adopting similar strategy. The loading efficiency of curcumin is a factor which gets compromised despite high encapsulation efficiency. Curcumin delivery in self-assembling methoxy poly (ethylene glycol)–palmitate nanocarrier of Sahu et al exhibited loading efficiency of 1% despite an encapsulation close to 100% (Sahu et al, 2009). We carried out curcumin loading in Pluronic/PCL micelles at 9.09%, 11.76% and 14.28% w/w which afforded an encapsulation efficiency of 96 ± 1 , 87.03 ± 2.21 and 72.1 ± 4.3% respectively. This corresponded to an actual loading capacity of 8.78 ± 0.09, 10.2 ± 0.3 and 10.3 ± 0.6% w/w. Precipitation of curcumin was observed when 16.66 % w/w loading was performed and hence theoretical loading of 11.76% w/w was optimized

for further *in vitro* studies. We were able to attain a loading capacity of 10 % w/w which equated to an encapsulation efficiency of 87 %. The compatibility of curcumin with the Pluronic/PCL core was evaluated by determining χ_{sp}, the Flory-Huggins interaction parameter. The interaction parameter (χ_{sp}), was calculated as 0.172 for Pluronic/PCL core. Previously, a χ_{sp} value of 2.91 has been reported for the compatibility between curcumin and PCL core (Letchford et al., 2008). Incorporting Pluronic to PCL has evidently reduced the (χ_{sp})value.

Particle size is an important parameter as it can directly affect the physical stability, cellular uptake, biodistribution and drug release from the nanoparticles (Feng, 2004). The particle sizes of the unloaded Pluronic/PCL micelles determined by DLS are shown in Table 3. Encapsulation of curcumin was evident from the gradual increase in the size of micelles with the increased curcumin loading. The size of the micelles observed in the TEM image were smaller than that obtained in DLS and the reason could be attributed to the shrinkage of the hydrophilic backbone during the sample preparation for TEM (Hu et al, 2009).

Information regarding a charged active material being encapsulated within the centre of the nanocarrier or adsorbed onto the surface can be gathered by zeta potential determination (Mohanraj and Chen, 2007). The micelles had a zeta potential in the range of –14 to –17mV which is well within the optimal range (Table 2). Negligible change in the zeta potential indicated that curcumin was encapsulated inside the Pluronic/PCL micelles.

The physical status of curcumin encapsulated in the polymeric micelles was investigated by DSC. DSC is an accurate and rapid thermo-analytical technique,

widely used by the pharmaceutical industry and in drug research, to investigate several physicochemical phenomena, such as polymorphism, melting and crystallization, purity, drug excipient interaction, polymer properties, etc (Pignatello and Castelli, 2011). Free curcumin has an endothermic melting peak at 177.2^{o}C implying its crystalline state. This peak was absent in the thermogram of curcumin loaded Pluronic/PCL copolymers which only exhibited the characteristic melting peaks of Pluronic/PCL co polymer around 57^{o}C (Figure 42). The absence of detectable crystalline domains of curcumin in the loaded micelles indicated that encapsulated curcumin was in the amorphous form in the polymeric matrix (Acharya et al., 2009). The presence of drug in crystalline form inside nanoparticles can pose as an obstacle during its release due to the difficulty in the diffusion of the large sized molecules from the small pores of the nanoparticles.

Encapsulation of curcumin in the micelles was further confirmed by spectral characterization studies. Free curcumin showed an absorption peak at 425 nm. Similar peak with a decrease in absorption intensity was exhibited by curcumin loaded Pluronic/PCL micelles (Figure 43A). In the fluorescence spectra, curcumin showed a weak broad peak at 550 nm and the curcumin loaded Pluronic/PCL micelles showed a well- defined high intensity blue-shifted fluorescent peak at 495 nm (Figure 43 B). This suggested the binding of curcumin to the hydrophobic core of the micelles.

Hemocompatibility is a significant parameter to evaluate the responses that arises between the drug carrier and blood. Negligible percentage (less than 1 %) of hemolysis was observed in the case of empty and curcumin loaded micelles which

indicated that the synthesized nanoparticles were compatible with the erythrocytes (Table 4). This was an expected observation as both the components of the micelles, Pluronic and PCL, are widely used matrices for biological applications. The blood compatibility of the micelles was further visually revealed through aggregation studies. Blood cell aggregation is a highly undesirable phenomenon that can induce serious circulatory disorders, even lethal toxicity. Evaluation of blood compatibility is essential for materials designed for biological applications. Negligible aggregation was detected in RBC, WBC and platelets incubated with the micelles indicating the non-toxic effect of the micelles on normal cells. The micrographs of human blood cells (RBC, WBC and platelets) upon interaction with the loaded and unloaded micelles along with normal saline and polyethylene imine (PEI) as controls are shown in Figure 44. It was observed that the micelles did not promote aggregation like the positive control, PEI. The non-aggregation of the micelles could be attributed to the Pluronic moiety. The use of Pluronic for modifying blood compatibility of materials is well reported and the improved anti-thrombogenicity of Pluronic can be attributed to the long polyethylene oxide chains which are capable of suppressing blood cell adhesion (Mao et al., 2009). Understanding nanoparticle-protein interaction is a prominent factor which helps in promoting applications of nanoparticles in the biomedical field and reducing/preventing possible adverse effects to the biological systems caused by nanoparticles. The binding extent of plasma proteins with Pluronic/PCL micelles was examined by native PAGE (Figure 45). Lane 2 and 3 corresponded to Pluronic/PCL and curcumin loaded Pluronic/PCL, respectively. It was observed that the protein bands corresponding to most of the low

molecular weight globular proteins were present in all the polymer- plasma samples. The protein bands were similar to the band obtained in lane 1 which corresponded to normal saline indicating that the micelles did not bind with the plasma proteins. The lack of adherence of plasma proteins on the Pluronic/PCL micelles could be attributed to the PEO units in Pluronic which are capable of prohibiting adsorption of proteins and cells depending on the surface density of PEO chains, their length and dynamics (Jeon et al., 1991). The bio-distribution of the carrier is mainly dictated by the nature of the hydrophilic shell which is responsible for micelle stabilization and interactions with plasma proteins and cell membranes (Yokoyama, 1998). Incorporation of PCL modulated the release of curcumin at the physiological pH. Low release of curcumin was observed at pH 7.4 compared to the previously synthesized Pluronic linolenate. After 72 hours, the release of curcumin was 56.2 ± 3.6% at pH 7.4 and 89.3 ± 5.2% at pH 4.5 (Figure 46).

Free curcumin was found to be sparingly soluble in aqueous solution with formation of visible undissolved microscopic flakes compared to the curcumin loaded micellar solution (Figure 47). We attempted to study the biodegradation and stability of curcumin by incubating both free and encapsulated curcumin in PBS and estimated its concentration with time, spectrophotometrically. It was observed that only 5% of free curcumin remained intact after an incubation of 8 hours where as 94 % of curcumin encapsulated in the Pluronic/PCL micelles remained intact (Figure 47). Curcumin, due to its hydrophibicity, was presumed to be inside the core of the micelles and the copolymeric micelles were capable of protecting the encapsulated curcumin against biotransformation and hydrolysis.

MTT assay was performed on the empty and curcumin loaded Pluronic/PCL micelles. It was observed that Pluronic/PCL micelles did not exhibit any toxicity which was in accordance with the hemolytic study. 100% cell viability was encountered at 3 mg/ml copolymer concentration (Figure 48 a). The potential of curcumin to elicit apoptosis signals in a variety of tumor tissues including colorectal, lung breast, pancreatic and prostate carcinoma is well documented in the literature (Lev-Ari et al., 2005; Ma et al., 2008). Levi-Ari et al have suggested that the apoptotic ability of curcumin is related to the inhibition of the activation of mitogen-activated protein kinase which subsequently down regulates the expression of COX-2 (cyclooxygenase) (Lev-Ari et al., 2007). Inadequate water solubility and subsequent precipitation decreased the effective exposure time of the cells with free curcumin leading to relatively less cytotoxicity compared to the curcumin loaded micelles (Figure 48 b). Less than 60% cells were viable at a curcumin concentration of 10 μM in the curcumin loaded micelles. Low cell viability of Caco2 cells was attributed to the enhanced aqueous solubility and effective cell internalization of the curcumin loaded Pluronic/PCL micelles. Enhanced cytotoxicity was attributed to the presence of Pluronic. Yan et al recently observed that the docetaxel-loaded PLGA/poloxamer 188 nanoparticles achieved a significantly higher level of cytotoxicity than that of docetaxel-loaded PLGA nanoparticles and Taxotere (Yan et al., 2010). Similar observation had been reported by Mei et al with docetaxel loaded PCL/Pluronic F68 nanoparticles in docetaxel resistant human breast cancer cell line, MCF-7 TAX (Mei et al., 2009). From the cytotoxicity study affirmed that the transition of crystalline phase of curcumin to the amorphous state upon encapsulation did not hinder its

anticancer potential and that the micellar encapsulation did not compromise the therapeutic activity of curcumin. Green intrinsic fluorescence of curcumin is a widely exploited factor in the cellular uptake studies of curcumin. Curcumin has the advantage to be traced inside cells without being tagged by other fluorescent dyes. We confirmed the cellular internalization of curcumin loaded Pluronic/PCL micelles by fluorescence microscopy in Caco2 cells. The empty Pluronic/PCL micelles did not exhibit any fluorescence (Figure 49 a). Curcumin loaded micelles showed intracellular green fluorescence proving that the Caco2 cells efficiently took up the micelles compared to the free curcumin. However, entry of free curcumin was not prominent in the cells owing to its low aqueous solubility (Figure 49 b,c). Similar observations on the effect of curcumin encapsulated Pluronic micelles in HeLa cells have been reported (Sahu et al., 2011). Micelles with Pluronic moiety have been known to undergo internalization in cells (Batrakova et al., 2001). Sahay et al studied the endocytosis mechanism of Pluronic block copolymers where they interfere with selected membrane trafficking processes by inserting their hydrophobic PPO chains into lipid bilayers and decreasing membrane microviscosity (Sahay et al., 2008). The uptake of curcumin loaded Pluronic/PCL micelles in the Caco2 cells could be attributed to these mechanisms induced by the Pluronic moiety.

5.2.2 Curcumin loaded calix arene conjugated Pluronic/PCL micelles

Calix arenes are versatile macrocyclic compounds endowed with well-defined conformational properties and molecular dimensional cavities that are capable of encapsulating drug molecules (Specht et al., 2002). This section focuses on

conjugating calix arene to Pluronic/PCL to impart enhanced hydrophobicity so as to attain greater loading efficiency for curcumin. The tert-butyl groups of tert-butyl calix[4]arene offer steric hindrance to the encapsulation of curcumin and so it was necessary to remove them (Tu et al., 2011). Calixarene was conjugated at the lower rim with PCL/Pluronic and the presence of aromatic peaks of calix arene, disappearance of the OH peak at 3122 cm^{-1}, in addition to the peaks corresponding to Pluronic/PCL in the IR spectrum confirmed the conjugation (Figure 51). Curcumin loading was performed in the CX-Pluronic/PCL micelles via dialysis method. Calix arenes are known to promote supramolecular recognitions by host-guest chemistry where chemical entities are held together by non-covalent interactions like hydrogen bonding, π-π interactions or ion-pairing (de Fátima et al., 2009). These host-guest interactions form the keystones that encourage the applications of calix arene in various fields like food, pharmaceutical and sensor technology. The presence of π-conjugation domains in curcumin enables π- π interaction with CX-Pluronic/PCL to form supramolecular self-assembling micelles in aqueous medium (Figure 52). The curcumin loading capacity in CX-Pluronic/PCL obtained was 17.6 ± 1.2% w/w which corresponded to an encapsulation efficiency of 78.2 ± 4.4 %. The size of the curcumin loaded micelles was found to 230 ± 9.2 nm from DLS measurements and the zeta potential was -26.1 ± 3.2 mV (Figure 54). CX-Pluronic/PCL micelles exhibited a reduced size in the TEM measurements due to the drying up of the micelles. The CMC value of CX-Pluronic/PCL was determined as 0.013 mg/ml. Conjugating calix arene to Pluronic/PCL led to a drastic lowering of the CMC value from 0.195 to 0.013mg/ml. At concentrations above the CMC value, amphiphilic

calix [n] arenes undergo a structural reorganization upon aggregation to attain the cone conformation in the micelles which is considered to be the stabilized confirmation (Basílio et al., 2012). In CX-Pluronic/PCL micelles, calix [4] arene and hydrophobic moieties of Pluronic/PCL moieties point to the hydrophobic interior with hydrophilic PEO chains in contact with the solvent. The value obtained for the interaction parameter (χ_{sp}) of curcumin with CX-Pluronic/PCL core was –0.799. Occurrence of negative interaction parameter has been reported as evidence of thermodynamic compatibility where the inter-molecular interactions between the mixtures are dominated by directional interactions (Choi et al., 1996). This implied a high miscibility between the curcumin and the CX-Pluronic/PCL core. The improved core-drug compatibility is attributed to the π- π interactions between the aromatic rings of calix arene and curcumin. The presence of aromatic groups on the core-forming block improves the stability and loading of an aromatic drug (Carstens et al., 2008). Observations regarding the spectral characterization were similar to the previously synthesized micelles. The trend of enhanced peak intensity at 425 nm was seen in the UV spectrum which is the characteristic of curcumin loaded in the the micellar core. In the fluorescence spectrum, the typical blue shift associated with curcumin in loaded micelles was encountered (Figure 55).

Calix arenes have been proved to be ideal candidates for pharmaceutical applications as they have been considered innocuous with regard to hemolytic effects (Mokhtari and Pourabdollah, 2012). The non-toxic effect was also confirmed from our blood compatibility studies. Negligible hemolysis was afforded with curcumin loaded

CX-Pluronic/PCL micelles. Aggregation studies further reinforced the fact that the micelles were compatible with blood components as no aggregation was induced.

Calix arenes, in addition to molecular recognition of targets, can also actively tune their molecular shape under external stimuli which plays a significant role in releasing or binding of the guest molecule (Lagugné-Labarthet et al., 2005). This explains the high release of curcumin from CX-Pluronic/PCL micelles at acidic pH. 88.3 ± 7.6% of curcumin was released in 72 hours at pH 4.5 whereas the release at pH 7.4 was 35.2 ± 6.5% (Figure 58). Calix arene, encapsulating a guest, exist in a vase conformation and upon lowering of the pH, it switches to kite conformation and this facilitates the release of the guest molecule. This process is defined by the couloumbic repulsion between the protonated wings of calix arene in vase conformation at acidic pH (Sliwa and Kozlowski, 2009). This pH-sensitive release could be extremely significant for tumour targeting. Cytotoxicity studies on curcumin loaded CX-Pluronic/PCL micelles revealed enhanced cell death in C6 glioma cells. Curcumin loaded CX-Pluronic/PCL exhibited a cell viability of 11.3 ± 3.7% compared to free curcumin which showed 70.7 ± 4.5% at curcumin concentration of 20 µM (Figure 59). Enhanced loading, aqueous solubility and accelerated release of curcumin at acidic pH contributed to the reduction of cancer cells. The empty micelles of CX-Pluronic/PCL did not induce any reduction in cell viability which indicated its non-toxicity. This was also corroborated through the blood compatibility studies. Encapsulation of curcumin in CX-Pluronic/PCL micelles also afforded enhanced cellular internalization in the glioma cells compared to unencapsulated curcumin as evident from the intense green fluorescence (Figure 59).

Recent studies on a fluorescent water-soluble calix[4] arene ruled out the possibility of active endocytosis as a the route for cellular internalization as the uptake could not be inhibited by endocytosis inhibitors and suggested that calix arenes could make pores in the membrane and enter by diffusion (Redshaw et al., 2012).

5.3 Curcumin dextran conjugates

Conjugating hydrophobic drugs to hydrophilic polymers enhance their aqueous solubility in addition to improving drug targeting to the tumour , limiting toxicity and overcoming the mechanisms of drug resistance (Duncan, 2006). In this section, we attempted to conjugate curcumin to hydrophilic polymer dextran. We hypothesized that conjugation of curcumin on to dextran can itself form an amphiphilic entity which can self- assemble into micelles and furthermore, dextran could endure a good loading capacity as it is endowed with many hydroxyl groups onto which conjugation with curcumin is possible. Curcumin was conjugated to dextran through succinic acid spacer to produce curcumin-dextran conjugate (Cur-Dex) [Figure 61]. The IR spectrum of Cur-Dex exhibited CH aliphatic stretching at 2882 cm^{-1} (Figure 62). Reduction of the –OH stretching peak dextran at 3250 cm^{-1} confirmed the conjugation. However, peak at 3505 cm^{-1} which corresponded to the hydroxyl group of curcumin was present, implying the mono-esterification of curcumin. In the ^{1}H NMR spectrum, the conjugation was confirmed through the presence of the protons of the dextran backbone seen between 2-5 ppm along with the aromatic protons of curcumin observed between 6.3 ppm and 6.6 ppm (Figure 63). An amphiphilic matrix was constructed by attaching hydrophobic curcumin to the hydrophilic

dextran chains (Figure 64). In order to determine whether the curcumin dextran conjugates could self-assemble into micelles, CMC was determined (Figure 65). The CMC of Cur-Dex was calculated to be 0.469mg/ml and was much lower compared to that of mPEG fatty esters, synthesized in the first section. In fact, it was evident that Cur-Dex could self-assemble into stable micelles.

The size of the micelles was 222 ± 33 nm from DLS measurements and less than 50 nm in TEM data. The zeta potential of Cur-Dex was measured to be − 15.2 ± 2.2 mV (Figure 66). The conjugated curcumin showed the amorphous characteristics of encapsulated curcumin as seen in the previous sections which was evident from the absence of crystalline peak of curcumin, usually exhibited around 180^{o}C, in the DSC thermogram of Cur-Dex conjugate (Figure 67). The curcumin loading capacity in Cur-Dex conjugates was 3.3 ± 1.2%. It was believed that the steric hindrance caused by the conjugated curcumin on the dextran backbone prevented further conjugation of curcumin molecules on to it affecting the loading capacity. The presence of curcumin in a micellar environment was further affirmed by spectral characterization. The UV-visible spectrum of Cur-Dex exhibited an enhanced absorption peak at 425 nm and the fluorescence spectrum showed a blue shifted emission at 522 nm.

Dextran is a widely implemented polymer for drug delivery due to its to an inherent biocompatibility (Draye et al., 1998). This was apparent as Cur-Dex conjugates neither induced any lysis of erythrocytes nor caused aggregation of blood components (Figure 69). The susceptibility of biomaterials to nonspecific protein adsorption on their surfaces poses as a chief limitation to their performance and

lifespan. Surfaces grafted with dextran have been reported for 65-90% reduction in protein adsorption (Frazier et al., 2000; Österberg et al., 1995). It was observed that hydrophilic chains of dextran prevented adsorption of proteins on the conjugates as evident from the PAGE study (Figure 70). Conjugation of drugs to water-soluble polymers increases their stability. The degradation of curcumin was prevented upon conjugation with dextran and was efficient in retaining its stability by 80% (Figure 71 a). Self-assembly of the conjugates pushed curcumin into the micelle core with the hydrophilic chains of dextran surrounding it from aqueous environment, thereby preventing the rapid degradation of curcumin. This is a significant factor as it ensures longer circulation of the drug after systemic administration without losing its stability. Another criterion is the release of the drug at physiological pH as this too contributes to the loss of the drug during systemic circulation. Conjugation of curcumin helped in modulating its release at pH 7.4 to achieve 30.2 ± 5.5 % sustained release of curcumin in 72 hours. However, an accelerated release of 97.4 ± 3.6 % of curcumin from the conjugate was observed at pH 4.5 (Figure 71 b). This was attributed to the ester hydrolysis of the succinic acid spacer which provided the labile linkage between curcumin and dextran at acidic pH (Won and Chu, 1998).

The efficacy of Cur-Dex conjugates in exerting cell death in C6 glioma cells was assessed through MTT assay. Curcumin concentration above 30µM in the conjugate form induced cytotoxic effects in glioma cells. A dose dependent cytotoxicity was observed. In case of free curcumin, about 60% of glioma cells were viable at 50 µM whereas for similar curcumin concentration in the conjugated system less than 20% cells were viable (Figure 72). The profound cytotoxicity was attributed to the

enhanced aqueous solubility of curcumin which was achieved by conjugating to water soluble dextran associated with release of curcumin at acidic pH. The enhanced cell death was further corroborated by live dead assay results (Figure 72). Dextran has been noted to enter cells via fluid endocytosis and hence is used widely as a fluid-phase marker to investigate endocytosis (Racoosin and Swanson, 1993). Conjugation of curcumin with dextran helped effective cellular internalization of curcumin in glioma cells which was evident from enhanced green fluorescence compared to free curcumin (Figure 74).

5.4 Curcumin loaded micelles based on POxs

5.4.1 Curcumin loaded Poly [2-ethyl-2-oxazoline-b-2-(but-3-enyl)-2-oxazoline] P(EtOx-b-ButenOx) micelles

POxs are a class of polymers which possess numerous potential applications (Hoogenboom, 2009). The living cationic ring-opening polymerization of 2-oxazolines affords the preparation of well-defined polymers with narrow average molecular weight distributions (Kagiya et al., 1966b; Seeliger et al., 1966; Tomalia and Sheetz, 1966). Incorporation of appropriately substituted monomers can fine-tune the properties of the corresponding polymers (Wiesbrock et al., 2005). Block copolymers that consist of hydrophilic and hydrophobic segments are capable of self assembling in aqueous solution. The hydrophobic core is capable of encapsulating low aqueous soluble drugs whereas the hydrophilic corona proves efficient in imparting stealth properties to the micelles (Mikhail and Allen, 2009). In this regard, we synthesized di-block polymers of EtOx and ButenOx which constituted the

hydrophilic and hydrophobic segments, respectively. ButenOx polymerization was carried out so as to incorporate hydrophobic chains for micelle formation. However, it can be further exploited for functionalization by click chemistry through their double bonds (Kempe et al., 2010). P($EtOx_{30}$-b-$ButenOx_5$) , P($EtOx_{33}$-b-$ButenOx_{26}$) and P($EtOx_{17}$-b-$ButenOx_{44}$) di-block polymers were synthesized by the living cationic ring opening polymerization and the block architecture was ensured by complete polymerization of the first monomer i.e. EtOx monomer before reacting the second monomer (ButenOx). The disappearance of the monomer peaks and appearance of the backbone protons of the polymer at 3.45 ppm was confirmed from ^{1}H NMR. The number average molecular weights of P($EtOx_{30}$-b-$ButenOx_5$), P($EtOx_{33}$-b-$ButenOx_{26}$) and P($EtOx_{17}$-b-$ButenOx_{44}$) di-block polymers were deduced from ^{1}H NMR and were found to be 3631.89 g/mol, 6555.79 g/mol and 7224.83 g/mol , respectively. The glass transition temperatures of P($EtOx_{30}$-b-$ButenOx_5$) , P($EtOx_{33}$-b-$ButenOx_{26}$) and P($EtOx_{17}$-b-$ButenOx_{44}$) were observed at 22.7, 23.2 and 17.8^{o}C, respectively (Figure 75). The glass transition of a polymer is indicative of the chain mobility of the polymer chains and share an inversely proportional relationship i.e. higher the Tg , lower is the chain mobility (Wiesbrock et al., 2005). Gress et al had reported the Tg values for P(ButenOx) homopolymers weights where the increment in the glass transition temperatures were observed with increase in the molecular weights (Gress et al., 2007a). It was observed from their study that the block polymer containing EtOx units showed higher Tg. Presence of EtOx led to a Tg of 38^{o}C compared to ButeOx homopolymers which had Tg in the range of 9^{o}C-

17^{o}C. Similarily, we encountered a decrease in Tg in PEtOx-b-ButenOx polymers due to the decrease in EtOx units (Figure 76).

The CMCs of the synthesized POx micelles were determined by using DPH as the fluorescent probe. DPH is a fluorescent molecule which is hydrophobic in nature and thus can readily incorporate itself into the hydrophobic core of micelles. The transition from the aqueous environment of the probe to the micelle hydrophobic core results in significant increase in fluorescence intensity (Shaik et al., 2009; Zeng and Pitt, 2006). The CMC of P($EtOx_{33}$-b-$ButenOx_{26}$) and P($EtOx_{17}$-b-$ButenOx_{44}$) was calculated to be 0.12 mg/ml and 0.07 mg/ml respectively. The relative lower CMC value of $PE_{17}B_{44}$ was attributed to the higher number of hydrophobic ButenOx units. A similar trend of decreasing CMC values for increasing hydrophobic units of poly oxazolines is in accordance with the literature (Hruby et al., 2010; Luxenhofer et al., 2010). Increase in the fluorescence intensity of DPH was more prominent in P($EtOx_{17}$-b-$ButenOx_{44}$) micelles and is in accordance with previous reports (Luxenhofer et al., 2010; Naka et al., 1995). However, a correlation could not be obtained between the CMC values for our di-block polymer with the values calculated for the triblock polymers synthesized by Luxenhofer and co-workers, in terms of number of hydrophobic units(Luxenhofer et al., 2010). We believe that comparisons between different hydrophobic moieties would not give relevant results. But even in terms of similar hydrophobic moieties, Bonne et al found differences in CMC with varying polymer architectures (Bonné et al., 2007). They observed that the CMCs of the tri-block polymers were lower than the ones of the di-block polymers, despite being contradictory to previous reports. However, the reason for

poly (2-oxazoline) copolymers to behave differently was not identified and further research would be needed to gain insight into this. For, $PE_{30}B_5$ the CMC value could not be derived as it did not give a definite inflection curve. This could be attributed to the less number of hydrophobic units which lead to low cohesion force to hold the micelle structure together. It is imperative for the micelles intended for drug delivery to have a low CMC value as higher CMC would make the micelles face the dire consequences of disassembling into unimers upon dilution after intravenous injection, thereby releasing the drug without attaining the desired physiological action. Micelle dissociation is related to the composition and the cohesion of the hydrophobic core. Increment in the hydrophobic units results in enhanced cohesion of the core leading to lower CMC (Gaucher et al., 2005; Lee et al., 2004; Van Domeselaar et al., 2003).

Empty and loaded micelles of the block polymers were prepared by nano-precipitation method which is based on the interfacial deposition due to the displacement of a solvent with non-solvent. This technique has been widely embraced owing to its facile procedure and low energy costs (Aubry et al., 2009). In contrast to the emulsion/solvent diffusion technique which uses immiscible solvents, nanoprecipitation utilizes a non-solvent that is miscible with the solvent. Furthermore, emulsion/ solvent diffusion technique might include addition of surfactants which could cause toxic effects. We attempted dialysis method initially but formation of large sized particles persuaded us to choose the nano-precipitaion technique. In our preparation, we dissolved curcumin and POx in acetone and added the polymer drug solution drop wise to stirring water followed by dilution which can

favour the decrease of free energy of the system by rapid removal of hydrophobic fragments from the aqueous environment to form the drug loaded micellar core [Figure 77] (Torchilin, 2001).

The block polymers self-assembled into micelles of size in the range of 70-110 nm as confirmed by DLS measurements (Table 4). Particle size of a micelle defines various crucial parameters like cellular uptake, bio-distribution and stability (Feng, 2004a). Polymeric micelles usually have the size of 10-200 nm and due to their small size they are able to home in on the tumour cells by enhanced permeation and retention (EPR) effect (Maeda et al., 2000). Relative large size of our micelles to the previously synthesized micelles of tri-block copolymers could be attributed to the polymer architecture (Luxenhofer et al., 2010). Micelles formed from di-block copolymer undergo stretching of the core block through the micellar core ,in addition to the space demands of the hydrophilic block (Bonné et al., 2007). Increase in micelle size was concomitant with curcumin loading. However, P($EtOx_{17}$-b-$ButenOx_{44}$) exhibited smaller size than P($EtOx_{33}$-b-$ButenOx_{26}$), despite possessing more number of hydrophobic units. This relatively smaller size of could be attributed to the lower number of ethyl 2-oxaline units. The shorter and less extended hydrophilic chains could have resulted in smaller hydrodynamic volume leading to reduction in overall particle size.

Size of particles obtained by TEM was smaller compared to the DLS measurements (Figure 80). This was a result of drying up of the hydrophilic chains of micelles during sample preparation. It is perceived that longer hydrophobic and shorter hydrophilic chains can cause formation of non-spherical aggregates due to increase

in the number of crystalline folds in the core leading to a reduction in crowding of the corona(Owen et al., 2012). Interestingly, from our TEM images it was seen that P($EtOx_{17}$-b-$ButenOx_{44}$) micelles did not deviate from the usual spherical morphology despite possessing longer hydrophobic and shorter hydrophilic chains. Curcumin loading of 7.5 ±1.7 and 11.75 ±2.2 % were obtained from P($EtOx_{33}$-b-$ButenOx_{26}$) and P($EtOx_{17}$-b-$ButenOx_{44}$) micelles, respectively. The P(EtOx-b-ButenOx) micelles had lower χ_{sp} value than our previously investigated micelles which explained the relatively better loading capacity of the POx micelles. Low value of χ_{sp} , indicating good compatibility, between curcumin and ButenOx could be attributed to the π-π interaction between the double bond of the butenyl side chains and curcumin.

Spectral characterization studies further confirmed the encapsulation of curcumin in the micelles (Figure 79). Curcumin absorption peak in the loaded micelles was evident at 425 nm with enhanced intensity. In the fluorescence spectra, curcumin showed a weak broad peak at 560 nm and the curcumin-loaded P($EtOx_{33}$-b-$ButenOx_{26}$) and P($EtOx_{17}$-b-$ButenOx_{44}$) micelles showed a well-defined high intensity blue shifted peak at 548 and 538 nm , respectively. This suggested the binding of curcumin to the hydrophobic core of the micelles through the hydrogen bond interaction between the hydroxyl groups of curcumin and ButenOx core.

Stability is an important parameter to take into account when designing micelles for drug delivery purposes. Micelles designed for drug delivery should remain intact to prevent release of the drug payload before reaching the target cells. The size of the P($EtOx_{17}$-b-$ButenOx_{44}$) micelles was almost constant for over a period of 30 days and was evidently more kinetically stable than P($EtOx_{33}$-b-$ButenOx_{26}$) (Figure 80 a).

Increased hydrophobic chain length which indicates lower CMC values correlates to increased stability of micelles. Empty micelles of P($EtOx_{33}$-b-$ButenOx_{26}$) exhibited increase in size after 8 days, however the curcumin, loaded micelles of the same did not follow similar trend. It is evident that curcumin loaded in the core of the micelles enhanced the hydrophobicity of the core and prevented the disassociation of the micellar structure. Additional hydrophobic interactions of an encapsulated drug is known to stabilize the core of micelles (Owen et al., 2012).

The ability to ultimately release the drugs, in addition to sequestration and solubilization of hydrophobic drugs completes the profile of efficient drug delivery systems. It was interesting to note from our release experiments that P(EtOx-ButenOx) polymers depicted a pH dependent curcumin release. About 12.6 ± 4.5 % and 34.3 ± 4.8 % of curcumin were released from P($EtOx_{17}$-b-$ButenOx_{44}$) and P($EtOx_{33}$-b-$ButenOx_{26}$) , respectively in 168 hours at pH 7.4 whereas at pH 4.3 , 86 ± 3% and 87 ± 5% of curcumin was released, respectively (Figure 80 b). Similar pH dependent release pattern is in accordance with previous studies dealing with polyoxazoline (Hsiue et al., 2006). Acidic pH induces the protonation of tertiary amide groups on oxazoline chains which can subsequently enable intra/intermolecular interactions between micelles leading to aggregation and finally, micellar deformation (Hsiue et al., 2006). Faster release in acidic pH is significant as it relates to the lower pH in the endocytic compartment of tumor cells (pH 4.5-6.5). It was also observed that the release of curcumin from the micelles was dependent on the hydrophobicity of the micelles. Relatively lower release of curcumin was put

forth by P($EtOx_{17}$-b-$ButenOx_{44}$) micelles and this could be explained by the enhanced hydrophobic cohesive interaction due to greater number of ButenOx units.

The biocompatibility of POxs was demonstrated as early as 1989 (Goddard et al., 1989b). The evidence of biocompatibility and steatlth behavior of POxs was provided by Zalipsky and co-workers (Zalipsky, 1995; Zalipsky et al., 1996). It was observed in our study that the empty POxs micelles did not exhibit any toxic effect on the cell lines, thus highlighting their biocompatibility (Figure 81 a). Cytotoxicity of a range of homo and block POx copolymers were investigated by Luxenhofer et al and it was confirmed that POxs were well tolerated by mammalian cells (Luxenhofer et al., 2011). Curcumin loaded POx micelles exhibited profound cell death compared to free curcumin which could be related to enhanced solubility of curcumin in the micelles and accelerated release of curcumin in acidic environment (Figure 81 b). The cytotoxic effects were further corroborated by live dead assay (Figure 73). Amphiphilic POxs have been known to enter cells efficiently by endocytosis and uptake of the polymers was determined by structure-property relationships. It was noted that a reduction in the hydrophobicity of the hydrophobic block diminished the cellular uptake of POx polymer (Luxenhofer et al., 2011). The hydrophilic blocks played insignificant role in the cellular internalization. From the fluorescence microscopy images, it was observed that curcumin loaded P(EtOx-b-ButenOx) micelles exhibited prominent green fluorescence indicating relatively better uptake than the free curcumin. (Figure 74). Moreover, the uptake of curcumin loaded P($EtOx_{17}$-b-$ButenOx_{44}$) micelles was relatively better compared to P($EtOx_{33}$-b-

$ButenOx_{26}$) micelles and this could be explained by the greater hydrophobicity of P($EtOx_{17}$-b-$ButenOx_{44}$) .

5.4.2 Curcumin loaded block and gradient P(MeOx-isoPropOx) micelles

The micelles of the block and gradient polymers were prepared by nano-precipitation method. CMCs of the block and gradient polymers were determined using DPH as the fluorescent probe and the results have been tabulated (Table 6 and 7). The polymers followed the standard trend of decreasing CMCs for increasing number of hydrophobic (isoPropOx) units. The block copolymers had relatively lower CMCs than their gradient counterparts and this behaviour is consistent with previous studies (Sandoval et al., 2008; Wong et al., 2007). This is attributed to the key differences between the interfacial properties of block copolymers and gradient copolymers where the zone of mixing between two repeat units in gradient polymers is controlled by the copolymer radius of gyration, and not by the thermodynamic incompatibility between the repeat units which usually occurs in block polymers (Shull, 2002). Block polymers are capable of forming micelles at lower concentrations preventing their individual molecules to diffuse into the interface (Lyatskaya et al., 1996; Shull and Kramer, 1990).

The particle sizes of the micelles were evaluated by DLS. Interestingly, the DLS results showed that size of the micelles decreased after loading of curcumin which was contradictory to the P(EtOx-b-ButenOx) micelles. It was evident that hydrophobic interactions between the drug and isoPropOx core played a vital role in stabilizing and decreasing the size of the micelle. However, curcumin loaded block

$MeOx_{50}$-b-$IsoPropOx_{10}$ showed a size increase compared to the empty micelle. It is believed that the hydrophobic interaction between curcumin and the core was not prominent due to lesser number of isoPropOx units. This is validated by the determination of χ_{sp} between curcumin and isoPropOx. Value of χ_{sp} was calculated to be 0.625. Curcumin was definitely more compatible with ButenOx core (χ_{sp} = 0.07) and it was obvious that the presence of the double bonds in the butenyl group gave a massive difference in group contribution calculations, thereby accounting for the very low of χ_{sp}. The gradient polymers also exhibited similar trend in size decrease with curcumin loading except $MeOx_{40}$-g-$IsoPropOx_{20}$ and $MeOx_{50}$-g-$IsoPropOx_{10}$ which had lower number of hydrophobic units. The gradient polymers had larger size compared to block ones and could be attributed to the uneven sequence distribution of hydrophilic and hydrophobic segments. The TEM images depicted smaller sizes compared to DLS results due to the drying up of hydrophilic chains during sample preparation. Block polymers with greater number of hydrophobic units retained their spherical structure. It was observed that curcumin loading in P($MeOx_{50}$-b-$isoPropOx_{10}$) helped in retaining the spherical structure. The loading efficiency was calculated for these groups of polymers and was observed to be dependent on the number of hydrophobic units. The gradient polymers, however, showed very low loading compared to the block polymers and this is not unusual. The gradient sequence distribution of hydrophilic and hydrophobic units resulted in less cohesive interaction with encapsulated curcumin. Comparing with the P(EtOx-ButenOx) polymer the loading in P(MeOx-isopropOx) is relatively low as

P($MeOx_{20}$-b-IsoPropOx$_{40}$) had a loading efficiency of 5.7% whereas P($EtOx_{33}$-b ButenOx$_{26}$) exhibited 7% loading.

Curcumin loaded micelles exhibited the characteristic absorbance peak at 420 nm. (Figure 86 a). Higher intensity peaks were afforded by the block polymers. Among the block polymers, enhancement of peak intensity was achieved with increasing hydrophobic units. Random arrangement of hydrophobic units in gradient polymers led to lower intensity peaks. Fluorescence emission spectra of the block and gradient polymers with same concentration of curcumin were recorded. The intensity of curcumin emission was higher in the block polymers compared to the gradient polymers. The transition of curcumin into the hydrophobic domain of the micelles is the reason for enhanced intensities and this trend could be correlated with the CMC of the polymers (Figure 85 b). Polymers with low CMC showed enhanced emission intensity of curcumin. However, curcumin loaded P($MeOx_{40}$-b-isoPropOx$_{20}$), P($MeOx_{50}$-b-isoPropOx$_{10}$) and P($MeOx_{10}$-b-isoPropOx$_{50}$) show slight red shift in the intensity. We assume this could be due to the lesser number of hydrophobic units in case of block polymers and intrusion of more hydrophilic segments in case of the gradient polymer.

The *in vitro* release of curcumin from the block and gradient polymers were performed at two different pH conditions (Figure 86). Gradient polymers of sizes around 300 nm were only studied. The polymers afforded slow release of curcumin at pH 7.4 and faster release at acidic pH similar to the observations with ButenOx polymers, except P($MeOx_{50}$-b-$EtOx_{10}$) which put forth a faster release in PBS. The number of hydrophobic units is the factor which controls the release of curcumin.

The more number of hydrophobic units, the more strongly curcumin is held in the core and slower would be the release. However, at acidic pH, this scenario does not come into play as the tertiary amide bonds get protonated subsequently leading to micelle dissociation and faster release of the drug.

P(MeOx $_{30}$-b-EtOx$_{30}$) exhibited favourable results based on loading, size and release studies prompting us to investigate this particular ratio for further *in vitro* experiments. Cytotoxicity studies revealed that the empty P(MeOx$_{30}$-isoPropOx$_{30}$) micelles did not exhibit any toxic effect on the cell lines (Figure 88 a). Profound cell death in cancer cells was achieved by curcumin loaded P(MeOx$_{30}$-isoPropOx$_{30}$) micelles compared to free curcumin due to the enhanced solubility of curcumin (Figure 88 b). Live dead assay results were consistent with the MTT assay evaluation of curcumin loaded P(MeOx$_{30}$-isoPropOx$_{30}$) micelles . Curcumin loaded P(MeOx$_{30}$-isoPropOx$_{30}$) micelles exhibited greater cell death compared to free curcumin (Figure 89).Curcumin loaded P(MeOx$_{30}$-isoPropOx$_{30}$) micelles exhibited prominent green fluorescence indicating relatively better cellular internalization than the free curcumin (Figure 90). Free curcumin exhibited diminished green fluorescence indicating low uptake by the cancer cells.

CHAPTER 6 - SUMMARY AND CONCLUSION

Clinical application of curcumin has been limited due to poor aqueous solubility and consequently minimal systemic bioavailability. Polymeric micelles prove to be a viable and versatile platform capable of significantly improving curcumin delivery. However, most of the polymer micelles intended for anti-cancer application, exhibit low curcumin loading capacity and accelerated release at physiological pH which impedes the *in vivo* therapeutic efficacy of curcumin. This study was focused on synthesizing amphiphilic polymer matrices that could self-assemble into micelles and were further explored for their feasibility for effective curcumin delivery to cancer cells. It was understood that altering the constituents in the amphiphilic matrix influenced the performance related parameters like micelle size, curcumin-micelle core compatibility, loading capacity and kinetics of release.

Initial investigations were performed by synthesizing curcumin loaded mPEG-laurate and mPEG-linolenate micelles. However, these micelles exhibited low curcumin loading capacity. Therefore, in an attempt to enhance the hydrophobibity, Pluronic was incorporated. It was noted that loading capacity increased to 8% by enhancing the hydrophobicity of the micelles. Cytotoxic studies on Caco2 cells revealed the coupled effects of linolenic acid and curcumin combined in a single nano-carrier. However, higher drug release was evident at pH 7.4 with the Pluronic linolenate micelles which was considered as a disadvantage. In the second section, PCL was explored for its superior hydrophobicity. Curcumin loading of 10% w/w was obtained in Pluronic/PCL micelles. In addition, it was observed that

the release was lowered at pH 7.4. Further, conjugation of calix[4] arene to Pluronic/PCL was successful in enhancing the loading to 17% w/w. The ability of calix arenes to switch conformations at lower pH aided in the high release of curcumin at pH 4.5 and attenuated release at pH 7.4. Unfortunately, low reaction yield and use of dioxane for micelle preparation posed as setbacks to work with these calix arene matrices on a larger scale.

Micelles	Loading Capacity (% w/w)	χ_{sp}	Release (%) after 72 h	
			At pH 7.4	At pH 4.5
1. PEG fatty esters				
• mPEG-laurate	2.4 ± 0.2	0.74	95.2±2.5	95.3 ± 4.6
• mPEG-linolenate	2.91 ± 0.06	0.71	85.6± 2.7	95.2 ± 5.9
• Pluronic linolenate	7.9 ± 0.3	0.55	73.5 ±1.7	88.2 ± 2.5
2. Pluronic/PCL				
• Pluronic/PCL	10.3 ± 0.6	0.17	56.3 ±2.3	85.5 ± 4.3
• CX-Pluronic/PCL	17.6 ± 1.2	− 0.79	35.1±6.5	88.3 ± 5.6
3. Cur-Dex	3.3 ± 1.2	−	30.2±5.5	97.4 ± 3.6
4. POxs				
• $PEtOx_{33}$-$ButenOx_{26}$	7.47 ± 1.7	0.07	24.1 ± 4.8	67.5 ± 4.7
• $PEtOx_{17}$-$ButenOx_{44}$	11.8 ± 2.2	”	6 ± 1	57.2 ± 4.9
• $MEtOx_{30}$-b-$isopropOx_{30}$	5.4 ± 0.9	0.63	44.1 ± 3.2	90.9 ± 5.2

Table 7. Summarized results on curcumin loading and release profile from the synthesized polymeric micelles

The third section investigated the efficacy of curcumin dextran conjugates. Curcumin dextran conjugates prevented curcumin degradation at physiological pH. In addition, it was observed that conjugation of curcumin did not compromise its therapeutic property and induced cytotoxicity on C6 glioma cells at 50 μM curcumin

concentration. These conjugates had control over the release rate at physiological pH. However, a low loading capacity of 3% was afforded with the conjugates. The fourth section evaluated the efficiency of POxs polymers. Micelle characteristics were seen to be highly dependent on the polymer architecture. From the investigated POx micelles, it was observed that favourable results were obtained with P(EtOx-b-butenOx) micelles, P($EtOx_{17}$-$ButenOx_{44}$) in particular. Curcumin loaded P($EtOx_{17}$-$ButenOx_{44}$) exhibited particle size less than 100 nm with curcumin loading of 12%. pH-sensitive release was observed with a release of 6% at pH 7.4. Enhanced cytotoxicity and cellular internalization was also afforded with this POx ratio. These attributes project the potential of P($EtOx_{17}$-b-$ButenOx_{44}$) to be employed as a promising nano-carrier for curcumin among the other investigated matrices. It was also realized from the study that the assessment of polymer-curcumin compatibility using Flory-Huggins interaction parameter (χ_{sp}) could expedite the selection of highly compatible micelle cores. Lower χ_{sp} value was related to higher curcumin loading (Table 5). Therefore, this technique could be considered as a reliable approach to screen suitable micelle systems for curcumin delivery. Future perspectives of the study include designing a strategy to enhance the experimental yield of CX-Pluronic/PCL and *in vivo* investigation of curcumin loaded P($EtOx_{17}$-b-$ButenOx_{44}$) to further establish its potential for safe and efficient cancer therapy.

REFERENCES

Abd Ghafar SA, Ismail M, Yagan LS, Fakurazi S, Ismail N, Chan KW,Tahir PM (2013) Cytotoxic activity of kenaf seed oils from supercritical carbon dioxide fluid extraction towards human colorectal cancer (HT29) cell lines. *Evid Based Complement Alternat Med* 1-8.

Adhikary R, Carlson PJ, Kee TW, Petrich JW (2010) Excited-state intramolecular hydrogen atom transfer of curcumin in surfactant micelles. *J Phys Chem B* 114: 2997-3004.

Aggarwal BB, Bhatt ID, Ichikawa H,Ahn KS,Sethi G,Sandur SS , Sundaram C,Seerum N,Shishodia S (2007) Curcumin–biological and medicinal properties. In: Ravindran PN, Nirmal babu K, Kandaswamy S (eds) *Turmeric: the genus Curcuma*, Taylor and Francis, New York pp. 297-368.

Aliabadi HM, Lavasanifar A (2006) Polymeric micelles for drug delivery. *Expert Opin Drug Deliv* 3:139-162.

Anand P, Sundaram C, Jhurani S , Kunnumakkara AB, Aggarwal BB (2008) Curcumin and cancer: an "old-age" disease with an "age-old" solution. *Cancer Lett* 267: 133-164.

Aubry J, Ganachaud F, Cohen Addad JP , Cabane B (2009) Nanoprecipitation of polymethylmethacrylate by solvent shifting: 1. Boundaries. *Langmuir* 25: 1970-1979.

Avgoustakis K, Beletsi A, Panagi Z, Klepetsanis P, Livaniou E, Evangelatos G, Ithakissios DS (2003) Effect of copolymer composition on the physicochemical characteristics, in vitro stability, and biodistribution of PLGA–mPEG nanoparticles. *Int J Pharm* 259: 115-127.

Balkwill F, Mantovani A (2001) Inflammation and cancer: back to Virchow? *Lancet*, 357: 539-545.

Barz M, Luxenhofer R, Zentel R, Vicent MJ (2011) Overcoming the PEG-addiction: well-defined alternatives to PEG, from structure–property relationships to better defined therapeutics. *Polym Chem* 2: 1900-1918.

Basílio N, Garcia-Rio L, Martín-Pastor M (2012) Calixarene-based surfactants: Evidence of structural reorganization upon micellization. *Langmuir* 28: 2404-2414.

Batrakova EV, KabanovAV (2008) Pluronic block copolymers: evolution of drug delivery concept from inert nanocarriers to biological response modifiers. *J Control Release* 130: 98-106.

Batrakova EV, Li S, Li Y, Alakhov VY, Elmquist WF, Kabanov AV. (2004) Distribution kinetics of a micelle-forming block copolymer Pluronic P85. *J Control Release* 100: 389-397.

Batrakova EV, Li S, Vinogradov SV, Alakhov VY, Miller DW, Kabanov AV (2001) Mechanism of pluronic effect on P-glycoprotein efflux system in blood-brain barrier: contributions of energy depletion and membrane fluidization. *J Pharmacol Exp Ther* 299: 483-493.

Bisht S, Feldmann G, Soni S, Ravi R, Karikar C, Maitra A, Maitra A (2007) Polymeric nanoparticle-encapsulated curcumin ("nanocurcumin"): a novel strategy for human cancer therapy. *J Nanobiotechnology* 5: 1-18.

Blanco E, Kessinger C W, Sumer BD, Gao J (2009). Multifunctional micellar nanomedicine for cancer therapy. Exp Biol Med 234: 123-131.

Bonné TB, Lüdtke K, Jordan R, Papadakis CM (2007) Effect of Polymer Architecture of Amphiphilic Poly (2-oxazoline) Copolymers on the Aggregation and Aggregate Structure. *Macromol Chem Physic* 208: 1402-1408.

Boukany PE, Morss A, Liao WC, Henslee B, Jung H, Zhang X, Yu B, Wang X, Wu Y, Li L, Gao K, Hu X, Zhao X, Hemminger O, Lu W, Lafyatis GP, Lee LJ (2011)Nanochannel electroporation delivers precise amounts of biomolecules into living cells. *Nat Nanotechnol* 6: 747-754.

Bray F , Ren J.S , Masuyer E , Ferlay J (2013) Global estimates of cancer prevalence for 27 sites in the adult population in 2008. *Int J Cancer* 132: 1133-1145.

Carlson LJ, Cote B, Alani AW, Rao DA (2014) Polymeric Micellar Co-delivery of Resveratrol and Curcumin to Mitigate In Vitro Doxorubicin-Induced Cardiotoxicity. *J Pharm Sci* 103: 2315-2322.

Carothers WH (1929) Studies on polymerization and ring formation. I. An introduction to the general theory of condensation polymers. *J Am Chem Soc* 51: 2548-2559.

Carrstensen H, Müller, R.H, Müller B (1992) Particle size, surface hydrophobicity and interaction with serum of parenteral fat emulsions and model drug carriers as parameters related to RES uptake. *Clinical nutrition*, 11: 289-297.

Carstens MG, de Jong PH, van Nostrum CF, Kemmink J, Verrijk R, de Leede LG, Crommelin DJ , Hennink WE (2008) The effect of core composition in biodegradable oligomeric micelles as taxane formulations. *Eur J Pharm Biopharm* 68: 596-606.

Castelli F, Caruso S, Uccella N (2003) Biomimesis of linolenic acid transport through model lipidic membranes by differential scanning calorimetry. *J Agr Food Chem* 51: 851-855.

Chabner BA, Roberts TG (2005) Chemotherapy and the war on cancer. *Nature Reviews Cancer*, 5: 65-72.

Chattopadhyay I, Biswas K, Bandyopadhyay U, Banerjee RK (2004) Turmeric and curcumin: Biological actions and medicinal applications. *Current science*, 87: 44-53.

Chen A , Xu J, Johnson A (2005) Curcumin inhibits human colon cancer cell growth by suppressing gene expression of epidermal growth factor receptor through reducing the activity of the transcription factor Egr-1. *Oncogene* 25: 278-287.

Chen X, Liu Y, An Y, Lü J, Li J, Xiong D, Shi L (2007) Novel structured composites formed from gold nanoparticles and diblock copolymers. *Macromol Rapid Comm* 28: 1350-1355.

Choi P, Kavassalis T, Rudin A (1996) Measurement of three-dimensional solubility parameters of nonyl phenol ethoxylates using inverse gas chromatography. *J Colloid Interface Sci* 180: 1-8.

Clogston JD, Patri AK (2011) *Zeta potential measurement, Characterization of Nanoparticles Intended for Drug Delivery*. Springer, pp. 63-70.

Costache AD, Sheihet L, Zaver K, Knight DD, Kohn J (2009) Polymer-drug interactions in tyrosine-derived triblock copolymer nanospheres: a computational modeling approach. *Mol Pharm* 6: 1620-1627.

Coussens LM , Werb Z, (2002) Inflammation and cancer. *Nature*, 420: 860-867.

Couvreur P, Barratt G, Fattal E, Legrand P, Vauthier C (2002) Nanocapsule technology: a review. Critic Rev Ther Drug 19: 99-134.

Culver KW , Michael Blaese R (1994) Gene therapy for cancer. *Trends Genet*, 10: 174-178.

Das RK, Kasoju N, Bora U (2010) Encapsulation of curcumin in alginate-chitosan-pluronic composite nanoparticles for delivery to cancer cells. *Nanomed-Nanotechnol* 6: 153-160.

de Fátima Â , Fernandes SA, Sabina AA (2009) Calixarenes as new platforms for drug design. *Current Drug Discovery Technol* 6: 151-170.

Desai D, Kothari S, Chen W, Wang J, Huang M, Sharma L (2011) Fatty acid and water-soluble polymer-based controlled release drug delivery system. *J Pharm Sci*, 100: 1900-1912.

Deshpande R , Mansara P, Suryavanshi S and Kaul-Ghanekar R (2013) Alpha-linolenic acid regulates the growth of breast and cervical cancer cell lines through regulation of NO release and induction of lipid peroxidation. *J Mol Biochem* 2: 6-17.

Dikshit R et al. (2012) Cancer mortality in India: a nationally representative survey. *Lancet* 379: 1807–16.

Dorai T , Aggarwal BB (2004) Role of chemopreventive agents in cancer therapy. *Cancer letters*, 215: 129-140.

Dougan M, Dranoff G (2001) *The Immune Response to Tumors: Current Protocols in Immunology*. John Wiley & Sons, Inc.

Draye JP, Delaey B, Van de Voorde A, Van Den Bulcke A, De Reu B, Schacht E (1998) In vitro and in vivo biocompatibility of dextran dialdehyde cross-linked gelatin hydrogel films. *Biomaterials* 19: 1677-1687.

Duncan R (2006) Polymer conjugates as anticancer nanomedicines. *Nat Rev Cancer* 6: 688-701.

Ebrahim Attia AB. Ong ZY, Hedrick L, Lee PP, Ee PLR, Hammond PT , Yang YY (2011) Mixed micelles self-assembled from block copolymers for drug delivery. *Current Opin Colloid Interface Sci* 16: 182-194

Eferl R, Wagner EF (2003) AP-1: a double-edged sword in tumorigenesis. *Nat Rev Cancer* 3: 859-868.

Esatbeyoglu T , Huebbe P, Ernst IM, Chin D, Wagner AE, Rimbach G (2012). Curcumin-from molecule to biological function. *Angew Chem Int Ed*, 51: 5308-5332.

Fedors RF (1974) A method for estimating both the solubility parameters and molar volumes of liquids. *Polym Eng Sci*, 14: 147-154.

Feng SS(2004) Nanoparticles of biodegradable polymers for new-concept chemotherapy. *Expert Rev Med Devices* 1: 115-125.

Ferlay J, Shin HR, Bray F, Forman D, Mathers C, Parkin DM (2010) Estimates of worldwide burden of cancer in 2008: GLOBOCAN 2008. *Int J Cancer* 127(12): 2893-2917.

Frazie RA, Matthijs G, Davies MC, Roberts CJ, Schacht E, Tendler SJ (2000) Characterization of protein-resistant dextran monolayers. *Biomaterials* 21: 957-966.

Gaucher G, Dufresne MH, Sant VP, Kang N, Maysinger D, Leroux JC (2005). Block copolymer micelles: preparation, characterization and application in drug delivery. *J Controlled Release* 109: 169-188.

Gescher A, Pastorino U, Plummer SM, Manson MM (1998). Suppression of tumour development by substances derived from the diet-mechanisms and clinical implications. *Br J Clinical Pharmacol* 45: 1-12.

Goddard P, Hutchinson LE, Brown J, Brookman LJ (1989) Soluble polymeric carriers for drug delivery. Part 2. Preparation and *in vivo* behaviour of N-acylethylenimine copolymers. *J Controlled Release*, 10: 5-16.

Goel A, Kunnumakkara AB, Aggarwal BB (2008) Curcumin as "Curecumin": From kitchen to clinic. *Biochem Pharmacol* 75: 787-809.

Gress A, Völkel A, Schlaad H (2007). Thio-click modification of poly [2-(3-butenyl)-2-oxazoline]. *Macromolecules* 40: 7928-7933.

Gunjur A, Duong C, Ball D, Siva S (2014) Surgical and ablative therapies for the management of adrenal 'oligometastases'-A systematic review. *Cancer Treat Rev* 40:838-46.

Guo LD, Chen XJ, Hu YH, Yu ZJ, Wang D, Liu JZ (2013) Curcumin inhibits proliferation and induces apoptosis of human colorectal cancer cells by activating the mitochondria apoptotic pathway. *Phytother Res* 27: 422-430.

Gupta SC, Kismali G, Aggarwal BB(2013) Curcumin, a component of turmeric: from farm to pharmacy. *Biofactors* 39: 2-13.

Gutsche CD (1998) *Calixarenes Revisited, Monographs in Supramolecular Chemistry*, Royal Society of Chemistry: Cambridge, UK.

Ha JC, Kim SY, Lee YM (1999) Poly (ethylene oxide)–poly (propylene oxide)–poly (ethylene oxide)(Pluronic)/poly (ε-caprolactone)(PCL) amphiphilic block copolymeric nanospheres: I. Preparation and characterization. *J Controlled Releas*e 62: 381-392.

Hanahan D, Weinberg RA (2011) Hallmarks of cancer: the next generation. *Cell* 144: 646-674.

Heard CM , Gallagher SJ, Congiatu C, Harwood J, Thomas CP, McGuigan C, Nemcová M, Nouskova T (2005). Preferential π–π complexation between

tamoxifen and borage oil/γ linolenic acid: Transcutaneous delivery and NMR spectral modulation. *Int J Pharm* 302: 47-55.

Hoogenboom R (2009) Poly (2-oxazoline)s: A Polymer Class with Numerous Potential Applications. *Angew Chem Int Ed* 48: 7978-7994.

Horbett TA (1993) Principles underlying the role of adsorbed plasma proteins in blood interactions with foreign materials. *Cardiovasc Pathol* 2: 137-148.

Hruby M, Filippov SK, Panek J, Novakova M, Mackova H, Kucka J, Vetvicka D, Ulbrich K (2010) Polyoxazoline thermoresponsive micelles as radionuclide delivery systems. *Macromol Biosci* 10: 916-924.

Hsiue GH, Chiang HZ, Wang CH, Juang TM (2006) Nonviral gene carriers based on diblock copolymers of poly (2-ethyl-2-oxazoline) and linear polyethylenimine. *Bioconjugate Chem* 17: 781-786.

Hsiue GH, Wang CH, Lo CL, Wang CH, Li JP, Yang JL (2006) Environmental-sensitive micelles based on poly (2-ethyl-2-oxazoline)-b-poly (l-lactide) diblock copolymer for application in drug delivery. *Int J Pharm* 317: 69-75.

Hsu CH, Cheng AL (2007) *Clinical studies with curcumin, The Molecular Targets and Therapeutic Uses of Curcumin in Health and Disease*. Springer, pp. 471-480.

Ireson C, Orr S, Jones DJ, Verschoyle R, Lim CK, Luo JL, Howells L, Plummer S, Jukes R, Williams Steward WP, Gescher AM (2001) Characterization of metabolites of the chemopreventive agent curcumin in human and rat hepatocytes and in the rat in vivo, and evaluation of their ability to inhibit

phorbol ester-induced prostaglandin E2 production. *Cancer Res* 61: 1058-1064.

Iyer AK, Khaled G, Fang J, Maeda H (2006). Exploiting the enhanced permeability and retention effect for tumor targeting. *Drug Discov Today* 11: 812-818.

Jackson JK, Springate CM, Hunter WL, Burt HM (2000) Neutrophil activation by plasma opsonized polymeric microspheres: inhibitory effect of Pluronic F127. *Biomaterials* 21: 1483-1491.

Jemal A, Bray F, Center MM, Ferlay J, Ward E, Forman D (2011) Global cancer statistics. *CA Cancer J Clin* 61: 69-90.

Jeon S, Lee J, Andrade J, De Gennes P (1991) Protein-surface interactions in the presence of polyethylene oxide: I. Simplified theory. *J Colloid Interface Sci* 142: 149-158.

Johnson BK, Prud'homme RK (2003) Chemical processing and micromixing in confined impinging jets. *AIChE J* 49: 2264-2282.

Johnstone RW, Ruefli AA, Lowe SW (2002) Apoptosis: a link between cancer genetics and chemotherapy. *Cell* 108: 153-164.

Jovanovic SV, Steenken S, Boone CW, Simic MG(1999) H-atom transfer is a preferred antioxidant mechanism of curcumin. *J Am Chem Soc* 121: 9677-9681.

Kabanov AV, Batrakova EV, Miller DW (2003) Pluronic block copolymers as modulators of drug efflux transporter activity in the blood-brain barrier. *Adv Drug Delivery Rev* 55: 151-164.

Kabanov AV et al (1989) The neuroleptic activity of haloperidol increases after its solubilization in surfactant micelles: micelles as microcontainers for drug targeting. *FEBS lett* 258: 343-345.

Kagiya T,Narisawa S, Maeda T, Fukui K (1966). Ring-opening polymerization of 2-substituted 2-oxazolines. *J Poly Sci Part B: Polym Lett* 4: 441-445.

Kempe K, Vollrath A, Schaefer HW, Poehlmann TG, Biskup C, Hoogenboom R, Hornig S, Schubert US (2010) Multifunctional Poly(2-oxazoline) Nanoparticles for Biological Applications. *Macromol Rapid Comm* 31: 1869-1873.

Klein J (2007) Probing the interactions of proteins and nanoparticles. *PNAS* 104: 2029-2030.

Knop K, Hoogenboom R, Fischer D, Schubert US (2010) Poly (ethylene glycol) in drug delivery: pros and cons as well as potential alternatives. *Angew Chem Int Ed* 49: 6288-6308.

Kwon GS, Kataoka K (1995) Block copolymer micelles as long-circulating drug vehicles. *Adv Drug Delivery Rev* 16: 295-309.

Lagugné-Labarthet F, An YQ, Yu T, Shen YR, Dalcanale E, Shenoy DK (2005). Proton driven vase-to-kite conformational change in cavitands at an air-water interface monitored by surface SHG. *Langmuir* 21: 7066-7070.

Lampe V, Milobedzka J, Kostanecki V (1910) Structure of curcumin. *Ber Dtsch. Chem Ges* 43: 2163-2170.

Lao CD, Ruffin MT , Normolle D, Heath DD, Murray SI, Bailey JM, Boggs ME, Crowell J, Rock CL, Brenner DE(2006). Dose escalation of a curcuminoid formulation. *BMC Complement Altern Med* 6: 1-10.

Latere Dwan'Isa JP, Rouxhet L, Préat V, Brewster ME, Ariën A(2007) Prediction of drug solubility in amphiphilic di-block copolymer micelles: the role of polymer-drug compatibility. *Pharmazie* 62: 499-504.

Lee J, Cho EC, Cho K (2004) Incorporation and release behavior of hydrophobic drug in functionalized poly (D, L-lactide)-block–poly (ethylene oxide) micelles. *J Controlled Release* 94: 323-335.

Letchford K, Liggins R, Burt H (2008) Solubilization of hydrophobic drugs by methoxy poly (ethylene glycol)-block-polycaprolactone diblock copolymer micelles: Theoretical and experimental data and correlations. *J Pharm Sci* 97: 1179-1190.

Leung MH, Colangelo H, Kee TW (2008) Encapsulation of curcumin in cationic micelles suppresses alkaline hydrolysis. *Langmuir* 24: 5672-5675.

Lev-Ari S, Strier L, Kazanov D, Madar-Shapiro L, Dvory-Sobol H, Pinchuk I, Marian B, Lichtenberg D, Arber N (2005) Celecoxib and curcumin synergistically inhibit the growth of colorectal cancer cells. *Clin Cancer Res* 11: 6738-6744.

Lev-Ari S, Vexler A, Starr A, Ashkenazy-Voghera M, Greif J, Aderka D, Ben-Yosef R (2007) Curcumin augments gemcitabine cytotoxic effect on pancreatic adenocarcinoma cell lines. *Cancer Invest* 25: 411-418.

Lim Soo P, Luo L, Maysinger D, Eisenberg, A(2002) Incorporation and release of hydrophobic probes in biocompatible polycaprolactone-block-poly (ethylene oxide) micelles: implications for drug delivery. *Langmuir* 18: 9996-10004.

Lipinski CA (2000) Drug-like properties and the causes of poor solubility and poor permeability. *J Pharmacol Toxicological Methods* 44: 235-249.

Liu J, Lee H, Huesca M, Young A, Allen C (2006) Liposome formulation of a novel hydrophobic aryl-imidazole compound for anti-cancer therapy. *Cancer Chemother Pharmacol* 58: 306-318.

Liu J, Xiao Y, Allen C(2004) Polymer–drug compatibility: a guide to the development of delivery systems for the anticancer agent, ellipticine. *J Pharm Sci* 93: 132-143.

Loprinzi CL, Barton DL, Jatoi A, Sloan J, Martenson J, Steensma D, Rao R, Novotny P, Sood A, Grothey A, Minasian L, Windschitl H (2007) Symptom control trials: a 20-year experience. *J Support Oncol* 5: 119-25.

Lukyanov AN, Torchilin VP (2004) Micelles from lipid derivatives of water-soluble polymers as delivery systems for poorly soluble drugs. *Adv Drug Delivery Reviews* 56: 1273-1289.

Luthra PM, Kumar R, Prakash A (2009) Demethoxycurcumin induces Bcl-2 mediated G2/M arrest and apoptosis in human glioma U87 cells. *Biochem Biophys Res Commun* 384: 420-425.

Luxenhofer R, Sahay G, Schulz A, Alakhova D, Bronich TK, Jordan R, Kabanov AV (2011) Structure-property relationship in cytotoxicity and cell uptake of poly (2-oxazoline) amphiphiles. *J Controlled Release* 153: 73-82.

Luxenhofer R, Schulz A, Roques C, Li S, Bronich TK, Batrakova EV, Jordan R, Kabanov AV(2010) Doubly amphiphilic poly (2-oxazoline)s as high-capacity delivery systems for hydrophobic drugs. *Biomaterials* 31: 4972-4979.

Lyatskaya Y, Gersappe D, Gross NA , Balazs AC (1996) Designing compatibilizers to reduce interfacial tension in polymer blends. *J Phys Chem* 100: 1449-1458.

Ma Z, Haddadi A, Molavi O, Lavasanifar A, Lai R, Samuel J (2008) Micelles of poly (ethylene oxide)-b-poly (ε-caprolactone) as vehicles for the solubilization, stabilization, and controlled delivery of curcumin. *J Biomed Mater Res Part A* 86: 300-310.

Maechling-Strasser C, Déjardin P, Galin JC, Schmitt A, Housse-Ferrari V, Sébille B, Mulvihill JN, Cazenave JP (1989) Synthesis and adsorption of a poly(n-acetylethyleneimine)-polyethyleneoxide-poly(n-acetylethyleneimine) triblock-copolymer at a silica/solution interface. influence of its preadsorption on platelet adhesion and fibrinogen adsorption. *J Biomed Mater Res* 23(12): 1395-1410.

Maeda H, Greish K, Fang J (2006) The EPR effect and polymeric drugs: a paradigm shift for cancer chemotherapy in the 21st century *Adv Polym Sci* 193: 103–121.

Maeda H, Wu J, Sawa T, Matsumura Y, Hori K (2000) Tumor vascular permeability and the EPR effect in macromolecular therapeutics: a review. *J Controlled Release* 65: 271-284.

Mahmud A, Xiong XB, Aliabadi HM, Lavasanifar A (2007) *J Drug Target* 15: 553-584.

Manju S, Sreenivasan K (2011) Enhanced drug loading on magnetic nanoparticles by layer-by-layer assembly using drug conjugates: blood compatibility evaluation and targeted drug delivery in cancer cells. *Langmuir* 27: 14489-14496.

Mao C, Liang CX, Mao YQ, Li L, Hou XM, Shen J(2009). Modification of polyethylene with Pluronics F127 for improvement of blood compatibility. *Colloids Surf B Biointerfaces* 74: 362-365.

Martin AN, Sinko PJ, Singh Y (2011) *Martin's Physical Pharmacy and Pharmaceutical Sciences: Physical Chemical and Biopharmaceutical Principles in the Pharmaceutical Sciences.* Lippincott Williams & Wilkins.

Matsumura Y, Maeda H (1986) A new concept for macromolecular therapeutics in cancer chemotherapy: mechanism of tumoritropic accumulation of proteins and the antitumor agent SMANCS. *Cancer Res* 46: 6387-6392.

McDonald DM, Baluk P (2002) Significance of blood vessel leakiness in cancer. *Cancer Res* 62: 5381-5385.

Mei L, Zhang Y, Yi Zheng Y, Tian G, Song C, Yang D, Chen H, Sun H,[3] Tian Y, Kexin Liu K, Li, Z , Huang L (2009) A novel docetaxel-loaded poly (ε-caprolactone)/pluronic F68 nanoparticle overcoming multidrug resistance for breast cancer treatment. *Nanoscale Res Letters* 4: 1530-1539.

Mikhail AS, Allen C (2009) Block copolymer micelles for delivery of cancer therapy: transport at the whole body, tissue and cellular levels. *J Controlled Release* 138: 214-223.

Milner JA, McDonald SS, Anderson DE, Greenwald P (2001). Molecular targets for nutrients involved with cancer prevention. *Nutr Cancer* 41: 1-16.

Miyata K, Christie RJ, Kataoka K (2011) Polymeric micelles for nano-scale drug delivery. *React Funct Polym* 71: 227-234.

Mohanraj V, Chen Y (2007) Nanoparticles-a review. *Trop J Pharm Res* 5: 561-573.

Mokhtari B, Pourabdollah K (2012) Applications of calixarene nano-baskets in pharmacology. *J Inclusion Phenom Macrocyclic Chem* 73: 1-15.

Nagarajan R, Barry M, Ruckenstein E(1986) Unusual selectivity in solubilization by block copolymer micelles. *Langmuir* 2: 210-215.

Naka K, Nakamura T, Ohki A, Maeda S (1995) Aggregates of amphiphilic block copolymers derived from poly [(N-acylimino) ethylene] s and their complexes with lipase in water. *Polym J* 27: 1071-1078.

N Nakatsuji T, Kao MC, Fang JY, Zouboulis CC, Zhang L, Gallo RL, Huang CM (2009) Antimicrobial property of lauric acid against Propionibacterium acnes: its therapeutic potential for inflammatory acne vulgaris. *J Investigative Dermatol* 129: 2480-2488.

Naksuriya O, Okonogi S, Schiffelers RM, Hennink WE (2014) Curcumin nanoformulations: A review of pharmaceutical properties and preclinical studies and clinical data related to cancer treatment. *Biomaterials* 35: 3365-3383.

Nam JP, Park SC, Kim TH, Jang JY, Choi C, Jang MK, Nah JW (2013) Encapsulation of paclitaxel into lauric acid- O-carboxymethyl chitosan-

transferrin micelles for hydrophobic drug delivery and site-specific targeted delivery. *Int J Pharm* 457: 124-135.

Neises B, Steglich W (1978) Simple method for the esterification of carboxylic acids. *Angew Chem Int Ed* 17: 522-524.

Niidome T, Huang L (2002) Gene therapy progress and prospects: nonviral vectors. *Gene Ther* 9: 1647-1652.

Nimse SB, Kim T(2013) Biological applications of functionalized calixarenes. Chem Soci Rev, 42: 366-386.

Osterberg E, Bergström K, Holmberg K, Schuman TP, Riggs JA, Burns NL, Van Alstine JM, Harris JM (1995) Protein-rejecting ability of surface-bound dextran in end-on and side-on configurations: Comparison to PEG. *J Biomed Mater Res* 29: 741-747.

Owen SC, Chan DP, Shoichet MS (2012) Polymeric micelle stability. *Nano Today* 7: 53-65.

Owens III D, Peppas NA (2006) Opsonization, biodistribution, and pharmacokinetics of polymeric nanoparticles. *Int J Pharm* 307: 93-102.

Pathan IB, Setty CM (2009) Chemical penetration enhancers for transdermal drug delivery systems. *Trop J Pharm Res* 8:173-179.

Payton F, Sandusky P , Alworth WL (2007) NMR study of the solution structure of curcumin. *J Nat Prod* 70: 143-146.

Pignatello R, Castelli F (2011) Calorimetric techniques to study the interaction of drugs with biomembrane models. *J Pharm Bioallied Sci* 3: 1-2.

Plenderleith IH (1990) Treating the Treatment: Toxicity of Cancer Chemotherapy. *Can Fam Physician* 36: 1827-1830.

Podaralla S, Averineni R, Alqahtani M, Perumal O (2012) Synthesis of Novel Biodegradable Methoxy Poly (ethylene glycol)–Zein Micelles for Effective Delivery of Curcumin. *Mol Pharm* 9: 2778-2786.

Pratten MK, Lloyd JB, Hörpel G, Ringsdorf H (1985) Micelle-forming block copolymers: Pinocytosis by macrophages and interaction with model membranes. *Die Makromol Chemie*, 186: 725-733.

Racoosin EL, Swanson JA (1993) Macropinosome maturation and fusion with tubular lysosomes in macrophages. *J Cell Biol* 121: 1011-1020.

Raveendran R, Bhuvaneshwar GS, Sharma CP (2013) *In vitro* cytotoxicity and cellular uptake of curcumin-loaded Pluronic/Polycaprolactone micelles in colorectal adenocarcinoma cells. *J Biomater Appl* 27: 811-827.

Redshaw C, Elsegood MRJ, Wright JA, Baillie-Johnson H, Yamato T, De Giovanni S , Mueller A (2012) Cellular uptake of a fluorescent vanadyl sulfonylcalix [4] arene. *Chem Comm* 48: 1129-1131.

Sahay G, Batrakova EV, Kabanov AV(2008) Different internalization pathways of polymeric micelles and unimers and their effects on vesicular transport. *Bioconjugate Chem* 19: 2023-2029.

Sahu A, Bora U, Kasoju N, Goswami P (2008) Synthesis of novel biodegradable and self-assembling methoxy poly (ethylene glycol)–palmitate nanocarrier for curcumin delivery to cancer cells. *Acta Biomater* 4: 1752-1761.

Sahu A, Kasoju N, Goswami P. and Bora U(2011) Encapsulation of curcumin in Pluronic block copolymer micelles for drug delivery applications. *J Biomater Appl* 25: 619-639.

Salem M, Rohani S, Gillies ER (2014) Curcumin, a promising anti-cancer therapeutic: a review of its chemical properties, bioactivity and approaches to cancer cell delivery. *RSC Adv* 4: 10815-10829.

Samanta S, Roccatano D (2013) Interaction of Curcumin with PEO–PPO–PEO block copolymers: a molecular dynamics study. *J Phys Chem B* 117: 3250-3257.

Sandoval RW, Williams DE, Kim J, Roth CB, Torkelson JM (2008) Critical micelle concentrations of block and gradient copolymers in homopolymer: Effects of sequence distribution, composition, and molecular weight. *J Polym Sci Part B: Polym Phys* 46: 2672-2682.

Rejinold NS, Muthunarayanan M, Divyarani VV, Sreerekha PR, Chennazhi KP, Nair SV, Tamura H, Jayakumar R (2011) Curcumin-loaded biocompatible thermoresponsive polymeric nanoparticles for cancer drug delivery. *J Colloid Interface Sci* 360: 39-51.

Scarano W, de Souza P, Stenzel MH (2015) Dual-drug delivery of curcumin and platinum drugs in polymeric micelles enhances the synergistic effects: a double act for the treatment of multidrug-resistant cancer. *Biomater Sci* 3:163-174.

Seeliger W, Aufderhaar E, Diepers W, Feinauer R, Nehring R, Thier W, Hellmann H (1966) Recent syntheses and reactions of cyclic imidic esters. *Angew Chem Int Ed Engl* 5: 875-888.

Shaik N, Giri N, Elmquist WF (2009) Investigation of the micellar effect of pluronic P85 on P-glycoprotein inhibition: Cell accumulation and equilibrium dialysis studies. *J Pharm Sci* 98: 4170-4190.

Shehzad A, Lee J, Lee YS (2013) Curcumin in various cancers. *Biofactors* 39: 56-68.

Shen L, Ji HF (2007) Theoretical study on physicochemical properties of curcumin. *Spectrochim Acta A Mol Biomol Spectrosc* 67: 619-623.

Shoba G, Joy D, Joseph T, Majeed M, Rajendran R, Srinivas PS (1998). Influence of piperine on the pharmacokinetics of curcumin in animals and human volunteers. *Planta Med* 64: 353-356.

Shull KR (2002) Interfacial activity of gradient copolymers. *Macromolecules* 35: 8631-8639.

Shull KR, Kramer EJ (1990) Mean-field theory of polymer interfaces in the presence of block copolymers. *Macromolecules* 23: 4769-4779.

Siepmann J Siegel RA, Rathbone MJ (2012) *Fundamentals and applications of controlled release drug delivery*. Springer, New York.

Sinha R, Anderson D, McDonald S, Greenwald P (2003). Cancer risk and diet in India. *J Postgrad Med* 49: 222-228.

Sliwa W, Kozlowski C (2009) *Calixarenes and resorcinarenes: Synthesis, properties and applications*. Wiley,Weinheim .

Song Z, Feng R, Sun M, Guo C, Gao Y, Li L, Zhai G (2011). Curcumin-loaded PLGA-PEG-PLGA triblock copolymeric micelles: Preparation,

pharmacokinetics and distribution *in vivo. J Colloid Interface Sci* 354: 116-123.

Specht A, Bernard P, Goeldner M, Peng L (2002) Mutually Induced Formation of Host–Guest Complexes between p-Sulfonated Calix [8] arene and Photolabile Cholinergic Ligands. *Angew Chem Int Ed* 41: 4706-4708.

Surh YJ (2003) Cancer chemoprevention with dietary phytochemicals. *Nat Rev Cancer* 3: 768-780.

Tadros TF (2006) *Applied Surfactants: Principles and Applications*, John Wiley & Sons.

Takada Y, Fang X, Jamaluddin MS, Boyd DD, Aggarwal BB (2004) Genetic deletion of glycogen synthase kinase-3β abrogates activation of IκBα kinase, JNK, Akt, and p44/p42 MAPK but potentiates apoptosis induced by tumor necrosis factor. *J Biol Chem* 279: 39541-39554.

Takada , Ichikawa H, Pataer A, Swisher S, Aggarwal BB (2006) Genetic deletion of PKR abrogates TNF-induced activation of IκBα kinase, JNK, Akt and cell proliferation but potentiates p44/p42 MAPK and p38 MAPK activation. *Oncogene* 26: 1201-1212.

Tomalia D, Sheetz D (1966) Homopolymerization of 2-alkyl-and 2-aryl-2-oxazolines. *J Polym Sci Part A-1: Polym Chem* 4: 2253-2265.

Tominaga Y, Mizuse M, Hashidzume A, Morishima Y, Sato T (2010) Flower micelle of amphiphilic random copolymers in aqueous media. *J Phys Chem B*, 114: 11403-11408.

Torchilin VP (2001) Structure and design of polymeric surfactant-based drug delivery systems. *J Controlled Release* 73: 137-172.

Torchilin VP (2008) Cell penetrating peptide-modified pharmaceutical nanocarriers for intracellular drug and gene delivery. *Peptide Sci* 90: 604-610.

Tu C, Zhu L, Li P, Chen Y, Su Y, Yan D, Zhu X, Zhou G.Tu (2011) Supramolecular polymeric micelles by the host–guest interaction of star-like calix [4] arene and chlorin e6 for photodynamic therapy. *Chem Commun* 47: 6063-6065.

Tyrrell ZL, ShenY and Radosz M (2010) Fabrication of micellar nanoparticles for drug delivery through the self-assembly of block copolymers. *Progr Polym Sci* 35: 1128-1143.

Uchegbu IF, Schatzlein AG (2010) *Polymers in drug delivery*, CRC Press, Taylor & Francis Group, Boca Raton.

Van Domeselaar GH, Kwon GS, Andrew LC,Wishart DS (2003) Application of solid phase peptide synthesis to engineering PEO–peptide block copolymers for drug delivery. *Colloid Surf B* 30: 323-334.

Van Krevelen D (1997) *Properties of polymers: their correlation and chemical structure: their numerical and prediction and additive group contributions.* Elsevier, Amsterdam.

Varshosaz J (2012). Dextran conjugates in drug delivery. *Exp Opin Drug Deliv* 9: 509-523.

Verstappen CC, Heimans JJ, Hoekman K, Postma TJ (2003) Neurotoxic complications of chemotherapy in patients with cancer. *Drugs* 63: 1549-1563.

Vogel, H. and Pelletier, J., 1815. Curcumin-biological and medicinal properties. J Pharma, 2: 50-50.

Wahlström B, Blennow G (1978) A study on the fate of curcumin in the rat. *Acta Pharmacol Toxicol* 43: 86-92.

Wang YJ, Pan MH, Cheng AL, Lin LI, Ho YS, Hsieh CY, Lin JK (1997) Stability of curcumin in buffer solutions and characterization of its degradation products. *J Pharm Biomed Anal* 15: 1867-1876.

Wang YZ, Fang XL, Li YJ, Zhang ZW, Han LM, Sha XY (2008) Preparation, characterization of paclitaxel-loaded Pluronic P105 polymeric micelles and in vitro reversal of multidrug resistant tumor. *Acta Pharm Sin B* 43: 640-646.

Wiesbrock F, Hoogenboom R,Leenen M, van Nispen SFGM , van der Loop M , Abeln CH , van den Berg AMJ , Schubert US (2005). Microwave-assisted synthesis of a 42-membered library of diblock copoly (2-oxazoline) s and chain-extended homo poly (2-oxazoline) s and their thermal characterization. *Macromolecules* 38: 7957-7966.

Winnik FM, Ringsdorf H, Venzmer J (1991) Interaction of surfactants with hydrophobically-modified poly (N-isopropylacrylamides). 2. Fluorescence label studies. *Langmuir* 7: 912-917.

Won CY, Chu CC (1998) Dextran–estrone conjugate: synthesis and *in vitro* release study. Carbohydrate polymers, 36: 327-334.

Wong CL, Kim J, Roth CB ,Torkelson JM (2007) Comparison of critical micelle concentrations of gradient copolymer and block copolymer in homopolymer:

Novel characterization by intrinsic fluorescence. *Macromolecules* 40: 5631-5633.

Woodruff MA, Hutmacher DW (2010) The return of a forgotten polymer-polycaprolactone in the 21st century. *Prog Polym Sci* 35(10): 1217-1256.

Yallapu MM, Khan S, Maher DM, Ebeling MC, Sundram V, Chauhan N, Ganju A, Balakrishna S, Gupta BK, Zafar N, Jaggi M, Chauhan S (2014) Anti-cancer activity of curcumin loaded nanoparticles in prostate cancer. *Biomaterials* 35: 8635-8648.

Yan F, Zhang C, Zheng Y, Mei L, Tang L, Song C, Sun H, Huang L (2010) The effect of poloxamer 188 on nanoparticle morphology, size, cancer cell uptake, and cytotoxicity. *Nanomedicine* 6: 170-178.

Yang C, Tan JPK, Cheng W,Ebrahim Attiaa AB, Yi Ting CT,Nelson A, Hedrick JB,

Yang YY (2010). Supramolecular nanostructures designed for high cargo loading capacity and kinetic stability. *Nano Today* 5: 515-523.

Yang D, Pornpattananangkul D, Nakatsuji T, Chan M, Carson D, Huang CM, Zhang L (2009). The antimicrobial activity of liposomal lauric acids against Propionibacterium acnes. *Biomaterials* 30: 6035-6040.

Yang KY, Lin LC, Tseng TY, Wang SC, Tsai TH (2007). Oral bioavailability of curcumin in rat and the herbal analysis fromCurcuma longa by LC–MS/MS. *J Chromatogr B Analyt Technol Biomed Life Sci* 853: 183-189.

Yano M, Kishida E, Iwasaki M, Kojo S, Masuzawa Y(2000). Docosahexaenoic acid and vitamin E can reduce human monocytic U937 cell apoptosis induced by tumor necrosis factor. *J Nutr* 130: 1095-1101.

Yokoyama M (1998) Novel passive targetable drug delivery with polymeric micelles.In:Okano T (ed) *Biorelated Polym Gels*, Academic Press, San Diego,pp. 193-229.

Yue J, Lui S, Xie Z, Xing Y, Jing X (2013) Size-dependent biodistribution and antitumor efficacy of polymer micelle drug delivery systems. *J Mater Chem B* 1: 4273-4280.

Zalipsky S (1995) Chemistry of polyethylene glycol conjugates with biologically active molecules. *Adv Drug Delivery Rev* 16: 157-182.

Zalipsky S, Hansen CB, Oaks JM, Allen TM (1996) Evaluation of blood clearance rates and biodistribution of poly (2-oxazoline)-grafted liposomes. *J Pharm Sci* 85: 133-137.

Zeng Y, Pitt WG (2006) A polymeric micelle system with a hydrolysable segment for drug delivery. *J Biomater Sci, Polym Ed* 17: 591-604.

Zitvogel L, Apetoh L, Ghiringhelli F, Kroemer G (2008). Immunological aspects of cancer chemotherapy. *Nat Rev Immunol* 8: 59-73.

List of Publications

1) Original papers

- Raveendran R, Bhuvaneshwar GS, Sharma CP (2013) *In vitro* cytotoxicity and cellular uptake of curcumin-loaded Pluronic/Polycaprolactone micelles in colorectal adenocarcinoma cells. *J Biomater Appl* 27: 811-827.
- Raveendran R, Pillai CKS, Bhuvaneshwar GS, Sharma CP (2014) Enhanced cytotoxicity and cellular internalization of hemocompatible curcumin loaded Pluronic linolenate micelles in cancer cells. *J Nanopharmaceutics Drug Delivery* 2:36-51.
- Raveendran R , Bhuvaneshwar GS, Sharma CP (2016) Hemocompatible water soluble dextran curcumin conjugates: Enhanced *in vitro* cytotoxicity and cellular uptake in C6 glioma cells *Carbohydrate Polymers*137, 497-507

2) Book Chapter

Raveendran R and C P Sharma, Applications of Interpenetrating Polymer Networks in Micro- and Nano-Structured Interpenetrating Polymer Networks: From Design to Applications John Wiley & Sons, Incorporated , 2016.

3) Conferences/ Symposiums

- R Raveendran, Bhuvaneshwar GS, Sharma CP, "Curcumin loaded calix-arene conjugated Pluronic/PCL amphiphiles for anti-cancer drug delivery" at the 9th World Biomaterials Congress (WBC), 2012 in Chengdu, China (Poster presentation).

- R Raveendran, Sharma CP, "Hemocompatible water soluble dextran curcumin conjugates: Evaluation of their anticancer potential in C6 glioma cells" at the 22nd Australasian Society for Biomaterials and Tissue Engineering (ASBTE) conference, Barossa valley, Australia (Oral Presentation).

- R Raveendran, Sharma CP, Mullen K, Dargaville TR, "Polymeric micelles for curcumin delivery to cancer cells" at annual RACI polymer student symposium, QUT, Brisbane, Australia (Oral presentation).

****